Development and Characterisation of Polymeric Nano-carriers for Oral Delivery of Biopharmaceuticals

Li, Molly

Award date:
2017

Awarding institution:
University of Bath

Development and Characterisation of Polymeric Nano-carriers for Oral Delivery of Biopharmaceuticals

Ruiying Li

A thesis submitted for the degree for Doctor of Philosophy

University of Bath

Department of Pharmacy and Pharmacology

Table of Contents

Acknowledgement

Doctoral study time is the most unforgettable experience in my life, it is bitter and sweet. I am so grateful for all these people who have helped me during this period of time.

First and foremost, I would like to give my deepest and sincere gratitude to, Professor **Randy Mrsny**, who has been always supporting, encouraging and inspiring me over the years. He has led me to discover the beauty of science and to enjoy exploring the unknown. He is also a life mentor, opens my eyes to see things from different perspectives.

My deepest thanks go to Dr **Paul De Bank**, he has been always helpful and supportive, I really appreciated all his suggestions during the course of this study, which has taught me to become a more organised and independent researcher.

I am really grateful to Dr **Magdalena Perez Ortiz**, her encouraging words, all stimulating discussions and valuable advice on this work are all greatly appreciated. I would like to express my thanks to Dr **Sarah Cordery**, for her patient proofreading and suggestions on this thesis. My thanks also go to **Iain Johnson**, his time and proofreading on this work is highly appreciated. I also want to thank **Alistair Taverner** who helped me with the *in vivo* work and Dr **Julia MacKay** for the practical help in the lab.

I gratefully acknowledge Professor **Alexander (Sandy) Florence** and Dr **Albert Bolhuis** for accepting to evaluate this work.

I would like to acknowledge my sponsors: University of Bath and Chinese Scholarship Council.

My deepest thanks go to my friends and family, for always being on my side, cheering me up, accepting me and loving me unconditionally.

Finally, I give deepest gratitude to God, who created everything for me to explore and learn, also gives me the ability and all the help I needed to finish this work.

Abstract

Biopharmaceuticals represent a variety of biological products for diagnostic and therapeutic purposes, of which developments are driven by the recent advances in biotechnology. However, oral administration of biopharmaceuticals is challenging due to the low absorption of macromolecules and the potential degradation that occurs in the harsh environment of the gastrointestinal tract. Various strategies have been explored to improve the bioavailability of these therapeutic agents, and some strategies have the potential to protect these fragile proteins from the harsh environment. The low permeability of these macromolecules across the intestinal epithelium remains the main challenge.

This work focuses on providing a strategy to increase the intestinal epithelium permeability of biopharmaceuticals. In nature, bacterial toxins, such as *Pseudomonas aeruginosa* exotoxin A (PE), are able to travel across the intestinal epithelium and target the immune cells underneath. The hypothesis of this study is that these toxins can facilitate the trans-epithelial transport of toxin-conjugated nanoparticles. Two biodegradable and mucoadhesive polymers, alginate and chitosan, were selected for the preparation of nanoparticles.

Alginate-chitosan nanoparticles had a diameter of 179 ± 3 nm and a zeta potential of 17 ± 5 mV. After the conjugation with ntPE, the size and zeta potential changed to 202 ± 20 nm and -6 ± 5 mV, respectively. Transcytosis of ntPE-coupled nanoparticles was evaluated on Caco-2 cell monolayers *in vitro*. The transport rate was 4.36 ± 2.24 %, compared to 4.18 ± 2.05 % for nanoparticles conjugated with bovine serum albumin (BSA) and 2.83 ± 1.29 % for unmodified ones. The trans-epithelial transport of ntPE-coupled nanoparticles was then examined in the living rat small intestine. Nanoparticles coupled with ntPE were found to accumulate in the *lamina propria* of the rat small intestine, while no BSA-coupled nanoparticles or unmodified nanoparticles were found in the tissue sections. Finally, green fluorescent protein served as a model for biopharmaceuticals, and was loaded into alginate-chitosan nanoparticles to study the trans-epithelial delivery ability of these nano-carriers.

Overall, this thesis tests the feasibility of using a bacterial toxin to facilitate the trans-epithelial transport of nano-carriers loaded with biopharmaceuticals. Results support this hypothesis and suggest these alginate-chitosan nanoparticles are worthy of continued work to develop into nano-carriers for oral administration of biopharmaceuticals.

List of Abbreviations

AC NPs	Alginate-chitosan nanoparticles
AEE	Apical early endosome
ASBT	Apical sodium-dependent bile salt transporter
BSA	Bovine serum albumin
CaP NPs	Calcium phosphate nanoparticles
CT	Cholera toxin
CD	Circular dichroism
CTCF	Corrected total cryosection fluorescence
DAPI	4', 6-diamidino-2-phenylindole, dihydrochloride
DCs	Dendritic cells
DOCA	Deoxycholic acid
DLS	Dynamic light scattering
EDC	N-(3-Dimethylaminopropyl)-N′-ethylcarbodiimide hydrochloride
EDTA	Ethylenediaminetetra-acetic acid
EE	Early endosome
EGTA	Ethylene glycol tetraacetic acid
ELISA	Enzyme-linked immunosorbent assay
EMCH	N-ε-maleimidocaproic acid hydrazide
ER	Endoplasmic reticulum
FcRn	Neonatal Fc receptor
FITC	Fluorescein isothiocyanate
fPS NPs	Fluorescence polystyrene nanoparticles
FSH	Follicle-stimulating hormone
FTIR	Fourier transform infrared spectroscopy
FTSC	Fluorescein-5-thiosemicarbazide

GALT	Gut-associated lymphoid tissue
GFP	Green fluorescent protein
GI tract	Gastrointestinal tract
GM1	Monosialoganglioside
HC	Haptocorrin
HIM2	Hexyl-insulin monoconjugate 2
IgG	Immunoglobulin
IF	Intrinsic factor
IFR	Intrinsic factor receptor
IMAC	Immobilised metal ion affinity chromatography
IPTG	Isopropyl β-D-1-thiogalactopyranoside
IV	Intravenous
LRP-1	Low density lipoprotein receptor-related protein
LE	Late endosomes
LK	Lumbrokinase
MCT	Mercury cadmium telluride
NHS	N-hydroxysuccinimide
NMR	Nuclear Magnetic Resonance
NPs	Nanoparticles
NTA	Nanoparticle Tracking Analysis
ntPE	Non-toxic *Pseudomonas* exotoxin
PBS	Phosphate-buffered saline
PCL	Polycaprolactone
PE	*Pseudomonas* exotoxin A
PEC	Polyelectrolyte complexes
PEG	Polyethylene glycol
PEG-PLA	Polyethylene glycol-D, L-polylactide

pI	Isoelectric point
PLA	Polylactic acid
PLG	Polyglycolic acid
PLGA	Polylactic-co-glycolic acid
PVDF	Polyvinylidene difluoride
REC	Recycling endosome compartment
RIPA buffer	Radioimmunoprecipitation assay buffer
RT	Room temperature
SDS-PAGE	Sodium dodecyl sulphate polyacrylamide gel electrophoresis
SEC	Size exclusion chromatography
SEM	Scanning electron microscopy
SIF	Simulated intestinal fluid
TBS	Tris-buffered saline buffer
TCII	Transcobalamin II
TEER	Trans-epithelial electrical resistance
TEM	Transmission electron microscopy
TEV	Tobacco etch virus
TGN	*Trans* Golgi network
TJ	Tight junctions
$VitB_{12}$	Vitamin B_{12}
WGA	Wheat germ agglutinin
ZO-1	*Zona occludens*

Chapter 1 Introduction

Overview: The field of biopharmaceuticals is growing fast with emerging biotechnology, unfortunately, most of the therapeutic proteins on the market are restricted to the injection route, which is invasive and has low patient compliance. The clinical potential of biopharmaceuticals would therefore be greatly expanded by the ability to deliver these therapeutics as oral dosage forms. However, biopharmaceuticals are vulnerable to the acidic and enzymatic environment in the gastrointestinal (GI) tract, and the therapeutic effect is also extremely limited by their low permeability across the intestinal epithelium.

In order to provide a successful oral delivery strategy, approaches must be developed to overcome these issues of instability and poor uptake following oral dosing. This chapter gives a brief description of the anatomy of the GI tract, emphasising its characteristics that hinder the administration of biopharmaceuticals. In this respect, strategies based on absorption enhancers, enzyme inhibitors, chemical conjugation, and nano-carriers are discussed. In addition, this chapter describes different transport routes for nano-carriers, including the paracellular pathway, and transcytosis via M cells or absorptive epithelial cells (enterocytes). The approach of modifying nano-carriers with ligands to facilitate their transcytosis is the subject of this thesis.

The specific approach examined in this thesis involves ligand-mediated nano-carrier uptake where the ligand used is a non-toxic version of *Pseudomonas* exotoxin A (ntPE). Finally, the main physicochemical properties of nano-carriers favoured for absorption and transport is discussed.

1.1 Challenges and advantages of oral biopharmaceutical delivery

Biopharmaceuticals (i.e. protein, peptide, or nucleic acid-based agents) are manufactured by using biotechnology or synthetic methods for the purpose of therapeutic or diagnostic applications. In particular, the development and commercialisation of protein-based biopharmaceuticals has changed the direction of healthcare. This area has undergone a boom since two discoveries were reported in the mid-1970s: hybridoma technology for producing large numbers of identical antibodies, and genetic engineering for the large-scale production of proteins (11). The first recombinant protein drug (human insulin) was approved by the US Food and Drug Administration in 1982, and the proportion of biopharmaceuticals on the market has been increasing ever since. By 2016, around 650 protein drugs had been approved worldwide, and over 1300 recombinant pharmaceuticals are under development (12). Biopharmaceuticals have been used for treating different types of cancer, autoimmune diseases, as well as various genetic and metabolic diseases (13, 14). Overall, the annual market for biopharmaceuticals is predicted to reach $386.7 billion by the end of 2019 globally (15).

Compared to conventional small drug molecules, therapeutic proteins offer several distinct advantages: 1) the unique structure and function allows for a highly specific pharmacological effect, thereby, interfering less with normal biological processes (16); 2) since the body produces many of the proteins used as therapeutics, these agents are well tolerated and less immunogenic; 3) the specific structures and effects of proteins enable pharmaceutical companies to gain far-reaching patent protection, providing critical financial benefits for the companies developing them (17).

While recombinant proteins have been used clinically for more than ~35 years, their administration is still restricted largely to the parental route (i.e. intravenous, intramuscular, and subcutaneous injection). Frequent injections might cause reactions at the site of administration, and reduce patient compliance (18). On the other hand, injections also carry the risk of infection resulting from inappropriate use or reuse of needles; there is also a social stigma associated with injecting drugs (19). Delivering biopharmaceuticals via the oral route is a very attractive alternative to parental delivery, but this approach is severely limited by the physical, chemical and biological barriers established by the GI tract.

The oral route presents several advantages over other means of administration, not only because it is the most convenient way of delivering drugs compared to other non-invasive routes (i.e. pulmonary, intranasal, and transdermal), but also has high patient compliance (20). From a more practical perspective, an oral formulation does not require the direct involvement of health

care professionals, which makes it cheaper compared to parenteral administration (21). Further, an oral dosage form must be aseptic, but not sterile in the same way as a parenteral formulation, which saves manufacturing costs (21). Finally, there is a number of biopharmaceuticals that could have improved benefit by oral administration. For example, insulin delivered orally results in its direct targeting to the liver via hepatic portal circulation, replicating its physiological direct targeting to the liver after its release from the pancreatic beta cells. The current form of subcutaneous injection of insulin delivers the dose to the systemic circulation firstly with only a fraction (10 – 20 %) reaching the liver. By better mimicking this physiological route, oral insulin is likely to bring additional advantages on clinical effects, including reducing the risk of hypoglycaemia, weight gain associated with systematic insulin therapy, and reduction of hyperinsulinemia (22).

1.2 Anatomy and physiology of the gastrointestinal tract

The GI tract is composed of the mouth, oesophagus, stomach, small and large intestine; its primary role is to macerate and digest foodstuffs with the goal of nutrient absorption (Figure 1-1). The stomach is a muscular, hollow organ that secretes gastric acid and digestive enzymes to break down substances such as carbohydrates, proteins, and fats. The absorption of these nutrients takes place primarily in the small intestine, which is composed of the duodenum, jejunum, and ileum. The large intestine is mainly responsible for extracting water and salts from solid wastes before the elimination from the body, and working together with resident bacteria to derive nutrients from materials poorly digested in the upper GI tract.

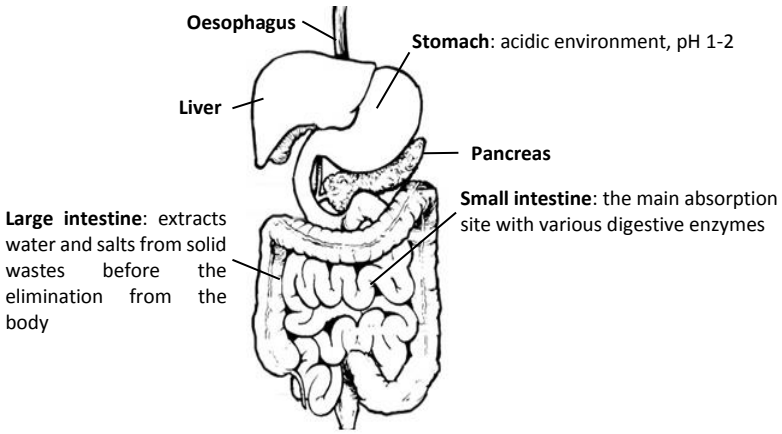

Figure 1-1: Diagram of the human GI tract. The GI tract is an organ system that digests food and absorbs nutrients, as well as expels the remaining waste. It is composed of the mouth, oesophagus, stomach, small intestine and large intestine. The image is modified from (1).

The innermost layer of the GI tract is called the epithelium, which acts as a physical and biological barrier separating the body from the lumen that is contiguous with the external environment. The luminal space is enriched with many digestive enzymes, ingested compounds in various states of degradation, and potentially noxious substances (23). The small intestinal epithelium is responsible for selectively absorbing major nutrients from the lumen as well as for maintaining the homeostatic conditions in the small intestine, while restricting the uptake of unwanted or dangerous materials. Underlying the epithelium is the *lamina propria*; this tissue functions as scaffold, in turn the *lamina propria* is supported by a thin layer of smooth muscle, called the *muscularis mucosa* (23).

Numerous finger-like structures called villi protrude into the lumen (~0.5 – 1.6 mm), which increase the surface area for nutrient absorption by ~30-fold (Figure 1-2) (24). The intestinal villi mainly consist of a monolayer of columnar absorptive epithelial cells (named enterocytes) that are interspersed with goblet cells. Blood and lymphatic vessels (termed lacteals) are connected with the villi, for the purpose of absorbing nutrients from the lumen.

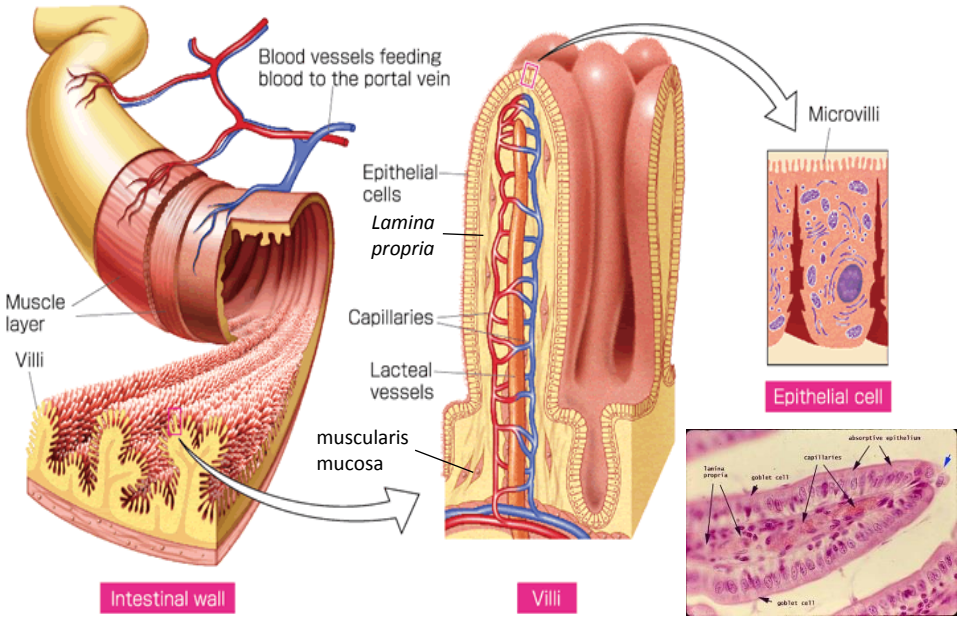

Figure 1-2: Illustration of the small intestine. The innermost layer of the small intestine is the epithelium, and it is supported by a layer of connective tissue named *lamina propria*. Numerous finger-like structures (called villi) extend toward the lumen, and a network of capillaries and lacteal vessels are the routes for the absorbed nutrients to be transported away. Image was modified from (6).

At the base of villi are crypts (Figure 1-3), which contain Paneth cells, stem cells and enteroendocrine cells. Epithelial stem cells are constantly proliferating to renew the epithelial cells in the crypts that then work their way up to the tip of each villus. Paneth cells, named after physiologist Joseph Paneth in the 1880s, secrete anti-bacterial products such as lysozyme and defensins that help to protect the intestinal epithelium from pathogens (25). Enteroendocrine cells are specialised cells for producing gastrointestinal hormones, which function as intercellular messengers for regulation of the nervous-immune responses to specific stimuli (26).

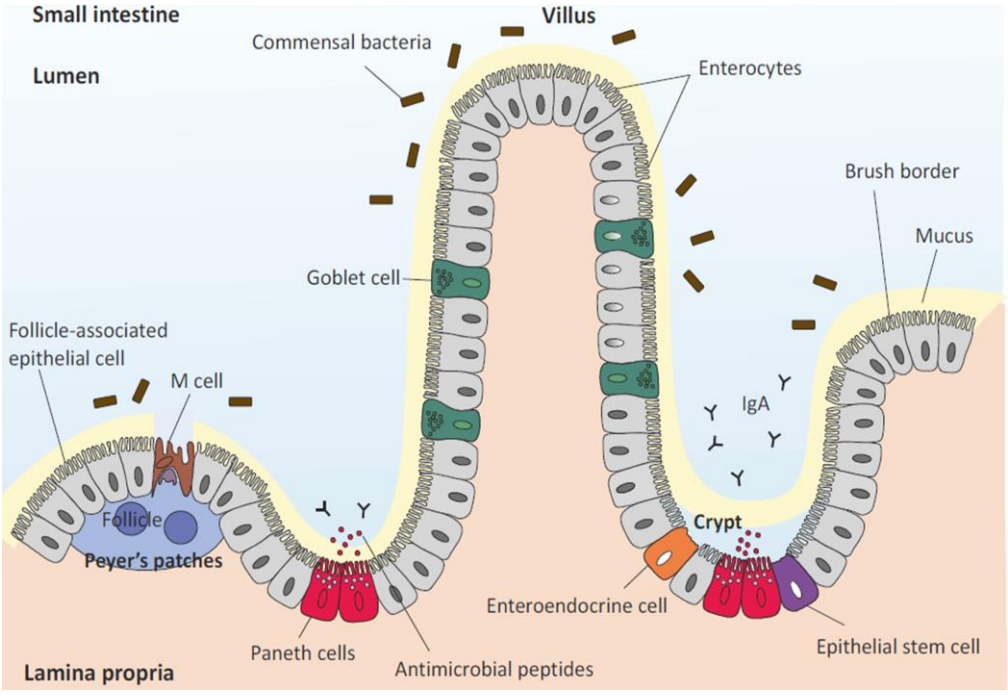

Figure 1-3: Diagram of small intestinal epithelium. The surface of the epithelium is covered by a mucus layer as a protective barrier for the underlying epithelial cells. The folded epithelium, villi, are composed of a single layer of enterocytes interspersed with goblet cells. Paneth cells, entero-endocrine and epithelial stem cells are found in the crypts, which are important for the regulation of the small intestine. Peyer's patches are aggregations of lymphatic tissue, their surfaces are covered by follicle-associated epithelial cells mainly consisting of M (for microfold) cells. Image is from (2) .

Enterocytes are the most abundant cells in the GI tract. These polarised cells are known for their actions in metabolism and nutrient absorption. Each enterocyte has numerous hair-like structures that extend into the lumen known as microvilli (~1 μm by length), expanding the membrane surface available for absorption by 600-fold (27). These cells have an apical-basal polarity; the apical membrane faces the intestinal lumen, and the basolateral membrane is connected to the basement membrane (28). The apical and basolateral membranes are composed of different types of proteins and lipids; sphingolipids and cholesterol are enriched in the apical membrane, while the basolateral membrane is mainly composed of phospholipids (8). Some

enterocytes contain a primary cilium which is a long, thin extension of the plasma membrane (Figure 1-4). The segregation of apical from basolateral plasma membrane is controlled and stabilised by lateral cell-cell adhesion junctions, containing desmosomes, gap junctions, adherens junctions, and tight junctions shown in Figure 1-4.

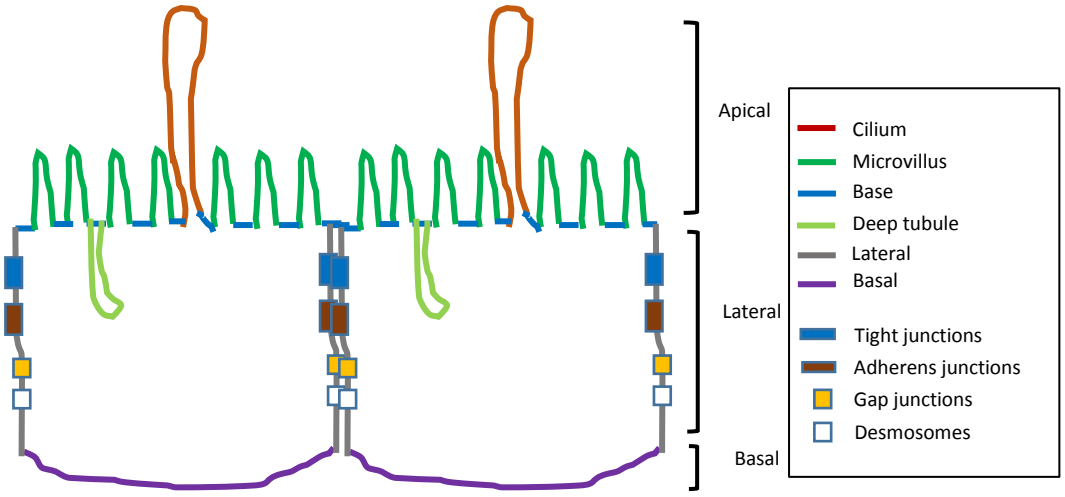

Figure 1-4: Illustration of the polarised enterocytes. Different proteins and lipids are located on the apical and basolateral membranes. This segregation of apical from basolateral membrane is stabilised by the lateral cell-cell adhesion junctions, containing tight junctions, adherens junctions, gap junctions and desmosomes. Image was modified from (8) with the kind permission from Elsevier.

Desmosomes are adhesive intercellular junctions that are critical for maintaining stable cell-cell adhesion (29); gap junctions form cell-to-cell channels that only allow the diffusion of small molecules (< 1 kDa) between adjacent enterocytes. Adherens junctions are cytoskeletal-membrane microdomains located the basal side of tight junctions, which provide adherent strength at cell-cell contacts (8). Tight junctions consist of a network of transmembrane proteins involving claudins, occludin, tricellulin and junctional adhesion molecules. The function of tight junctions is not only preventing the mixing of apical and basolateral membrane components, but also restricting the movement of solutes, ions, and water between adjacent cells via the so-called paracellular route (30). Extracellular domains of occludin can regulate the paracellular permeability between adjacent enterocytes, but the properties of this regulation are dominated by the actions of claudins.

Tight junction proteins can be a target for manipulating the paracellular permeability in order to enhance trans-epithelial drug absorption (31). Claudin proteins constitute a family of 24 transmembrane proteins, of which claudin-2, -4, -7, and -15 are predominantly expressed in the intestinal epithelium (32). Interactions between claudins and ZO proteins are required for the assembly of tight junction structures. ZO-1, ZO-2 and ZO-3 are members of the family of *zona*

occludens proteins, which bind to adherens and tight junction proteins in addition to the actin cytoskeleton (30).

Another type of cell in small intestinal villi is the goblet cell, which functions to produce mucin, a substance used to maintain a hydration layer over the surface of the epithelium and to entrap bacterial and viral pathogens (33). The GI tract also contains gut-associated lymphoid tissue (GALT), which consists of isolated or aggregated lymphoid follicle-associated epithelium (Peyer's patches) (Figure 1-3). M (microfold) cells are located within Peyer's patches. In contrast to enterocytes, M cells lack an extensive mucus layer and display poorly organised and irregular shaped microvilli (34). These specialised cells play an important role in immune surveillance as they internalise antigens from the intestinal lumen via endocytosis, and deliver them to the underlying lymphoid tissue in the *lamina propria* (35).

1.3 Anatomical, biochemical, and physiological barriers

Although the oral route is attractive for delivering biopharmaceuticals, there are still challenges to overcome for efficient delivery of therapeutic proteins: 1) the harsh environment in the GI tract; 2) the defensive mucus layer; and 3) the low permeability of intact proteins across the epithelium.

Acidic and enzymatic environment in the GI tract

The acidic environment (pH ~1 – 2) in the stomach alters the ionisation state of amino acids, which acts to unfold proteins through the disruption of interactions involved in secondary or tertiary structures (36). Additionally, such acidity can also break some peptide bonds (37). All of these effects could cause a loss of specific structure and function for a biopharmaceutical. In general, four categories of digestive enzymes are present in the GI tract: lipases, proteases, amylases, and nucleases, which are responsible for breaking down fats, proteins/peptides, carbohydrates, and nucleic acids, respectively. Exposure of therapeutic proteins to proteases, such as trypsin and chymotrypsin released from the pancreas into the duodenum, may lead to the hydrolysis of peptide bonds or the chemical modification of the functional groups, for example, oxidation and de-phosphorylation. All these biochemical reactions will denature or degrade proteins, which may change their pharmacological effects (38).

The Mucus layer

Mucus is a viscous material that is adherent to the surface of the intestinal epithelium. It is composed predominantly of secretions released from specialised goblet cells. Mucus is a complex hydrogel composed of proteins, carbohydrates, lipids, salts, antibodies, bacteria, and cellular debris; but the main protein component of mucus is the glycoprotein mucin that is viscous and has elastic gel-like properties (39). Mucus is responsible for lubricating the GI tract to assist the passage of substances as well as providing a barrier to protect the epithelium from pathogens and noxious substances (40). At the apical surface is the glycocalyx; membrane-bound mucins (MUC) entangle and cross-link with other molecules, such as glycolipids and glycoproteins, to form an adherent ~500 µm thick coating layer between the cells and loosely held mucus (33). Specifically, MUC 3 is expressed in the apical membrane of enterocytes and goblet cells as part of this process to produce extended rod-like structures, that form a component (200 – 1500 nm) of the glycocalyx (41). Frey *et al.* (1996) showed the glycocalyx is a size-selective barrier with a functional pore size of 7.4 – 28.8 nm (42). There is constant turnover of the adherent layer and the glycocalyx to remove the potentially damaging compounds on the lumen surface (43).

Low permeability across the epithelium

A greater challenge than these two hurdles of harsh environment and mucus layer is the low permeability of crossing the intestinal epithelium. The size of most therapeutic proteins ranges from ~3.5 kDa (calcitonin) to ~150 kDa (monoclonal antibodies), all being too large and too hydrophilic to readily diffuse across enterocytes driven by the concentration gradient in a manner similar to many small molecule drugs; this transcellular pathway is size-dependent (< 700 Da) (44, 45) and a minimum level of lipophilicity is needed for molecules to partition into the cell membrane, and to be transported across the cell (46). Molecules with a lower degree of lipophilicity can travel across the epithelium via the paracellular pathway, meaning via the intercellular spaces between two adjacent cells. Unfortunately, this pathway is restricted to relatively small compounds (< 3.5 kDa), which is not applicable for most therapeutic proteins (9).

The low permeability of therapeutic proteins has direct impact on their bioavailability and thus limits their pharmacological effects (20). That is to say, even when the biopharmaceutical is extensively protected from the harsh environment in the GI tract, less than 1 % of therapeutic protein can reach the systemic circulation.

1.4 Overcoming these barriers

Based on the anatomy of the GI tract and challenges of transporting therapeutic proteins via the oral route, various attempts have been made to improve the bioavailability of therapeutic proteins over the years. These approaches have attempted to overcome one or more of the barriers to oral protein delivery listed above.

Enzyme inhibitors

Co-administration of protein drugs with protease inhibitors, such as aprotinin (an inhibitor of trypsin and chymotrypsin), soybean trypsin inhibitor, and FK-448 (a chymotrypsin inhibitor), has shown increased permeability of proteins (47). The choice of protease inhibitor depends on the structure of delivered protein and its specificity towards the enzyme. For example, Yamamoto *et al.* (1994) showed significant hypoglycaemic effect following large intestinal co-administration of insulin with Na-glycocholate, camostat mesilate and bacitracin, while marginally enhanced insulin absorption was observed following co-administration with soybean trypsin inhibitor and to a moderate degree for aprotinin (48). In addition, the cocktail of enzymes present in different segments of the GI tract is different, which would make the choice of enzyme inhibitors more difficult. Furthermore, due to the potential denaturation of enzyme inhibitor itself in the gut, excessive amount of inhibitor is required. If a long-term treatment is considered, normal protein digestion might be affected (18).

Some mucoadhesive polymers are promising candidates as enzyme inhibitors. Hutton *et al.* (1990) firstly reported the inhibitor properties of polyacrylate on intestinal proteases (49). Lueßen *et al*. (1995) proposed that the inhibitor effect of polyacrylate derivatives is due to the formation of complexation with divalent cation ions (calcium ions), so that the ion-dependent enzymatic effects are prevented (50). Although these polymers are generally regarded as safe, protective effects on the polymer-embedded proteins might not be sufficient (47).

Absorption enhancers

Absorption enhancers are substances that can promote the absorption of a poorly absorbed drug across the intestinal epithelium. Various mechanism(s) of absorption enhancers have been proposed: 1) disrupting the structural integrity of the cell membrane temporarily to make it more permeable for drug transport (51); 2) increasing the retention time on the mucus layer; 3) opening

tight junctions to utilise the paracellular pathway (this will be discussed in detail at section 1.5.1) (52).

Some absorption enhancers result in enhanced permeability not only by one mechanism. For example, the cationic polymer chitosan has the combined effects of mucoadhesion and reversibly opening tight junction structures; and carbopol and polyacrylate derivatives can inhibit enzymatic activities as well as opening tight junctions through the removal of extracellular calcium ions (53, 54). Recently, bile acid/salt derivatives have attracted considerable interest as absorption enhancers. Mournir *et al.* (2002) demonstrated that co-administration of insulin with bile acid/salt derivatives (such as deoxycholate and cholate) led to a hypoglycaemic effect in rabbits. Perhaps, bile salts were masking the hydrophilic protein surface via micelle formation (55, 56). It has been suggested that the apical sodium-dependent bile salt transporter in the ileum can be targeted for enhancing oral absorption of macromolecules physically complexed with bile acid/salt derivatives (56). It is important to note that this pathway is used for the reabsorption of bile acid from the proximal and distal ileum back to the liver.

Since absorption enhancers have the potential to reduce the barrier function of the intestinal epithelium, toxicological effects clearly need to be evaluated. Taking into consideration the physiological environment in the small intestine, it appears difficult to control and maintain the enhancer concentration sufficiently well to use this strategy; these enhancers would be dispersed and diluted in varied volumes of intestinal fluid (57).

Chemical modification of proteins

Some absorption enhancers described above can also be conjugated to proteins, for example, DOCA (deoxycholic acid) was conjugated with heparin to target ASBT (58). Attempts have been made to chemically conjugate proteins with functional groups in order to improve their lipophilicity, and thereby to enhance their uptake. Hashizume *et al.* (1992) demonstrated that conjugation of insulin with fatty acids (palmitic acid) not only increased the lipophilicity of insulin but also reduced its degradation (59). The oral insulin product hexyl-insulin monoconjugate 2 (HIM2) has demonstrated efficacy in both type I and type II diabetics, HIM2 contains recombinant human insulin covalently modified with a single amphiphilic oligomer (60, 61). However, this strategy has not resulted in any marketed product to date.

Ideally, functional groups (conjugation groups) would detach or cleave from the delivered protein before its arrival in the systemic circulation, so that the structure and efficacy of protein would remain the same. Otherwise, the conjugated protein would be considered to be a new drug, requiring thorough safety and toxicology data for a regulatory filing. Thus, the conjugation effects

on pharmacokinetics and other pharmacological activities of such delivered proteins must be considered carefully (9).

Novel carrier systems

Numerous carriers have been exploited for oral protein delivery, such as microspheres, liposomes, emulsions, and nanoparticles (NPs). All of these systems have the potential to increase the bioavailability of a protein loaded into them, but each also has unique challenges to overcome before being developed into an efficient delivery system. For example, the physiochemical stability of emulsions is one critical drawback for this strategy (21).

Advantages of nanoparticles

The formulation strategy discussed herein involves using nano-carriers. The concept of pharmaceutical NPs was first introduced by Peter Speiser (1960s) (62). Mohanraj and Chen (2006) listed several advantages of developing NPs as a drug delivery system in general for oral, nasal, and parenteral administrations: 1) they have relatively high drug loading, 2) normally no chemical reaction is required for the encapsulation of drugs, this is important for preserving the bioactivity of fragile drugs; 3) they can achieve site-specific targeting so as to increase therapeutic effects of the drugs and reduce the unintended side effects; 4) the release properties of an entrapped drug can theoretically be controlled during the transportation or at the site of localisation; and 5) their size, charge and other characteristics can be manipulated to achieve both active or passive drug targeting after various routes of administrations (63).

Another potential advantage, specific to the oral route, is that NPs have a high surface area per mass, allowing increased contact with the epithelia and therefore more chance of uptake, and studies have shown the increased bioavailability of NPs (64). In addition, the architecture of the NPs can protect the loaded proteins from the enzymatic or acid environment (65).

Biodegradable polymeric nanoparticles

Biodegradable polymers are materials that can break down naturally either by inherent instability or through the action of enzymes (66). The first record of biodegradable polymer in medicine is the catgut suture (made from sheep intestine), dating back to at least 100 AD (67). Although the first industrialisation of a synthetic polymer was started in the 1910s by Baekeland, the concept of synthetic biodegradable polymer was not introduced until the 1980s (68). Since

then, biodegradable polymers have innumerable uses in the biomedical field, particularly in tissue engineering and drug delivery (69).

Various biodegradable polymers have been emerging for the preparation of NPs, such as PLA (polylactic acid), PLG (polyglycolic acid), PLGA (poly (lactic-co-glycolic acid)), PEG (polyethylene glycol), and PCL (polycaprolactone). Four methods are commonly used for the preparation of NPs from these polymers, their advantages and disadvantages are listed in Table 1-1 (70).

Table 1-1: Different preparation methods using biodegradable polymers.

Method	Advantages	Disadvantages
Solvent evaporation (69)	Ease of performing on a laboratory-scale	1) High energy required for homogenous NPs, this can damage protein structure; and 2) is limited to amphiphilic or hydrophobic polymers
Nanoprecipitation (70)	1) No need of high energy or high pressure devices, such as homogenisation or ultra-sonication	1) Organic solvent choice is limited to water miscible; 2) the encapsulated drug is also limited to one that can dissolve in this type of solvent; 3) total removal of organic solvent can be an issue
Salting out (71)	1) No need of high energy or high pressure devices; 2) high yields of drugs; and 3) it is easy for scaling up	1) Limited to hydrophobic drugs; 2) special requirements for salting-out agents and soluble stabilisers; and 3) issues related to recycling salts used in large quantities
Emulsion diffusion (72)	1) Use of pharmaceutically acceptable organic solvents; 2) no need of homogenisation steps; 3) high yields generally obtained; 4) high batch-to-batch reproducibility; and 5) ease of scale-up	1) High volume of water is required; and 2) the potential leakage of water-soluble drugs into the saturated-aqueous external phase during the diffusion

1.5 Epithelial transport of biodegradable polymeric nanoparticles

Biopharmaceuticals can be protected from the harsh environment in the GI tract, by using enteric coating (71). Therefore, the low permeability across the intestinal epithelium remains as the main challenge for efficient delivery via the oral route. Three theoretical pathways have been utilised for transporting NPs across the epithelium.

1.5.1 The paracellular pathway

The paracellular space is the intercellular space between two adjacent enterocytes, this channel is mainly controlled by the tight junctions that only allow the passage of compounds < 3.5 kDa (72). Regulating the tight junction is one strategy to allow NPs to cross via the paracellular route.

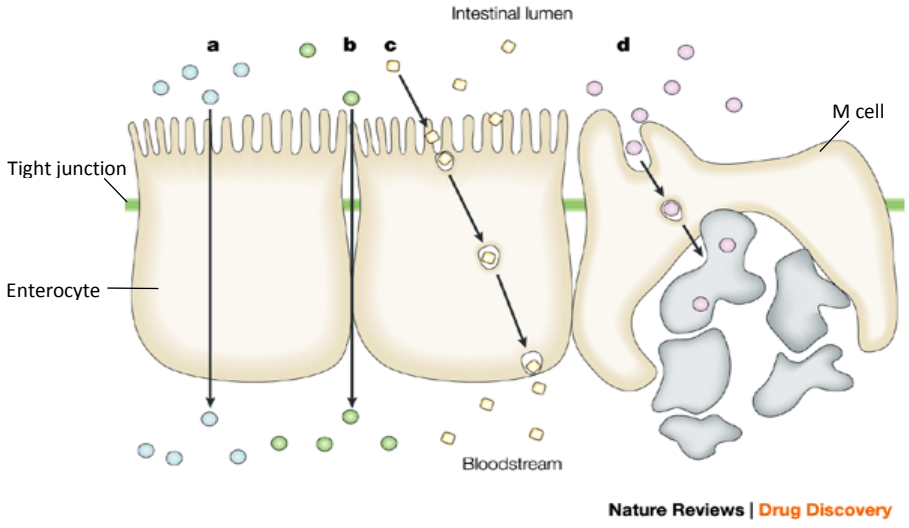

Figure 1-5: Diagram of different transport routes across the intestinal epithelium. (a) Transcellular pathway: small molecules (<700Da) can transport passively or actively through this route; (b) paracellular pathway: extracellular transport between two adjacent enterocytes under the regulation of tight junctions; (c) transcytosis across the enterocytes: travel across the enterocyte involving forming transport vesicles; (d) vesicle-based transcytosis across the M cell: being taken up by M cell and transport into the immune cells under the epithelium. Image was modified from (9) with permission from Nature Publish Group.

Some absorption enhancers (anionic polymers and bile acids) mentioned earlier have been used to open tight junction structures by removal of extracellular calcium ions, which are important in the maintenance of tight junction integrity. For example, Chuang *et al.* (2013) demonstrated a reversible tight junction opening in the Caco-2 cell line after treatment with EGTA (ethylene glycol tetraacetic acid)-conjugated NPs (73). Chitosan-based NPs are another widely studied system, which have shown the ability to reversibly open tight junction structures. Lin *et*

al. (2007) showed that insulin-loaded NPs, prepared by chitosan and poly (γ-glutamic acid), reduced the blood glucose level more effectively compared to an oral insulin solution (74). This group (2011) also demonstrated that chitosan-induced tight junction opening is linked to changes in claudin-4, an important protein for tight junction integrity of polarised epithelial cells. The interaction between claudin-4 and chitosan leads to the redistribution of claudin-4 from the cell membrane to lysosomal degradation and an increased paracellular permeability (75).

It is important to note that the paracellular space regulated by tight junctions comprises only ~0.01 % of the total absorptive surface area of the GI tract (76). Opening tight junctions also carries the risk of introducing unintended substances into the body (77). Thus, altering tight junctions to enhance the uptake of a biopharmaceutical is not without difficulty.

1.5.2 Transcytosis across M cells

Transcytosis involves particles being taken up into the cell via endocytosis from the apical membrane, being transported through the cell in endosomal vesicles and released from the basolateral side (77).

M cells present in Peyer's patches have less organised microvilli, and are also less protected by the mucus layer compared to the rest of the intestinal epithelium (33). Optimal NP characteristics for targeting the Peyer's patches, in terms of size, hydrophobicity and surface charge, have been studied. It is generally agreed that particles less than 1 μm in diameter can be taken up by M cells. Besides size, Eldridge *et al.* (1990) showed that hydrophobic NPs were taken up by Peyer's patch more efficiently than less hydrophobic ones (78).

M cells can take up NPs mainly via phagocytosis and pinocytosis (79). Recent studies by Yin *et al*. (2009) and Camile *et al.* (2011) demonstrated enhanced drug (loaded into NPs) absorption was mainly due to uptake by M cells (80, 81). Nevertheless, the importance of M cells might have been over-emphasised as Hussain *et* al. (1997) pointed out, considering they only make up ~1 % of the total intestine surface (77, 82). Fievez *et al.* (2009) suggested that M cells might be a target for oral vaccination, as they are specialised cells for transporting antigens from the lumen to immune cells residing in the *lamina propria* (83).

1.5.3 Transcytosis across enterocytes

Transcytosis across enterocytes appears to provide a route for NPs transporting across the epithelium, since they are the most abundant cells in the epithelium and have an extensive surface area available for absorption. A specific transport route is required for an efficient delivery of NPs, as passive diffusion only applies to small molecules. In this regard, several studies have attached NPs to transport ligands, such as Vitamin B_{12} ($VitB_{12}$), lectin, IgG (immunoglobulin), and transferrin (Tf), with the intention of using these ligands to facilitate the trans-epithelial transport of NPs.

Vitamin B_{12}

$VitB_{12}$ is a hydrophilic molecule that cannot be absorbed via simple or facilitated diffusion like other small molecules. After $VitB_{12}$ is released from food, it forms a complex with haptocorrin (HC) (Figure 1-6), which protects $VitB_{12}$ from degradation in the acidic environment of the stomach. The $VitB_{12}$-HC complex travels to the small intestine, where the HC is degraded by the action of trypsin and chymotrypsin. Intrinsic factor (IF), produced in the stomach, then forms a complex with $VitB_{12}$, and this complex is recognised by the intrinsic factor receptor (IFR) at the apical surface of enterocytes. This $VitB_{12}$-IF-IFR complex is then internalised via a receptor-mediated endocytosis, with $VitB_{12}$ being transported across the enterocyte through a process that involves transcobalamin II (TCII) binding to $VitB_{12}$ once IF is released (84).

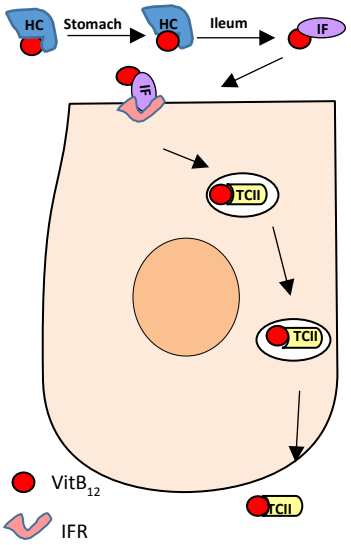

Figure 1-6: Diagram of $VitB_{12}$ transcytosis across the enterocyte. $VitB_{12}$ is complexed to HC, which is believed to protect $VitB_{12}$ from degradation in the acidic environment of the stomach. The $VitB_{12}$-HC travels to the small intestine where IF binds to $VitB_{12}$ after the degradation of HC. $VitB_{12}$-IF is internalised by the enterocyte and $VitB_{12}$ is transported to the basolateral membrane after binding with TCII after the IF is released.

$VitB_{12}$ has been used as a ligand to facilitate the transport of NPs across the epithelium. Chalasani *et al.* (2007) showed a reduction of blood glucose levels in rats when insulin was loaded in $VitB_{12}$ conjugated-NPs that was much greater than comparing to NPs without the conjugation with $VitB_{12}$ (85). More recently, Fowler *et al.* (2013) investigated the mechanism of uptake and transport of NPs mediated by $VitB_{12}$ in airway epithelial cells. NP uptake was reduced when filipin and chlorpromazine were added, suggesting that caveolae-mediated and clathrin-mediated endocytosis might be involved in the uptake (86). Using the $VitB_{12}$-mediated pathway is not without disadvantage, since $VitB_{12}$ has a minimal oral uptake capacity (1-2 µg), which might limit its applications (87).

Lectin

Lectins are plant proteins that can recognise glycosylated protein and lipid on most of the cell surface. The concept of using lectins for GI target delivery was first proposed by Woodley in 1988, bioadhesion of tomato lectin was shown to slow down the intestinal transit of oral drugs and increase their bioavailability (88). The bioadhesion of lectin-conjugated NPs was also tested in gastric pig mucin, an *ex vivo* model based on rat intestinal mucosa, and also in a Caco-2 cell line (89-91). Hussain *et al.* (1997) demonstrated the total systemic circulation of lectin-conjugated NPs reached 23 % compared to < 0.5 % uptake of the same NPs with a lectin inhibitor (N-acetylchiototraose), and the majority of them were considered to be taken up via non-lymphoid tissue. Tissue analysis revealed that 12 % of the NPs were associated with the intestine (enterocytes) as compared to < 1 % associated with the Peyer's patches (82).

Wheat germ agglutinin (WGA) is another commonly studied lectin, which binds to N-acetyl-D-glucosamine and sialic acid found at the luminal surface of both M cells and intestinal epithelial cells (92). Russell-Jones *et al.* (1999) showed significant uptake and transport of WGA-conjugated NPs (80 %) compared to unmodified NPs (10 %) when tested in Caco-2 cell monolayers (91). The uptake of WGA-conjugated NPs was reduced when other lectins were used, but not with the addition of bovine serum albumin; the uptake and transport mechanisms,

however, are unknown. Yin *et al.* (2006, 2007) encapsulated an immunomodulating peptide (thymopentin) into WGA-conjugated NPs, and reported a ~2-fold increase in the ratio of $CD4^+/CD8^+$ T cell populations in immunosuppressed rats as compared to unconjugated NPs (93). Interestingly, orally administered WGA-conjugated NPs had similar effects as thymopentin solution administered by intravenous injection in these studies. In a subsequent study, systemic uptake of these NPs was reported to be as high as 6 – 13% of dose at 1 day and 7 – 15 % at 7 days, comparing to ~4.8 % at 1 day and ~4.9 % at 7 days for the unconjugated ones (94). Ensign *et al*. (2013) suggested that the high overall systemic uptake of both conjugated and unconjugated NPs could have been due to large gavage volumes in these two studies, but the specific volume was not stated (33). Overall, lectin-mediated NPs have advantages for delivering vaccines, as they could elicit an immune response (95).

IgG

Another pathway that transports a macromolecule is the transcytosis of IgG, which is a process that involves the specific binding of this class of antibodies to a specific membrane receptor known as the neonatal Fc receptor (FcRn). As suggested from the name, FcRn binds IgG antibodies via their faction crystallisable (Fc) domain at the apical enterocyte surface. Human FcRn was initially discovered in the placenta where it transports IgG from mother to foetus, and later on, it was detected in the epithelial cells present in the lung and the intestine of an adult (96). Dickinson *et al*. (1999) showed *in vitro* that FcRn is the receptor for transporting IgG across human intestinal epithelial cells (97). As shown in Figure 1-7, IgG can be internalised by binding to FcRn at the apical surface of epithelial cell, undertaking transcytosis involving vesicles that are trafficked to the basolateral side of the enterocyte where the IgG molecule is released (98).

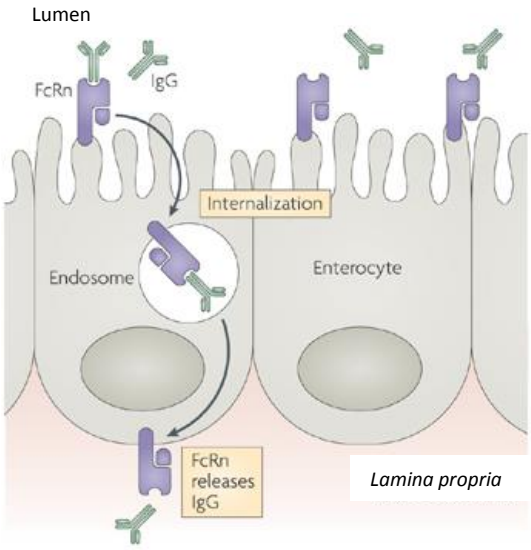

Figure 1-7: Diagram of the transcytosis of IgG across the enterocyte. IgG firstly binds to FcRn on the apical membrane of the enterocyte, and then IgG travels across the enterocyte via a transport vesicle involving FcRn. The image was modified and reused with the permission from Nature Publish Group (5).

The concept of using Fc as a transport ligand was tested by Low *et al.* (2005) using the oral administration of FSH (follicle-stimulating hormone) fused with Fc in rats; ~2-fold greater stimulation of ovarian weight compared to the equimolar dose of FSH was reported (96). In

addition, Fc-mediated NP transcytosis was tested using polarised monolayers of an airway epithelial cell line, Calu-3, by Vllasaliu *et al.* (2012). Comparing Fc-coated NPs to unmodified NPs showed increased uptake and transport that was reduced with the presence of additional Fc (99). Pridgen *et al.* (2013) encapsulated insulin into Fc-conjugated PLGA NPs, and demonstrated ~13.7 % absorption of IgG-conjugated NPs, compared to ~1.2 % for unmodified NPs. Furthermore, IgG-decorated NPs showed distinct effects on blood glucose compared to unmodified NPs, and this effect was reduced with the extra addition of IgG, suggesting the transport of these Fc-NPs involved interactions with the FcRn (100).

Transferrin

Transferrin (Tf), is an iron-transporting glycoprotein that has been used to facilitate nano-carrier transport across the blood brain barrier and the GI epithelium, since the Tf receptors (TfR) are highly expressed on both of these two barriers (101). Tf binds two ferric (Fe^{3+}) ions to form the holo-Tf, resulting in a conformational change favourable for binding to TfR at the cell membrane. In non-polarised cells, holo-Tf is internalised and, once reaching an acidic vesicular compartment Fe^{3+} ions are discharged from the Tf protein to help supply cells with this essential ion.

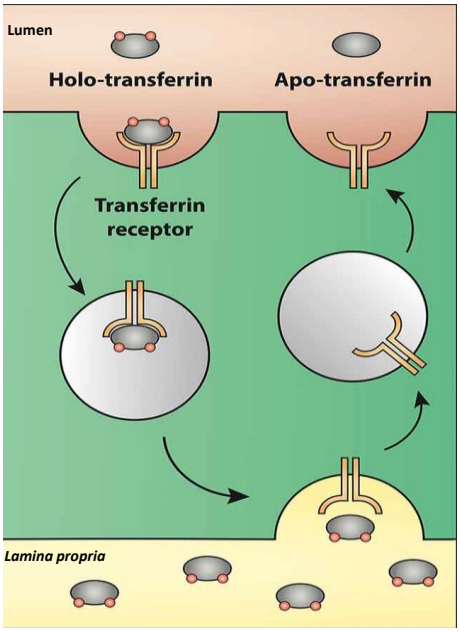

Figure 1-8: Presumed transport route of ions across the enterocyte. Tf binds to two ions (Fe^{3+}) to form holo-Tf, which is internalised into the cell via a receptor-mediated endocytosis and translocated to the basolateral membrane. This image is modified and reused with the permission of Frontier Media S.A(7).

However, for polarised cells, holo-Tf is believed to transport Fe^{3+} in vesicles that traffic across the cell to reach the basolateral membrane; the exact transport mechanism is not elucidated (102). TfR is expressed in both apical and basolateral sides of the polarised epithelial cells, while the majority of these receptors are localised at the basolateral membrane of the intestinal epithelial cells (103).

Xia *el al.* (2000) demonstrated that a Tf-insulin conjugate exhibited a slow but prolonged hypoglycaemic effect in streptozotocin-induced diabetic rats (104). The same group (2005) showed that an oligomeric Tf-conjugate had ~2-fold higher intracellular retention in Caco-2 cells than a monomeric Tf-conjugate; an *in vivo* study in rats showed the same trend (105). A full understanding of the Tf-mediated transport mechanism, however, is required for the safe use of this approach for chronic application.

Bacterial toxins

Bacterial toxins have been examined for their ability to transport across intestinal epithelia. Several of these proteins secreted from a variety of bacteria are able to travel across the mucus epithelial barrier and target underlying immune cells. Examples of these toxins and the bacteria they are derived from include, shiga toxin from *Shigella sp.*, cholera toxin from *Vibrio cholera*, and cytolethal distending toxins from *Salmonella typhi*. These toxins exist as A-B_n subunit molecules, where the subunit A is the active/toxic component to kill the cell by various means, while the subunit(s) B appears responsible for internalisation and translocation of subunit A (106).

Cholera toxin B (CTB) has been used to form a fusion protein with lumbrokinase (LK), which is used for the treatment of vascular thrombus. According to *in vivo* studies in rats and mice, the fusion protein CTB-LK exhibited distinct anti-thrombotic effects compared to the oral administration of LK alone (107). Salman *et al*. (2005) decorated NPs with flagella-enriched *Salmonella* extract, in order to increase the adhesion of these NPs to rat GI epithelium. NPs were found in enterocytes and Peyer's patches 2 h after oral administration, and the coated NPs exhibited competitive binding to Peyer's patches with *Salmonella*. More studies are needed to determine the uptake and transport process of *Salmonella* flagella prior to using this ligand in an oral delivery strategy (108). In terms of the systemic effect of NPs coated by bacterial toxins, Hussain *et al.* (1998) demonstrated that 13 % of NPs conjugated with invasin C192 (from *Yersina pseudotuberculosis*) were detected in the systemic circulation, compared to 2 % of the unmodified NPs after the oral administration (109).

1.6 Bacterial toxin-mediated transcytosis

Toxin-conjugated NPs may be useful for delivery of biopharmaceuticals across the intestinal epithelium where the NPs can be loaded with biopharmaceuticals. To achieve this goal, characteristics of NPs capable of loading a biopharmaceutical must be optimised in favour of uptake and transcytosis.

1.6.1 Transport ligand

Pseudomonas exotoxin A (PE) is a virulence factor secreted by *Pseudomonas aeruginosa*, belonging to the family of A-B toxins as mentioned earlier in the section 1.5.3. Subunit A is composed of domain I and II, and subunit B consists of domain III (Figure 1-9) with diphtheria toxin being the first and best known protein of this toxin family. Most studies for this A-B family of proteins have focused on their intoxication of non-polarised cells. For PE, domain Ia (residues 1-252) binds to LRP-1 (low-density lipoprotein receptor-related protein, also known as CD91) on the surface of the host cell. Once bound, a PE molecule is internalised via a clathrin-mediated endocytosis. After cleavage by the protease furin, domain II (amino acids 253-364) participates

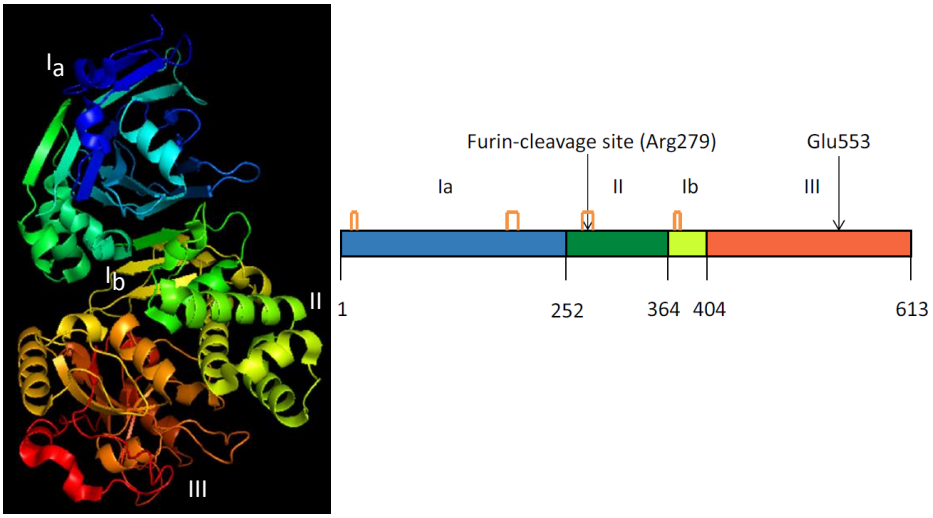

Figure 1-9: Diagram for the structure of PE. The protein is composed of domain Ia (1-252) responsible for cell recognition and receptor binding (blue); domain II (253-364) functions for protein translocation and contains furin-cleavage site for toxin activation (green); domain Ib (364-404) (yellow) and domain III (405-613), which contains the active component (red).

in translocation of domains Ib (amino acids 365-404) and III (amino acids 405-613) of the protein into the cytosol through a vesicle trafficking process that avoids the lysosomal pathway. Once in

the cytoplasm, domain III functions enzymatically to kill the cell by inhibiting protein synthesis through ADP ribosylation of elongation factor 2 (110).

The trafficking pathway used by PE in non-polarised cells is well characterised. Following the internalisation by a receptor-mediated endocytosis, PE travels to the early endosome (EE), where the protein undergoes a conformational change in the decreased pH, so that a furin cleavage site can be cut for toxin activation (111, 112). Once in the EE, PE has been reported to utilise several pathways to reach the cytosol. One pathway is mediated by the KDEL-receptor, where the toxin is driven to the late endosomes (LE) in a Rab9/Arf1-dependent pathway and transported to the *trans* Golgi network (TGN) where a C-terminal REDL motif binds to the KDEL receptor, which facilitates its transport to the endoplasmic reticulum (ER) in a retrograde manner (113). An alternative pathway involves PE trafficking directly from the EE to the TGN and ER via a Rab-6 controlled lipid-dependent sorting pathway (114). The intracellular pathways of PE appear to be cell-dependent, as Chaudhary *et al*. (1990) demonstrated PE trafficking in Swiss mouse 3T3 cells is fully dependent on the Rab-9-mediated pathway and the presence of the REDL sequence, while Smith *et al.*(2006) reported that PE can use either pathway to reach the ER in HeLa cells (114, 115).

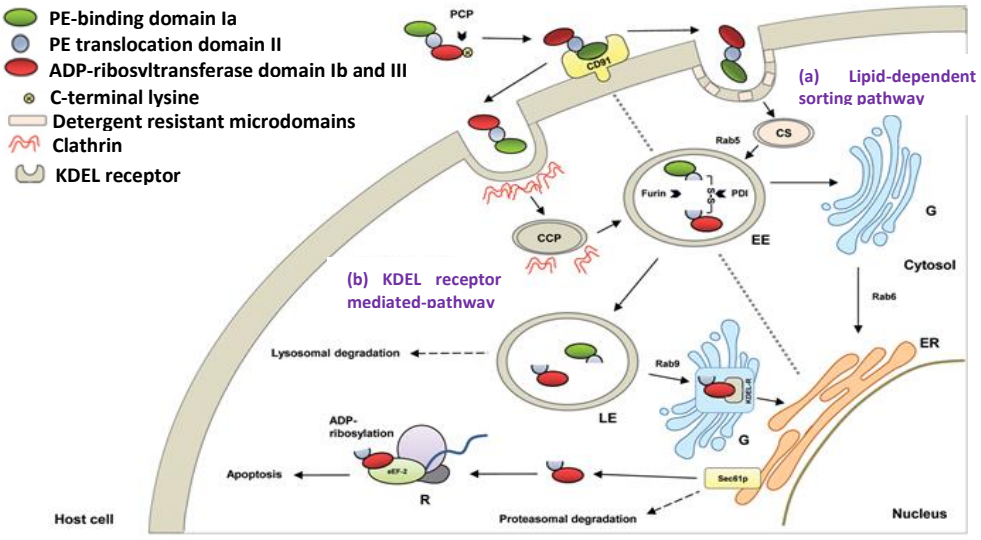

Figure 1-10: Potential cellular pathways of PE in the non-polarised cell. PE is internalised into clathrin-coated vesicle following recognition by its receptor (CD91) on the cell surface. PE is then cleaved by furin at a site in domain II while the two fragments are still linked via a disulphide bond in the EE. Once in the EE, PE has the potential to utilise two possible pathways to reach the cytosol: (a) lipid-dependent sorting pathway, where PE travels directly from the EE to the TGN and ER or (b) PE transports to the TGN network, where it interacts with KDEL-receptor and travels to the ER in a retrograde manner. In the cytosol, domain III of PE inhibits protein synthesis through ADP ribosylation of elongation factor 2. Image is modified and reused with the permission from Frontiers Media SA (10).

Based on this understanding of the PE intoxication pathway, this protein has been constructed as recombinant immunotoxin (Figure 1-11), in which the receptor-binding domain of the toxin (domain I) has been replaced by a cell-specific ligand to enhance its targeting for more directed cell killing (110). Recombinant immunotoxins based on PE have been widely studied as an approach for cancer treatment. For example, the domain I of PE has been replaced by a Fv fragment which targets CD22 on B cell malignancies, and monoclonal antibody K1 has also been fused to truncated PE for targeting mesothelin, which is overexpressed on mesothelioma and ovarian cancer cells (116, 117); both of these two immunotoxins have reached clinical trial.

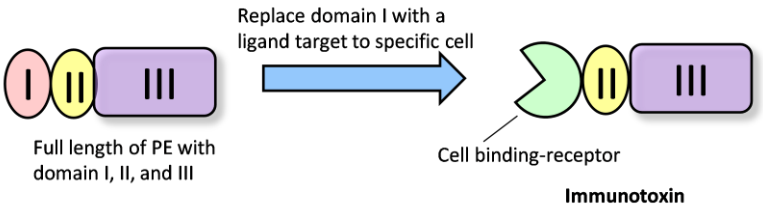

Figure 1-11: The diagram of immunotoxin based on PE. Immunotoxin is a recombinant protein, in which domain I has been replaced by another cell-binding ligand for the specific cell killing effect.

The rationale of using PE as a trans-epithelial ligand is based on the fact that for this exotoxin to reach the non-polarised, antigen-presenting cells in the submucosa, it must first translocate across the polarised epithelium such as that present in the airway and intestinal epithelium (118). Importantly, the cytotoxicity can be completely lost by the deletion of a glutamic acid at the position 553; this non-toxic version of PE (ntPE) becomes applicable to facilitate the transport of NPs (119).

Mohammed *et al.* (2012) replaced the catalytic domain of PE (domain III) with a therapeutic protein and fused a cell-penetrating peptide onto the N-terminus of domain II to facilitate the cytosolic delivery of cargo protein (120). Recently, Carter (2014) showed that PE can deliver siRNA across polarised intestinal epithelial cells and also delivered the cargo to elicit knockdown effect in the macrophages present in the basolateral compartment below the cell monolayer (121). The strategy utilised in this work conjugated ntPE to NPs to enhance their trans-epithelial transport. The conjugation strategy to connect ntPE to NPs was achieved by inserting a tobacco etch virus (TEV) protease-specific sequence into the plasmid, which allows for introduction of a single free thiol group available for chemical coupling.

1.6.2 Methods for the preparation of mucoadhesive nanoparticles

The concept of mucoadhesion as an approach to improve drug targeting and absorption was first introduced in the early 1980s (122). These mucoadhesive materials/polymers can interact with mucus by means of electrostatic interaction and hydrogen bonds (123). There are many widely used mucoadhesive polymers, such as cellulose derivatives, polyacrylates, chitosan, pectin, alginate, and starch.

Alginate is a water-soluble anionic polysaccharide produced by brown algae and bacteria. It has been widely used in food and pharmaceutical areas, due to its biodegradability and high biocompatibility. Structurally, it consists of α-L-guluronic acid (G) and β-D-mannuronic acid (M) residues, linearly linked by 1, 4-glycosidic linkages. Alginate gelation is mainly achieved by exchanging Na^+ in the guluronic acid with Ca^{2+}, which results in stacking the guluronic groups to form the characteristic "egg-box" structure (Figure 1-12). The ease of gelation has broadened applications of alginate in tissue engineering, wound healing, and drug delivery. The first report of alginate-based NPs was from Rajaonarivony *et al.* (1993), the prepared NPs were in the size range of 250 – 850 nm in diameter (124). In addition, from a manufacturing perspective, alginate has an abundant supply and is relatively inexpensive.

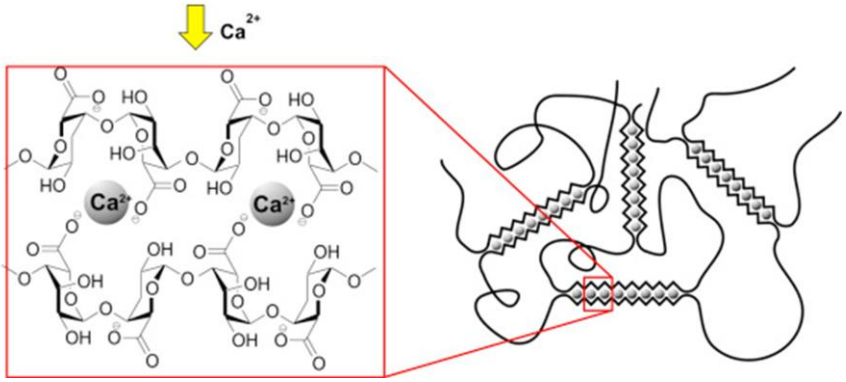

Figure 1-12: Diagram for the alginate-Ca^{2+} complex. Ca^{2+} ionically cross-links with the guluronic acid of alginate and form an "egg-box" structure. Image is reused with the permission from Elsevier (3).

Chitosan shares similar advantages attributed to alginate, also being relatively inexpensive, biodegradable, and having abundant supply from natural sources. This cationic polymer is produced by deacetylation of chitin, which results in randomly distributed β-(1-4)-linked D-glucosamine (deacetylated unit) and N-acetyl-D-glucosamine (acetylated unit). The positively charged amine groups in chitosan are believed to interact with the negatively charged proteins in

the mucus layer (125). Chitosan-based NPs have been widely investigated using *in vitro* and *in vivo* models, and some chemical modifications on chitosan have been also carried out, with the intention of increasing its retention time with mucus and enhancing its capability to affect tight junction function (126-128).

These two biopolymers, alginate and chitosan, are generally regarded as safe, mucoadhesive, abundantly available, and relatively inexpensive, providing the rationale for their selection in NP preparation in the present studies. Preparation methods based on these two biopolymers are different from methods used for synthetic and hydrophobic polymers listed in Table 1-1. Instead, these preparation methods are mainly performed in aqueous solution with a mild process, which is favoured for the encapsulation of labile biopharmaceuticals.

Chitosan-based nanoparticles

Preparation methods of chitosan-based NPs can be classified into ionic gelation, polyelectrolyte complexation, chemical cross-linking, and emulsification solvent diffusion.

Ionic gelation: Gelation can be achieved through ionic interactions between protonated amine groups of chitosan and small negatively charged molecules, such as triphosphate (TPP), citrate, or sulphate. This preparation process is relatively simple, mild, and without the involvement of organic solvent. In addition, this preparation method allows the encapsulated labile molecules in a biologically active form (129). Chitosan-TPP NPs have been used for the delivery of RNA/DNA (130).

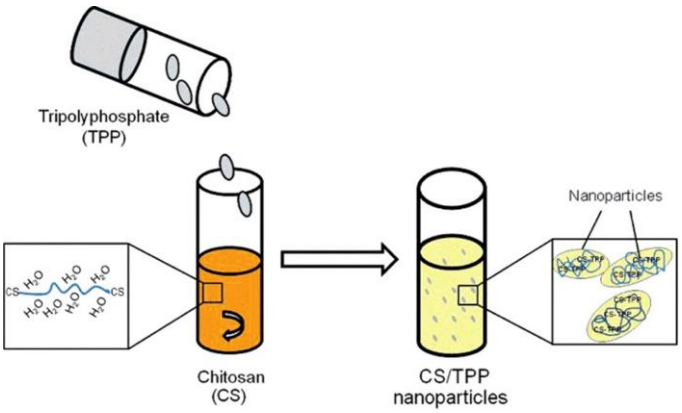

Figure 1-13: Schematic diagram for the ionic gelation method. NPs are formed with the addition of TPP into chitosan solution dropwise, the negatively charged molecules cross-link with the positively charged amine groups of chitosan. The image is reused with the permission from Taylor & Francis (4).

Chemical cross-linking in water in oil (w/o) emulsion system: A w/o emulsion can be prepared by emulsifying a chitosan aqueous solution in an oil phase (*e.g.* toluene), with the suitable surfactant as a stabiliser (*e.g.* Span 80®). Chemical cross-linking is between the reactive amine groups of chitosan with the aldehyde groups of a cross-linking agent such as glutaraldehyde (131). This method can produce a narrow particle size distribution, but it suffers from the negative effects of residual solvent and/or cross-linking agent on the cell viability, and the integrity of the entrapped biopharmaceutical (132).

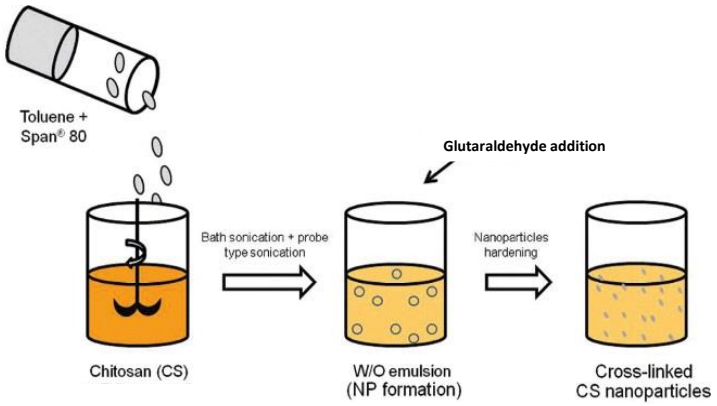

Figure 1-14: **Schematic diagram of the method of emulsification and cross-linking. A w/o emulsion is formed by chitosan (in aqueous solution) and oil phase (*e.g.* toluene) with a surfactant (Span 80®), NPs are formed with the addition of cross-linking agent such as glutaraldehyde. The image is reused with the permission from Taylor & Francis (4).**

Chemical modification: By simple covalent modification of chitosan, its physicochemical properties can be changed, and it becomes more suitable for oral protein delivery. For example, addition of thiol groups into the chitosan chain would enhance its interactions with mucus; this is mainly due to the potential covalent bonds between the thiolated polymers and cysteine-rich subdomains of glycoproteins in the mucus layer (80).

Emulsion solvent diffusion: An organic phase, containing dichloromethane and acetone, is added to an aqueous solution containing chitosan and stabiliser with constant stirring. This leads to the formation of an oil in water (o/w) emulsion which is then subjected to high pressure homogenisation. Subsequent evaporation of dichloromethane from the organic phase leads to the diffusion of acetone (water miscible) into the aqueous phase. This solvent diffusion decreases the solubility of chitosan, and results in the formation of NPs (133). However, these preparation conditions are harsh, with high shear forces and the presence of organic solvent, which might not be suitable for labile biopharmaceuticals. In addition, hydrophobic drugs are more suitable for encapsulation using this method (4).

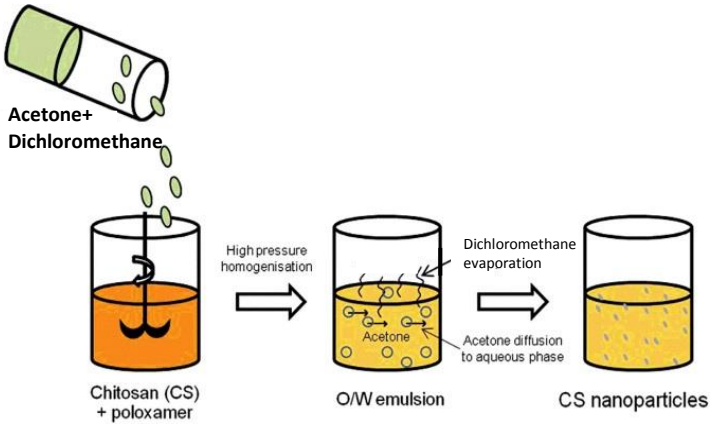

Figure 1-15: Schematic diagram of the emulsion solvent diffusion method of NP production. An o/w emulsion is formed with acetone and dichloromethane in the oil phase and with chitosan in the aqueous phase. After homogenisation, NPs are formed when acetone diffuses into the aqueous phase followed by the evaporation of dichloromethane. The image is modified and reused with the permission from Taylor & Francis (4).

Polyelectrolyte complexes (PECs): These associated complexes are formed due to the electrostatic interactions between oppositely charged polyions, such as between chitosan and alginate. The preparation process avoids the use of a chemical cross-linking agent, and the preparation conditions are mild, which should help preserve the structure of an entrapped biopharmaceutical as well as reducing possible toxic effects at targeted sites (4). A protein or DNA/RNA biopharmaceutical can be loaded into PECs by polyion coacervation between charged groups, and other molecular forces are involved at the same time, such as hydrogen bonds and hydrophobic interactions (134).

In contrast to chitosan, the study of alginate-based NPs is relatively scarce (135). Besides modification of alginate with thiol groups, forming polyelectrolyte complexes, w/o nanoemulsion is another method which is applicable for the encapsulation of biopharmaceuticals (136).

1.6.3 Importance of specific nanoparticle characteristics

Size: Particle size and size distribution are the most important characteristics, as they determine the pharmacokinetics, biodistribution, toxicity, and target ability of NPs. In addition, size can influence drug loading and release, as well as the stability of NPs. It is well known that NP size plays a key role in their cellular uptake and transcytosis, and the impact of size is also cell-dependent (137). Desai *et al.* (1997) suggested that NP uptake by polarised Caco-2 monolayers is size-dependent, and Win *et al.* (2005) showed that 100 – 200 nm is the optimal size range (137, 138).

Surface properties: The nature of NP surface properties determine their interactions with the surroundings, thus influencing their fate *in vivo*. NP hydrophobicity determines the extent of adsorption of blood components, mainly proteins. Coating the surface of NPs with a hydrophilic polymer/surfactant, like polyethylene glycol, polysorbate 80, and polyoxamer, can reduce the adsorption of serum proteins, known as opsonisation, which acts as bridge between NPs and phagocytes (63).

NP surface charge can also affect their fate and behaviour at specific sites in the body or within a tissue. In turn, their uptake behaviour is also influenced by the cell type (139). For example, charged polystyrene NPs are taken up better than their uncharged counterparts (140) and positively charged NPs are better taken up than negatively charged NPs (128). Although it is generally agreed that positively charged NPs result in higher uptake rate, Bannunah *et al.* (2014) showed that a larger number of negatively charged NPs are able to transport across intestinal epithelial cells (141).

Based on current understandings of the importance of the physicochemical properties of NPs to their behaviours, one can summarise an optimal size characteristic for intestinal transcytosis of 100 – 200 nm diameter. Since there is still uncertainty with respect to the impact of surface charge, it would be preferable to use NPs with some capacity to tune their surface charge.

1.7 Thesis Outline

The overall goal of this work was to design and prepare nano-carriers for transporting a protein cargo across the intestinal epithelium. The hypothesis is that a bacterial toxin, specifically ntPE, can facilitate transcytosis of polymeric NPs across the intestinal epithelium. By testing the feasibility of this hypothesis, we hope to identify a strategy for the oral delivery of biopharmaceuticals. Specific objectives to address this hypothesis were:

1) develop and characterise biodegradable NPs;

2) conjugate ntPE onto the surface of these NPs;

3) evaluate ntPE-coupled NP transcytosis *in vitro* using Caco-2 cell monolayers;

4) assess ntPE-coupled NP transcytosis *in vivo*, and test their ability to deliver biopharmaceuticals across the intestinal epithelium.

Chapter 2 explores different methods of making biodegradable NPs using alginate and chitosan. The physicochemical properties of NPs were optimised and the preparation method was selected for the chemical conjugation with ntPE.

Chapter 3 describes a method for the chemical conjugation between ntPE and NPs. The feasibility of the conjugation was first tested on polystyrene NPs before applying the strategy to alginate-chitosan NPs. The physicochemical properties of these NPs were characterised by a variety of methods, to better understand NP behaviours in the later *in vitro* and *in vivo* tests.

Chapter 4 evaluates the transcytosis of polystyrene and alginate-chitosan NPs in an *in vitro* model using Caco-2 cell monolayers. Secondary structural studies of ntPE after coupling to the surface of NPs were performed. The expression of LRP-1 on Caco-2 cells was evaluated and the effect of serum on LRP-1 expression was studied.

Finally, in Chapter 5 the transcytosis of both polystyrene and alginate-chitosan NPs was assessed in living rat small intestine. The feasibility of this nano-carrier strategy for delivering a cargo protein was tested by loading green fluorescent protein into alginate-chitosan NPs.

Chapter 2 Preparation of polymeric nanoparticles

Overview:

Aim: The aim of this chapter was to prepare biodegradable nano-carriers in the size range of ~100 –200 nm, and to test the ability of these nanoparticles to encapsulate biopharmaceuticals.

Methods: Chitosan-triphosphate nanoparticles were prepared using an ionic gelation method. Calcium phosphate nanoparticles were prepared by the co-precipitation of calcium nitrate and ammonium hydrogen phosphate. These two types of nanoparticles were characterised in terms of size, charge and morphology using dynamic light scattering and scanning electron microscopy. Chitosan was coupled onto the surface of calcium phosphate nanoparticles using carbodiimide as a cross-linking agent. This conjugation was characterised using Fourier transform infrared spectroscopy and ^{31}P nuclear magnetic resonance spectroscopy. In addition, alginate and chitosan nanoparticles were prepared by ionic pre-gelation of alginate cores followed by chitosan polyelectrolyte complexation. The resulting nanoparticles were characterised in size, charge, and shape by dynamic light scattering and transmission electron microscopy. The influence of pH, polymer concentration, stirring speed, and polymer ratios were studied. Finally, green fluorescent protein was used to represent a potential biopharmaceutical to be encapsulated into alginate-chitosan nanoparticles.

Results: Chitosan triphosphate nanoparticles had an average diameter of 93 ± 2 nm, 98 ± 18 nm, and 171 ± 25 nm when ratios of chitosan to TPP of 1:20, 1:10, and 1:5 were used, respectively; zeta potential values were determined to be 7 ± 5 mV, 17 ± 11 mV, and 16 ± 9 mV, respectively. Calcium phosphate nanoparticles had an average diameter of 181 ± 13 nm with zeta potential of -42 ± 5 mV. Their size and zeta potential changed to 173 ± 63 nm and 11 ± 1 mv, respectively, after coating with chitosan. Infrared spectra of chitosan-conjugated calcium phosphate nanoparticles were not consistent with the spectra anticipated for ^{31}P nuclear magnetic resonance, suggesting that additional studies will be required to confirm conjugation outcomes. After optimising preparation parameters, such as pH, polymer concentrations, and polymer ratios, alginate-chitosan nanoparticles had a diameter of 179 ± 3 nm, and a zeta potential of 17 ± 5 mV. When green fluorescent protein was loaded into alginate-chitosan nanoparticles (92 % encapsulation efficiency), these nanoparticles had a diameter of 196 ± 13 nm, and a zeta potential of 14 ± 7 mV.

2.1 Introduction

As mentioned in Chapter 1, the overall goal of this thesis is to test the hypothesis that ligand-conjugated nanoparticles (NPs) could be used to carry biopharmaceuticals across the intestinal epithelium. In this chapter, studies are described that had the goal of preparing biodegradable NPs in the size range of 100 – 200 nm that were capable of encapsulating a model protein, green fluorescent protein (GFP). This chapter also discusses the ability of these NPs for surface conjugation with a ligand.

Several aspects of ligand-conjugated NPs for the oral delivery of a biopharmaceutical must be considered to make this approach pharmaceutically acceptable. These NPs must 1) have the capacity to readily release the biopharmaceutical following the process of transcytosis, 2) be biodegradable, and 3) have no potential toxicity as these systems are likely to be used in chronic dosing strategies. Chitosan and alginate fit these criteria and were selected for this study; both are generally regarded as safe and are also cost-effective since they have abundant sources of extraction. Alginate is produced by brown algae and bacteria, and chitosan is isolated from shrimp shells.

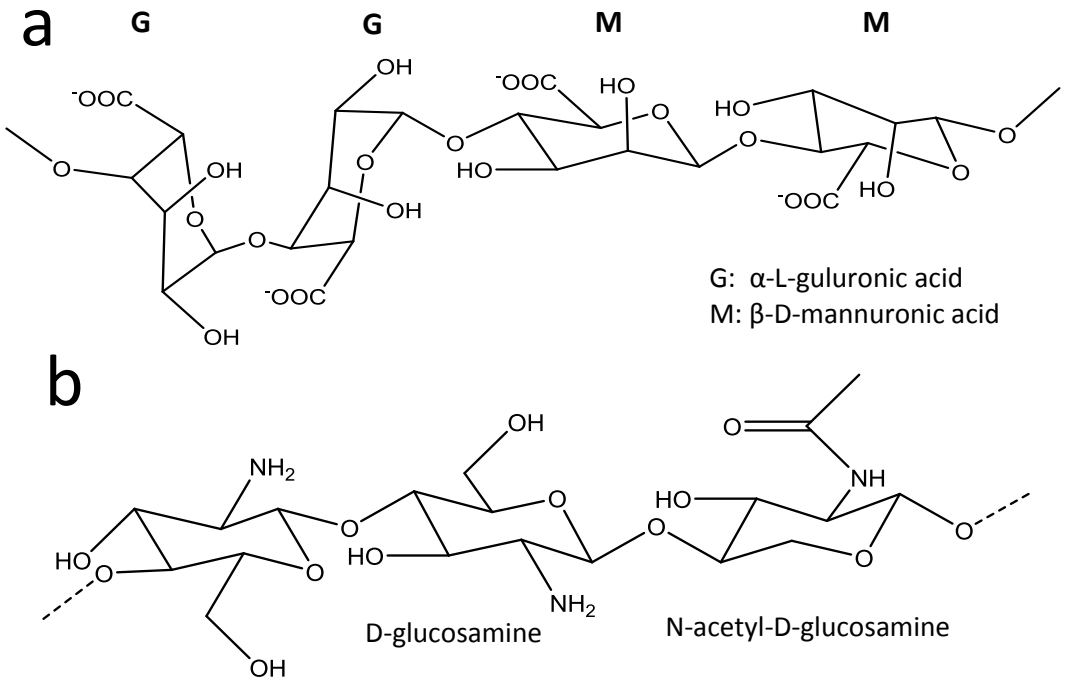

Figure 2-1: Chemical structure of alginate and chitosan. (a) Alginate, a linear copolymer with α-L-guluronic acid (G block) and β-D-mannuronic acid (M block); (b) Chitosan is a linear cationic polymer composed of randomly distributed D-glucosamine and N-acetyl-D-glucosamine.

Alginate is a water-soluble anionic linear polysaccharide, which consists of α-L-guluronic acid (G) and β-D-mannuronic acid residues (M), linearly joined by 1, 4-glycosidic linkages (Figure 2-1a) (142). On the other hand, chitosan is a cationic polymer and the second most abundant biopolymer after cellulose. It is produced by deacetylation of chitin, which is a long-chain polymer of an N-acetylglucosamine, resulting in randomly distributed β-(1-4)-linked D-glucosamine (deacetylated unit) and N-acetyl-D-glucosamine (acetylated unit) (Figure 2-1b). The amine groups on chitosan provide a potential site for chemical conjugation with a ligand; alginate carboxyl groups provide a similar potential site for chemical conjugation with a ligand or easy modification for the purpose of conjugation. Both of these polymers have demonstrated mucoadhesive properties, which can increase their residence time at the epithelial surface of the small intestine (143).

It has been suggested that the physicochemical properties of NPs have great impact on their uptake and transcytosis behaviour. Based on these understandings, desirable characteristics of NPs to enhance the oral delivery of a biopharmaceutical could be proposed. Firstly, the uptake of NPs by small intestinal enterocytes occurs in a size-dependent manner. In this regard, spherical NPs between 20 and 50 nm have the highest uptake rate by non-phagocytic cells (144, 145); while enterocytes have shown preferential uptake particles in the range of 100 – 200 nm (137). Surface charge is another important parameter to be considered. In general, charged NPs are internalised more readily than their uncharged counterparts (140). Positively charged NPs, prepared from chitosan have demonstrated better uptake compared to negatively NPs composed of poly (ethylene glycol)-D, L-polylactide (PEG-PLA) and polystyrene NPs (128, 146, 147). However, Bannunah *et al.* (2014) showed that although positively charged NPs seemed to be internalised by Caco-2 cells to a greater extent than the negatively charged ones, a larger number of negatively charged NPs was transported across the Caco-2 cells (141). Thus, it is still unclear how NP surface charge may affect transcytosis. Furthermore, NPs uptake and transport behaviours are shown to be cell-specific (147).

A robust and consistent method of NP preparation would be required to assess their transcytosis across the intestinal epithelium. Additionally, efficient entrapment and stability of a biopharmaceutical in NPs would be essential. For commonly used preparation methods, such as emulsification-solvent evaporation, solvent displacement, and solvent diffusion, the use of an organic solvent (acetone, ethyl acetate) is unavoidable. The presence of organic solvent trace results in a potential toxicological issue as well as increasing the potential to cause damage to the entrapped biopharmaceutical (148). Recently, polyelectrolyte complexes have become recognised as an attractive delivery system, due to their ease of preparation, and organic solvent-free preparation process (149). These complexes are formed due to electrostatic interaction between oppositely charged polyions; a process that avoids the use of covalent cross-linkers and organic

solvents (134). Additionally, the mild preparation conditions favour encapsulating fragile biopharmaceuticals.

Chitosan and alginate can form a polyelectrolyte complex due to their opposite charges. The protonated amine groups of chitosan can also cross-link with small molecules, like phosphate, citrate, and sulphate to form NPs through a process known as ionic gelation (150). Another biodegradable type of NP, prepared using calcium phosphate (CaP), was also studied. Because of its biocompatibility and biodegradation, CaP NPs have been used for cell transfection since the 1970s and more recently have shown potential as an oral delivery carrier for insulin (151, 152). Furthermore, the process of preparing CaP NPs is easy to perform and cost-effective. The conjugation of ligands on CaP NPs can be achieved by coating CaP NPs with a polymer on the surface.

2.2 Methods

2.2.1 Preparation of chitosan-triphosphate nanoparticles (Chitosan-TPP NPs)

20 mL of 0.25 mg/mL sodium triphosphate (TPP, MW=367.86 g/mol, T5883, Sigma-Aldrich) solution was added dropwise into 10 mL of 2.5 mg/mL chitosan solution (pH 4.5 – 5.0, chitosan deacetylation at 83 %, 448869-50G, Sigma-Aldrich) under magnetic stirring. The resulting suspension was allowed to stabilise for 30 min at room temperature (RT). Different ratios of chitosan to TPP (*w/w*) were performed: 20:1, 10:1, 5:1, and 2:1. The concentration of chitosan was kept the same during these preparations. 9 batches of each ratio were prepared (3 batches per day, over 3 days). Each batch was characterised 3 times using the following equipment (see in 2.2.5). This approach was used throughout this chapter.

2.2.2 Preparation of calcium phosphate nanoparticles (CaP NPs)

100 mL of a 20 mM calcium nitrate solution (27607, BDH chemicals Ltd.) and 100 mL of a 12 mM ammonium hydrogen phosphate solution, pH 10 (Fisons Scientific Apparatus LTD) were prepared in Milli-Q water. 10 mL of both solutions were warmed independently to 80 °C and then mixed in a beaker (50 mL) with magnetic stirring at 80 °C for 7 min. Afterwards, 20 mL of a 10 mM sodium citrate solution (S1804-500G, Sigma-Aldrich) was slowly added over 5 min with constant stirring. The resulting suspension was sonicated using a probe sonicator for 10 min (Model 2501450, Sonifier, Branson, discontinuous mode: pulse on for 4 s and pulse off for 2 s). Following sonication, NPs were washed and suspended in Milli-Q water, with the NPs being

pelleted by ultracentrifugation at 80640 × *g* (Rotor type: 70.1 Ti, L8-M Ultracentrifuge, Beckman) for 20 min at 20 °C (153).

Conjugation between chitosan and CaP NPs was carried out using carbodiimide as a cross-linker (154). Washed CaP NPs were suspended in 10 mL of MES buffer (2-ethanesulfonic acid, 10 mM, pH 6.0, M3671-50G, Sigma-Aldrich). While shaking at 100 rpm, 100 mg of EDC (N-(3-dimethylaminopropyl)-N′-ethylcarbodiimide hydrochloride, E1769-1G, Sigma-Aldrich) were added and the mixture was shaken for 1 h at RT. NPs were then washed twice using PBS (phosphate-buffered saline, 10 mM of phosphate buffer in 137 mM sodium chloride, pH 7.4, Dulbecco "A" Tablets, BR0014G, Oxoid Ltd), pelleted by ultracentrifugation, and suspended in 10 mL of PBS. Finally, 200 µL of 1 % (*w/w*) chitosan, dissolved in acetic acid solution (1 %, *v/v*; 537020, Sigma-Aldrich) was diluted in 1 mL PBS before adding dropwise into a CaP NPs suspension, and the reaction was allowed to proceed overnight at RT.

The linkage between CaP NPs and chitosan was analysed using a Perkin Elmer Frontier Optica FTIR spectrometer equipped with a mercury cadmium telluride (MCT) detector. Suspensions of CaP NPs and chitosan conjugated-CaP NPs were applied onto the crystal of the spectrometer for analysis. Spectra were collected at RT over wavenumber range of 5000-600 cm^{-1} in the transmission mode, and at the resolution of 1 cm^{-1}. Conjugation between chitosan and CaP NPs was also characterised using ^{31}P nuclear magnetic resonance (NMR) spectroscopy, with NMR spectra of CaP NPs and chitosan-conjugated CaP NPs being obtained at 25°C on a Bruker Advance 500 spectrometer (Bruker, UK).

2.2.3 Preparation of alginate-chitosan nanoparticles (AC NPs)

The method used to prepare AC NPs was adapted from that described by De and Robinson (2013) (155). Specifically, 2 mL of a 0.51 mg/mL calcium chloride (C3881-500G, Sigma-Aldrich) solution was added dropwise into 10 mL of a 0.6 mg/mL sodium alginate (W201502-sample, Sigma-Aldrich) solution under a micro-tip probe ultra-sonicator (Figure 2-2) at 4 °C. The resulting pre-gel was stirred for 30 min before the addition of 2 mL of 0.3 mg/mL chitosan solution (dissolved in 0.01 % (*v/v*) acetic acid) at RT. The suspension was then equilibrated overnight to allow the formation of NPs at RT. All materials were filtered through 0.45 µm membranes (MF-Millipore™ Membrane, 0459, Merck Millipore Ltd.) prior to use. Characteristics of the alginate-chitosan complexes formed at different ratios of calcium chloride to alginate (0, 0.08, 0.17, and 0.25, *w/w*) and different ratios of chitosan to alginate (0, 0.05, 0.1, and 0.2, *w/w*) were studied using a Malvern ZetaSizer Nano ZS instrument (Malvern Instruments Limited, Malvern, UK) (details in section 2.2.5). AC NPs formation was also performed at different pH (3.8, 4.5, 5.0 and 5.5) and characterised using the ZetaSizer.

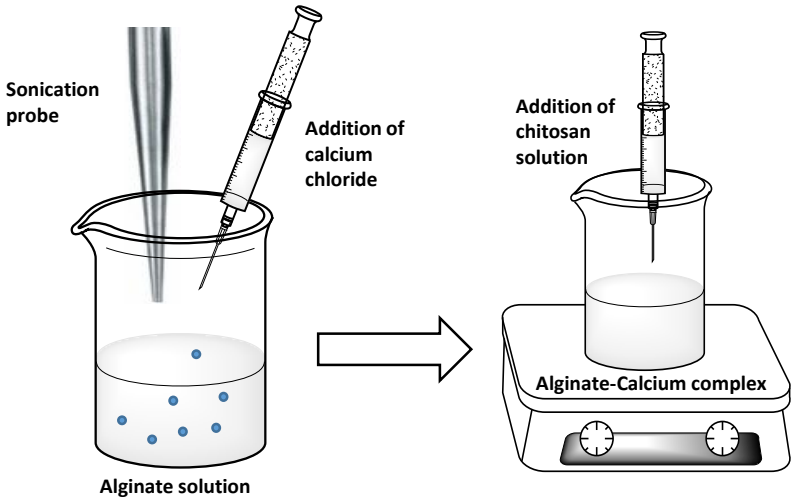

Figure 2-2: Schematic diagram of method used to prepare alginate-chitosan nanoparticles. Calcium chloride solution was added into alginate solution during sonication, and polyelectrolyte complexes were formed by the addition of chitosan.

2.2.4 Preparation of green fluorescent protein-loaded AC NPs

After the formation of alginate and calcium complex as described in 2.2.3, 0.3 mg of green fluorescent protein (GFP, MW=26 kDa, pKa=5.7) was mixed with 2 mL of 0.3 mg/mL chitosan solution which was added dropwise into the alginate-calcium complex. The suspension was then equilibrated at RT for 2 h. Unloaded GFP was separated from NPs by ultracentrifugation at 61740 × g for 30 min at 4 °C. Supernatant from the NP's suspension was assayed on a 96 well microplate in triplicate (655086, Cell culture microplate, 96 well, F-bottom, black, Cellstar®, Greiner bio-one) and measured using a fluorescence microplate reader (FLUOstar Omega, BMG Labtech). The amounts of unloaded GFP were quantified according to a standard curve. The encapsulation efficiency of GFP was calculated by the following equation:

$$Encapsulation\ efficiency = \frac{total\ amount\ of\ GFP - the\ amount\ of\ GFP\ in\ the\ supernatant}{total\ amount\ of\ GFP} \times 100$$

Different ratios of GFP to polymer (1:5, 1:3, 1:2 and 2:1) were prepared and characterised in triplicate while the ratio of chitosan to alginate was kept 1:1.

2.2.5 NPs characterisation

Size and zeta potential measurements of NPs were performed in triplicate using a ZetaSizer at 25 °C.

Chitosan-TPP NPs and CaP NPs morphology was observed by scanning electron microscopy (SEM; JEOL FESEM6301F, JEOL Ltd.). Both sets of samples were freeze-dried using a Micro Modulyo 230 lyophilizer (Thermo Scientific) and the freeze-dried samples were placed on Leit Adhesive Carbon Tabs (AGG3357N, Agar scientific) adhered to SEM stubs. Samples were stored in a desiccator prior to SEM analysis.

Morphological analysis of AC NPs was performed using a transmission electron microscope (TEM; JEOL JEM1200EXII). NP suspensions were diluted 10-fold in PBS (pH 7.4) and dropped onto carbon-coated copper grids (FC300Cu, EM Resolutions) with the liquid being quickly removed by touching the edge of the grid with filter paper. Negative staining was performed by exposing samples to 2 % uranyl acetate for 30 seconds, which was also removed by filter paper absorption. Samples were stored in a desiccator after air drying until being viewed in the TEM.

A preliminary stability test of NPs was performed. 1 mL of AC NPs was dispersed in 10 mL of simulated intestinal fluid (SIF, pH 6.8) for 15, 30 and 60 min. At each time interval, 1 mL of sample was withdrawn and used to prepare TEM samples using the protocol described above. AC NPs were kept at RT for over 7 days, and the size of AC NPs was measured using ZetaSizer at day 1, day 2, day 3 and day 7.

2.2.6 Data Analysis

Data reported as mean ± standard deviation of the mean throughout.

2.3 Results and discussion

2.3.1 Chitosan-triphosphate nanoparticles (Chitosan-TPP NPs)

Chitosan-TPP NPs were prepared by ionic gelation by dropwise addition of TPP to a chitosan solution at RT. This preparation method is relatively simple and inexpensive; it also avoids the use of an organic solvent and harsh conditions, such as high temperature or high speed homogenisation. Nano-scale chitosan-TPP complexes prepared for the encapsulation of 5-fluorouracil were first published by Ohya *et al.* (1994). This cross-link complex was not a new delivery system, and an earlier study can be found in 1989 by Bodmeier (156). Later on, thanks to the mild preparation conditions, chitosan-TPP NPs have been used to deliver fragile molecules, like protein and genetic materials (DNA/RNA), through establishment of ionic interactions between negatively charged biomolecules with positively charged chitosan (130, 157, 158).

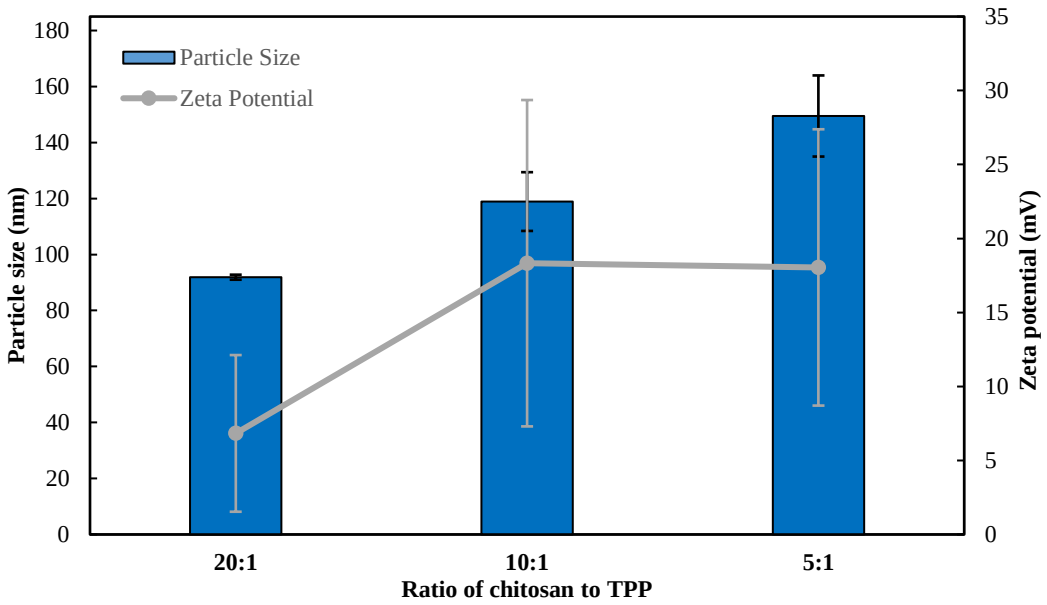

Figure 2-3: The effects of polymer ratios on NPs size and zeta potential. The size of NPs, by DLS was 92 ± 1 nm, 119 ± 10 nm, and 149 ± 14 nm for the ratios of chitosan to TPP, of 20:1, 10:1, and 5:1, respectively; and corresponding zeta potential values were 7 ± 5 mV, 17 ± 11 mV and 16 ± 9 mV. The size of NPs increased with the increasing amount of chitosan in the suspension. The zeta potential also increased with the addition of chitosan, but kept steady from the ratio of 10:1 (n=3).

When preparing NPs with different ratios of chitosan and TPP, the concentration of chitosan was kept constant. NP size and zeta potential appeared to be influenced by the ratio of TPP to chitosan (*w/w*). Chitosan-TPP NPs are believed to be formed by ionic interactions between the phosphate groups and the protonated amine groups of chitosan (159). In this study, the ratio of chitosan to TPP was changed from 20:1 to 10:1 and to 5:1, resulting in NPs with a diameter average of 92 ± 1 nm, 119 ± 10 nm, and 149 ± 14 nm, and zeta potential of 7 ± 5 mV, 17 ± 11 mV and 16 ± 9 mV. The higher TPP concentration appeared to result in larger NPs, and the suspension visibly turned from opalescent to turbid, consistent with observations made by others (158). At a ratio of chitosan to TPP at 2:1, the suspension could not be measured by ZetaSizer, so this preparation was not depicted in the data sets. Rampino *et al.* (2013) reported the same phenomenon that increasing amounts of TPP resulted in greater particle aggregations (157). Overall, these observations were consistent with the mechanism proposed by Koukaras *et al.* (2012) where the addition of TPP reduces the solubility of chitosan, and when the amount of TPP exceeds the amount of amine groups on chitosan, aggregated particles are produced (158).

The measured polydispersity by ZetaSizer for NPs was 0.610 ± 0.02, 0.457 ± 0.01, and 0.425 ± 0.06, respectively, for the ratio of chitosan: TPP, 20:1, 10:1 and 5:1, respectively. Chitosan-TPP NPs appeared to have a low polydispersity under SEM analysis (Figure 2-4). No significant changes were observed for samples prepared at different polymer ratios. Chitosan-TPP NPs

prepared at these three different polymer ratios were in the size range of 100 – 200 nm, which would be desired for protein delivery across the intestinal epithelium. However, conjugation of chitosan-TPP NPs with ligands at the same time as conjugation with a fluorescent tag for *in vitro* or *in vivo* visualisation, is challenging. Therefore, further studies with chitosan-TPP NPs were not carried out.

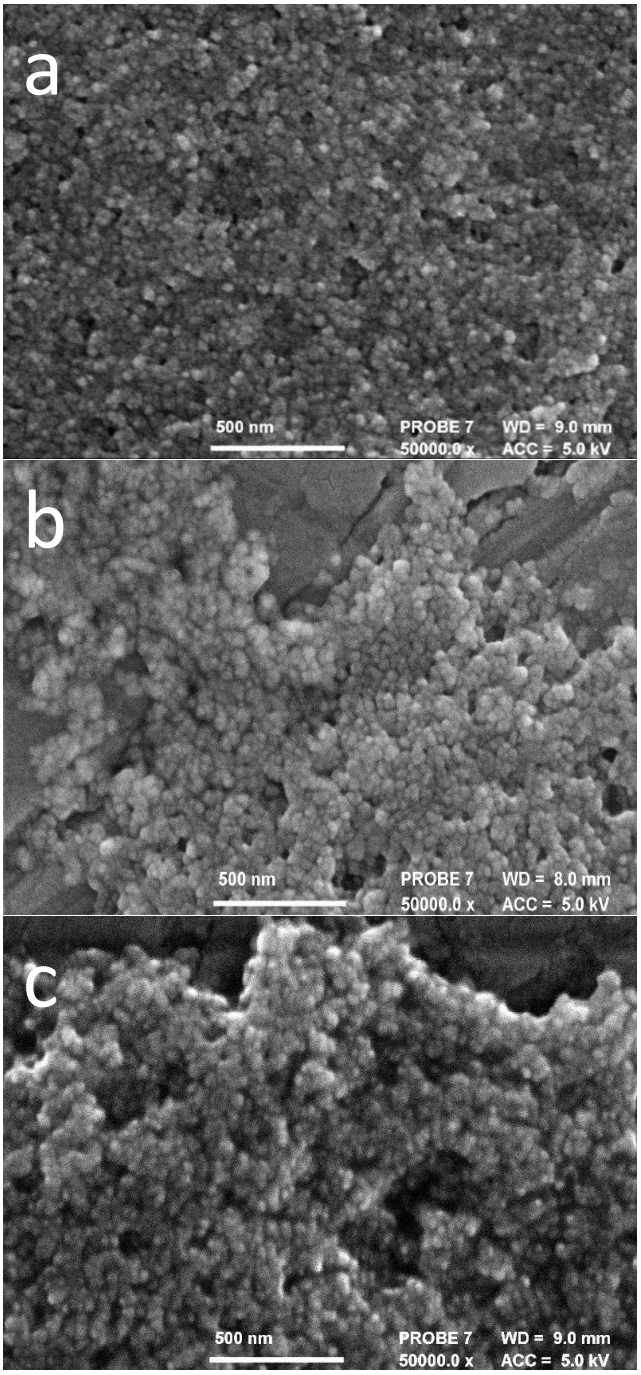

Figure 2-4: Representative SEM images of chitosan-TPP NPs. (a) The ratio of chitosan: TPP was 20:1; (b) the ratio of chitosan: TPP was 10:1; and (c) the ratio of chitosan: TPP was 5:1. Chitosan-TPP NPs appeared to have low polydispersity, and no significant changes were observed in the morphology of NPs at the different chitosan-TPP ratios.

2.3.2 Calcium phosphate nanoparticles (CaP NPs)

Calcium phosphate was used for fracture treatment in the 1920s, and since then it has been applied broadly in orthopaedics, dentistry, and as a carrier for protein and gene delivery (160-162). Its wide application is attributed to a simple and cheap preparation process (163).

Table 2-1: Characterisation of CaP NPs before and after coating with chitosan (n=3).

	Before coating with chitosan	After coating with chitosan
Particle size (nm)	181 ± 13	173 ± 63
Zeta potential (mV)	-42 ± 5	11 ± 1
Polydispersity index	0.287 ± 0.018	0.410 ± 0.167

CaP NPs in this study were prepared using a co-precipitation method: calcium nitrate and ammonium hydrogen phosphate were the reactants, and sodium citrate served as the stabilising agent. This method is a simple and quick process, as other methods either require a reactor or are time-consuming (164).

Using DLS, CaP NPs were determined to have a diameter of ~181 ± 13 nm, and their zeta potential averaged -42 ± 5 mV (Table 2-1) (153). CaP NPs showed a larger size in SEM (Figure 2-5, 438 ± 107 nm, n=50) compared to these DLS measurements. The larger size in SEM could have been due to the freeze-drying process that was carried out without lyoprotectant, which might have allowed aggregation of NPs (165). Chitosan was chosen to link with CaP NPs, since it could be readily used for conjugation with ligands. Additionally, a surface layer of this polymer was also anticipated to improve the colloidal stability of CaP NPs (166). Phosphate groups present in the CaP NPs were conjugated to chitosan amine groups by using carbodiimide cross-link chemistry. Carbodiimide activates the phosphate group to an intermediate phosphate ester similar to its reaction mechanism demonstrated for carboxylates. Then, in the presence of an amine, the ester reacts to form a stable phosphoramidate bond (167).

After coating CaP NPs with chitosan, their size was determined to be 173 ± 63 nm in diameter, and their zeta potential changed from -42 ± 5 mV to 11 ± 1 mV (Table 2-1). The positive zeta potential values suggested that chitosan was presumably on the surface of CaP NPs. Consequently, the presence of chitosan also increased the polydispersity of NPs (Table 2-1), as could be seen by SEM and from the polydispersity values by DLS. This higher polydispersity could be due to the unreacted chitosan forming complexes with phosphate in the suspension (Figure 2-5).

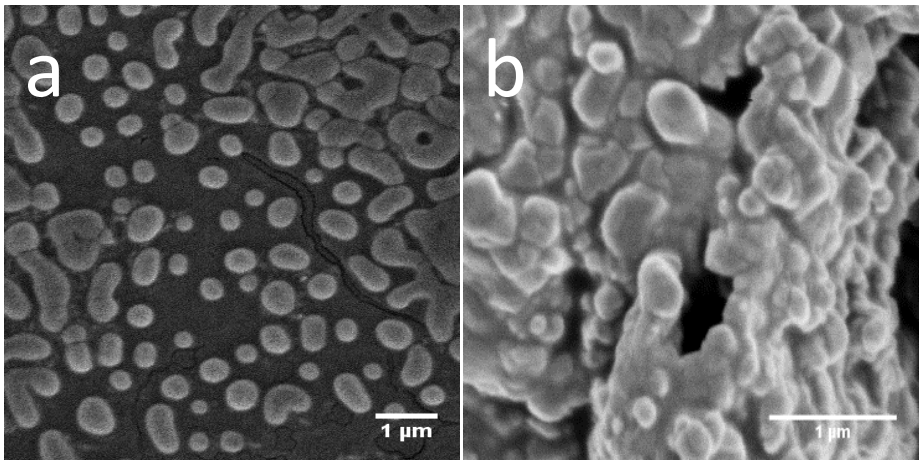

Figure 2-5: Representative SEM images of CaP NPs. (a) CaP NPs were spherical and oval in shape, some NPs were aggregated; (b) CaP NPs were coated with chitosan, and appeared not uniform in size and shape.

One potential problem with these NPs was their propensity to aggregate, as noted by the high polydispersity. This might result in a reproducibility issue, resulting in inaccurate dosing when therapeutic agents are loaded. Also, large CaP NPs agglomerates would limit the efficiency of receptor-mediated endocytosis, and the extended extracellular exposure to these materials could disturb intracellular calcium homeostasis and result in cell death (168).

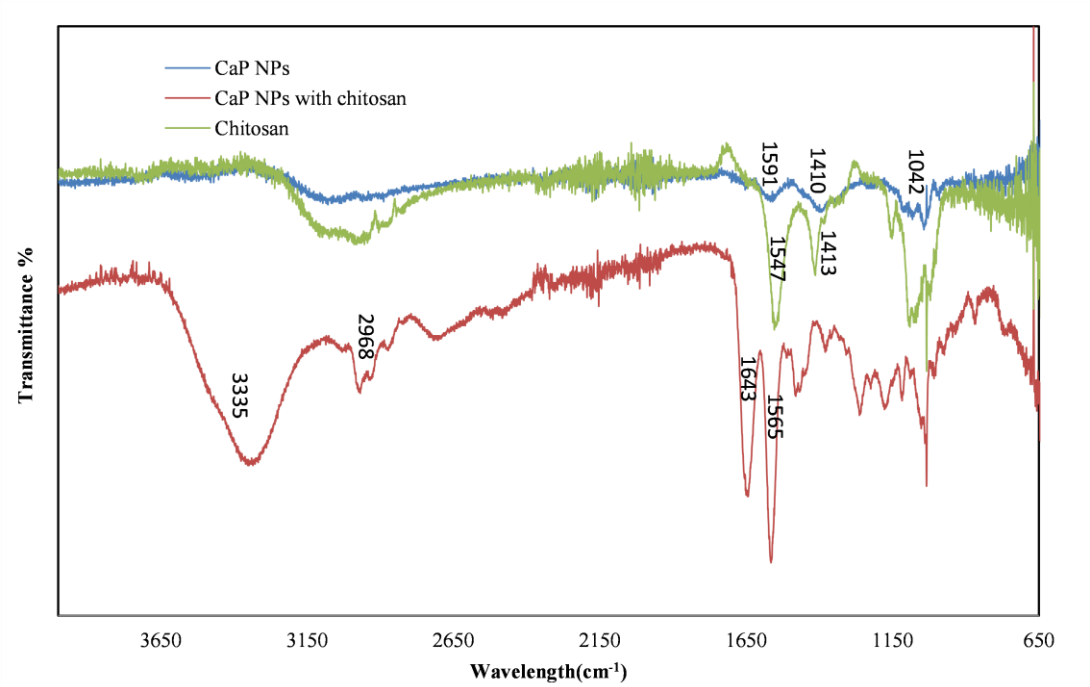

Figure 2-6: FTIR spectra of CaP NPs, chitosan-coated CaP NPs and chitosan. Characteristic bands of PO_4 at 1042 cm^{-1} were found in the spectrum of CaP NPs. The appearance of bands at 1643 cm^{-1} and at 1563 cm^{-1} in the spectrum of the chitosan-coated CaP NPs were attributed to the presence of chitosan in the NPs suspension.

The ability of chitosan-coated CaP NPs to be conjugated with proteins was assessed using FTIR and ^{31}P NMR. The FTIR spectrum acquired from CaP NPs demonstrated a characteristic band of PO_4 at 1042 cm^{-1} (Figure 2-6). The band at 1410 cm^{-1} was considered to describe the alkaline C–H bond present in citrate (169). The FTIR spectrum from chitosan showed a band at 1413 cm^{-1} that probably represented an alkaline C-H bond and the band at 1547 cm^{-1} was assigned to $–NH_2$ scissoring (170). In the spectrum acquired from chitosan coated-CaP NPs, the absorption bands at 1643 cm^{-1} and at 1563 cm^{-1} were attributed to the presence of chitosan (170).

In summary, these studies confirmed that chitosan was present on the CaP NPs. Whether this was due to covalent bonds between phosphate groups of CaP NPs with amine groups of chitosan was not verified. To know if chemical conjugation between chitosan and phosphate had occurred, these NPs were characterised using ^{31}P NMR (171). As shown in Figure 2-7, peaks at δ=0.913 and 0.396 ppm were both considered to be the phosphate groups from CaP NPs, while the anticipated phosphoarimidate group, which was reported at δ =3.3 and 3.1, was not found in the spectrum (172).

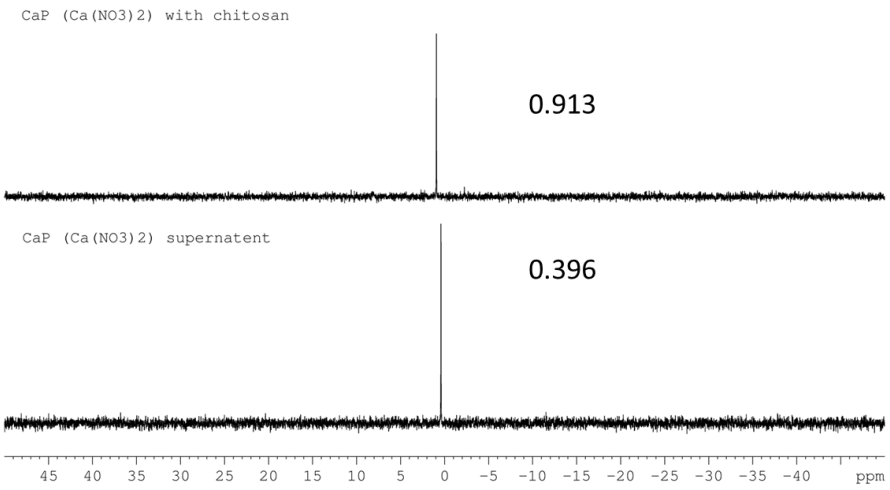

Figure 2-7: ^{31}P NMR spectra of CaP NPs and chitosan coated-CaP NPs. Peaks at δ=0.913 and 0.396 ppm were both considered to be phosphate groups from CaP NPs. The expected phosphoarimidate group was not found at δ =3.3 and 3.1 ppm. This outcome suggested that chitosan was not covalently bonded to CaP NPs.

More studies are required to confirm the conjugation between chitosan and CaP NPs, in order to ensure the possibility of linking NPs with ligands in the next step. Considering the additional complication of particle aggregation and the limited chance of conjugation with ligands, further studies on CaP NPs were not carried out.

2.3.3 Alginate and chitosan nanoparticles (AC NPs)

2.3.3.1 Preparation and characterisation of AC NPs

Alginate is a linear polysaccharide composed of repeating units of glucuronate (G) and mannuronate (M). Gelation of alginate occurs when sodium ions in the glucuronate residues are exchanged with multivalent cations, like calcium ions, and stacking of these G blocks form an "egg-box" like structure. In general, alginate hydrogels are considered to be biologically inert and are commonly used since the 1980s for biomedical purposes, especially in wound dressing, controlled release systems and in tissue engineering (173). More recently, NPs in the size range of 250 – 850 nm prepared from alginate were published by Rajaonarivony *et al.* (1993), and their formation required lower concentrations of sodium alginate and calcium compared to conventional methods of alginate gelation (124).

Different particle sizes caused by reagent concentrations were also observed in the present studies; lower concentrations of alginate formed NPs, while higher concentrations resulted in the formation of gels. As shown in Figure 2-8, a relatively higher concentration of alginate (6 mg/mL) led to gelation, while at lower concentrations (0.06 mg/mL and 0.6 mg/mL), NPs were obtained. For example, NPs prepared using 0.06 mg/mL of alginate had a diameter of 192 ± 15 nm, and when the alginate concentration was increased to 0.6 mg/mL, the diameter of NPs increased to 255 ± 38 nm (Figure 2-9).

Figure 2-8: Appearance of AC NP preparations using different alginate concentrations (from left to right, 0.06 mg/mL, 0.6 mg/mL, and 6 mg/mL). 6 mg/mL of alginate formed a gel when calcium was added, while NPs were formed at lower concentrations of alginate (0.6 mg/mL and 0.06 mg/mL).

Surface charge of AC NPs was also influenced by alginate concentration (174); measured zeta potential values were -34 ± 1 mV when the concentration of alginate was 0.6 mg/mL, and increased to -21 ± 1 mV when the alginate concentration was 0.06 mg/mL, which is related to more chitosan (cationic polymer) remaining unreacted.

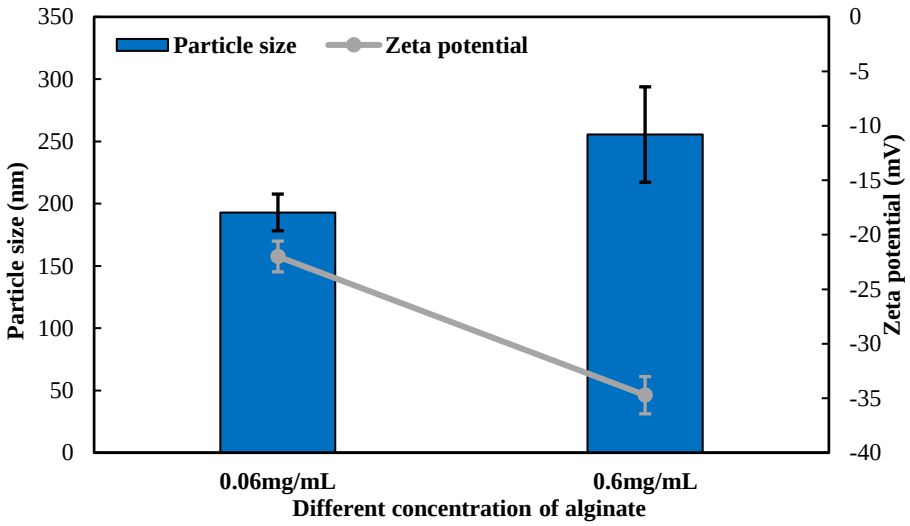

Figure 2-9: Characterisation of AC NPs prepared using different alginate concentrations. The size of AC NPs prepared using 0.06 mg/mL and 0.6 mg/mL of alginate was 192 ± 15 nm, and 255 ± 38 nm, respectively, and zeta potential was measured to be -21 ± 1 mV and -34 ± 1 mV, respectively (n=3).

AC NPs were formed by first adding calcium chloride into an alginate solution, which was followed by adding chitosan solution to form polyelectrolyte complexes. It is known that calcium ions and guluronate (G) residues in alginate interact to form a gel, thereby greater amounts of G blocks in alginate lead to greater interactions and stronger gels. Calcium ions have shown to be important for the formation of AC NPs (175). Different calcium to alginate ratios (0, 0.08, 0.17, 0.25, *w/w*) were used to prepare AC NPs, with optimal complexes being obtained at a ratio of 0.17 (*w/w*, data not shown) (176). Thus, it is necessary to have a calcium ions/alginate ratio < 0.2 for the formation of NPs, as De and Robinson (2003) concluded (155).

Alginate and chitosan are both pH-sensitive polymers, thus their charges at different pH values would have considerable impacts on the formation and characteristics of AC NPs. Alginate has low aqueous solubility in an acidic environment, and chitosan is poorly water soluble at neutral or alkaline pH (177).

Different pH conditions were evaluated to assess the influence of this parameter on AC NPs characteristics. When pH was higher than 5.5, most of the amine groups of chitosan were considered to be un-protonated (chitosan pKa = 5.5 – 6.5), and therefore, unable to have ionic interactions with alginate (178). The insolubility of chitosan at pH 5.5 caused flocculation and the particle size was above the detection limit of the ZetaSizer. Interestingly, lower pH conditions did not necessarily mean smaller AC NPs; the size of NPs prepared at pH 3.8 was 265 ± 30 nm, while the size of AC NPs prepared at pH 4.5 was 179 ± 5 nm (Figure 2-10) (176). This outcome was consistent with other studies where smaller NPs were obtained when chitosan amine groups and carboxyl groups of alginate were ionised, which indicates ionisation state is important for the formation of polyelectrolyte complex (179, 180). When the NP formation was performed at pH 3.8, alginate started to precipitate due to decreased solubility (alginate pKa ~3.5), providing a possible explanation for the observed size differences at pH 3.8 versus 4.5 (180).

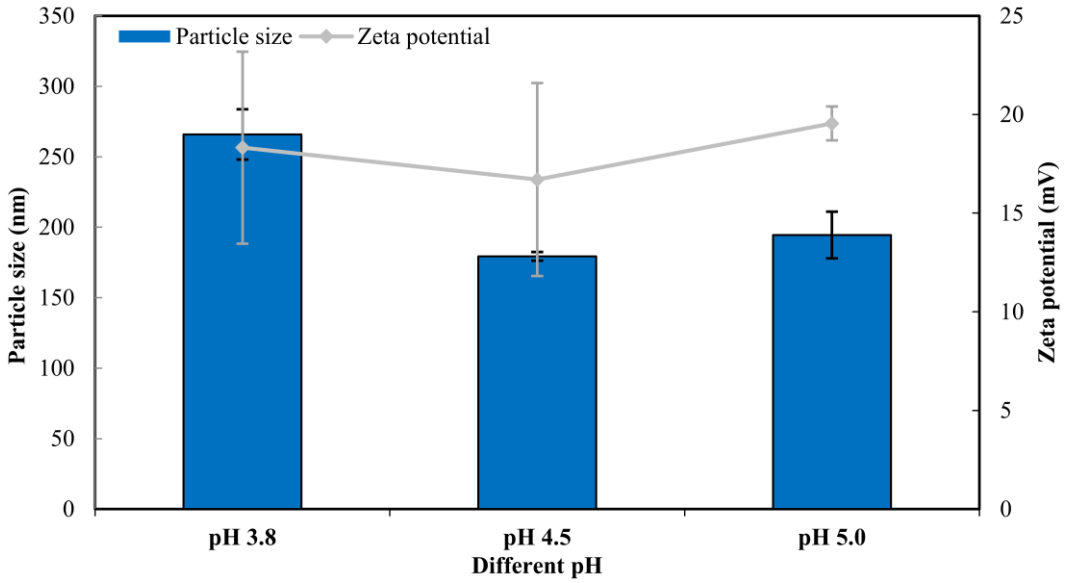

Figure 2-10: Characterisation of AC NPs prepared at different pH. The particle size was 266 ± 18 nm, 179 ± 3 nm, and 194 ± 16 nm when prepared at pH 3.8, 4.5, and 5.0, respectively. Measured zeta potential values of the corresponding NPs were 18 ± 5 mV, 17 ± 5 mV and 19 ± 1 mV. The smallest NPs were obtained when the pH was 4.5, consistent with the possibility that maximising the ionisation of the alginate carboxyl groups and the chitosan amine groups optimises the formation of polyelectrolyte complexes (n=3).

Characteristics of nano-complexes formed by ionic interactions are dependent on the relative concentrations of soluble, charged forms of the two polymers involved. So, the influence of different ratios of alginate: chitosan (*w/w*) to generate NPs were also investigated.

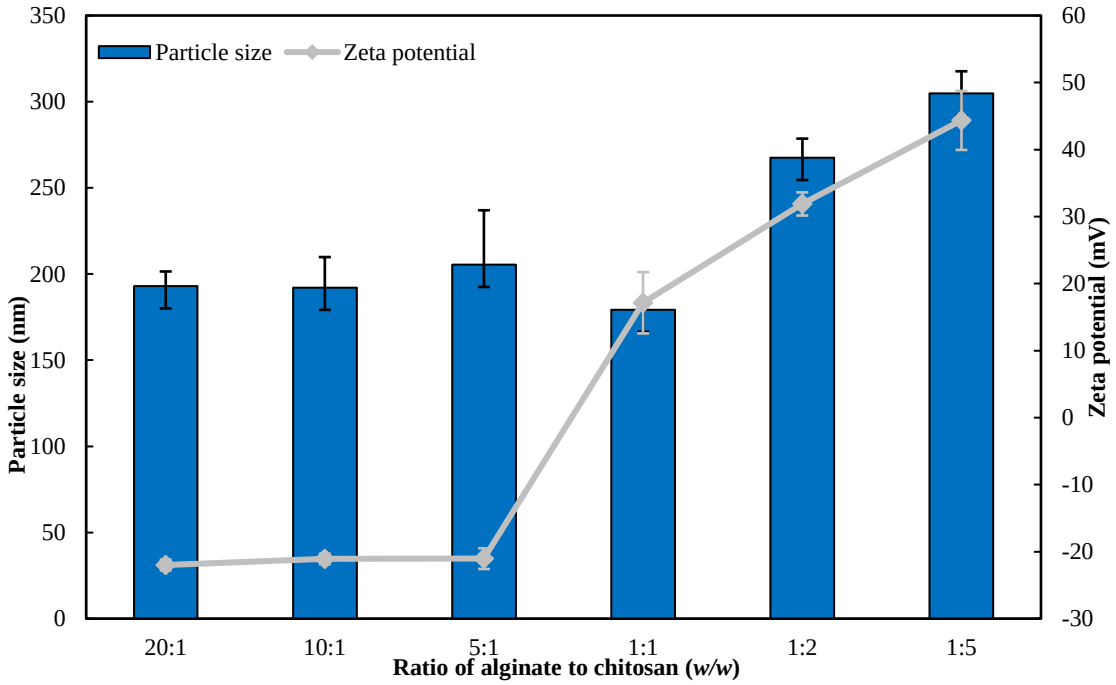

Figure 2-11: Characterisation of AC NPs at different polymer ratios (*w/w*). Chitosan to alginate ratios (20:1, 10:1, 5:1, 1:1, 1:2, and 1:5) resulted in NPs having average diameters of 193 ± 8 nm, 192 ± 18 nm, 205 ± 32 nm, 179 ± 3 nm, 267 ± 11 nm, and 305 ± 13 nm, respectively. The smallest NPs size occurred at the ratio of 1:1. Zeta potential values measured for these different ratios were -22 ± 1 mV, -21 ± 1 mV, -21 ± 2 mV, 17 ± 5 mV, 32 ± 2 mV, and 37 ± 4 mV, respectively. Zeta potential was observed to change from negative to positive as the amount of chitosan was increased (n=3).

AC NP sizes were larger for conditions with increasing amounts of chitosan in the suspension. Interestingly, the smallest NPs were formed when the ratio of alginate: chitosan was 1:1 (Figure 2-11). This observations were consistent with the study by Douglas and Tabrizian (2005) where the smallest NPs were obtained when the alginate: chitosan ratio was between 1:1.5 and 1.5:1 (176). Data presented herein does not contradict the idea that smaller NPs are formed when the availability of the functional groups of two polymers are in stoichiometric proportion (176). It is also important to note that the zeta potential of AC NPs changed from negative to positive when the ratio changed from 5:1 to 1:1 (Figure 2-11), it is thought that when a higher amount of alginate was used (5:1 ratio) the chitosan was unable to "cover" the total amount of carboxyl groups (negative charge) in the alginate.

Stirring speed seemed to have less of an impact on AC NP characteristics in terms of particle size and zeta potential. All AC NPs prepared using stirring speeds of 500 rpm, 1000 rpm, and 1500 rpm were in the size range of 175 –180 nm (Figure 2-12), with 1000 rpm being considered to be the optimal stirring speed due to relatively smaller particle size outcomes. When the stirring speed increased from 500 rpm to 1000 rpm, the zeta potential of AC NPs increased from 16 mV

to 26 mV (Figure 2-12). This increase might indicate that extensive stirring facilitated the interactions between alginate and chitosan. No increase of zeta potential at the speed of 1500 rpm was measured, suggesting that 1000 rpm was sufficient to adequately mix these two polymers.

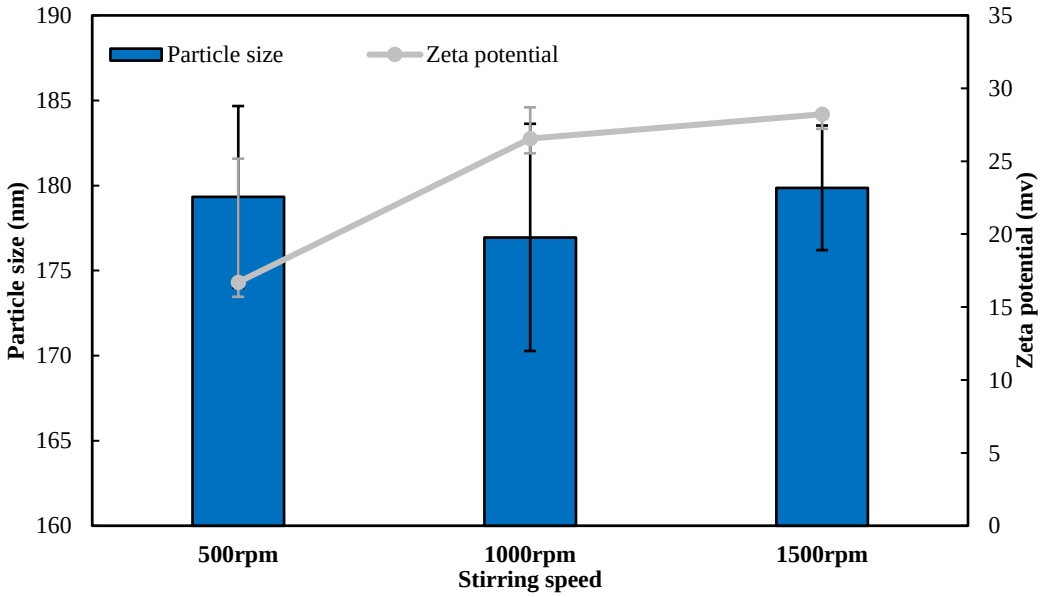

Figure 2-12: Characterisation of AC NPs prepared at different stirring speeds. Stirring speeds of 500 rpm, 1000 rpm, and 1500 rpm resulted in NPs with mean diameters of 179 ± 5 nm, 177 ± 7 nm, and 180 ± 4 nm, respectively; measured zeta potential values were 17 ± 8 mV, 26 ± 2 mV, and 28 ± 2 mV, respectively. The stirring speed seemed to have less impact on the size and zeta potential of AC NPs. The stirring speed at 1000 rpm was considered to be the optimal speed for the formation of NPs (n=3).

In addition to the parameters studied herein, such as alginate concentrations, pH, ratio of polymers, and stirring speeds, others parameters might also influences the formation of AC NPs. In this regard, Douglas and Tabrizian (2005) investigated the influence of polymer molecular weight, demonstrating that the molecular weight of chitosan has much more of an impact than the molecular weight of alginate on NP size. In general, NPs prepared using low molecular weight chitosan were smaller than those prepared with high or medium molecular weight chitosan (176). Nevertheless, chitosan molecular weight does not significantly influence surface charge, as different molecular weights of chitosan may have a similar degree of deacetylation, which means they have a similar proportion of functional groups to interact with alginate (181).

Deacetylation degree of chitosan is another important parameter which determines physicochemical and biological properties of chitosan (182). Lavertu *et al.* (2006) observed a slight increase of NP zeta potential as deacetylation degree (72 %, 80 %, 92 %, and 98 %) of chitosan was increased (183). It is important to point out that the influence of deacetylation degree

is also pH-dependent, as the ionisation state of polymer is sensitive to the pH of the suspension (184).

The morphology of AC NPs was evaluated using TEM (Figure 2-13). AC NPs appeared to be individual spherical NPs, although a tendency for these particles to agglomerate was observed. The measured average diameter of these particles was 48 ± 14 nm (n=100). Particle size measured by TEM was smaller than the measurement from DLS, which has been reported previously (185). This discrepancy is perceived to be due to the fact that DLS measurements give the hydrodynamic diameter of NPs in hydrated conditions, while TEM images are obtained from samples following dehydration. In addition, particle size differences can also be a result of the multiple scattering effect in the DLS technique; multiple scattering refers to the process when light scattered by the diffusing particle is re-scattered by one or more particles before reaching the detector (186).

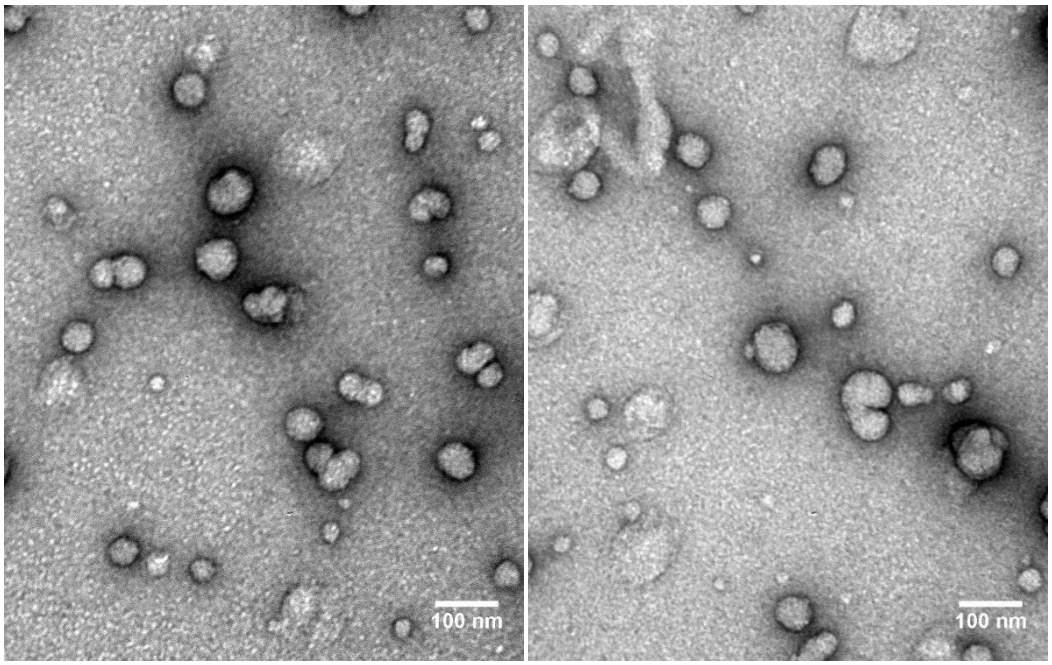

Figure 2-13: Representative TEM images of AC NPs. Particles were generally spherical in shape and had an average diameter measured by using Image J of 48 ± 14 nm (n=100).

The aim of this study was to develop a nano-carrier that could be loaded with biopharmaceuticals. As the pH in the small intestine is between pH 6 to pH 7.4, the morphology of these AC NPs in simulated intestinal fluid (SIF, pH 6.8) after 60 min was examined using TEM (187). While a considerable number of AC NPs was observed in TEM after the exposure to SIF for 15 min (Figure 2-14a), fewer AC NPs were observed after longer times of incubation in SIF (Figure 2-14b and c). It should be pointed out that SIF at pH 6.8 is close to the pK_a of chitosan (~ 6.5) (180). Thus, ionic interactions between alginate and calcium ions may reduce dramatically (188). An increased number of counter-ions in the suspension can also interact with protonated

amine groups of chitosan, as well as alginate carboxyl groups, so that the electrostatic interactions between them are no longer the dominant force involved in maintaining AC NP integrity (189).

Particle size stability over a short time frame is important and relevant for subsequent *in vitro* and *in vivo* studies. AC NP particle size was determined to be constant during 7 days of storage at RT (Table 2-2).

Table 2-2: Change of NPs size and polydispersity over 7 days at RT

	Day 1	Day 2	Day 3	Day 7
Particle size (nm)	174 ± 3	170 ± 1	174 ± 3	165 ± 2
Polydispersity index	0.245 ± 0.01	0.224 ± 0.01	0.233 ± 0.01	0.244 ± 0.01

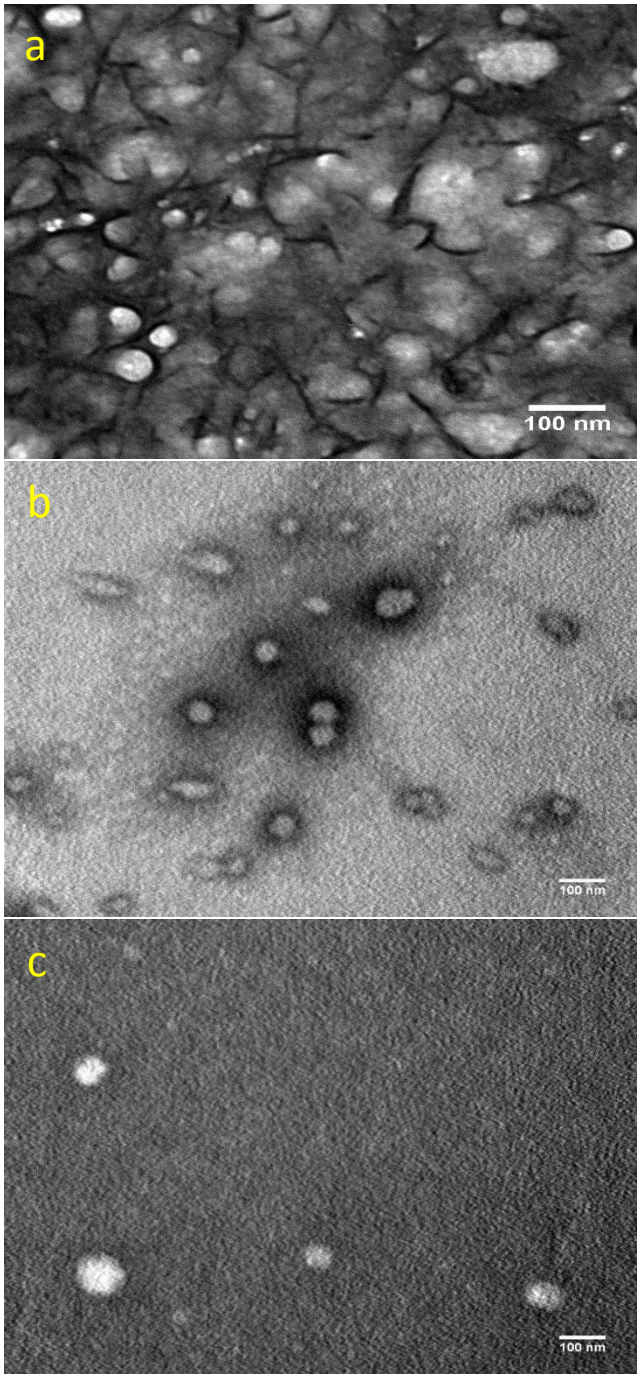

Figure 2-14: Representative TEM images of AC NPs incubated in SIF at pH 6.8. The numbers of detected AC NPs were observed to decrease over time (×100,000; scale bar=100 nm).

2.3.3.2 Encapsulation of green fluorescent protein (GFP) into AC NPs

Once the size (179 ± 3 nm) and zeta potential (16 ± 5 mV) of AC NPs were optimised, the ability of AC NPs for encapsulating biopharmaceutical was tested using green fluorescent protein (GFP) as a model. This protein has a molecular weight of 26.9 kDa and an isoelectric point (pI) of 5.7.

Different ratios of GFP to alginate (1:5, 1:3, 1:2 and 2:1, *w/w*) were tested using a constant ratio of alginate: chitosan (1:1). Encapsulation efficiency of each ratio was calculated and compared, as well as the particle size and zeta potential (Figure 2-15 and Figure 2-16). AC NPs prepared using the ratio of 1:2 appeared to have the highest encapsulation efficiency of 91.7 %, while AC NPs prepared at the ratio of 2:1 had an encapsulation efficiency of only 61.6 %, the lowest amongst the ratios tested (Figure 2-15). For AC NPs prepared at ratio of 1:2, the average diameter measured by DLS was 196 ± 13 nm and measured zeta potential was 14 ± 7 mV (Figure 2-16). When the ratio of GFP: polymer was adjusted to 2:1, the measured size increased to 207 ± 4 nm and zeta potential changed to 23 ± 5 mV (Figure 2-16).

These changes in encapsulation efficiency and physicochemical properties of AC NPs suggested that the excess GFP molecules, which are positively charged, were on the surface of NPs after reaching the ratio of 1:2. This ratio is believed to have the highest level of interactions possible between polymers. Comparing with AC NPs without loading GFP, which had a diameter of 179 ± 5 nm and a zeta potential of 16 ± 5 mV, the size of AC NPs loaded with GFP was increased, but no significant changes were observed in zeta potential.

Protein encapsulation in AC NPs are likely dependent upon electrostatic interactions between the protein molecule and the alginate and chitosan polymer (184). Under the conditions used to form AC NPs (pH 4.5), GFP (pI=5.7) was positively charged, which means it should preferentially interact with the negative charges provided by the alginate. This electrostatic interaction normally exhibits a saturation kinetic which reaches a peak value at high concentration of loaded material. Gan *et al.* (2007) found an almost linear increase of protein encapsulation in relation to protein concentration. A direct relationship between encapsulation efficiency and the concentration of loaded material (GFP) was not observed in this study (184). This might have suggested that other interactions were involved in the encapsulation of GFP, as there is no consensus in the literature for the relation between the protein concentration and the encapsulation efficiency. Akbuga and Bergisadi (1999) suggested that the concentration of the loaded material (cisplatin) had no effect on the encapsulation efficiency, but the small molecule nature of the encapsulated drug should be taken into consideration (190). In addition, Xu and Du (2003)

showed that lower concentrations of loaded proteins (BSA) resulted in higher encapsulation efficiency outcomes (191).

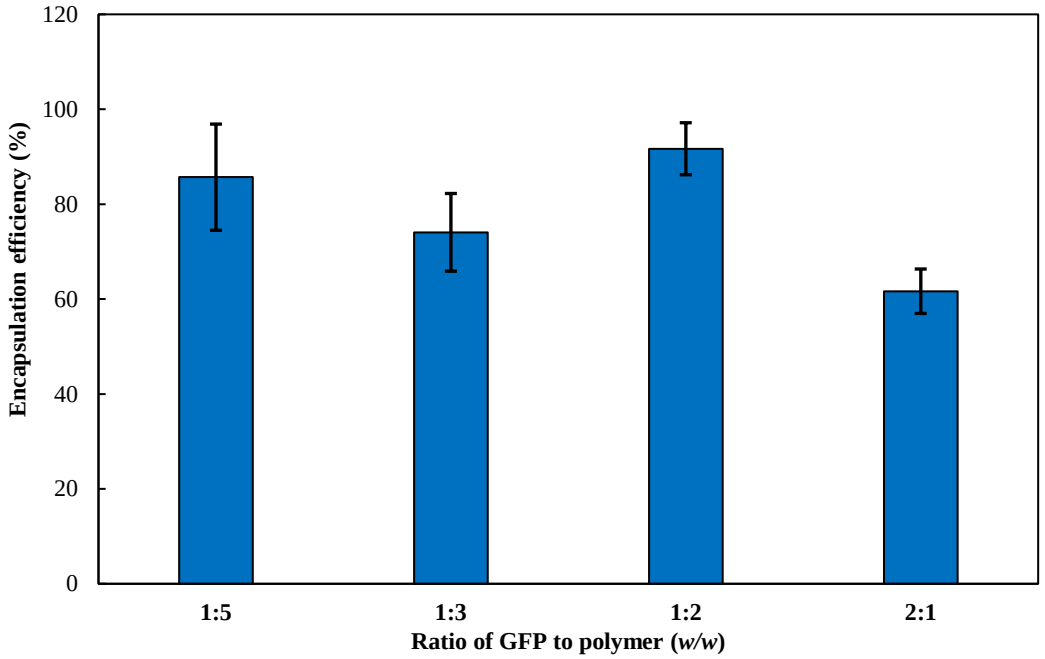

Figure 2-15: Encapsulation efficiency of GFP in AC NPs at different ratios of GFP to polymer (*w/w*). GFP encapsulation efficiency was 85 ± 6 %, 74 ± 5 %, 91 ± 3 %, and 61 ± 3 % when NPs were prepared at ratios of 1:5, 1:3, 1:2, and 2:1, respectively (n=3).

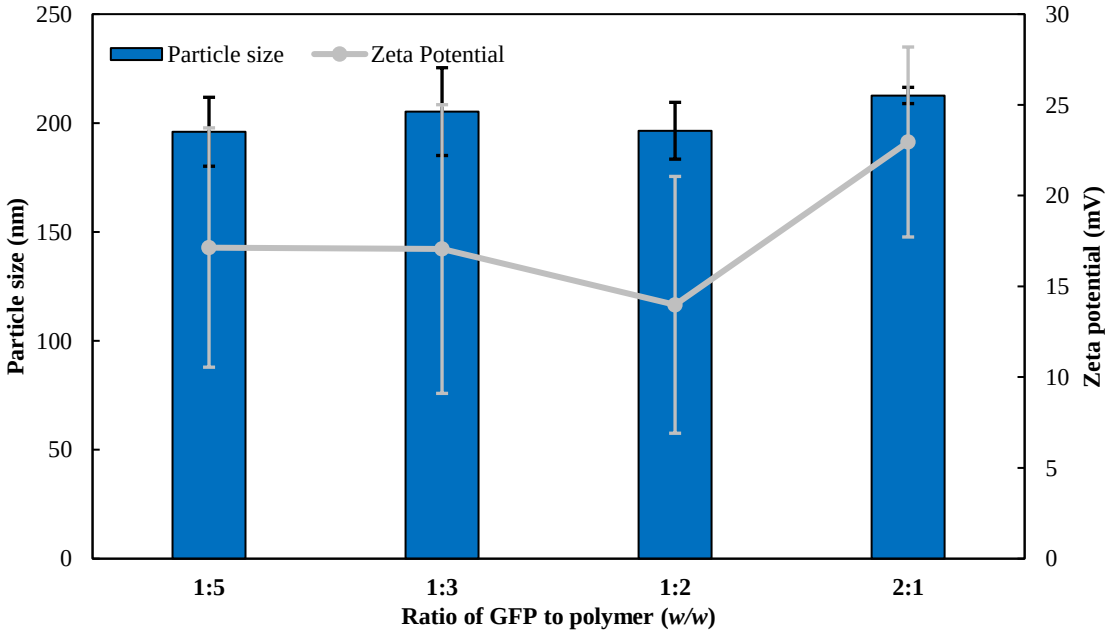

Figure 2-16: Characterisation of GFP-loaded AC NPs prepared using different ratios of GFP to polymer (*w/w*). NPs prepared at GFP: polymer ratios of 1:5, 1:3, 1:2, and 2:1, had hydrodynamic diameters of 196 ± 16 nm, 205 ± 20 nm, 196 ± 13 nm, and 207 ± 4 nm, respectively; zeta potential values for these preparations were measured to be 17 ± 6 mV, 17 ± 8 mV, 14 ± 7 mV, and 23 ± 5 mV, respectively (n=3).

It is also important to note that electrostatic interactions could occur between negative groups of GFP and chitosan amine groups, as well as between the positive charges of GFP with alginate carboxyl groups. Furthermore, GFP can also interact with alginate and chitosan via hydrogen bonds. As chitosan molecules would be fully extended at pH 4.5, protein accessibility to amine groups would be without serious steric hindrance (184).

At the GFP: polymer ratio of 1:2 most of the positive groups of GFP were interacting with alginate negative groups, which led to a high encapsulation efficiency (Figure 2-15) that was consistent with a low measured zeta potential (Figure 2-16). When the GFP: polymer ratio was increased to 2:1, the excess amount of GFP molecules resulted in higher zeta potential. It is important to note that besides the electrostatic interaction, other interactions, like Van der Waals forces might be involved.

Apart from the GFP: polymer ratio, other parameters that could influence cargo protein encapsulation, including polymer concentration, polymer molecular weight, and degree of chitosan deacetylation would be relevant for the current studies. Xu and Du (2003) showed that increasing chitosan concentration decreases BSA encapsulation efficiency (191). Vanerberg *et al.* (2001) showed that the highly viscous nature of a gelation medium hinders the encapsulation of BSA (192). On the other hand, polymer molecular weight influences both NP size and the encapsulation efficiency, with higher chitosan molecular weight resulting in a higher encapsulation efficiency (191). This outcome could be explained by the idea that longer polymer chains can entrap greater amounts of protein during loading.

In contrast, Vila *et al.*(2004) showed that encapsulation of tetanus toxoid was irrespective of chitosan molecular weight, indicating that the entanglement of the protein within the chitosan chains was not affected by their molecular weight (193). This disagreement in literature about the effects of molecular weight on the encapsulation efficiency, may have resulted from the use of chitosan forms with different degrees of deacetylation. Lavertu *et al*. (2006) also showed that chitosan with a low degree of deacetylation results in physically unstable complexes with DNA. According to Köping-Höggård *et al*. (2001), the degree of deacetylation must exceed 65 % in order to obtain stable complexes with BSA for the purpose of cell transfection (194). As mentioned earlier, the ionised state of chitosan is also dependent on pH (184). That is to say, the behaviour of chitosan polymers with different molecular weight is partially dependent on their deacetylation degree, and the behaviour of the deacetylated chitosan is affected by the pH.

The present studies using AC NPs have shown their ability of encapsulating a model biopharmaceutical (GFP), resulting in particles with size and surface charge in the desirable range. In terms of chemical linkage with ligands, alginate and chitosan provide flexibility for the direct conjugation of protein ligands via their functional groups at the surface of these particles. Specifically, the carboxyl groups on alginate can be used to cross-link with the amine groups from

ligand to enhance transcytosis, whilst the amine groups from chitosan can also be used to cross-link to carboxyl groups of a ligand (195). In addition, a cysteine residue could be integrated into either chitosan or alginate to facilitate site-directed chemical linkage with potential ligand to enhance transcytosis. A covalent attachment of cysteine onto alginate can be achieved by carbodiimide cross-link chemistry, and this thiolated alginate may also interact with cysteine-rich subdomains of mucus glycoproteins, improving its mucoadhesive properties (177). On the other hand, thiolated chitosan can also be prepared by coupling with reagents bearing thiol moieties (196).

2.4 Conclusion

Different preparation methods have been explored to generate biodegradable NPs in a desirable size range of 100 – 200 nm. These NPs had the capacity of encapsulating GFP representing a model biopharmaceutical. Importantly, these NPs should have surface accessible moieties that could be used to chemically cross-link a ligand to facilitate epithelial transcytosis of an NP loaded with a biopharmaceutical.

Chitosan TPP NPs could be prepared with a diameter of 92 ± 1 nm, and a zeta potential of 7 ± 5 mV when the ratio of chitosan: TPP was 20:1. While these characteristics would be considered promising for epithelial transcytosis, there may be limited applications for these NPs if one cannot identify ways to functionalise their surfaces for the chemical coupling of a transport ligand.

Another biodegradable nano-carrier, based on CaP NP was prepared and characterised. These NPs were 181 ± 13 nm in diameter and had a zeta potential of -42 ± 5 mV. In order to facilitate their conjugation with ligands and increase their bioadhesion in the intestine, chitosan was used to coat them. However, it was not possible to confirm the chitosan coating was on the surface. For this reason, no further study was carried out with this type of NP.

Finally, AC NPs were prepared by the ionic interactions between two oppositely charged polymers. The formation of this nano-carrier was influenced by pH, polymer concentrations and polymer ratios. We identified an optimised method involving an alginate concentration of 0.06 mg/mL, a polymer ratio of 1:1 for alginate to chitosan, pH 4.5, and stirring speed of 1000 rpm when preparations are performed at room temperature. The obtained NPs were 179 ± 5 nm in diameter, with a zeta potential of 16 ± 5 mV. Both alginate and chitosan have the ability to conjugate ligands and/or to be chemically modified for conjugation. The ability of AC NPs to encapsulate biopharmaceuticals was tested using GFP as a model. The best encapsulation efficiency of GFP (92 %) was reached at a GFP: polymer ratio of 1:2. GFP-loaded AC NPs were 196 ± 13 nm in diameter and with a zeta potential of 14 ± 7 mV. These AC NPs had the desired

size, the ability to encapsulate a biopharmaceutical, and the ability to conjugate a transport ligand on the surface.

Therefore, a nano-carrier using alginate and chitosan was developed and characterised sufficiently to warrant subsequent studies involving surface conjugation with ligands to mediate epithelial transcytosis.

Chapter 3 Chemical linking of proteins with nanoparticles

Overview:

Aim: To chemically link non-toxic *Pseudomonas* exotoxin (ntPE) with stable fluorescent polystyrene nanoparticles (fPS NPs) and biodegradable alginate chitosan nanoparticles (AC NPs).

Methods: The gene sequence for expressing ntPE with a C-terminal extension composed of a cleavable, constrained loop followed by a hexa-histidine (H_6) tag was expressed in *Escherichia coli* K12 bacteria. This protein was then purified using immobilised metal ion affinity chromatography (IMAC) and size exclusion chromatography (SEC). Following cleavage of the constrained loop, a free thiol group was exposed and was used to link ntPE with fPS NPs or AC NPs via a heterobifunctional cross-linking reagent (EMCH; N-ε-maleimidocaproic acid hydrazide). Bovine serum albumin (BSA) was similarly coupled to fPS NPs or AC NPs to serve as a negative control in subsequent studies. Protein-modified NPs were characterised by dynamic light scattering (DLS), transmission electron microscopy (TEM) and ZetaSizer to determine the particle size and zeta potential. For the purpose of validating proteins on the surface of fPS NPs, the change in fluorescence intensity of fPS NPs after the conjugation with BSA or ntPE was recorded using the fluorescence intensity detector in a microplate reader. To check the presence of proteins in the BSA- or ntPE-coupled AC NPs, each NP preparation was characterised by using Fourier transform infrared spectroscopy (FTIR). Fluorescein-5-thiosemicarbazide (FTSC) was used to detect and compare the extent of residual functional sites on AC NPs before and after the linkage with proteins, with the intention of revealing molecular level information about the conjugation.

Results: The diameter of blank fPS NPs, fPS NPs-BSA and fPS NPs-ntPE was 134 ± 22 nm, 151 ± 26 nm, and 111 ± 10 nm, respectively. After conjugation with BSA or ntPE on the surface of fPS NPs, the zeta potential of these particles changed from -30 ± 2 mV to -20 ± 5 mV and to -20 ± 0.4 mV, respectively. Observed fluorescence quenching on fPS NPs-BSA and fPS NPs-ntPE suggested that proteins might be located on the surface of fPS NPs. The conjugation of BSA or ntPE onto AC NPs altered the particle sizes from 215 ± 8 nm to 280 ± 9 nm for AC NPs-BSA and to 202 ± 20 nm for AC NPs-ntPE. The zeta potential of the AC NPs changed from 20 ± 8 mV to -19 ± 11 mV for AC NPs-BSA and to -6 ± 5 mV for AC NPs-ntPE. FTIR spectral analysis of AC NPs-BSA and AC NPs-ntPE supported the possibility of the chemical linkage between BSA and ntPE with AC NPs.

Conclusion: BSA and ntPE appear to have been successfully linked to fPS NPs and AC NPs, this was sufficient to warrant biological studies that would assess the role of these proteins to facilitate trans-epithelial transport of these NPs.

3.1 Introduction

Chapter 2 explored NP preparation methods to achieve desired physicochemical properties that could facilitate their uptake and transport in the gastrointestinal tract (GI tract). It has been generally accepted that NPs in the size range of 100 – 200 nm are favoured for cell uptake (138). Although NPs can be internalised into the enterocytes of the GI tract, the fate of NPs after endocytosis into these cells is presumed to be degradation in lysosomes or non-specific exocytosis (197). Consequently, very small amounts of NPs are able to travel across the epithelium: from the apical to the basolateral side (transcytosis). It has been hypothesised that specific ligands on NPs might lead to receptor-mediated transport, which could possibly evade digestion and facilitate efficient transcytosis (34).

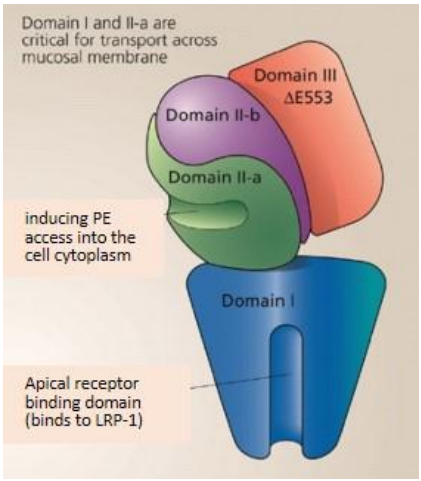

Figure 3-1: Schematic diagram of the structure of PE. It consists of three domains, domain I is responsible for the recognition on the cell membrane, the function of domain II is to translocate the protein after internalisation, and domain III leads to the cytotoxic effect.

Pseudomonas aeruginosa secrete a virulence factor, exotoxin A that can efficiently cross an epithelial barrier. *Pseudomonas* exotoxin A (PE) consists of three domains: domain I binds to the low-density lipoprotein receptor-related protein (LRP-1) at the apical surface of simple polarised epithelial cells such as those in the intestine and airway (by inhibiting protein synthesis through ADP ribosylation (110). In non-polarised cells, domain II is responsible for inducing PE access into the cell cytoplasm, and domain III functions as a cytotoxic enzyme that results in cell death by inhibiting protein synthesis through ADP ribosylation (110).

Remarkably, PE is able to travel across polarised epithelial cells without changing the toxicological properties determined by its structure (118). Deletion of a glutamic acid at position 533 of PE removes its cytotoxic effect, a mutant that has been widely used in immunotoxin development (198). In this present study, we hypothesised that attachment of ntPE at the surface of NPs would facilitate permeability of NPs across intact, simple, polarised epithelium. In order to achieve a controlled coupling to NPs, a unique construction was prepared that would generate a single available thiol group on ntPE.

Chitosan and alginate were selected to prepare biodegradable and biocompatible polymeric NPs. Both chitosan and alginate have shown great flexibility for conjugation with protein and for

chemical modification for conjugation (177). A mild chemical linking strategy was selected because of the fragile nature of proteins. It is critical to ensure that properly folded, biologically active proteins are coupled onto NPs so that these NPs could be tested *in vitro* and *in vivo*. Conjugation of ntPE onto the surface of preformed NPs was carried out in water using the cross-linking agent EMCH (N-ε-maleimidocaproic acid hydrazide). Using the maleimide group of EMCH, the free thiol groups on a C-terminal modified form of ntPE could be selectively linked, while the hydrazide group at the other end of EMCH was anticipated to link with carboxyl groups present at the surface of NPs (Figure 3-2). This linking strategy would allow unwanted byproducts

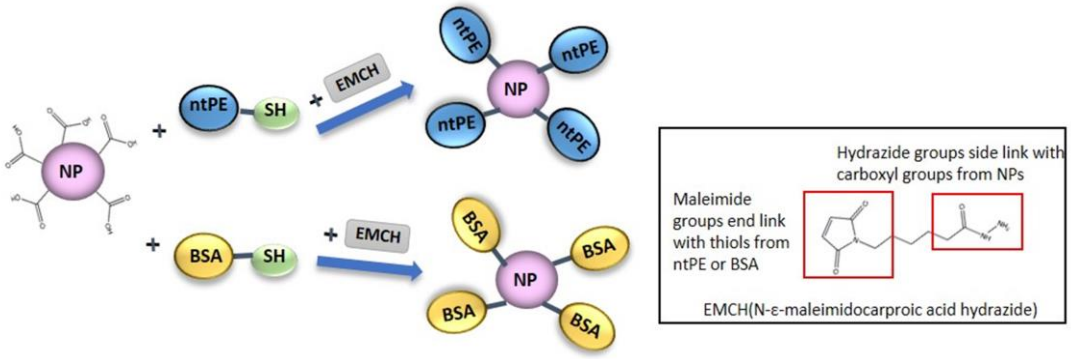

Figure 3-2: Illustration of the chemical linkage between NPs and ntPE or BSA. The carboxyl groups on NPs were linked with thiol-BSA or thiol-ntPE using the cross-linker EMCH (the particles and molecules depicted do not represent the actual size and location).

to be easily removed by nonchromatographic methods (199).

The chemical linking protocol was first developed using stable PS NPs before moving to the more labile NPs prepared from chitosan and alginate. Additionally, BSA was used to optimise chemical coupling conditions that could then be used with ntPE; BSA and ntPE have a similar isoelectric point (pI) and molecular weights (200, 201).

It is widely acknowledged that physicochemical properties of NPs, such as size and surface chemistry, dramatically affect their behaviours in biological systems (202). Therefore, the physicochemical characterisation of NPs and protein-conjugated NPs was performed in this study, anticipating they would provide important information for understanding the *in vitro* and *in vivo* behaviours of NPs surface-coupled with ntPE.

3.2 Methods

3.2.1 Production of ntPE used for selective coupling

A non-toxic mutant of *Pseudomonas* exotoxin A (ntPE) was used; deletion of the glutamic acid at position 553 (ΔE553) resulted in detoxification of the enzyme activity of domain III (119). A plasmid containing nt-PE (pVC 45D) was kindly donated by Dr David FitzGerald (NCI/NIH, Bethesda, MD, USA). A tobacco etch virus (TEV) protease-specific sequence followed by a hexa-histidine sequence (CENLYFQSGTCHHHHHH) was inserted into the plasmid at the C-terminus of the ntPE open reading frame (ntPE-TEV-H_6).

3.2.1.1 Protein expression in the periplasm

The bacterial strain used to express ntPE-TEV-H_6 was *Escherichia coli* K12. A single colony of SHuffle® T7 (C3026H, New England Biolabs) transformed with the ntPE-TEV-H_6 expression vector was used to inoculate 50 mL of Lysogeny Broth (LB) medium containing 50 μg/mL ampicillin (BP1760-25, Fisher Scientific) and grown overnight at 37 °C with shaking at 250 RPM. The protocol for making LB medium was: 10 g of tryptone (1279-7099, Fisher Scientific), 5 g of yeast extract (BPE9727-2, Fisher Scientific), and 10 g of sodium chloride (S9625-5KG, Sigma-Aldrich) in 1 L of water. The next day, 1 L of LB medium supplemented with 50 μg/mL ampicillin was inoculated with 25 mL overnight culture and cells were grown at 37 °C with shaking at 250 RPM until the OD600 reached 0.6 – 0.8. At this point, cell cultures were induced using 0.5 mM IPTG (isopropyl β-D-1-thiogalactopyranoside, C9H1805S, Fisher Scientific) and grown overnight at 18 °C. Cells were harvested by centrifugation at 1530 × *g* (calculated by r_{min}, refers to the distance between the centre of rotor to the top of the tube) at 4 °C for 20 min (JA-10 fixed angle rotor on Beckman J2-MC centrifuge), and the cell pellets were suspended in 30 mM Tris-HCl (T6066-1KG, Sigma-Aldrich), 20% sucrose (S7903-250G, Sigma-Aldrich), pH 8.0 at 80 mL per gram wet weight. 200 mM EDTA (Ethylenediaminetetra-acetic acid, E9884-100G, Sigma-Aldrich) was added dropwise to the cell suspension while on ice until a final concentration of 1 mM EDTA was reached. Following 10 min of gentle shaking, cell suspensions were centrifuged at 3225 ×*g* (Heraeus™ Primo™/ Primo R Centrifuge, Thermo Scientific) for 20 min at 4 °C, with the pellets suspended in ice-cold water and incubated on ice with gentle shaking for 10 min. Cell debris following this osmotic shock step was pelleted by centrifugation at 3225 ×*g* for 20 min at 4 °C. The supernatant, containing proteins from the periplasm, was collected and processed for the purification of ntPE-TEV-H_6 protein.

3.2.1.2 Protein purification

Purification of ntPE-TEV-H_6 was a two-step process. Firstly, immobilised nickel ion affinity chromatography (IMAC) was used to capture the full-length protein, then size exclusion chromatography (SEC) was used to capture monomeric protein. The H_6 tag at the C-terminus of ntPE-TEV was designed for high affinity capture using a His Trap column prepacked with nickel ion-Sepharose (5mL, HisTrap™ HP, 17-5248-02, GE Healthcare Life Sciences). A linear gradient of imidazole (20 mM to 500 mM, 301870010, Acros Organics) in a solution containing 50 mM Tris pH 8.0, and 300 mM sodium chloride at a flow rate of 4 mL/min was used to elute ntPE-TEV-H_6 captured by the His Trap column. Fractions with proteins were collected at every 5 mL (referred to as fractions A1-A12). These fractions were then concentrated by reducing the volume to 1 mL using a 10 kDa MWCO spin filter (Amicon® Ultra-4 Centrifugal Filter Unit with Ultracel-10 membrane, UFC801024, Merck Millipore Ltd.).

SEC was used to separate aggregated forms and other unwanted substances from monomeric ntPE-TEV-H_6. A concentrated protein solution obtained following the IMAC purification step was loaded onto a Superdex® 200 HR10/30 column (17517501, GE Healthcare Life Sciences) and eluted with PBS (10 mM of phosphate buffer in 137 mM sodium chloride, pH 7.4, Phosphate-buffered saline, Dulbecco "A" Tablets, BR0014G, Oxoid Ltd) at a flow rate of 0.5 mL/min. Sodium dodecyl sulphate polyacrylamide gel electrophoresis (SDS-PAGE; the full protocol can be found in Appendix 1) was used to identify column fractions containing ntPE-TEV-H_6. Protein concentrations were determined using a NanoDropTM 2000c spectrophotometer (Thermo Scientific) at the wavelength of 280 nm.

3.2.2 Preparation of EMCH-ntPE and EMCH-BSA for conjugation with NPs

3.2.2.1 Cleavage of ntPE-TEV-H_6 protein and preparation of EMCH-ntPE

The ntPE-TEV-H_6 protein sequence contains a TEV cleavage sequence (CENLYFQ√ SGTCHHHHHH) at its C-terminus where √ refers to a TEV-specific cleavage site. Mild reaction allows opening the disulphide bond present and exposes a linear form of the amino acid sequence identified and cleaved by the tobacco etch virus (TEV) protease. Removal of the C-terminal amino acids (SGTCHHHHHH) using a second IMAC step allowed for the preparation of ntPE-CENLYFQ that contained an unpaired cysteine residue, which could be used for selective conjugation. This was achieved by the following steps. 2 mg ntPE-TEV-H_6 protein was mixed with the TEV cleavage reaction buffer containing 50 mM Tris-HCL pH 8.0, 0.5 mM EDTA and 0.5 mM DTT (Dithiothreitol, 1452675, Novex® by Life Technology) and was incubated for 4 h

at room temperature (RT) after the addition of TEV enzyme (1351394, Novex® by Life Technology). A 1 mL HisTrap HP column (prepacked with nickel- Sepharose, 29-0510-21, GE Healthcare Life Sciences) was used to separate cleaved protein (ntPE-CENLYFQ) from the SGTCHHHHHH peptide. A PD-10 column (17-0851-01, GE Healthcare) was used to perform buffer exchange into PBS solution.

Chemical coupling between the free thiol group of the cysteine residue in ntPE-CENLYFQ and carboxyl groups present on the surface of NPs was achieved by using the heterobifunctional chemical linker EMCH (N-ε-maleimidocaproic acid hydrazide, 22106, Thermo Fisher Scientific). The maleimide moiety of EMCH was used to conjugate with thiol groups of ntPE-CENLYFQ, whilst the hydrazide moiety of EMCH was used to conjugate to the free carboxyl groups on NPs. The thiol-maleimide reaction was allowed to occur at RT for 2 h. Unreacted EMCH was removed by dialysis (SnakeSkin™ Dialysis tubing, 10K MWCO, 68100, Thermo Fisher Scientific) against water overnight at 4 °C.

3.2.2.2 Introduction of free thiol groups into BSA and the preparation of EMCH-BSA

BSA (A7906-100G, Sigma-Aldrich) was chosen as a control for ntPE due to its similarities in physicochemical properties (molecular weight, isoelectric point). In order to use a similar coupling approach for both molecules, free thiol groups were introduced into BSA to allow for the EMCH-based conjugation. Traut's reagent (2-iminothiolane, 26101, Thermo Fisher Scientific) was used to achieve a one-step conversion of free amines to free thiols. A 3-fold molar excess of Traut's reagent was added to BSA (12mM in PBS containing 3 mM EDTA) in a dropwise manner and the reaction solution was incubated at RT for 1 h. Afterwards, the number of thiol groups was determined to be ~1 per BSA molecule using Ellman's reagent (5,5'-Dithiobis(2-nitrobenzoic acid), S39637, Sigma-Aldrich). This reagent can react quantitatively with thiol groups to yield detectable reaction products, which can be quantitated spectrophotometrically (λ_{max}= 412nm; the full protocol can be found in Appendix 2). The thiol groups induced to BSA were reacted with EMCH in a manner identical to that used for ntPE-CENLYFQ as above (see section 3.2.2.1).

3.2.3 Conjugation of EMCH-ntPE and EMCH-BSA onto fPS NPs

fPS NPs ~100 nm in diameter and with carboxylate groups on the surface were used (Ex/Em: 580/605 nm, 50 mg/mL, F8801, Thermo Fisher Scientific). 0.5 mL of fPS NPs were rinsed twice by ultrafiltration at 5000 × *g* for 10 min using Amicon Ultra-15 Centrifugal Filter Units (10kDa MWCO, UFC901024, Merck Millipore) in MES buffer (2-ethanesulfonic acid, 50 mM, pH 6.0, M3671-50G, Sigma-Aldrich). Rinsed NPs were suspended in 10 mL MES buffer to the final concentration of 2.5 mg/mL.

2 mL of fPS NPs were reacted with 0.5 mg of EMCH-BSA or EMCH-ntPE prepared earlier, the reaction being allowed to occur in 3 mL of 50 mM phosphate buffer (50 mM of Na_2PO_4 71636-250G, Sigma-Aldrich) containing 0.9 % sodium chloride. After 15 min of incubation at RT, 4 mg of EDC (1-Ethyl-3-(3-dimethylaminopropyl), carbodiimide, E1769, Sigma-Aldrich) and 5 mg of NHS (N-hydroxysuccinimide, 24500, Thermo Fisher Scientific) was added to the reaction solution (203). After the addition of EDC and NHS, the pH was adjusted to 6.5 and the reaction was allowed to proceed overnight at RT. Unreacted proteins and reagents were excluded from the suspension through ultrafiltration (Amicon Ultra-4 Centrifugal Filter Units, 652000, 100K MWCO, Merck Millipore) at 2500 × *g* for 10 min; un-coupled proteins were collected and quantified by Bradford assay (described in section 3.3.2.5).

3.2.4 Alginate-chitosan nanoparticles coupling to EMCH-BSA or EMCH-ntPE

3.2.4.1 Oxidation of sodium alginate

Carboxyl groups on AC NPs were produced by the oxidisation of alginate. A 1 % (*w/v*) sodium alginate (W201502, Sigma-Aldrich) solution was mixed with sodium periodate (50 mM, 311448-5G, Sigma-Aldrich) and incubated at RT for 24 h with the reaction being quenched by the addition of an equimolar amount of ethylene glycol (102466-500ML,Sigma-Aldrich). Sodium chloride (2.5 g) was then added to the solution, followed by precipitation with 2 excess volumes of ethyl alcohol (200 mL). The precipitates were collected by centrifugation and dissolved in distilled water (100 mL) prior to a second precipitation using ethyl alcohol (200 mL). The resulting oxidised alginate was freeze-dried (MicroModulyo 230, Thermo Scientific) under reduced pressure to yield a white solid (0.8 g, 80 % yield).

3.2.4.2 Preparation of oxidised AC NPs

2 mL of 0.51 mg/mL calcium chloride (C3881-500G, Sigma-Aldrich) solution was added into 10 mL of 0.06 mg/mL oxidised alginate solution dropwise under micro-tip probe ultra-sonication (Model 2501450, Sonifier, Branson). The resultant material was stirred for another 30 min before the addition of 2 mL 0.3 mg/mL chitosan solution (448869-50G, Sigma-Aldrich). The suspension was equilibrated overnight at RT to allow the formation of NPs. All materials were filtered through 0.45 µm membranes (MF-Millipore™ Membrane, 0459, Merck Millipore Ltd) prior to use.

3.2.4.3 Conjugation of EMCH-ntPE and EMCH-BSA onto AC NPs

The carboxyl groups on oxidised alginate were reacted with the hydrazide groups on EMCH-BSA and EMCH-ntPE. 2 mL of oxidised AC NPs were mixed with 0.5 mg of EMCH-BSA or EMCH-ntPE in a 10 times diluted PBS buffer (1 mM for phosphate, 13 mM for sodium chloride, pH 7.4). After 2 h reaction at RT, the un-coupled EMCH-BSA or EMCH-ntPE was excluded by overnight dialysis against water at RT (Spectra/Por® Biotech membranes, 100K MWCO, SpectrumLabs). The extent of protein coupled onto AC NPs was quantified by Bradford assay.

3.2.5 Standard curve for Bradford assay and protein quantification

Bradford assay is a simple, fast and sensitive method to determine protein concentration. It relies on absorbance shift of the dye Coomassie blue after its binding to protein. In the acidic assay reagent solution, the dye is in the cationic form and has a λ_{max} of 470 nm. In contrast, the anionic form of the dye, which binds to protein, has a λ_{max} of 595 nm. Thus, the amount of protein can be quantified by the measurement of the absorbance of the solution at 595 nm.

A standard curve from 2.5 to 50 µg of BSA was used for protein quantitation, with 50 µL of a protein solution being mixed with 150 µL of Coomassie blue solution (1856209, Thermo Scientific) in a 96 well microplate (3370, 96 Well Flat Bottom, Costar®, Corning Incorporated). Coomassie blue-protein complexes were left for 10 min at RT before spectroscopic measurement. The standard curve of ntPE from 2.5 to 100 µg was generated the same way as the BSA standard curve. To quantify the amount of proteins on NPs, the values from blank NPs were subtracted for each reading.

3.2.6 Physicochemical characterisation of NPs

3.2.6.1 Measurement of size and zeta potential

The hydrodynamic size of NPs was measured using a NanoSight NS 500 instrument (NanoSight Ltd, Amesbury, UK), equipped with a sample chamber and syringe pump. All samples were diluted 10-fold in PBS (1 mM for phosphate, 13 mM for sodium chloride, pH 7.4) prior to measurement. Nanoparticle Tracking Analysis (NTA) 2.2 software was used to control the measurement process, to capture, and analyse data. The injection tube was immersed in 1 mL of sample solution, and the machine automatically loaded a sample into the viewing unit. Three recordings were obtained for each sample. The instrument settings were standardised for measuring each type of NP. Particle concentration was acquired from the NanoSight report. Protein density on each NP preparation was calculated as follows:

$$protein\ density\ (molecule\ per\ particle) = \frac{c \times 10^6 \times N}{M \times cp}$$

c: the concentration of protein on NPs in 1 mL

M: molecular weight of protein

cp: number of nanoparticles in 1 mL

N: Avogadro's number, 6.022×10^{23} mol^{-1}

Zeta potential measurements were performed in triplicate in a Malvern ZetaSizer Nano instrument (Malvern Instruments Limited, Malvern, UK) at 25 °C.

3.2.6.2 Transmission Electron Microscopy

The morphological analyses of fPS NPs and AC NPs were performed using TEM (JEOL JEM1200EXII). Samples were diluted 10-fold in PBS (pH 7.4). A suspension of NPs was then dropped onto carbon-coated copper grids (FC300Cu, EM Resolutions) with the liquid being quickly removed by touching the edge of the grid to filter paper. Negative staining was performed using uranyl acetate to treat samples for 30 seconds, which was also removed by filter paper absorption. Samples were stored desiccated after air drying (179).

3.2.6.3 Fluorescence excitation/emission spectra of fPS NPs

Fluorescence intensity is related to the concentration of a fluorescent molecule but also to its environment; under certain circumstances the intensity of a fluorescent molecule can be quenched (204). The change in fluorescence intensity of fPS NPs is probably one way of showing the presence of proteins on NPs surface. 100 µL volumes of fPS NPs, fPS NPs-BSA and fPS NPs-ntPE solutions were displayed in a 96 well microplate (655086, Cell culture microplate, 96 well, F-bottom, black, Cellstar®, Greiner bio-one), and the fluorescence spectra of these fPS NPs were performed using a microplate reader (FLUOstar Omega Microplate Reader, BMG LABTCH), with an excitation and emission wavelength range of 475 – 576 nm and 545 – 660 nm, respectively. Excitation and emission spectra of each fPS NPs were performed in triplicate.

3.2.6.4 Attenuated Total Reflection Fourier Transform Infrared Spectroscopy

FTIR is a well-established technique for providing information on molecular structure and interactions. ATR FTIR is able to measure a wide variety of solid and liquid samples without the need for complex preparations. FTIR spectra were obtained by using a Perkin Elmer Frontier Optica FTIR spectrometer equipped with a mercury cadmium telluride (MCT) detector (Perkin Elmer). Correction of the buffer was carried out before each measurement. A drop of AC NPs, AC NPs-BSA and AC NPs-ntPE solution was placed on the ATR crystal and the signals were obtained under the wavenumber from 4000 to 600 cm^{-1} at a resolution of 4 cm^{-1}.

3.2.6.5 Fluorescent labelling of AC NPs

In order to understand the chemical linkage of protein with AC NPs at a molecular level, a fluorescent label was used to detect the free aldehyde groups on the surface of AC NPs before and after the linkage with proteins. FTSC (fluorescein-5-thiosemicarbazide, MW=421.3 g/mole, 46985, Sigma-Aldrich, λ_{ex}= 492 nm; λ_{em}=516 nm) was used to react with aldehyde groups on oxidised AC NPs prior to reaction with proteins. 150 µg of FTSC was added into 2 mL of oxidised AC NPs solution and incubated for 4 h at 37 °C. Unreacted FTSC was removed by overnight dialysis (SnakeSkin™ Dialysis tubing, 10K MWCO, 68100, Thermo Fisher Scientific) against water at RT. The amount of FTSC on AC NPs was used to determine the total amount of aldehyde groups on AC NPs (labelled as A_T). The same batch of AC NPs were reacted with EMCH-BSA or EMCH-ntPE as described in section 3.2.4.3, and then 2 mL of AC NPs coupled to EMCH-

BSA or EMCH-ntPE were reacted with 150 µg of FTSC. The extent of FTSC reacted with free aldehyde groups on AC NPs coupled to EMCH-BSA or EMCH-ntPE was quantified and defined as A_N. Reacted aldehyde groups were calculated by the difference between the total amount of aldehydes on NPs and the free aldehyde groups ($A_R = A_T - A_N$) after the conjugation with proteins. The amount of FTSC was measured in a microplate reader (205). All experiments were performed in triplicate.

3.3 Results and discussion

3.3.1 Expression and purification of ntPE-TEV-H_6 protein

ntPE secretion into the bacterial periplasm was facilitated by the OmpA signal sequence in the plasmid. It is believed that the oxidising environment in the periplasm facilitates the formation of disulphide bonds in ntPE, promotes protein folding and preserves protein stability (206). A hexa-histidine sequence (CENLYFQSGTCHHHHHH) was inserted into the plasmid at the C-terminus of the ntPE open reading frame (ntPE-TEV-H_6), which facilitated capture purification methods. This C-terminus location of H_6 instead of an N-terminus ensures that only full-length protein, not partially expressed or truncated form of ntPE, would be captured by the initial purification step that involved immobilised nickel ion affinity chromatography (IMAC). Followed by the hexa-histidine sequence, a tobacco etch virus (TEV) protease-specific sequence was inserted into the plasmid which allowed the introduction of a single free thiol for the subsequent chemical coupling.

A representative IMAC purification step for ntPE-TEV-H_6 showed extensive amounts of UV-absorbing materials (280 nm) obtained from the bacterial periplasm that are present in the column flow through, as shown in Figure 3-3a and indicted by the blue arrow. Elution of the desired ntPE-TEV-H_6 was achieved by switching to the imidazole buffer (Figure 3-3a, red arrow). Eluted ntPE-TEV-H_6 material, captured in fractions A3-A4, was separated by SDS-PAGE (Figure 3-3b). Comparing proteins from *E.coli* before and after IPTG induction (shown in Figure 3-3b at lane 1 and lane 2 respectively), there was one band appearing around 70 kDa in lane 2, suggesting proteins were induced to express after the addition of IPTG. Following the initial purification using IMAC, the eluted proteins were collected, analysed and shown in Figure 3-3b at lane 4 and lane 5 around 70 kDa; their molecular weight corresponds to the molecular weight of ntPE-TEV-H_6 which is 68 kDa (207) .

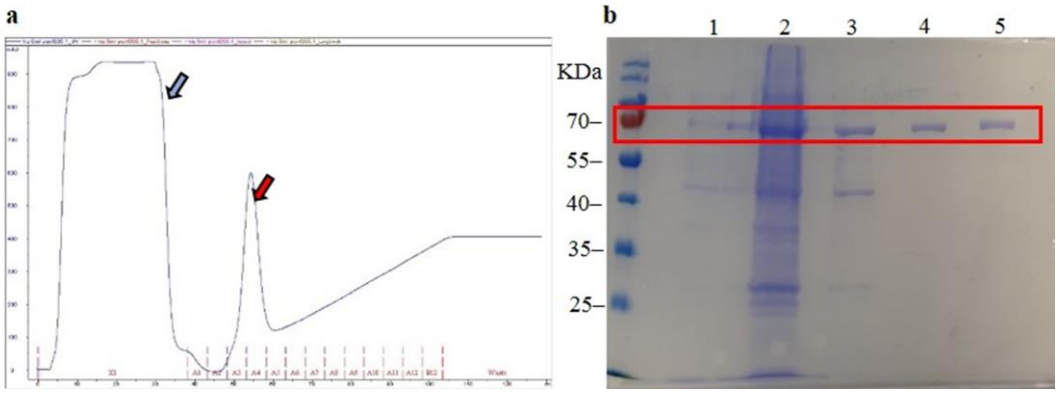

Figure 3-3: ntPE purification by IMAC. (a) Chromatogram obtained by IMAC. Extensive amounts of UV-absorbing materials passed through the column first (blue arrow) and then ntPE-TEV-H_6 were released from the column and collected in tubes A3–A4 (red arrow) with the elution of the imidazole buffer. (b) Coomassie blue-stained SDS-PAGE analysis shows how the IMAC step was used to isolate ntPE-TEV-H_6. Lane 1, protein from *E. coli* before the IPTG induction; lane 2, proteins from *E.coli* after IPTC induction; lane 3, protein extracted in osmotic shock solution; lane 4 and lane 5 protein fractions corresponding to the UV peaks in (a), A3–A4.

Following IMAC purification, SEC was used to further purify monomeric ntPE-TEV-H_6. As IMAC is an affinity purification process which would enrich aggregated or fragmented forms of this protein, as well as unrelated materials produced by *E. coli* that might interact with nickel ions within the histidine column.

Proteins eluted from the SEC column were collected corresponding to fractions A6–A12 (Figure 3-4, red arrow), and were analysed in SDS-PAGE (Figure 3-4b). It appeared that there were some aggregated forms of ntPE (as circled in Figure 3-4b, lane 1) and some fragments (as circled in Figure 3-4b, lane 6). Considering they were in low quantity, most of the protein shown in Figure 3-4 lanes 2–5 was believed to be monomeric ntPE-TEV-H_6.

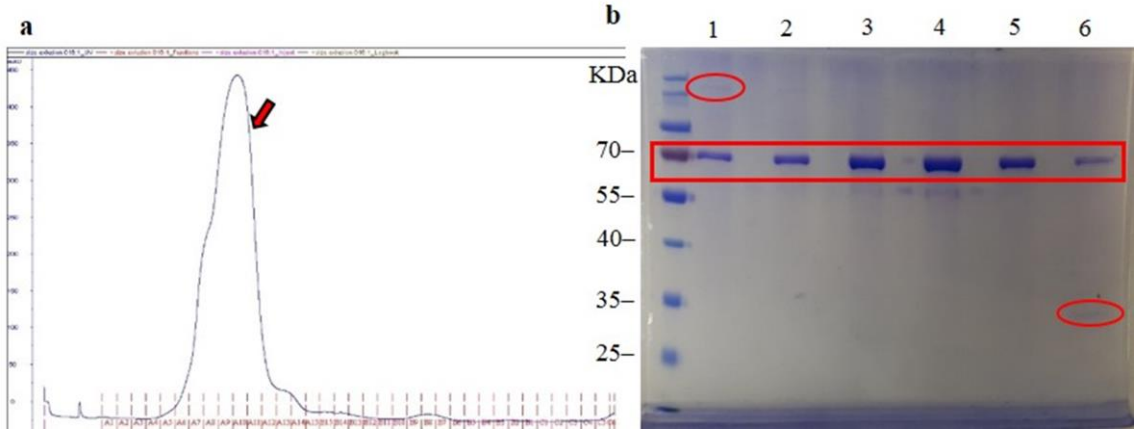

Figure 3-4: Purification of nt-PE by SEC. (a) Chromatogram obtained by SEC. Large amounts of UV-absorbing materials passed through the SE column and collected in the tube from A6 to A12 (red arrow). (b) Coomassie blue-stained SDS-PAGE analysis of nt-PE fractions corresponding to the UV peaks in (a), lane 1-lane 6, corresponding to A6–A12.There were some aggregated forms of ntPE-TEV-H_6 in lane 1, and some fragments in lane 6. The rest of the protein collected in A7–A11 corresponding to lane 2 – lane 5 was considered to be the monomeric form of ntPE-TEV-H6.

3.3.2 Preparation of protein for chemical linkage with NPs

3.3.2.1 TEV cleavage of ntPE-TEV-H_6 and the preparation of EMCH-ntPE for chemical linkage with NPs

The C-terminal TEV cleavage sequence (CENLYFQ√SGTCHHHHHH) in ntPE-TEV-H_6 exposed an unpaired cysteine residue for selective conjugation; the cleavage reaction and purification process is illustrated in Figure 3-5. The H_6 tag was separated from ntPE-CENLFQ using a HisTrap column, which would allow ntPE-CENLFQ to go through the column and to be collected, whilst the H_6 tag was trapped inside the column. The conjugation of ntPE and NPs was achieved by a heterobifunctional chemical cross-linker, EMCH, the maleimide end of which reacted with thiol groups on ntPE-TEV-H_6; while its hydrazide groups reacted with carboxyl groups at the surface of NPs (illustrated in Figure 3-5) (208).

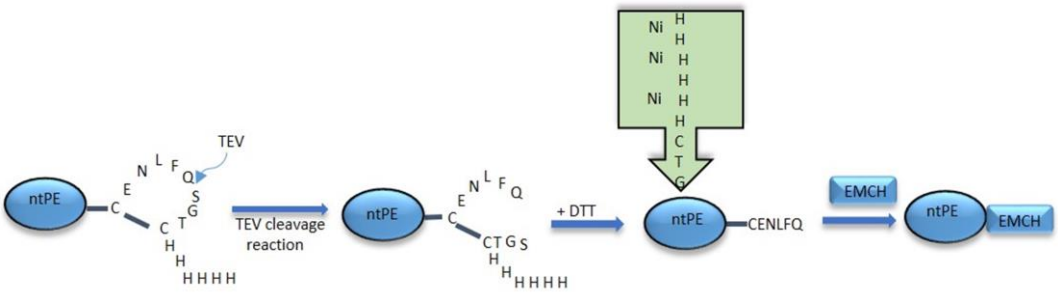

Figure 3-5: Illustration of the preparation process of EMCH-ntPE. TEV protease opened an unpaired cysteine residue of ntPE-TEV-H6 for thiol-maleimide reaction with EMCH, and the H_6 tag was removed using a HisTrap column.

3.3.2.2 Preparation of EMCH-BSA for chemical linkage with NPs

BSA served as a negative control due to its similarity in structure and physicochemical properties to ntPE (200, 201). Calculated by Ellman's reagent, there were 5 mM of thiol groups in a 12 mM BSA solution, suggesting that ~42 % of BSA molecules have free thiol groups on average. In order to mimic the organisation of thiol-ntPE (Figure 3-6), each BSA was allowed to carry one thiol group after different amounts of Traut's reagent had reacted with BSA (209). One thiol group for each BSA molecule was kept consistently with a 3-fold mole excess of Traut's reagent over BSA. EMCH was coupled to thiol-BSA using the same protocol as for thiol-ntPE.

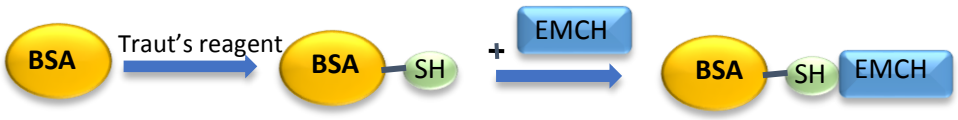

Figure 3-6: Illustration of the preparation process for EMCH-BSA. Amine groups on BSA were converted into thiol groups and linked with maleimide groups from EMCH

3.3.3 Preparation of fPS NPs-BSA conjugate and fPS NPs-ntPE conjugate

A commercial and stable nano-system, fPS NPs, was used to verify the chemical linking process. The carboxylate groups on the surface of the fPS NPs were linked with EMCH-BSA or EMCH-ntPE as illustrated in Figure 3-7.

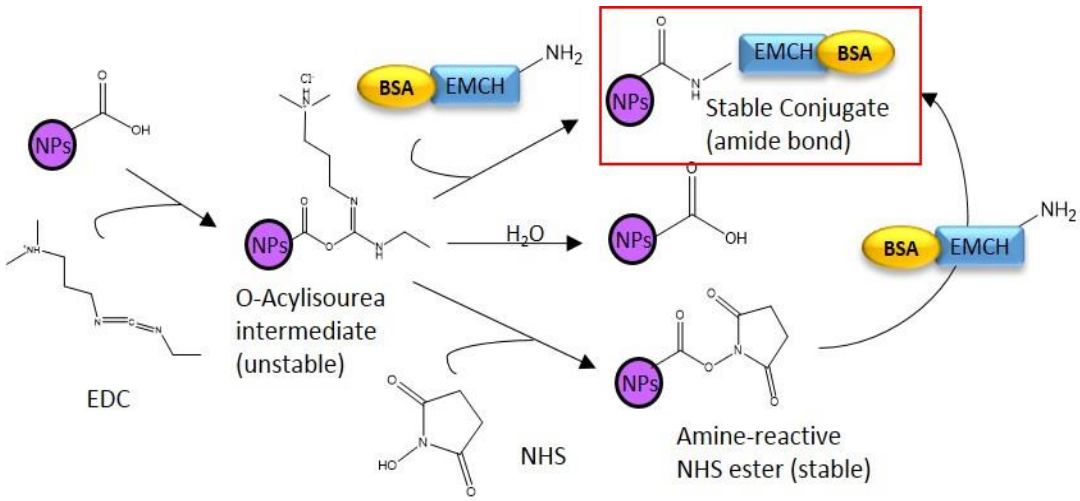

Figure 3-7: Illustration of EDC and NHS coupling. EDC and NHS form a more stable intermediate, amine-reactive NHS ester for improving the amine and carboxylate reaction efficiency between EMCH-BSA and fPS NPs.

Using EDC and NHS in the chemical reaction between fPS NPs and EMCH-BSA (or EMCH-ntPE) is believed to increase the amine-carboxylate reaction efficiency. It has been proposed that EDC reacts with carboxyl groups from fPS NPs and forms an active O-acylisourea intermediate. The intermediate is not stable and can hydrolyse easily in aqueous solutions (in Figure 3-7). NHS was added into the reaction mixture to improve the reaction efficiency by forming a more stable intermediate with EDC and allowing more efficient conjugation with hydrazine groups from EMCH (203). This conjugation reaction was carried out in a mild environment which favours preserving protein structures, and the by-products generated were excluded from the solution via ultra-centrifugation in this study.

3.3.4 Physicochemical characterisation of fPS NPs-BSA and fPS NPs-ntPE

Following the conjugation of proteins onto NPs, different techniques were used to verify the linkage and explore their physicochemical properties.

Particle size measurement was performed using a NanoSight instrument, which is based on the mechanism of DLS. Blank fPS NPs (fPS NPs without protein) had a diameter of ~134 ± 22 nm, the addition of BSA altered the size to ~151 ± 26 nm (see Table 3-1). It was anticipated from a previous study that adding BSA onto the surface of NPs would increase particle size (210). Based on the particle size measured in this study, the surface area for each particle was approximately ~5.6×10^4 nm^2, according to the calculated protein density (shown in Table 3-1), there were ~1.26×10^4 BSA molecules on each NP. It is known that the ellipsoid dimensions of BSA is 3.8 × 3.8× 14.0 nm (211), assuming the diameter of BSA was 4 nm when it was coupled onto a NP, BSA would occupy ~5.0×10^4 nm^2 on each particle, and thus, it is reasonable to propose that BSA molecules were distributed on NP with different orientations, considering there was 17 nm measured increase in thickness. It is also important to note that all these calculations were based on the assumption that NP and BSA molecules are spherical, however, that may not always represent the real situation.

The particle size of fPS NPs-ntPE was ~111 ± 10 nm in diameter, no size increase was observed comparing to blank fPS NPs. Particle size measured by DLS reflects the hydrodynamic size, i.e., NP size plus a hydration layer on the surface. Therefore, the observed small particle size of fPS NPs-ntPE might be due to the hydrophilic carboxylate groups on fPS NPs being replaced by less hydrophilic ntPE; or the hydrophilic carboxylate groups on the surface being blocked by the protein. Overall this may suggested a thinner hydration layer around fPS NPs, resulting in smaller measured size. The surface area of each fPS NP was calculated to be 5.6×10^4 nm^2, if

ntPE diameter was assumed to be 4 nm as BSA, then ntPE would occupy 3.76×10^4 nm^2, thus suggesting ntPE were presumably located on NP with different orientations.

Table 3-1: Characterisation of polystyrene nanoparticles (n=3)

	Blank fPS NPs	fPS NPs-BSA	fPS NPs-ntPE
Particle size (nm) from Nanosight	134 ± 22	151 ± 26	111 ± 10
Particle size (nm) from TEM	32 ± 10	44 ± 13	38 ± 14
Zeta potential (mV)	-30 ± 2	-20 ± 5	-20 ± 0.4
Protein density (protein molecule per particle)	---	$1.26 \pm 0.37 \times 10^4$	$9.38 \pm 3.3 \times 10^3$

Zeta potential is an indication of the NP surface charge, thereby, the observed changes in zeta potential can be considered as evidence of proteins conjugation on NPs. For blank fPS NPs, zeta potential was -30 ± 2 mV measured using ZetaSizer, while after conjugation zeta potential changed to -20 ± 5 mV for fPS NPs-BSA and -20 ± 0.4 mV for fPS NPs-ntPE. The changes in zeta potential might be related to the additional proteins on NPs surface. Since blank fPS NPs were prepared and measured using the same protocol as fPS NPs-BSA and fPS NPs-ntPE, it excluded potential changes brought from chemical reagents or experimental processes. Originally, fPS NPs were negatively charged due to carboxylate groups on the surface, which were ionised at the pH where the measurement was carried out (pH 6.5). It can be understood that the replacement of these carboxylate groups with less acidic molecules, for instance, ntPE (pI=5.53, calculated by using ExPASy ProtParam) and BSA (pI=4.7) (207, 212), resulted in the increase of zeta potential values, as shown in Table 3-1. In addition, some positively charged residues of proteins would compensate the negatively charged surface on NPs.

It was difficult to compare the protein density calculated in this study to other similar reports, since every report used different ways of interpreting protein density, for instance, $\mu g/m^2$ and protein per particle (213, 214). The lack of standard units and interpretation of protein density is due to the inaccurate and unstandardised NP counting methods. So far, each of the reported methods for determining the number of NPs has the potential of biased counting or misleading information. Some mathematical calculations were based on the assumption that an individual NP is an atom or a single sphere. These different underlying assumptions might lead to considerable errors when it comes to protein density (215). Besides, there is also discrepancy between

mathematical calculation of the numbers of NPs and the experimental data, therefore, the number of NPs in 1 mL was directly obtained from NTA measurements reported in this study.

The morphology of the NPs was observed using TEM. fPS NPs were spherical in shape and had a diameter of ~32 ± 10 nm (n=100, in Figure 3-8). Particle size measured by TEM was smaller than the measurement from NanoSight, this has been also reported by other researchers (185). Perhaps this discrepancy is because NanoSight measures the hydrodynamic diameter of NPs, which refers to NPs along with the solvent layer, while TEM images were taken on dried samples. In addition, the difference in particle size is probably a result of the multiple scattering effect in DLS; which occurs when the light scattered by the diffusing particle is re-scattered by one or more particles before reaching the detector (186).

After the conjugation with proteins, fPS NPs were still in a similar shape, with fPS NPs-BSA having a diameter of 44 ± 13 nm and fPS NPs-ntPE having a diameter of 38 ± 13 nm (in Figure 3-8 and Table 3-1). The contrast seemed to be stronger for fPS NPs-BSA and fPS NPs-ntPE than for blank fPS NPs. Perhaps the proteins on the surface of fPS NPs made the binding with uranyl ions stronger, which resulted in higher contrast in the TEM images (216).

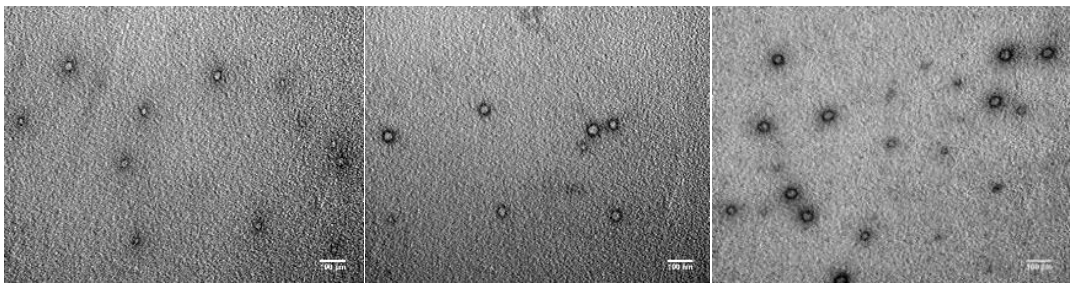

Blank fPS NPs fPS NPs-BSA fPS NPs-ntPE

Figure 3-8: TEM images of fPS NPs. NPs were in the size range of ~40 nm; after the addition of BSA or ntPE onto NPs, they appeared to be a similar size and shape (scale bar = 100 nm).

The fluorescent properties of fPS NPs also provide a perspective for physicochemical characterisation. Complex-formation is believed to be one of the causes of fluorescence quenching; it is reasonable to hypothesise that the fluorescence intensity of fPS NPs would change accordingly if proteins were on the surface of the NPs (204). The fluorescence excitation/emission spectra of fPS NPs were obtained before and after the conjugation with proteins. The excitation spectrum was determined by monitoring fluorescence emission at the wavelength of maximum intensity while the fluorophore is excited through consecutive wavelengths. Regarding the absorbed energy that molecules needed to be promoted to the excited electronic singlet state S_1, for fPS NPs-BSA and fPS NPs-ntPE (in Figure 3-9a), it seemed lower energy was needed. A reduced fluorescence intensity was also observed in the emission spectrum of fPS NPs-BSA and fPS NPs-ntPE compared to blank fPS NPs (Figure 3-9b). The observed fluorescence quenching in both excitation and emission spectra were considered and clarified as static quenching, which occurs when a ground state complex forms before excitation occurs (217). The ground state complex was understood to be the fPS NPs-protein conjugation in this study.

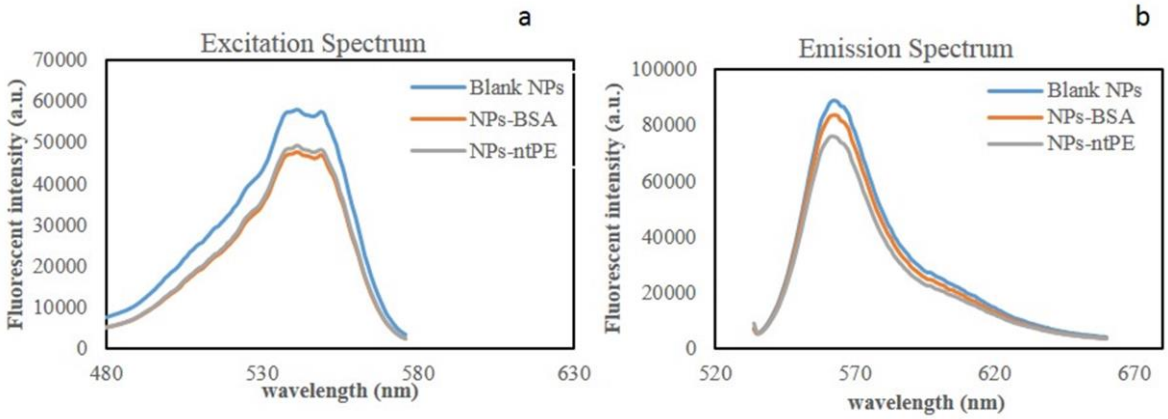

Figure 3-9: Fluorescence excitation and emission spectra of fPS NPs. The fluorescence quenching was observed in fPS NPs-BSA and fPS NPs-ntPE in both excitation and emission spectra compared to blank fPS NPs.

3.3.5 Conjugation of AC NPs-BSA and AC NPs-ntPE

3.3.5.1 Preparation of oxidised AC NPs

As discussed in chapter 2, AC NPs offer more chance for modification, since both alginate and chitosan can be directly coupled with proteins or chemically modified to be coupled. Aldehyde groups were introduced by the oxidation of alginate before particles were formed, for the purpose of conjugation with the hydrazide groups of EMCH.

The oxidised alginate was used to prepare AC NPs in the same way as un-oxidised alginate (details are in Chapter 2.2.3). Both oxidised and un-oxidised AC NPs were characterised by particle size and surface charge. By DLS, the diameter of the oxidised AC NPs was ~185 ± 5 nm, while the un-oxidised AC NPs was ~266 ± 18 nm (in Table 3-2), suggesting that AC NPs became smaller when oxidised materials were used. The size of the NPs was reported to be influenced by polymer concentrations and molecular weight (155). During the oxidation process, the reduction in molecular weight of alginate is not inevitable, therefore, the reduced NPs size might be due to the reduced molecular weight of alginate (188).

Table 3-2: Characterisation of oxidised AC NPs and un-oxidised AC NPs (n=3)

	Un-oxidised AC NPs	Oxidised AC NPs
Size from DLS (nm)	266±18	185±5
Polydispersity index	0.30±0.01	0.24±0.02
Zeta potential (mV)	18±5	28±4

Oxidised-AC NPs had a higher zeta potential compared to un-oxidised AC NPs. AC NPs were formed mainly due to the electrostatic interactions between oppositely charged alginate and chitosan (7). In the oxidisation process of alginate, sodium periodate broke down the guluronate ring at the position of C-2 and C-3 of alginate and induced two aldehyde groups (illustrated in Figure 3-10). The induced aldehyde groups were believed to give alginate polymer more negatively charged groups, with the result that more chitosan molecules were attracted on the surface and leading to a higher surface charge measurement (218).

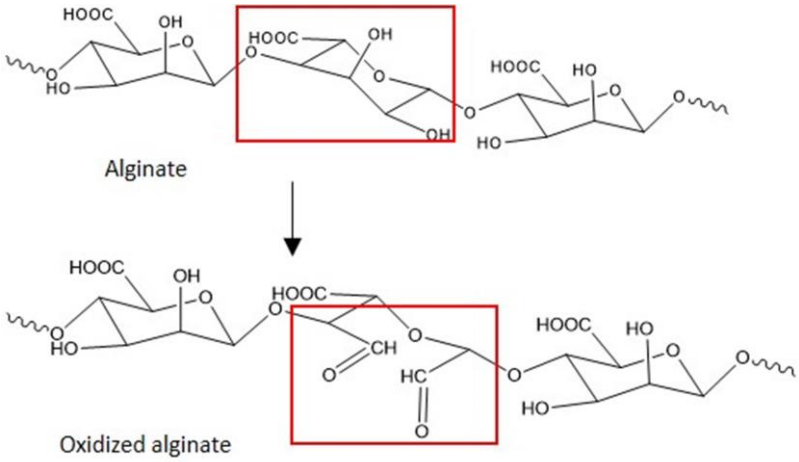

Figure 3-10: The oxidisation of alginate. The oxidation process induced two aldehyde groups on the guluronate ring of alginate.

3.3.5.2 Physicochemical characterisation of AC NPs-BSA and AC NPs-ntPE

By DLS measurement, the size of AC NPs had increased from 215 ± 8 nm to 280 ± 9 nm after the addition of BSA onto the surface (in Table 3-3), while it had reduced to 202 ± 20 nm after the conjugation with ntPE. Particle size increase in AC NPs-BSA and size decrease in AC NPs-ntPE was consistent with the findings for fPS NPs in section 3.3.4. The zeta potential of blank AC NPs was 20 ± 8 mV and it was attributed to the presence of chitosan on the surface; after the addition of BSA and ntPE, zeta potential dropped to -19 ± 11 and -6 ± 5 mV for AC NPs-BSA and AC NPs-ntPE respectively. The pIs of BSA and ntPE are both below the measurement condition, pH 7.4, thus these proteins were negatively charged in the solution. It seemed that the addition of negatively charged BSA and ntPE onto positively charged AC NPs resulted in a negatively charged surface as indicated in Table 3-3.

Table 3-3: Physicochemical Characterisations of AC NPs (n=3)

	Blank AC NPs	AC NPs-BSA	AC NPs-PE
Size (nm) from NanoSight	215 ± 8	280 ± 9	202 ± 20
Size (nm) from TEM	48 ± 14	48 ± 15	46 ± 24
Zeta potential (mV)	20 ± 8	-19 ± 11	-6 ± 5
Protein density	---	$3.30 \pm 0.90 \times 10^5$	$3.41 \pm 0.82 \times 10^5$

Protein density on AC NPs surface was calculated by the same equation used for fPS NPs (in 3.2.6.1). On average, there were 3.30 ± 0.90×10^5 BSA molecules on each AC NP and 3.41 ± 0.82×10^5 ntPE molecules on each AC NP. Comparing with fPS NPs, it seemed that AC NPs had more proteins on the surface. A possible explanation is that their different NP structures resulted in different organisations with protein. fPS NPs are solid NPs in the suspension and have a rigid spherical structure as shown in Figure 3-11. While, in contrast, AC NPs are polyelectrolyte complexes formed by polymeric interactions (7). In terms of structure, AC NPs were similar to a polymeric matrix, and might have some polymer extending out from the complex (142), as illustrated in Figure 3-11. These extended groups from AC NPs possibly linked with protein and left some distance between the NP and the protein. Therefore, perhaps the numbers of protein molecules were not restricted by the available functional sites on NP surface or by steric hindrance. In addition, proteins have shown a tendency to interact with the AC NPs via non-covalent bonds, such as hydrogen bonds or electrostatic interactions (219).

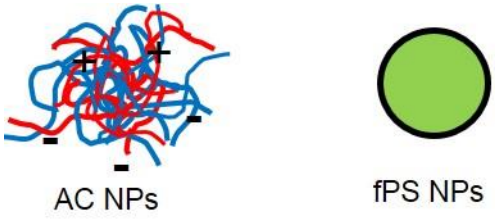

Figure 3-11: Illustration of AC NP and fPS NP. AC NP was formed by electrostatic interactions in a flexible structure, while fPS NP were solid and spherical.

Blank AC NPs were observed using TEM, and compared with AC NPs conjugated to BSA and ntPE. Blank AC NPs were ~48 ± 14 nm in size (n=100, see Figure 3-12), and some of them appeared to be aggregated forms. After the conjugation with proteins, AC NPs-BSA were ~48 ± 15 nm (n=100) in diameter and AC NPs-ntPE were ~46 ± 24 nm (n=100) in diameter. Although this may not represent all particles morphologies and sizes, TEM observation can at least provide a glimpse of NPs. Under TEM it appeared that the protein-coupled AC NPs have less aggregation. The presence of proteins on the surface can shield the NP from agglomeration, which could increase the colloidal stability and result in less aggregation (166).

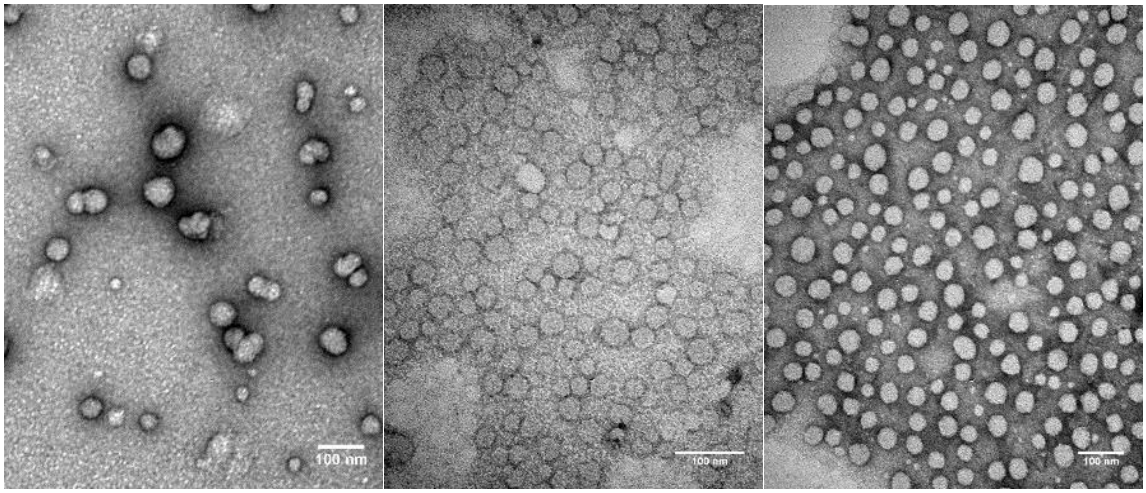

Blank AC NPs AC NPs-BSA AC NPs-ntPE

Figure 3-12: TEM images of AC NPs. Particles were ~48±14 nm in size, blank AC NPs tended to aggregate, while less aggregation was observed for AC NPs-BSA and AC NPs-ntPE.

.

3.3.5.3 FTIR spectra of AC NPs

AC NPs were characterised by FTIR and the spectra were compared before and after conjugation with BSA and ntPE.

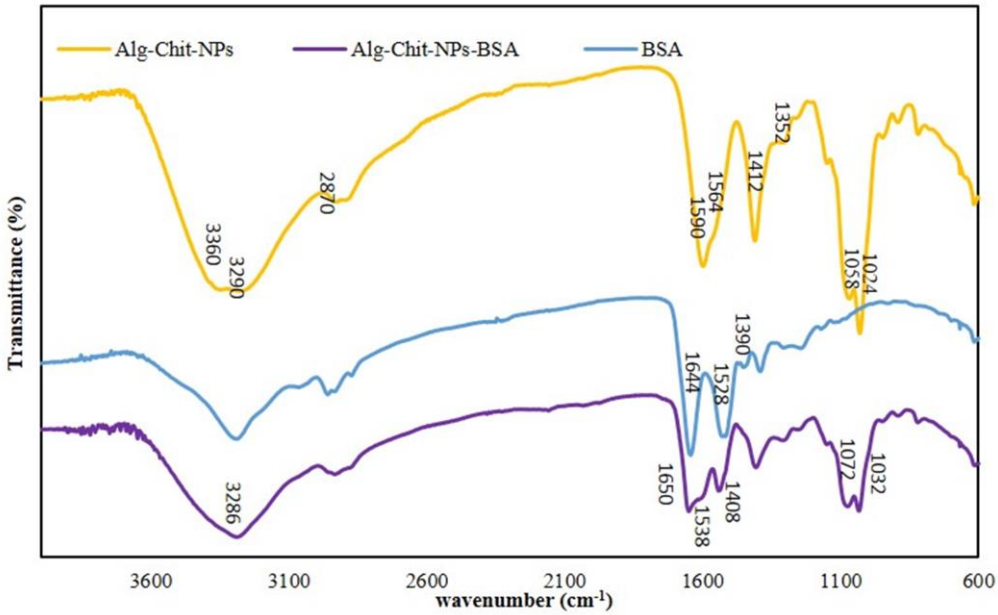

Figure 3-13: FTIR spectra of AC NPs and AC NPs-BSA. The broad peak at 3700-3000 cm^{-1} in AC NPs spectrum suggested the intermolecular hydrogen bonds between alginate and chitosan. The appearance of amine bonds (1538 cm^{-1}) in AC NPs-BSA suggested the presence of BSA.

The spectrum obtained from AC NPs showed strong intermolecular hydrogen bonds between alginate and chitosan at the broad peak of 3700-3000 cm^{-1} (in Figure 3-13), which is consistent with a previous study (220). The bands at 1590 cm^{-1} and 1412 cm^{-1} were identified as the antisymmetric stretch and symmetric stretch of alginate, respectively. Moreover, the band at 1564 cm^{-1} was assigned to bending vibrations of the N-H (N-acetylated residues, amide bond) from chitosan (170).

Proteins have characteristic absorption bonds in infrared spectra owing to the stretching vibrations of the C=O bond and the bending vibration of the N-H bond of the amine bond. The bands at 1644 cm^{-1} and 1528 cm^{-1} in the BSA spectrum was attributed to these two vibrations of amine bonds (221). In the spectrum generated from the AC NPs-BSA, the appearance of the peak at 1538 cm^{-1} was presumably due to the N-H bond of BSA. It suggested that there were BSA molecules associated with AC NPs, considering that the uncoupled BSA molecules were excluded from the system via dialysis.

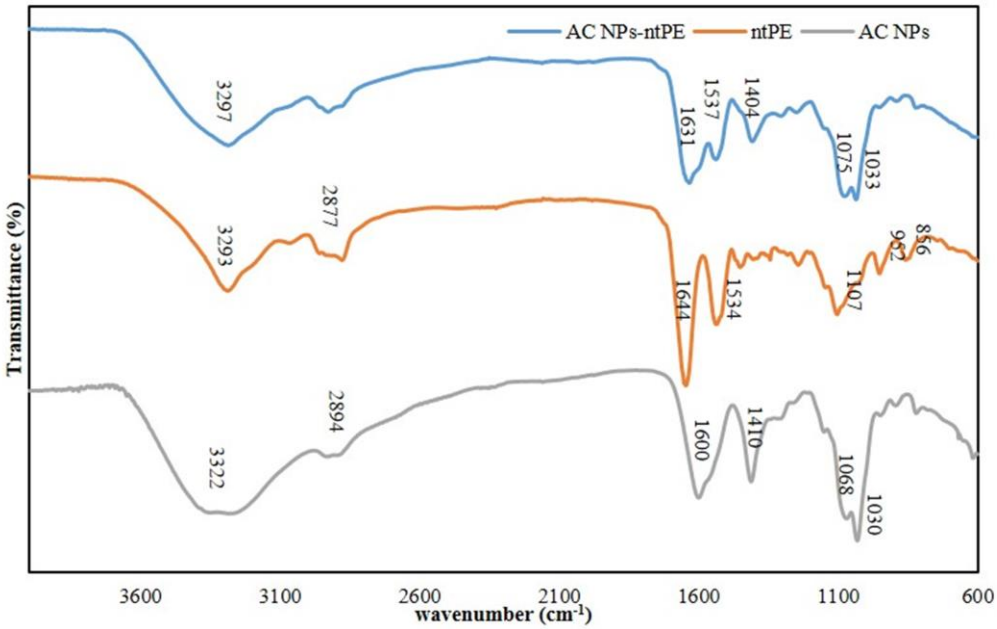

Figure 3-14: FTIR spectra of ntPE and AC NPs-ntPE. The appearance of the amine bonds (1631 cm^{-1}, 1537cm^{-1}) in AC NPs-ntPE spectrum confirmed the chemical conjugation of ntPE onto AC NPs.

In the spectrum of ntPE, the bands at 1644 cm^{-1} and 1534 cm^{-1} were considered to have resulted from the amine bonds (as shown in Figure 3-14). The appearance of the amine bonds in the AC NPs-ntPE spectrum suggested that ntPE was associated with AC NPs. In both cases, for BSA and ntPE, the detected protein bands in AC NPs system provided evidence that proteins were associated with AC NPs, however, further investigation is needed to establish whether they were covalently bonded or whether other types of bonding were involved.

3.3.5.4 Fluorescent labelling of AC NPs

A quantitative method was exploited in this study to understand the AC NP-protein conjugates. FTSC is a fluorescent label that can link with aldehyde groups on the AC NPs. Molecular level information about NP-protein conjugates may be revealed by comparing the FTSC on the surface of AC NPs before and after modifying the surface with proteins (illustrated in Figure 3-15).

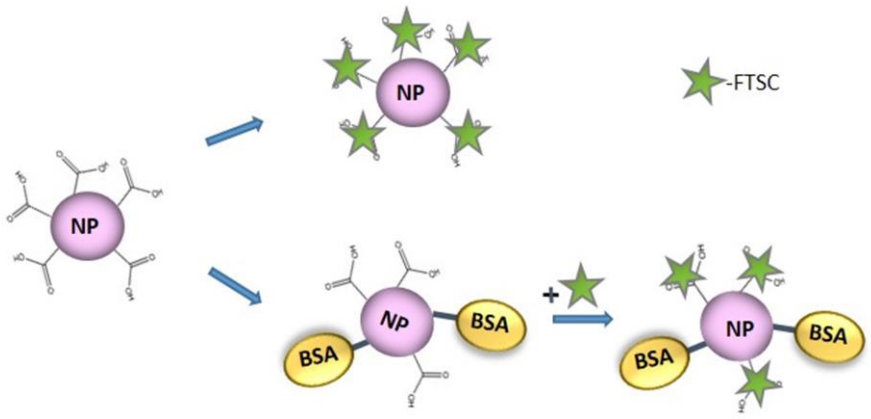

Figure 3-15: Illustration of labelling AC NP with FTSC. Before the conjugation of proteins onto NP, the amount of FTSC shows the amount of aldehyde groups on the surface of AC NP; after the conjugation with proteins, the amount of FTSC reflects the amount of functional groups that did not react with proteins.

Before the conjugation of proteins onto AC NPs, there were ~1.31 ± 0.15×10^{-9} moles of aldehyde groups on the surface of NPs per mL of suspension, suggested by the amount of FTSC which reacted with aldehyde groups on NPs (as shown in Table 3-4). After the conjugation with BSA, there were 1.01 ± 0.07×10^{-9} moles of free aldehyde groups on NPs accessible for FTSC to react with. This suggested that 2.98 ± 1.0×10^{-10} moles of aldehyde groups had reacted with BSA, and were therefore no longer accessible for FTSC. The same experiment was performed on AC NPs-ntPE. There were 1.19 ± 0.27×10^{-9} moles of aldehyde groups available on the surface of AC NPs before the protein-NP conjugation and 0.66 ± 0.24×10^{-9} moles of these aldehyde groups were occupied by proteins after the conjugation. The measurement and calculation of FTSC gave indirect quantitative information about the conjugation of AC NPs and BSA or ntPE.

Table 3-4: **Measurement of aldehyde groups on NPs (n=3)**

	AC NPs-BSA	AC NPs-PE
Total amount of aldehyde groups (mole) per mL of suspension	$1.31 \pm 0.15\times10^{-9}$	$1.19 \pm 0.27\times10^{-9}$
Amount of aldehyde groups which did not react with protein (mole) per mL of suspension	$1.01 \pm 0.07\times10^{-9}$	$0.66 \pm 0.24\times10^{-9}$
Amount of aldehyde groups which reacted with protein (mole) per mL of suspension	$2.98 \pm 1.0\times10^{-10}$	$5.26 \pm 2.32\times10^{-10}$

3.4 Conclusion

ntPE was expressed and purified for the purpose of conjugating with NPs. BSA was also prepared in a similar organisation, with one thiol group on each BSA molecule on average (as illustrated in Figure 3-16). These proteins were linked with NPs via a heterobifunctional cross-linker using EMCH.

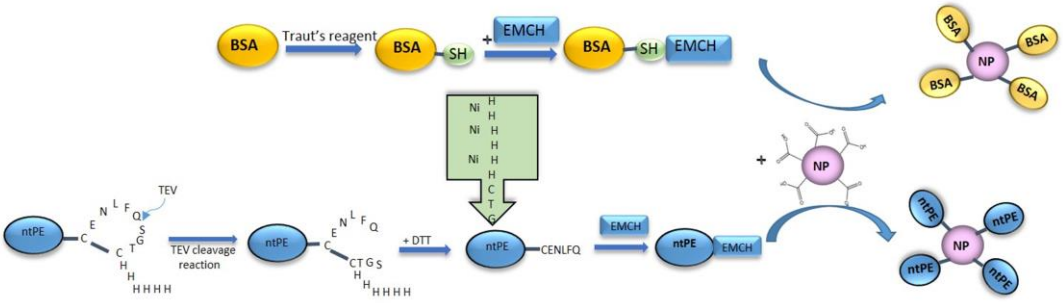

Figure 3-16: Diagram for preparing NPs-BSA and NPs-ntPE conjugate. TEV protease-specific sequence was used to induce a single free thiol group on ntPE for subsequent chemical coupling with EMCH, which served as a "bridge" between ntPE and NPs. BSA was prepared by converting amine groups into thiol groups using Traut's reagent, and linked with NPs involving EMCH in a similar manner as ntPE.

Commercial and stable fPS NPs were firstly used to test the conjugation method. With the conjugation of BSA and ntPE with NPs, the diameter of NPs changed from 134 ± 22 nm to 151 ± 26 nm for fPS NPs-BSA, and to 111 ± 10 nm for fPS NPs-ntPE. The increased size measurement in BSA-coupled fPS NPs was considered due to the conjugation of BSA on the surface of NPs. The relatively larger particle size of fPS NPs-BSA is consistent with the protein density values, of which $1.26 \pm 0.37\times10^{4}$ BSA molecules were measured on the surface of fPS NPs, while for

ntPE the value was 9.38 ± 3.3×10^3. The conjugation of proteins might have altered the hydrophobicity of NPs, which explains the reduced particle size for ntPE-coupled fPS NPs. The zeta potential of NPs also changed with the conjugation with BSA and ntPE, the zeta potential for blank fPS NPs, fPS NPs-BSA, and fPS NPs-ntPE was -30 ± 2 mV, -20 ± 5 mV and -20 ± 0.4 mV, respectively. Negative carboxylate groups on fPS NPs appeared to be covered by proteins on the surface. The reduced fluorescence intensity in the Ex/Em spectra suggested a static quenching, which involves the formation of a complex. These changes were attributed to the addition of BSA or ntPE on the NP's surface.

AC NPs were also conjugated with BSA and ntPE; changes in the physicochemical properties suggested the presence of proteins on AC NPs surface. The diameter of NPs changed from 215 ± 8 nm for blank AC NPs to 280 ± 9 nm for AC NPs-BSA, and to 202 ± 20 nm for AC NPs-ntPE. The zeta potential of blank AC NPs, AC NPs-BSA and AC NPs-ntPE was 20 ± 8 mV, -19 ± 11 mV, and -6 ± 5 mV respectively. On average, more protein molecules were present on the AC NPs than on the fPS NPs. This was considered due to their different NP structure, which leads to different arrangement of proteins on its surface. FTIR spectra suggested the presence of BSA and ntPE in the AC NPs suspension, and fluorescence labelling showed that certain amount of aldehyde groups on AC NPs (coupled with proteins) were no longer available for chemical coupling, which suggested these functional sites might have been occupied by proteins.

BSA and ntPE-coupled NPs were prepared and characterised in this chapter, enabling testing the hypothesis that ntPE would facilitate the transport of NPs *in vitro*, in the next Chapter.

Chapter 4 *In vitro* study of ntPE-coupled nanoparticles

Overview:

Aim: To study the transcytosis of NPs mediated by ntPE in an *in vitro* model using Caco-2 cell monolayers.

Methods: The trans-epithelial transport of fPS NPs (fluorescent polystyrene nanoparticles) and AC NPs (alginate-chitosan nanoparticles) mediated by ntPE (non-toxic *Pseudomonas* exotoxin) was tested in an *in vitro* model of human intestine using Caco-2 cell monolayers. Trans-epithelial electrical resistance was monitored during a 60-minute time course of transcytosis. Confocal microscopy was used to follow the fate of NPs with cell landmarks of Caco-2 cell nuclei and tight junction structures, being labelled with DAPI and an antibody to the tight junction-specific protein *zonula occludens* 1, respectively. Secondary structure of ntPE before and after its conjugation to AC NPs was examined using circular dichroism (CD). The effect of serum in the growth culture on the expression of the cell receptor for ntPE, LRP-1 (low density lipoprotein receptor-related protein 1), was analysed in the Caco-2 cell line by western blot.

Results and Discussion: Transcytosis rates across Caco-2 cell monolayers was 0.20 ± 0.13 %, 2.60 ± 1.1 %, and 0.21 ± 0.01 % for blank fPS NPs, fPS NPs-BSA, and fPS NPs-ntPE, respectively. A low transcytosis rate was also observed for all the AC NPs: for blank AC NPs it was 2.83 ± 1.29 %, for AC NPs-BSA it was 4.18 ± 2.05 %, and for AC NPs-ntPE it was 4.36 ± 2.24 %. The unexpectedly low transcytosis rates of NPs mediated by ntPE could have been due to a change in ntPE structure after attachment onto NPs. CD-based studies assessed the secondary structure of ntPE after its coupling onto AC NPs, however, the data did not suggest such changes were occurring. An attempt was made to examine the expression of LRP-1, a binding receptor of ntPE on the cells. The presence of serum in the growth medium did not significantly alter LRP-1 expression. Since ntPE has also been suggested to utilise the ganglioside GM1 as a cell receptor during intracellular trafficking (2), and a previous study demonstrated that GM1 has a considerable impact on the transport of ntPE (121), it is possible that the low expression of GM1 in the Caco-2 cell model may have led to disorganised cellular trafficking functions (222).

4.1 Introduction

Chapter 3 describes coupling ntPE onto fPS NPs and AC NPs. In this chapter, epithelial transcytosis of ntPE-coupled NPs across Caco-2 cell monolayers was examined.

Transporting NPs across the intestinal epithelium is a tremendous challenge, since the epithelium functions to selectively absorb nutrients while preventing the uptake of potential pathogenic materials and particles. The intestinal epithelium is a single layer of cells mainly composed of nutrient-absorbing enterocytes and mucus-secreting goblet cells. Much less frequently present are a wide variety of specialised cell types, such as micro-fold (M), Paneth, enteroendocrine, cup, and tuft cells (23). All of these are polarised cells, with the apical side exposed to the lumen and the basolateral side linked with *lamina propria* of the epithelium.

Three pathways are theoretically possible for NPs crossing the epithelium: 1) paracellular pathway; 2) transcytosis across the M cells involving mostly pinocytosis or phagocytosis; and 3) transcytosis across the enterocytes involving mostly endocytosis (Figure 4-1) (9).

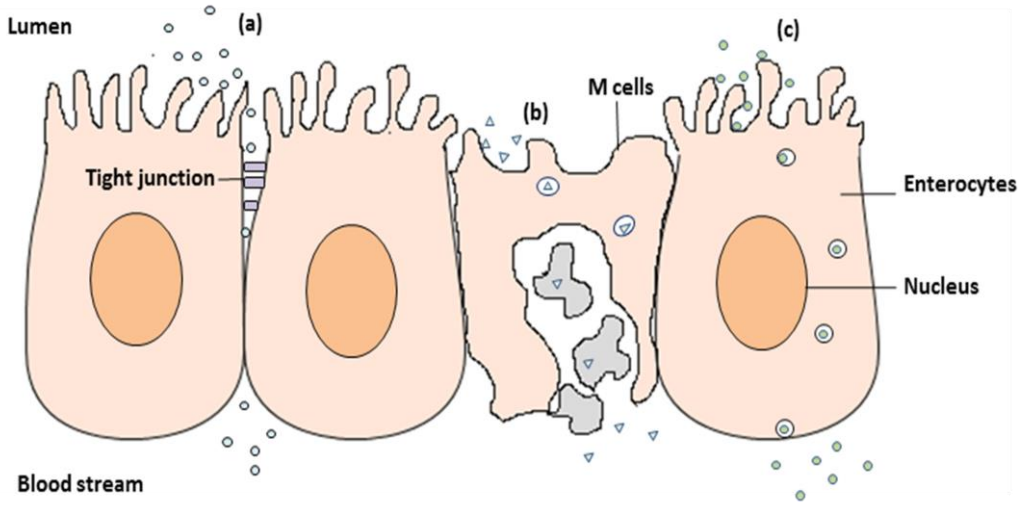

Figure 4-1: Three potential pathways for NPs crossing the epithelium. (a) Paracellular pathway: substances go across the epithelium by directly or indirectly opening tight junctions between two adjacent enterocytes; (b) Transcytosis across the M cells: M cells take up macromolecules and transport them into the underlying immune cells; (c) Transcytosis across the enterocytes: molecules are internalised into the cell via endocytosis and move from the apical to the basolateral side of the epithelium in an endosomal vesicle.

The intestinal epithelium is sealed by tight junctions, which contain transmembrane proteins that protrude into the intercellular space and regulate the paracellular movement of water, ions, and solutes (30). Opening tight junction is one strategy for overcoming the intestinal barrier for oral delivery of poorly-absorbed therapeutics. However, it carries the risk of introducing unintended substances into the body at the same time. In addition, the tightness of the junctions between the enterocytes (pore diameter between 3 and 10 Å) and the very small surface area of the intercellular spaces limits transporting NPs via the paracellular pathway (57, 223).

The second pathway for NPs to cross the epithelium is by transcytosis across M cells. Transcytosis involves particles being taken up into the cell via endocytosis on the apical membrane, and then being transported through the cells and released from the basolateral side (77). M cells are highly specialised microfold cells for the endocytosis and transport of antigens, i.e. macromolecules and bacteria, to immune cells residing under the epithelium (224). Although a certain amount of research has been conducted on attempting to deliver NPs via the M cells, Hussain *et al.* (1997) suggested that the pathway through M cells should not be over emphasised considering the numbers of M cells are limited in the intestine (82).

Finally, transcytosis across the enterocytes appears to be an alternative means of transporting NPs into the blood circulation. It involves endocytosis into the enterocyte, intracellular translocation and release from the basolateral side. This transport has the advantage of large surface area, as enterocytes are the most abundant cells in the epithelium. However, the transcytosis of NPs across the enterocytes is prone to generate a low transport rate. This is because either the endocytosed NPs would undertake the lysosome pathway leading to degradation, or the apical protein-NP complex would be easily delivered back to the apical side by exocytosis (197). A receptor-mediated transcytosis is needed to efficiently deliver NPs across the enterocytes. Lessons from nature have taught us some macromolecules can be transported across the enterocytes intact via a specific transport pathway, for instance, Vitamin B_{12}, lectins, Ig G, and bacterial toxins. Modifying NPs surface with these molecules has shown enhanced uptake and transport of NPs across the epithelium (87, 91, 95, 225).

The transport strategy in this study is to conjugate NPs with a bacterial toxin, so that the bacterial toxin could facilitate the transport of NPs via the transcytosis pathway utilised by the toxin. Specifically, *Pseudomonas* exotoxin A (PE) was used to try and enhance the uptake and transport of NPs. PE is a major virulence factor extracted from *Pseudomonas aeruginosa*. It can go across the epithelium and target the antigen-presenting cells present in the submucosal space. PE consists of three prominent domains: domain Ia binds to the low density lipoprotein receptor-related protein (LRP-1) on the cell membrane to allow entry into the cell (226); domain II facilitates the intracellular trafficking within the cell after internalisation in a clathrin-coated vesicle; and domain III is the catalytic domain which functions to enzymatically stop protein

synthesis and induce cell apoptosis (227, 228). The toxicity of PE can be removed by the deletion of the glutamic acid at position 553, referred to as ntPE (for non-toxic PE) (119). ntPE is able to transport across the polarised cells at equal rates to PE (229), therefore, it has been chosen as a transport ligand for NPs in this study.

The Caco-2 cell line, which is derived from human colorectal carcinoma, is a standard *in vitro* model, used in this work to mimic human intestinal epithelium. Importantly, a good correlation has been found for drug absorption in human jejunum and Caco-2 cells, especially for passively absorbed drugs; various transporters, enzymes, and receptors present in human intestinal epithelial are also expressed by Caco-2 cells (230). In a typical Caco-2 cell experiment, a confluent monolayer of cells are grown on a permeable filter until they become polarised. These Caco-2 monolayers differentiate both structurally and functionally into cells resembling mature enterocytes; they express the majority of morphological and functional characteristics of enterocytes. By culturing Caco-2 cells in this way, the apical and basolateral compartments of the Transwell® (Figure 4-2) correspond to the intestinal lumen side and the *lamina propria in vivo* (231).

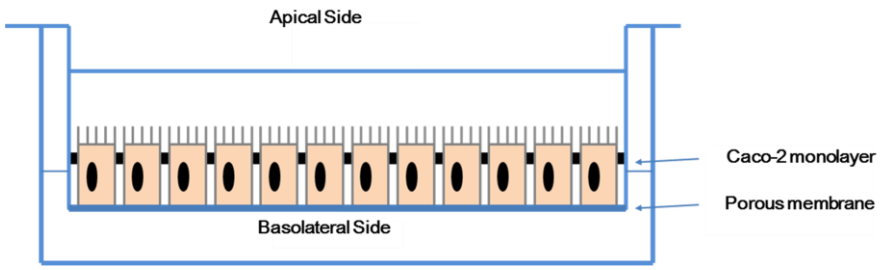

Figure 4-2 : Diagram for Caco-2 cell monolayers on Transwell®. Caco-2 cells are seated on the membrane of Tranwell® plate, as the apical side representing the luminal side of the epithelium and the basolateral side corresponds to the *lamina propria*.

In this chapter, the transport of stable fPS NPs and biodegradable AC NPs, which are both coupled with ntPE or BSA, were tested using Caco-2 cell monolayers, with BSA-coupled NPs severing as a negative control.

4.2 Methods

4.2.1 Subculture of Caco-2 cell line

Caco-2 cells were obtained from the American Type Culture Collection and grown in T75 flasks (156499, Thermo Scientific) in Dulbecco Modified Eagle Medium (1813348, Life Technologies) containing 10 % heat-inactivated foetal bovine serum (10500, Life Technologies) and 50 IU each of penicillin and streptomycin (P/S, P4333-100ML, Sigma-Aldrich). Cells were sub-cultured after reaching 60 – 70 % confluency. After medium removal, cells were rinsed with PBS before adding 0.25 % trypsin (*v/v*, 15090-046, Life Technologies) containing 0.02 % of EDTA (*w/v* Ethylenediaminetetra-acetic acid, E9884-100G, Sigma-Aldrich). Trypsin was inactivated by adding growth medium in a 1:1 ratio after a period of time when most of the cells had detached from the flask. Suspended cells were centrifuged at 125 × *g* for 5 min (accuSpin™ 400, Fisher Scientific). Pelleted cells were suspended in fresh growth medium, counted under a light microscope using a haemocytometer and diluted before being seeded at a desired cell density into a new T75 flask or onto Transwell® filters.

4.2.2 Transcytosis of fPS NPs

Sub-cultured Caco-2 cells were plated at a density of ~21,000 cells/well onto polycarbonate membrane Transwell® filters (6.5 mm, 0.4 µm pore size) from Corning Incorporated (Corning, NY, USA). Growth medium was changed every other day until cells differentiated into polarised epithelial cells (typically after 18 days). Cells were considered polarised when their trans-epithelial electrical resistance (TEER) was > 350 $\Omega \cdot cm^2$, as measured using an EVOM2 Epithelial Volt/Ohm Meter (World Precision Instruments).

Once polarised, each Caco-2 monolayer was prepared for transcytosis studies by washing both apical (150 µL) and basolateral (500 µL) surfaces twice for 5 min with warm HBSS (Hank's balanced salt solution, 14025-050, Invitrogen, Life Technologies) at 37°C. After equilibration in HBSS for 30 min at 37 °C, the basolateral compartment medium was collected to provide a baseline value for t=0. After replacing the basolateral compartment medium with fresh HBSS, test materials were applied onto the apical surface. Basolateral compartment medium was then collected with replacement after 30 and 60 min of incubation at 37 °C. These studies were used to assess the transcytosis of fPS-NPs conjugated with ntPE. Various control materials were tested, including fPS-NPs without any modification, and fPS NPs conjugated with BSA which was selected owing to its similar size and isoelectric point to ntPE.

Before performing a transcytosis study, the fluorescence intensity (termed Fb) of the materials being tested for transport was measured using a fluorescence microplate reader (FLUOstar Omega, BMG Labtech). 150 µL of fPS NPs, fPS NPs-BSA, or fPS NPs-ntPE (the concentration of protein in NPs suspension was kept at 66 µg/mL), were added to the apical compartment with transport studies being performed in triplicate. The fluorescence intensity of each sample (Fs) collected from the basolateral compartment was assayed in triplicate using a fluorescence microplate reader. Fluorescence values of the initial HBSS solutions collected at 0 min (F0) were subtracted to obtain the extent of fPS NP transcytosis. During the experiment, TEER was measured at each time interval to ensure cells were still polarised (>350 $\Omega \cdot cm^{-2}$). The transport efficiency of fPS NP preparations was calculated by the equation: $\frac{Fs-\mathrm{F0}}{Fb} \times 100\%$.

4.2.3 Confocal microscopy sample preparation

Following transcytosis, residual fPS NPs at the apical surface were removed by three washes with PBS before the cells were fixed in 4 % PFA (paraformaldehyde, P6148, Sigma-Aldrich) for 20 min at RT (room temperature). After PFA removal, cells were washed three times with PBS. These cells were permeabilised using 0.5 % of Triton-X 100 (X100-500ML, Sigma-Aldrich) in PBS and washed with blocking buffer containing 20 % BSA (*w/v*) for 1 h. To demonstrate cell-cell contacts at the plasma membrane, permeabilised samples were incubated overnight at 4 °C with a rabbit monoclonal antibody that recognised ZO-1 (diluted 1:50 in PBS, 8193S, Cell signalling Technology). Following three washes by PBS, ZO-1 distribution was visualised using a fluorescein-labelled goat anti-rabbit secondary antibody (diluted 1:100 in PBS, F1-1000, Vector) that was incubated with these cells for 30 min at RT prior to three washes with PBS. Cell nuclei were labelled with DAPI (4', 6-diamidino-2-phenylindole, Dihydrochloride, D1306, Thermo Fisher Scientific), by incubation for 30 min at RT. Following antibody and DAPI labelling, polycarbonate membranes were removed from the Transwell® filter and mounted onto microscope slides. A drop (~15 µL) of Fluoroshield Mounting Medium (ab104135, Abcam) was placed between the glass slide and Transwell® filter. Another drop of Fluoroshield Mounting Medium was added onto a coverslip so that it formed the organisation of "slide-medium-membrane-medium-coverslip". Cells were analysed using a Zeiss LSM 510 confocal microscope.

4.2.4 Western blot analysis of LRP-1 expression in non-polarised Caco-2 cells

LRP-1 expression can be influenced by the presence of serum in the growth medium (232). Since the cell surface receptor for ntPE is LPR-1, expression levels of this protein were assessed in triplicate in Caco-2 cells by western blot analysis. Caco-2 cells were grown in a 12-well plate format (150628, Nunclon™ Delta Surface, Thermo Scientific) and examined after reaching full confluence. Three different conditions were investigated: 1) no serum in the cell growth medium; 2) with serum in the cell growth medium; and 3) serum removed from growth medium 12 h prior to analysis. Cells lysed using RIPA buffer (Radioimmunoprecipitation assay buffer, R0278-50ML, Sigma-Aldrich) containing 5 % (*v/v*) of protease inhibitor (12841640, Fisher Scientific) and 5 % (*v/v*) phosphatase inhibitor (12841650, Fisher Scientific) were centrifuged at 9000 ×*g* (Heraeus Biofuge Primo R centrifuge, Thermo Scientific) for 10 min at 4 °C. Lysates were separated by 12 % polyacrylamide gels using sodium dodecyl sulphate-polyacrylamide gel electrophoresis (SDS-PAGE) at 100 V for 3 h. After SDS-PAGE, polyacrylamide gel bands were transferred onto a PVDF transfer membrane (polyvinylidene difluoride, 0.45 m, 26.5 cm × 3.75 m, pore size 0.45 µm, Immobilon®-FL, Merck-Millipore) at 30 V for 1.5 h. After blocking with 0.04 % BSA in TBS (Tris-buffered saline containing 0.1 % of Tween 20 (P1379, Sigma-Aldrich)), the PVDF transfer membrane was incubated overnight at 4 °C with rabbit monoclonal to LRP-1 antibody (ab92544, Abcam, diluted in 1:5000) and goat polyclonal IgG to β-actin (diluted in TBS 1:10,000, SC-1615, Santa Cruz Biotechnology). The recipe for 1 L of TBS buffer is: 10 mL of Tris-HCl 1 M pH 8.0, 37.5 mL of 4 M sodium chloride, and 952.5 mL of distilled water. PVDF membranes were rinsed three times with TBS (containing 0.1 % of Tween 20) and then incubated in secondary antibody for 1 h at RT: donkey anti-rabbit (IRDye® 680 RD, 926-68073, LI-COR®, diluted in TBS 1:5000) for visualising of LRP-1 and donkey anti-goat (IRDye® 800 CW, 926-32214, LI-COR®, diluted in 1:5000) to visualise β-actin. The PVDF membrane was washed in TBS buffer (containing 0.1 % of Tween 20) three times and imaged in Odyssey® CLx-0628 (LI-COR®).

4.2.5 Transcytosis of AC NPs

Unlike fPS NPs that could be readily followed due to the fluorescent label incorporated into the PS polymer, AC NPs lacked a straightforward means of detection. To overcome this challenge, a fluorescent tag was chemically coupled onto the chitosan of AC NPs using fluorescein isothiocyanate (FITC).

4.2.5.1 Preparation of FITC labelled AC NPs

4.2.5.1.1 Labelling chitosan with FITC

FITC (20 mg, fluorescein isothiocyanate isomer I, F7250-500MG, Sigma Aldrich) was dissolved in 10 mL methanol (16K144019, VWR chemicals) and added to 20 mL 1 % *w/v* chitosan (200 mg) in 0.1 M acetic acid solution (pH 2.8, 27225-2.5L-R, Sigma-Aldrich). After 3 h of reaction in the dark at RT, the FITC-labelled chitosan was precipitated by raising the pH to 10 with the addition of 0.5 M sodium hydroxide (72064-500ML, Sigma-Aldrich). Unreacted FITC was removed using centrifugation until no fluorescence was detected in the supernatant. FITC-labelled chitosan was dissolved in 20 mL 0.1 M acetic acid and then dialysed (SnakeSkin™ dialysis tubing, 10K MWCO, 68100, Thermo Fisher Scientific) against 4 L of distilled water at RT for 3 days under darkness, with water being replaced every day (233).

4.2.5.1.2 Formation of FITC-labelled AC NPs

2 mL of 51 µg/mL calcium chloride solution was added into 10 mL of 60 µg/mL oxidized alginate solution dropwise during micro-tip probe ultra-sonication. The resultant pre-gel was stirred for another 30 min before the addition of 2 mL of 0.3 mg/mL FTIC-labelled chitosan solution. The suspension was equilibrated overnight to allow the formation of NPs. All materials were filtered through 0.45 µm membranes prior to use.

4.2.5.2 Conjugation of BSA and ntPE onto FITC-labelled AC NPs

FITC-labelled AC NPs were linked with proteins (BSA or ntPE) via a bifunctional cross-linker EMCH, details can be found in Chapter 3.2.4.3. The aldehyde groups from AC NPs linked with hydrazide groups of EMCH, which has previously attached to thiol-ntPE and thiol-BSA (details can be found in Chapter 3.2.2.1 and 3.2.2.2).

4.2.5.3 Transcytosis of FITC-labelled AC NPs

Transcytosis of FITC-labelled AC NPs was performed in triplicate using essentially the same protocol as that used for fPS NPs (details can be found in 4.2.2). The amounts of AC NPs to be tested were determined by the amounts of ntPE or BSA on the surface, which were kept at 10 µg, and the amount of blank AC NPs were determined accordingly. AC NPs were visualised by

chemically labelling FITC onto NPs, therefore, the confocal microscopy sample preparation was performed in the same way as for fPS NPs, except that ZO-1 was visualised using Alexa Fluor® 546 donkey anti-rabbit secondary antibody (diluted 1:100 in PBS, A10040, Thermo Fisher Scientific).

4.2.6 Circular dichroism of ntPE and AC NPs-ntPE

Retention of a protein's native structure is essential for its biological function. Therefore, the secondary structure of ntPE following its coupling onto NPs was studied by circular dichroism (CD; Chirascan™, AppliedPhotophysics). CD spectra were acquired under the following conditions: temperature 20 °C, bandwidth 1 nm, time per point 0.5s, wavelength from 190 – 350 nm. A 5-mm path length quartz cuvette was used. Concentration of ntPE was 200 µg/mL and the concentration of AC NPs-ntPE was 17 µg/mL. Each sample was analysed in triplicate. Performance indices of each sample were calculated by the Selcon method available in DichroWeb (234, 235).

4.2.7 Transcytosis of ntPE-Alexa Fluor® 546 and FITC-BSA

Alexa Fluor® 546 C_5 maleimide (A10258, Life Technologies) was chemically linked to thiol groups of ntPE via the maleimide-thiol coupling. The procedure for exposing thiol groups of ntPE was described in Chapter 3.2.2.1. After 2 h of the maleimide-thiol coupling reaction, ntPE-A546 (ntPE coupled to Alexa Fluor® 546) was separated from reactants using size exclusion chromatography.

Confluent Caco-2 cell monolayers on Transwell® plates as described in 4.2.2 were used; 10 µg of ntPE-A546 and FITC-BSA (A23015, Thermo Fisher Scientific) were applied onto the apical compartment, and the transcytosis study was performed in triplicate for 120 min. The fluorescent secondary antibody to visualise ZO-1 was selected so as to not conflict with the fluorophore attached to BSA and ntPE. For cells treated with FITC-BSA, Alexa Fluor® 546 donkey anti-rabbit IgG was used to visualise ZO-1, while fluorescein goat anti-rabbit IgG was used accordingly for cells being treated with ntPE-A546.

4.2.8 Statistical analysis

Obtained data were analysed by using unpaired t-test (for comparing two groups of data). P values < 0.05 were considered to be statistically significant.

4.3 Results and discussion

4.3.1 *In vitro* transcytosis of fPS NPs

The transport percentage of fPS NPs across the Caco-2 cell monolayers was 0.20 ± 0.13 %, 2.60 ± 1.1 % and 0.21 ± 0.01 %, for blank fPS NPs, fPS NPs-BSA and fPS NPs-PE respectively (Figure 4-3).

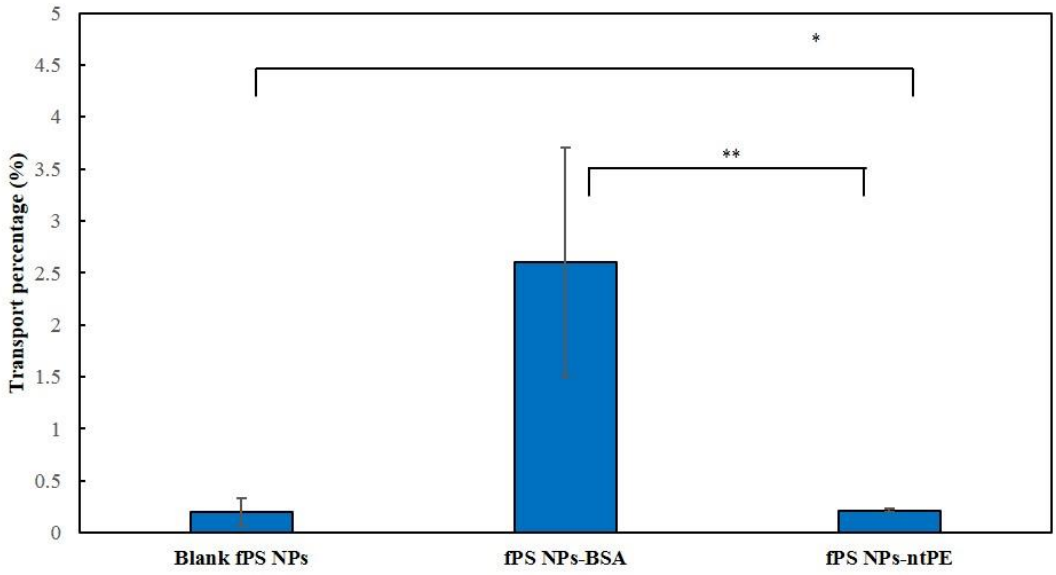

Figure 4-3: Transport percentage of fPS NPs across Caco-2 cell monolayers. The transport rate for blank fPS NPs, fPS NPs-BSA and fPS NPs-PE was 0.20 ± 0.13 %, 2.60 ± 1.1 % and 0.21 ± 0.01 %, respectively (n=3), *p=0.92 (>0.05), fPS NPs-ntPE compared to blank fPS NPs; **p=0.16 (>0.05), fPS NPs-ntPE compared to fPS NPs-BSA).

For blank fPS NPs, the transport percentage was consistent with the value reported by Fowler *et al.* (2013), which 0.825 % of NPs were detected in the basolateral side after 3 h incubation (236). Surprisingly, no increase in the transport was observed when fPS NPs were conjugated to ntPE, and a higher transport efficiency of fPS NPs-BSA compared to fPS NPs and fPS NPs-ntPE was detected. In this regard, it has been described that albumin-mediated transport can occur in alveolar epithelial cells by binding to gp-60 albumin-binding proteins on the cell membrane (237). This might also occur in the intestinal epithelial cells, as Howard *et al.* (2014) suggested that albumin has the potential to be a delivery system for oral delivery (237, 238). As described above,

the observed receptor-mediated uptake may contribute to or be the main cause of fPS NPs-BSA transport observed in the current studies.

Characteristics of NPs are known to have great impacts on their behaviours *in vitro* and *in vivo* (141, 239). Therefore, fPS NPs-ntPE and fPS NPs-BSA were prepared in the same protocol, so that they have similar characteristics (in Chapter 3), and would be more comparable for subsequent *in vitro* and *in vivo* study. Hydrodynamic size measured for fPS NPs-BSA was ~150 nm, and for fPS NPs-ntPE was ~110 nm, the zeta potential of both fPS NPs was ~ -20 mV. As reported in Chapter 3, on average, ~$1.26 \pm 0.37 \times 10^4$ BSA molecules were present on each fPS NP-BSA, while ~$9.38 \pm 3.3 \times 10^3$ ntPE molecules were present on each fPS NP-ntPE; the extent of surface attachment for these two proteins were similar. The extent of cell surface receptors on polarised Caco-2 cell monolayers for BSA and ntPE to bind to is unknown.

The arrangement of the ligands on NPs surface is another parameter which has impact on the cell uptake and transport (240). Carney *et al.* (2011) prepared gold NPs with surface coating with alternating hydrophobic and hydrophilic domains at different percentage ratios, as well as different shapes of the hydrophobic domains. Both the arrangement and shape of these ligands had an impact on the cellular internalisation, however the optimal NPs surface arrangement and structure was not concluded. In addition, for different ligands and NPs, the arrangement will be different too (240).

ntPE enters the cell via LRP-1 associated endocytosis, undertakes intracellular trafficking avoiding lysosomal degradation and releases from the basolateral side of the epithelium (229). This receptor-mediated pathway of ntPE was anticipated to facilitate the transport of NPs across the Caco-2 cell monolayers. The lack of appreciable difference between the transport of fPS NPs and fPS NPs-ntPE ($^*p=0.92$, >0.05), suggested that the transcytosis of fPS NPs-ntPE did not benefit from a specific transcytosis pathway. Studies were carried out with higher concentrations of fPS NPs-ntPE (up to 20 µg of proteins) and longer incubation times (up to 120 min). No increase in transport was observed (data not shown). Incubation beyond 120 min was not performed, as Desai *et al* (1997) reported that no significant increase of NPs uptake in Caco-2 cell monolayers was measured after 120 min (138). During the transcytosis study, TEER values were measured as an indication of the integrity of Caco-2 cell monolayers. As shown in Figure 4-4, Caco-2 cell monolayers used in these studies maintained TEER > 350 $\Omega \cdot cm^{-2}$, which was consistent with a polarised, differentiated state throughout the course of the experiment (241). Thus, none of fPS NPs tested appeared to induce significant changes in the functional properties of the Caco-2 cell monolayers used in this analysis.

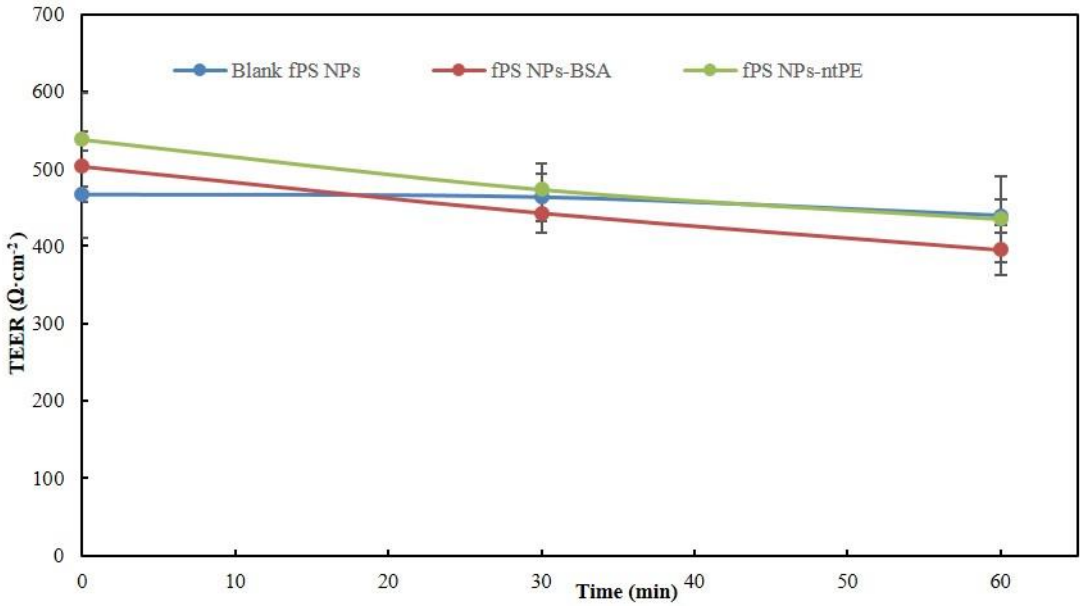

Figure 4-4: Measurement of TEER during the transcytosis of fPS NPs. TEER values remained above 350 Ω·cm^{-2} over the duration of the experiment (n=3).

To better understand the cellular fate of fPS NP preparations tested *in vitro*, confocal microscopy was used to examine fluorescence distributions and characteristics within the Caco-2 cell monolayers. The extent and distribution of red channel fluorescence, representing fPS NPs, was evaluated at conditions comparable to green channel fluorescence used for the tight junction-associated protein ZO-1 and blue channel fluorescence of DAPI-labelled nuclei (Figure 4-5). Results obtained for blank fPS NPs were consistent with the transcytosis data presented in Figure 4-3; there were minimal associations between blank fPS NPs and the Caco-2 cell monolayers. It is presumed that loosely-associated fPS NPs were removed from the apical surface during sample processing.

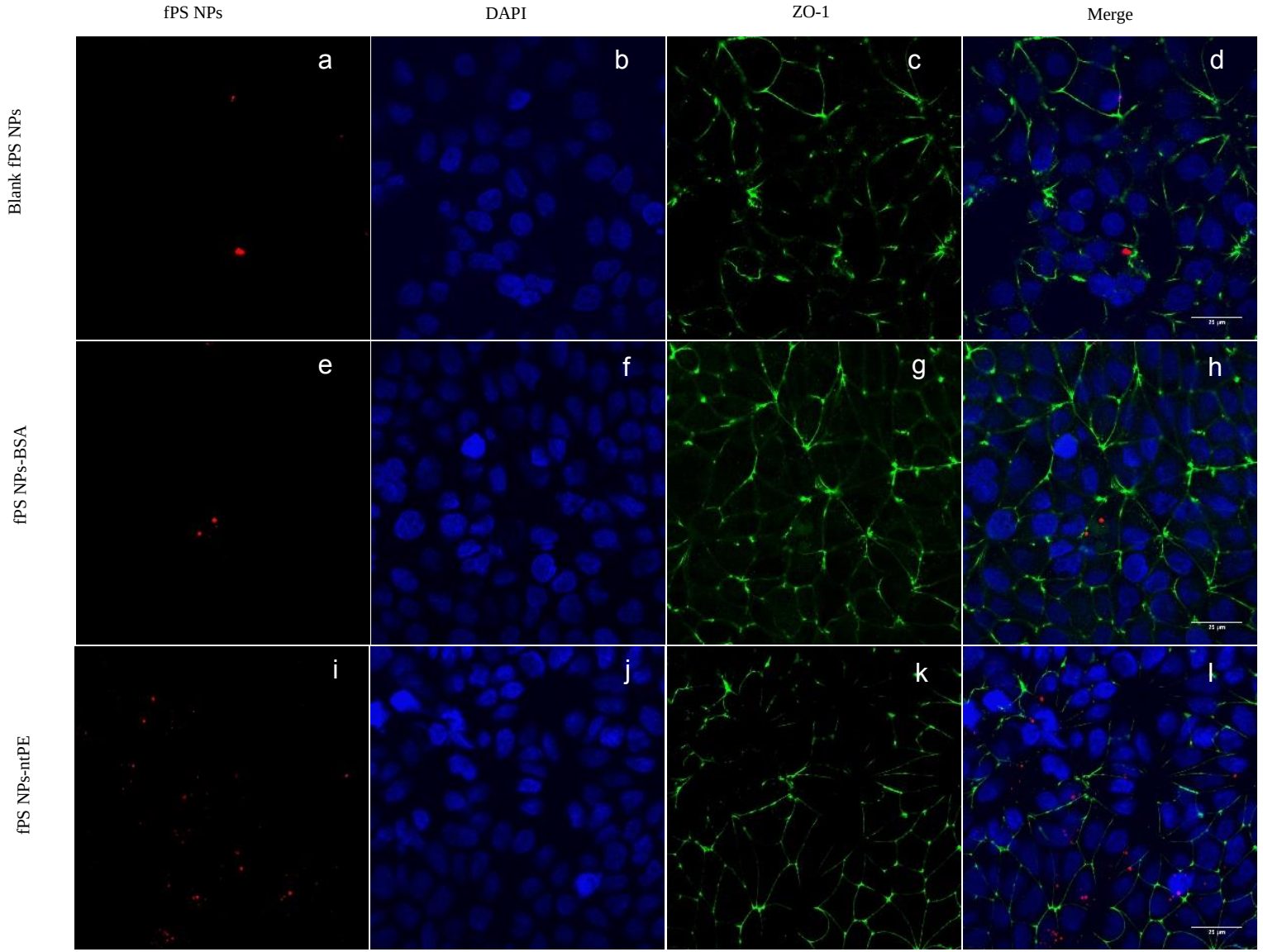

Figure 4-5: Representative confocal images of fPS NPs in Caco-2 cell monolayers. Few unmodified fPS NPs and fPS NPs-BSA were associated with Caco-2 cell monolayers; while considerable amounts of fPS NPs-ntPE were possibly located in the peri-nuclear compartment (red: fPS NPs, blue: nucleus, green: ZO-1, scale bar= 25 µm).

Few fPS NPs-BSA were demonstrated to associate with the Caco-2 monolayers by confocal microscopy, with the extent of those observed being comparable to blank fPS NPs (Figure 4-5d and Figure 4-5h). Interestingly, considerable amounts of ntPE-conjugated fPS NPs appeared in the peri-nuclear compartments (Figure 4-5l), which might be Golgi apparatus or endoplasmic reticulum (ER). This trend was consistent with other 16 images taken for Caco-2 cell monolayers treated with fPS NPs-ntPE at other independent experiments and at different locations on the membrane.

Bacterial toxins, like ntPE and cholera toxins, can exploit the retrograde trafficking pathway and translocate to Golgi apparatus or endoplasmic reticulum (242). In terms of the transport of NPs, Cartiera *et al.* (2009) demonstrated that PLGA NPs (95 ± 20 nm) were observed to accumulate in the Golgi network of human bronchial epithelial and opossum kidney renal tubule cells *in vitro* (243). He *et al.* (2013) showed that unmodified PLGA NPs can also transport to the recycling endosome compartment (REC) and ER through apical early endosome (AEE)/REC and AEE/ER pathways in polarised Caco-2 cell monolayers (197).

Research similar to that described herein has demonstrated the attachment of bacterial proteins onto microparticles can facilitate their uptake by Caco-2 cell monolayers. Rowland *et al.* (2005) coated 1 µm polystyrene particles with a fragment of internalin A, which the bacterium *Listeria monocytogenes* utilises to transport through the intestinal epithelium following an interaction with E-cadherin receptors; enhanced uptake by Caco-2 cell monolayers occurred for particles attached to internalin A, comparing with plain microparticles (244).

Cellular uptake and transport of NPs can be influenced by many factors. Not surprisingly, NPs size, surface charge, and surface coating have been identified to affect these events (245). Optimal NP size for uptake by Caco-2 cell is considered to be 100 – 200 nm in diameter (137); the size of the tested fPS NPs in this study was ~150 nm in diameter. In terms of surface charge, NPs decorated with negative materials have a higher uptake rate comparing with plain NPs, but the mechanism of the increased uptake has not yet been fully unravelled (137). Santos *el at.* (2011) tested the uptake of carboxylate PS NPs with sizes of 40 nm and 200 nm in HeLa and A549 cell lines (246). Uptake behaviours of these PS NPs appeared to be cell line-specific, and NPs showed to use multiple pathways to enter cells, which might include clathrin-mediated endocytosis, caveolae-mediated endocytosis, as well as other uptake processes involving microtubules (246, 247). It is also important to note that most of these studies were performed on non-polarised cells, for polarised cells, the effects of NPs characteristics on the uptake and transport are rarely studied. For polarised cells, such as Caco-2 cell monolayers herein, they have apical-basal polarity, and the apical and basolateral membranes are composed of different proteins and lipids. Accordingly, their uptake and transport of substances will probably be totally different from the non-polarised cells. These outcomes revealed complex internalisation pathways of NPs in cells, and suggested

that more work is needed in order to have a comprehensive understanding of NPs uptake and transport, specifically the knowledge for polarised cells.

The unexpectedly low transcytosis rate of ntPE-mediated fPS NPs might be due to absence of LRP-1, the cell receptor for ntPE. Data presented herein suggests that ntPE-mediated fPS NPs could enter polarised Caco-2 cells but may not be able to complete the transcytosis process to be detected in the basolateral compartment. Perhaps, AC NPs-ntPE entered the cell through a non-LRP-1 mechanism, which limited their ability to complete the intracellular trafficking processes involved in ntPE transcytosis. Interestingly, others have noted that compounds which need a carrier-mediated transport process, showed a lower transport rate when they were tested in Caco-2 cell monolayers compared to the test *in vivo* (248). If this is applicable to this study, the presence of the membrane-associated carrier proteins, in this case, LRP-1, needed to be verified.

4.3.2 Identification of LRP-1 on Caco-2 cells

Toquet *et al.* (2007) suggested that expression of LRP-1 is down-regulated by 48 % in adenocarcinoma cells; a lower LRP-1 expression in the Caco-2 cells used in these monolayers studies might explain why the transport levels of ntPE-mediated NPs were significantly lower than expected. Further, low expression of LRP-1 in adenocarcinoma cells can be a consequence of high albumin concentration in the culture medium (232, 249). Thus, the impact of albumin on LRP-1 expression in the Caco-2 cell model used in these studies was examined.

Three different conditions were used to culture Caco-2 cells and the expression of LRP-1 was compared between these conditions: 1) culture medium has serum all the time, labelled as “S+”; 2) “S-” stands for cells were in the absence of serum for 12 h before the analysis; 3) and culture medium has no serum all the time was labelled as “-”. Western blot analysis suggested that LRP-1 was equally expressed under these three conditions (no statistical difference) (in Figure 4-6).

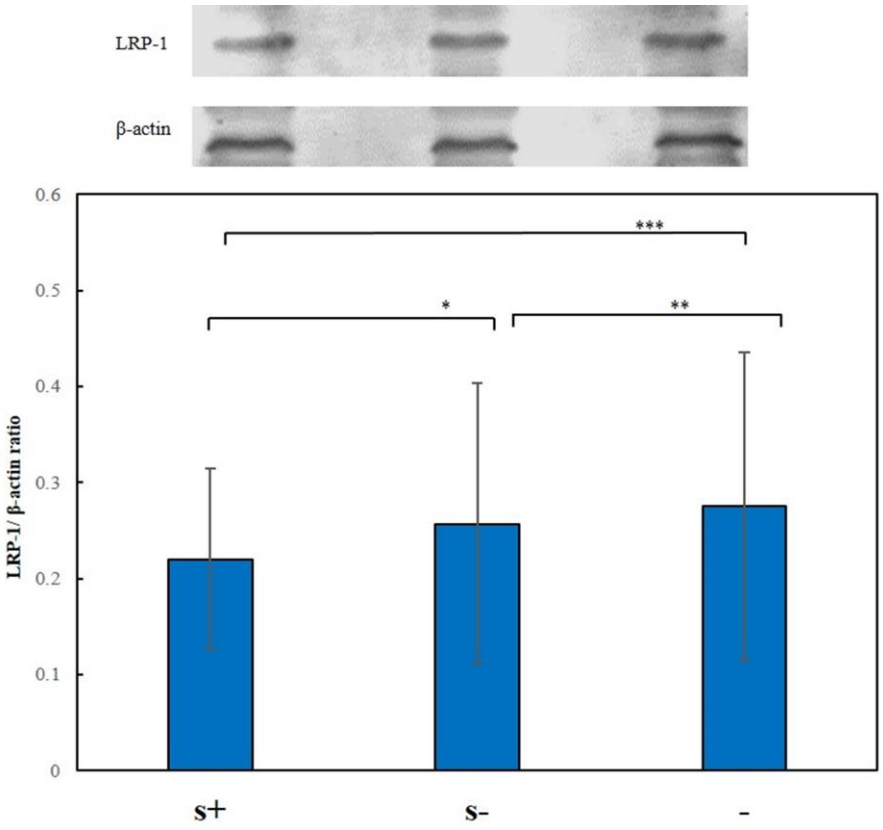

Figure 4-6 : Western blot analysis of LRP-1 expression in Caco-2 cells (n=3). The expression of LRP-1 in Caco-2 cells which were cultured with serum all the time ("S+") did not show significant difference comparing to "S-" (cells in the absence of serum for 12h before the analysis), $^{*}p=0.73 > 0.05$; nor comparing to "-" (cells were cultured without serum), $^{***}p=0.64 > 0.05$. There was so significant difference between the conditions of "S-" and "-" for the expression of LRP-1, $^{**}p=0.89 > 0.05$.

4.3.3 *In vitro* transcytosis of AC NPs

After a 60 min incubation the transport percentage for blank AC NPs was 2.83 ± 1.29 %, while for AC NPs-BSA and AC NPs-nPE was 4.18 ± 2.05 %, 4.36 ± 2.24 %, respectively (Figure 4-7).

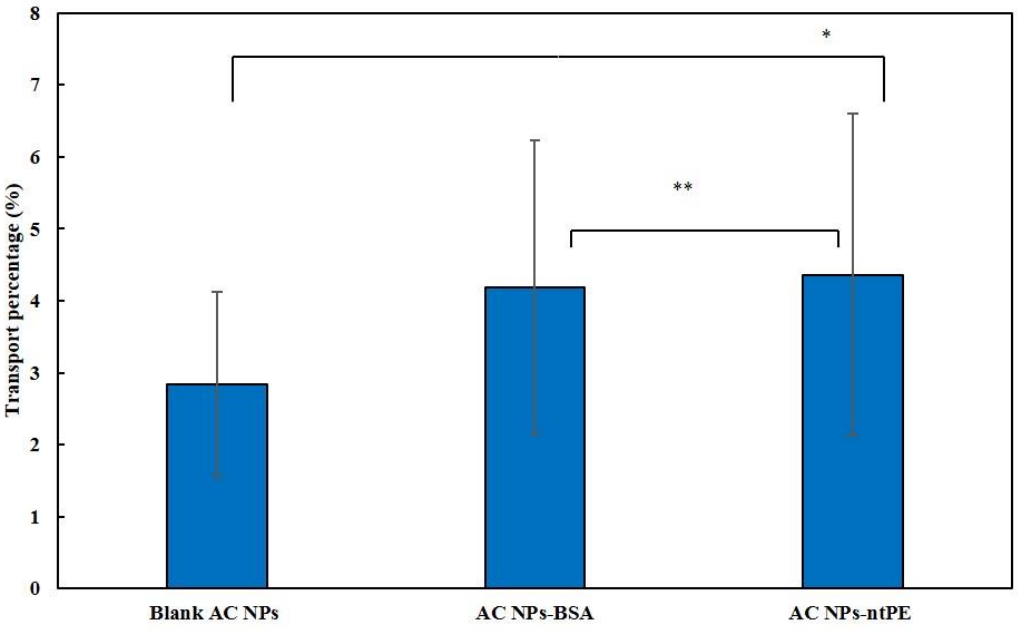

Figure 4-7: Transport percentage of AC NPs across Caco-2 cells monolayers. The transcytosis rate for unmodified AC NPs, AC NPs-BSA and AC NPs-PE was 2.83 ± 1.29 %, 4.18 ± 2.05 % and 4.36 ± 2.24 %, respectively (n=3, *p=0.60 > 0.05, AC NPs-ntPE compared to blank AC NPs; **p=0.84 > 0.05, AC NPs-ntPE compared to AC NPs-BSA).

Compared to fPS NPs, more AC NPs appeared to have transported across the Caco-2 cell monolayers after 60 min of incubation, although an exact comparison of these two studies cannot be made without some way of calibrating transport properly. One reason for the possible transport increase observed with AC NPs may have been greater particle flexibility allowing better accommodation into forming apical endosomal structures. Unlike rigid and stable fPS NPs structures, AC NPs are comparatively soft, flexible and labile structures (Figure 3-11), which are formed by electrostatic interactions between chitosan and alginate (142). In addition, these polyelectrolyte complexes are sensitive to the change of environment, such as the change of pH and ionic strength (218, 250). The ionic strength of the cell culture medium is higher than the solution in which these AC NPs were suspended. This change in ionic strength might have altered the structure of these AC NPs, making them more likely to transport across Caco-2 monolayers *in vitro*. As demonstrated in Chapter 2, fewer NPs were found in simulated intestinal fluid (pH6.8) using a transmission electron microscope. Furthermore, chitosan is able to reversibly alter the functional properties of tight junctions without altering cell viability (251). Therefore, the

chitosan component of these NPs might have additionally affected the paracellular pathway of these Caco-2 cells monolayers.

AC NPs coupled with BSA and ntPE showed an increased percentage transport compared to unmodified AC NPs (in Figure 4-7). Proteins coupled onto the surface of AC NPs changed the zeta potential from 20 ± 8 mV to -19 ± 11 mV for AC NPs-BSA, and to -6 ± 5 mV for AC NPs-ntPE, respectively (as described in Chapter 3). Although it is generally understood that positively charged NPs have higher cell internalisation rate compared to negatively charged NPs (146), Bannunah *et al.* (2014) demonstrated that the transport rate of negatively charged polystyrene NPs were two times higher than the positively charged ones in Caco-2 cell monolayers, even though the positive NPs were internalised more than the negative ones (141).

Chitosan and alginate are mucoadhesive polymers and generally regarded as safe. They have shown promise as nano-carriers for insulin, suggested by the observed pharmacological effects in rats compared to a solution of insulin alone (143). The physicochemical properties of AC NPs have been well characterised, as well as their *in vitro* release of the loaded drugs (insulin, nifedipin, and doxorubicin) in stimulated gastric and intestinal fluid (143, 252, 253). AC NPs have shown to be taken up by MCT-7 cells and HeLa cells with loading with doxorubicin and curcumin, respectively (253, 254). Katuwavila *et al.*(2016) proposed these AC NPs were non-selectively internalised via endocytosis by MCT-7 cells (253). Ma *et al*. (2003) suggested that clathrin-mediated endocytosis might be involved in the uptake of these NPs in Caco-2 cell monolayer, as the uptake was considerably reduced with the co-administration with chlorpromazine, which is considered to be an inhibitor of clathrin-related endocytosis (255). In addition, they reported that a low level of AC NPs was detected in the basolateral side of this cell monolayer. In a more recent study, Chen *et al.* (2008) assessed the transport of N-trimethyl chitosan NPs loaded with FITC-BSA across Caco-2 cell monolayers, and showed increased permeation when the NP surface was modified with alginate compared to control FITC-BSA NPs, but the mechanism of the uptake and transport is unknown (127).

Although NPs have demonstrated different levels of cell uptake, the fate after endocytosis and the potential transcytosis needs to be elucidated. In principle, three pathways could occur after NPs are internalised in the endosomal vesicle: 1) recycling back to the apical membrane; 2) transporting to the lysosomes for degradation; or 3) trafficking to the opposite membrane whereby NPs are released from the cell. He *et al.* (2013) showed a low transcytosis of PLGA NPs across the polarised Caco-2 cell monolayers. This low rate is mainly due to: 1) the exocytosis to the apical side, which is significantly regulated by Golgi complex and ER, and 2) the lysosome pathway following the early endosomes (EE) (197).

Compared to AC NPs coupled with BSA, AC NPs-ntPE did not show a significant increase in transport across the Caco-2 cell monolayers ($^{**}p=0.84 > 0.05$), suggesting these two types of NPs transported non-selectively across the cell monolayers. Considering the changes in the TEER values during the transcytosis study (Figure 4-8), the paracellular pathway might have been involved in the transport process due to the presence of chitosan in NPs composition. Chitosan has shown to induce a redistribution of tight junction-associated protein (Claudin-4) and it accompanies the increased paracellular permeability (75). It should be noted that the cell monolayers were cultured overnight in a fresh medium after the transcytosis study and showed that TEER values returned to pre-treatment levels (data not shown).

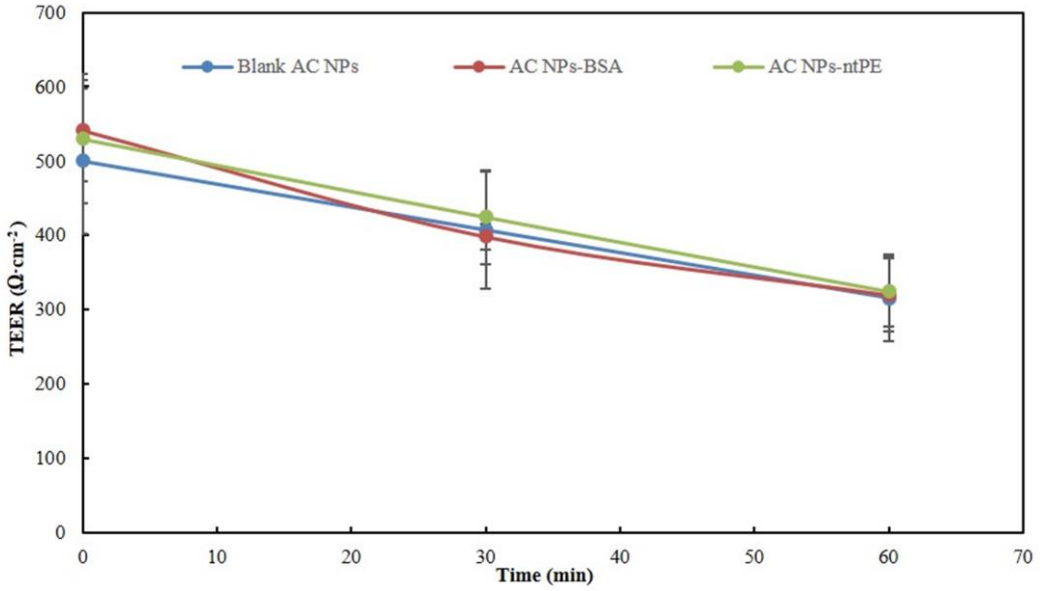

Figure 4-8: Measurement of TEER during the transcytosis of AC NPs. TEER values decreased with the addition of AC NPs, but remained above 300 Ω·cm^{-2} during the experimental course (n=3).

To better appreciate the transport process involving AC NPs, Caco-2 cell monolayers were observed using a confocal microscope following staining to demonstrate ZO-1 and nuclei after 60 min of apical exposure to the AC NPs. ZO-1 was stained red and nuclei were in blue; AC NPs became detectable after the chemical coupling of FITC to chitosan. For blank AC NPs, the green fluorescence was mostly co-localised with tight junctions (ZO-1), suggesting the possible effects of chitosan (in Figure 4-9d). The observed fluorescence signals from AC NPs-BSA were in a similar pattern as unmodified AC NPs, most of them were located on the edge of the cells (Figure 4-9h). Fluorescent green dots were detected in the cells which had been treated with AC NPs-ntPE for 60 min. In addition to the co-localisation with ZO-1, some AC NPs-ntPE (Figure 4-9l) were found to be in close proximity to nuclei as was observed for fPS NPs-ntPE (Figure 4-5l).

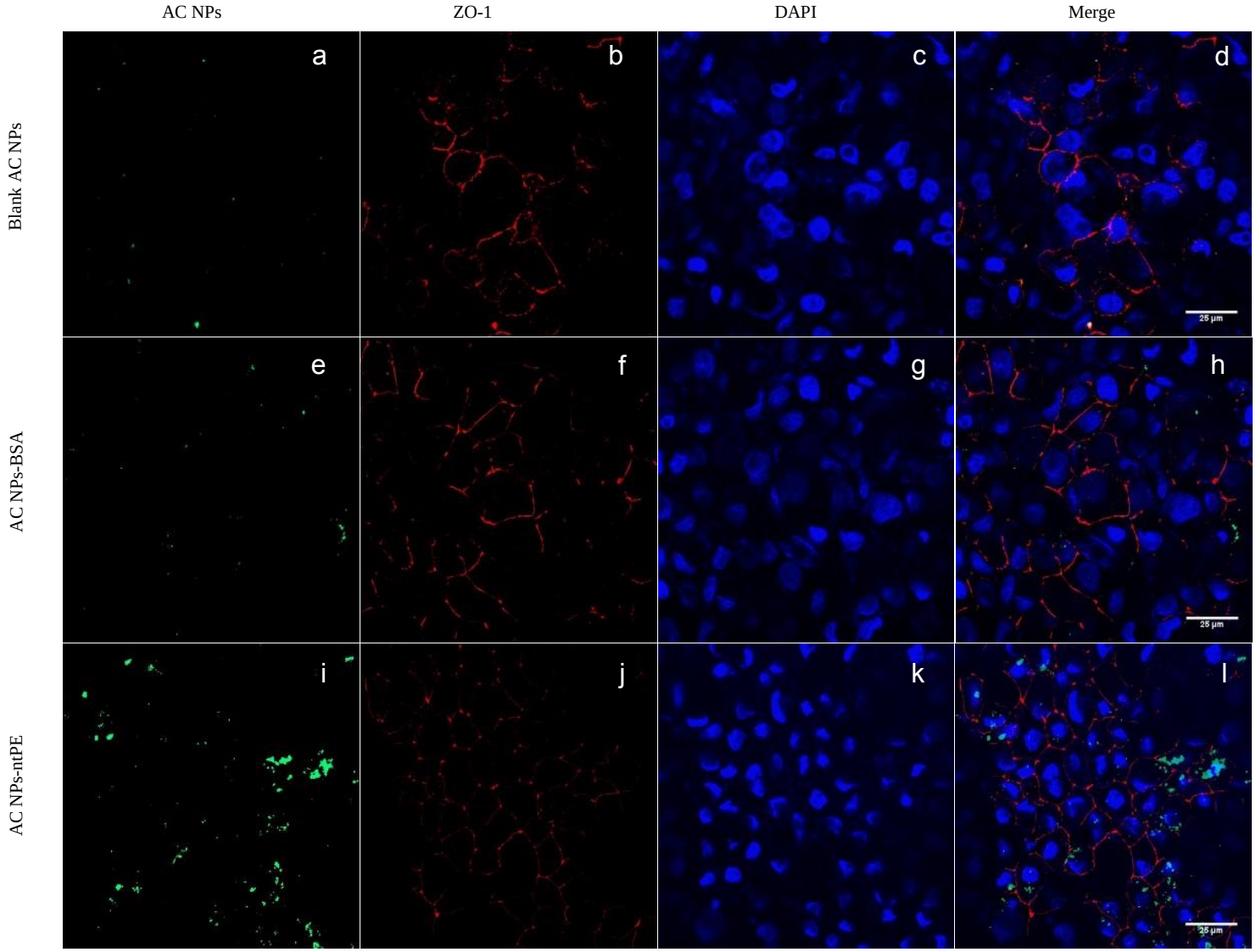

Figure 4-9: Representative confocal images of AC NPs on Caco-2 cell monolayers. Green signals from blank AC NPs and AC NPs-BSA appeared to associate with the tight junctions (labelled by red) on Caco-2 cell monolayers (in d and h), comparing to them, AC NPs-ntPE were found close to the nuclei of Caco-2 cells (green: FITC-labelled AC NPs, red: ZO-1, blue: nucleus, scale bar= 25µm).

These studies did not support the contention that ntPE can facilitate the transcytosis of AC NPs across Caco-2 cell monolayers. There were, however, a greater amount of AC NPs-ntPE in the Caco-2 cell monolayers compared to blank AC NPs and AC NPs-BSA (Figure 4-9). This phenomenon might be because the intracellular trafficking required for transcytosis did not occur as it would *in vivo*. One possible reason is that the structure of ntPE was altered by the process used to attach it onto NPs. Interestingly, others have noted that compounds which need a carrier-mediated transport process, showed a lower transport rate when they were tested in Caco-2 cell monolayers compared to the test *in vivo* (248). If this is applicable to this study, might suggesting an alternative model is needed.

4.3.4 Circular dichroism spectra of ntPE and AC NPs-ntPE

The measured low transport of ntPE-mediated AC NPs may be due to a loss of transcytosis capacity following ntPE's attachment to AC NPs surface. This might be caused by protein denaturation that occurs as part of the chemical coupling.

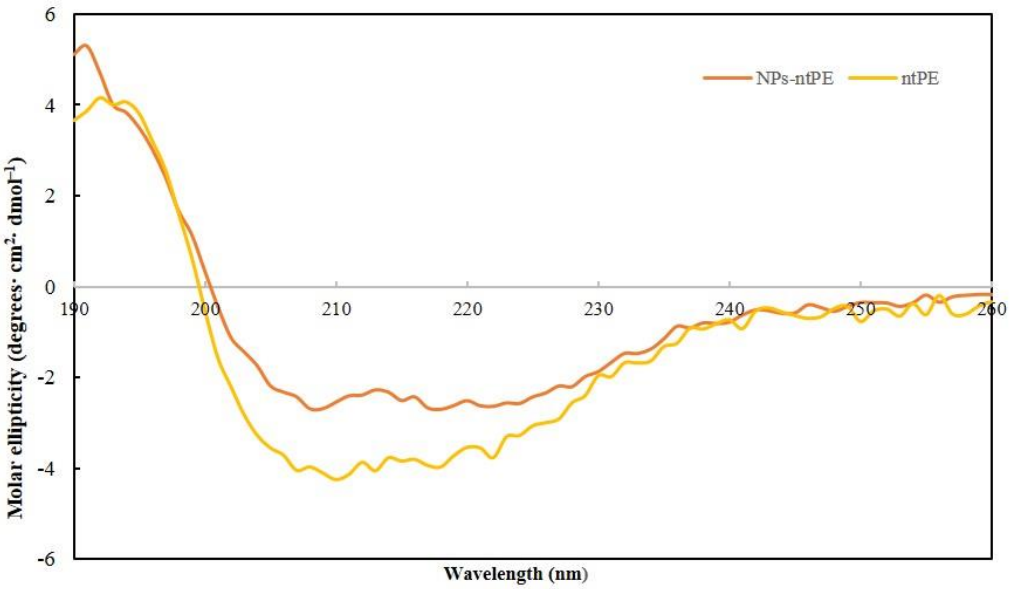

Figure 4-10: Far-ultraviolet CD spectra of free ntPE and ntPE on the surface of AC NPs. The spectra of the two samples were in a very similar pattern, suggesting that the secondary structure of ntPE did not change after the chemical conjugations with AC NPs.

The secondary structure of ntPE before and after conjugation was examined using CD spectrometry. CD spectra obtained for ntPE prior to and after its coupling to NPs were very similar (Figure 4-10), suggesting that conjugation with AC NPs did not change the secondary structure of ntPE significantly. These spectra were similar to data published previously (256). The

secondary structure performance index of free ntPE: α-helix, β-sheet, turns and random coil was 4.8 %, 35.5 %, 18.7 %, 41.0 %, respectively (in Table 4-1) (257), and after conjugating with AC NPs, it had the same performance index as ntPE molecules alone.

Table 4-1: Analysis of secondary structure of ntPE and AC NPs-ntPE

	α-helix	β-sheet	turns	random coil
ntPE	4.8 %	35.5 %	18.7 %	41.0 %
AC NPs-ntPE	4.8 %	35.5 %	18.7 %	41.0 %

4.3.5 *In vitro* transcytosis of ntPE-A546 and FITC-BSA

FITC-BSA served as a control for studying the transcytosis of ntPE-A546, and both of them have been applied onto the apical compartment of Caco-2 cell monolayers for 120 min incubation. The transport rate of FITC-BSA and ntPE-A546 were comparable when corrected for initial fluorescence values and final values. Limited amounts of FITC-BSA and ntPE-A546 molecules were detected in the basolateral compartments of Caco-2 cell monolayers (Figure 4-11). 0.06 % of FITC-BSA molecules were detected from the basolateral compartment after 120 min incubation, which had a similar transport outcome as Bies *et al.* (2004) reported (88). The measured transport rate of ntPE-A546 did not show statistically significant difference from FTTC-BSA ($^{*}p=0.67 > 0.05$), with 0.05 % of ntPE-A546 molecules transported from the apical to the basolateral side. Comparing to a previous study which showed 6 % of ntPE transported from the apical side to basolateral side of Caco-2 cell monolayers, suggesting that the specific transport pathway did not occur for ntPE-A546 in this study (229). However, this previous study is not totally comparable to the transcytosis study herein, as ELISA (enzyme-linked immunosorbent assay) was used to detect the transported ntPE, and this method is more sensitive than the fluorescence intensity measurement in this study.

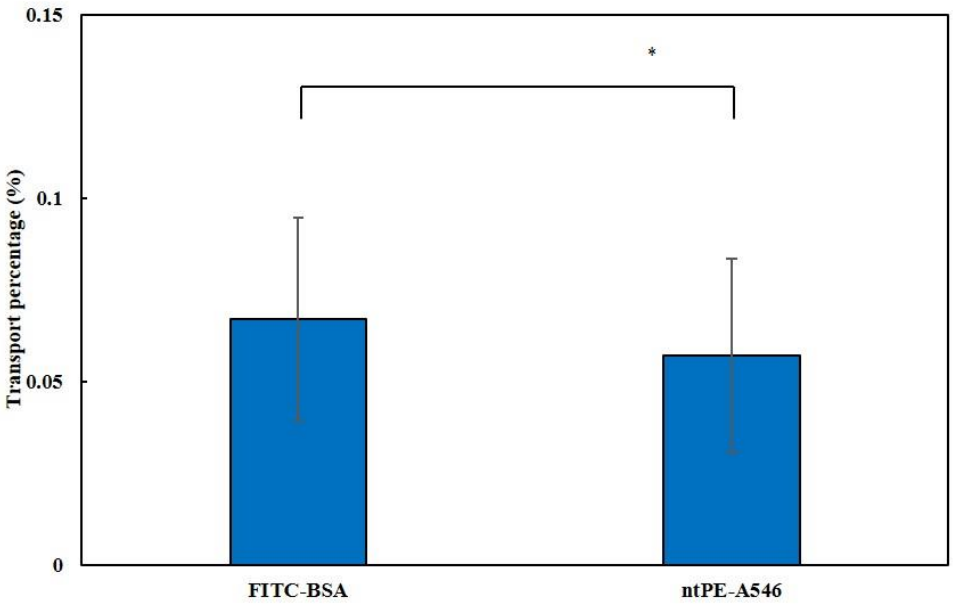

Figure 4-11: Transport percentage of FITC-BSA and ntPE-A546 across the Caco-2 cell monolayers. The transcytosis rate for FITC-BSA was 0.06 % and for ntPE-A546 was 0.05 % (*p=0.67 > 0.05, n=3).

There was little chance for FITC-BSA and ntPE-A546 molecules to go across the barrier via the paracellular pathway, as the TEER values were >350 Ω·cm^{-2} during the transcytosis study (Figure 4-12), suggesting sealed cell tight junctions have limited the extent of non-specific paracellular transport across these Caco-2 cell monolayers.

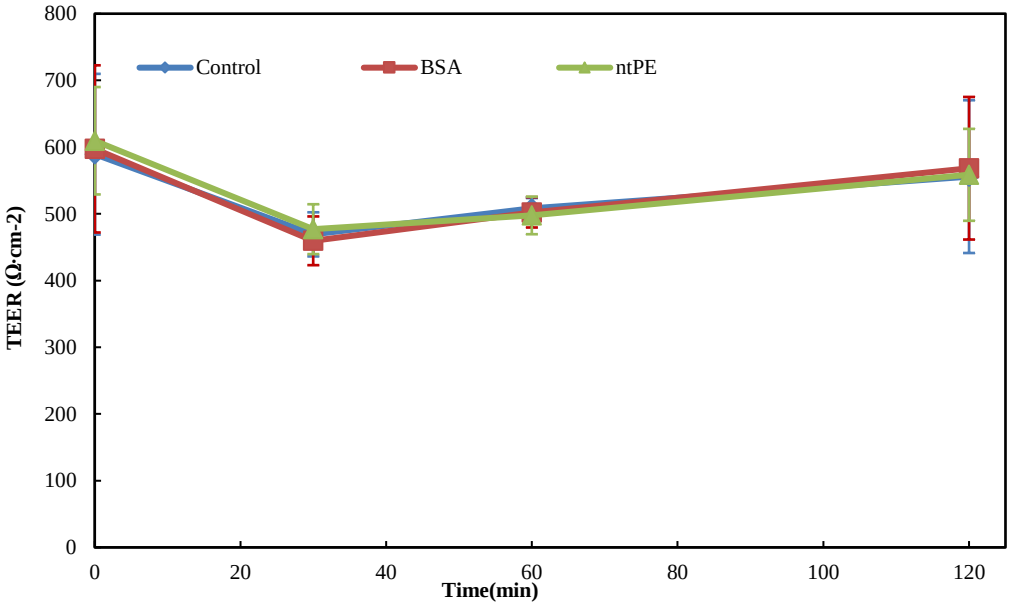

Figure 4-12: Measurement of TEER value during the transcytosis of FITC-BSA and ntPE-A546. The TEER values remained above 350 Ω·cm^{-2} during the transcytosis study, suggesting that tight junctions were kept integral (n=3).

Confocal microscopy showed limited amounts of FITC-BSA molecules associated with Caco-2 cell monolayer (Figure 4-13), which was consistent with the low transcytosis of FITC-BSA. Green fluorescent dots were found in the intercellular spaces. It is possible that FITC-BSA molecules interacted with cell membranes specifically, or just remained on the cell surface after the rinse in the apical compartment.

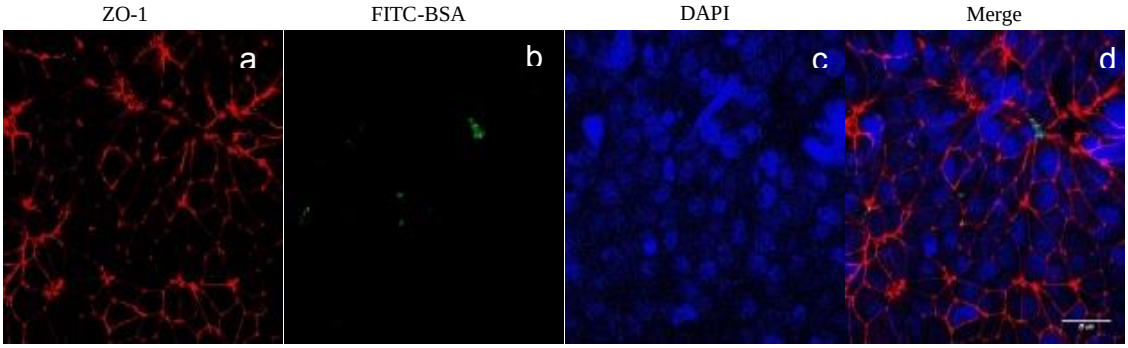

Figure 4-13 : Representative confocal images of FITC-BSA in Caco-2 cell monolayers. There were few FITC-BSA molecules associated with Caco-2 cells, and appearing between enteroctyes (green: FITC-labelled BSA, red: ZO-1, blue: nucleus, scale bar= 25µm).

Albumin is a metabolic transporter in the body, involved in the transport of copper, and fatty acid from the intestinal lumen into the capillaries (258, 259). Gp60 is a widely distributed cell-surface receptor, which has the ability to facilitate the internalisation and subsequent transcytosis of albumin across the endothelial cells (260, 261). Besides gp60, cubilin, a multi-ligand receptor on the cell membranes, and megalin, a large transmembrane protein, were shown to bind with albumin (262, 263). Birn *et al.*(2000) demonstrated that cubilin, in conjugation with megalin, has an essential role in the uptake of albumin (i.e. reabsorption) by the proximal tubules of the kidney (262). Since both of these two cell membrane proteins are expressed in the intestinal epithelial cells, a similar mechanism for transporting albumin may be involved in the current studies (264).

ntPE molecules were tracked by coupling Alexa Fluor® 546 onto the free thiol groups of ntPE, and ZO-1 on cell membrane was visualised by staining with FITC (Figure 4-14). Extensive amounts of ntPE-A546 molecules were observed to be localised in a peri-nuclear site of Caco-2 cells, after 120 min application to the apical surface of these cell monolayers.

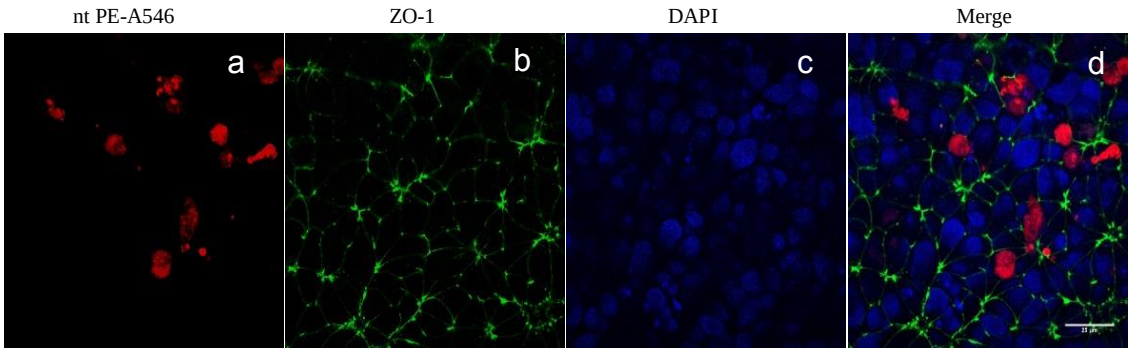

Figure 4-14: Representative confocal images of ntPE-A546 in Caco-2 cell monolayers. Considerable amounts of ntPE-A546 were on Caco-2 cell monolayers, and in close proximity to the nuclei (red: ntPE-A546, green: ZO-1, blue: nucleus, scale bar= 25µm).

Internalisation and early intercellular trafficking of PE in non-polarised cells is believed to involve multiple pathways. Smith *et al.* (2006) proposed that there are at least two possible pathways used by PE to reach the ER (endoplasm reticulum) in HeLa cells that avoid degradation in lysosomes (114). One of these is KDEL-receptor mediated pathway (Figure 4-15), where PE molecules bind to LPR-1 on the apical membrane and are internalised via clathrin-coated vesicles. Following LRP-1-mediated protein endocytosis, PE is subsequently trafficked from the EE (early endosomes) to the LE (late endosomes), and further to the TGN (*trans*-Golgi network). Once in the TGN, the C-terminal REDL motif of PE binds to the KDEL receptor and the molecule is transported to the ER in a retrograde manner (113, 114).

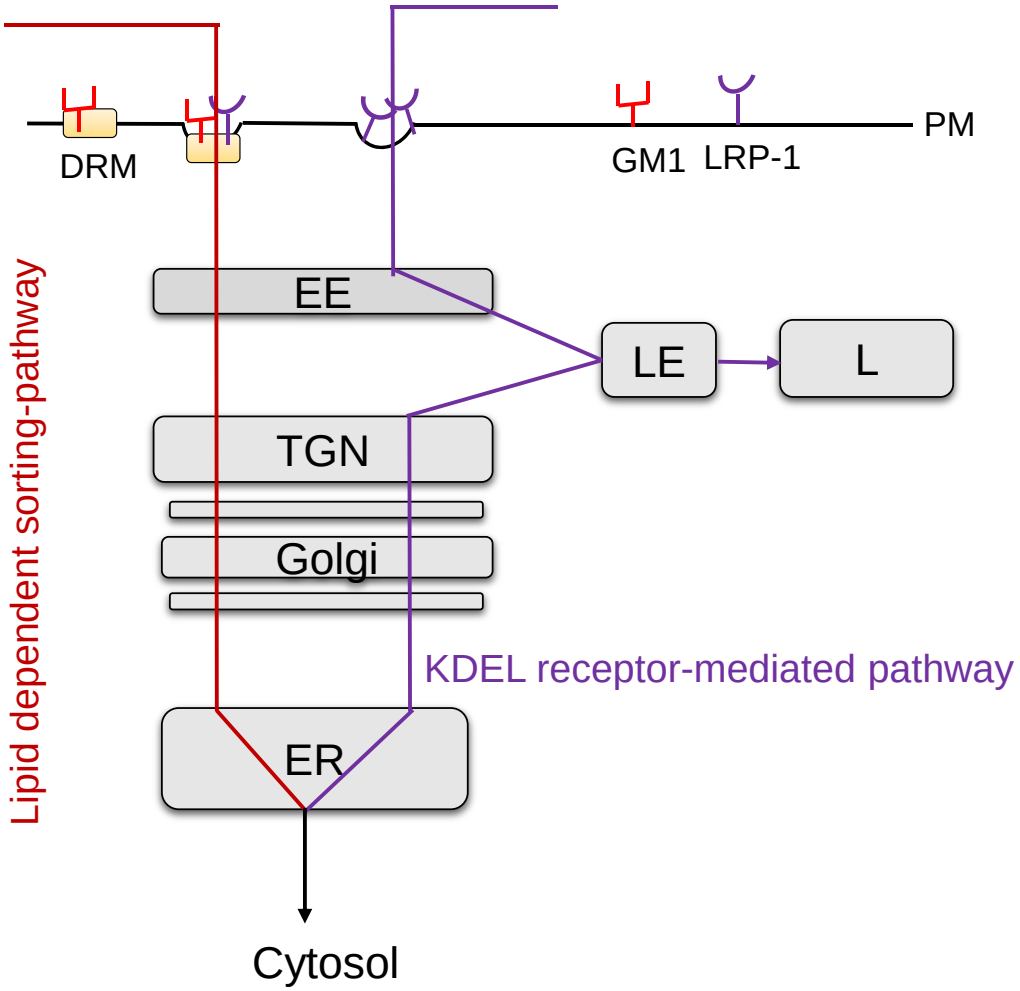

Figure 4-15: PE can utilise multiple pathways to move from the plasma membrane to the ER. One pathway is KDEL-receptor mediated pathway, where PE molecule is internalised following the recognition with LRP-1. Subsequently, PE travels from EE to LE and further to the TGN, where the C-terminal REDL motif of PE binds to the KDEL receptor and transports to ER. Lipid-dependent sorting pathway involves PE binding to LRP-1 and GM1, and transporting into Golgi and ER via a Rab-6 controlled lipid-dependent sorting pathway. PM, plasma membrane; DRM, detergent-resistant membrane micro-domain; EE, early endosome; LE, late endosome; L, lysosome; TGN, Trans Golgi network; KDEL-R, KDEL receptor. Adapted from (2).

The alternative pathway is the lipid-dependent sorting pathway (Figure 4-15). Laurent (2015) proposed that this pathway involves ntPE binding to the DRM (detergent-resistant microdomains) associated with GM1 ganglioside present on the plasma membrane, as well as to LRP-1 receptors in DRM. Whether these bindings occur simultaneously is unknown (2). It is possible, however, that ntPE binds to LRP1 (via domain I) and GM1 (via domain II), and the internalised proteins were being transported into Golgi and ER via a Rab-6 controlled lipid-dependent sorting pathway (114, 265).

In terms of polarised cells, the transport pathway has not been elucidated yet. By comparison to other bacterial toxins, like a member of the AB_5 toxin family, cholera toxin (CT), we might obtain clues regarding the transcytosis pathway of ntPE and better understand the low transcytosis measured in this study.

CT is one of the virulence factors secreted by the intestinal pathogen *Vibrio cholera*. Using polarised monolayers of the human epithelial cell line T84, CT transcytosis was shown to involve selected short chain or flexible fatty acid containing forms of GM1. In this case, CT-GM1 complexes in the Golgi apparatus transport to the ER in a retrograde manner (266).

Carter (2014) suggested that the transport of ntPE across the polarised Caco-2 cells might be influenced by GM1, as the addition of CT considerably reduced the transport of PE across the Caco-2 cell monolayers (121). The competition between CT and ntPE binding to GM1 seemed to suggest that the intracellular pathway, which involves GM1, is the optimal route for the transcytosis of ntPE across the polarised Caco-2 cell monolayers. Further, Pang *et al.* (2004) observed low internalisation of CT in Caco-2 cells and attributed it to the low expression of GM1 on the plasma membrane (267). This low expression of GM1 might explain the observed low transcytosis of ntPE across the Caco-2 cell monolayers reported here, as well as in Laurent's study (2).

4.4 Conclusion

Following the conjugation of ntPE onto fPS NPs and AC NPs in Chapter 3, the ntPE-mediated transport ability was tested in an *in vitro* model: Caco-2 cell monolayers. For stable fPS NPs, BSA-coupled fPS NPs showed increased transcytosis compared to unmodified fPS NPs and fPS NPs-ntPE. The gp60 proteins on the cell membrane might have facilitated the transport of fPS NPs-BSA across Caco-2 cell monolayers in this study. Unmodified fPS NPs and fPS NPs-ntPE appeared to transport via a non-specific pathway, there was no suggestion that the paracellular barrier was diminished in these studies.

In general, AC NPs had higher transcytosis rates than fPS NPs, possibly due to the greater flexibility of these structures and/or due to the presence of chitosan, which can reversibly open tight junctions. A lower than expected transcytosis rate was also observed for AC NPs coupled to ntPE. Decreased levels of LRP-1 was tentatively ruled out by western blot analysis, although the functional properties of LRP-1 were not examined. Initially, the low transcytosis observed for ntPE-mediated NPs was considered due to the alteration of ntPE's structure after the attachment onto NPs. However, CD analysis showed that the secondary structure of ntPE was not

dramatically changed by the process used to attach it to NPs. Free ntPE was also observed to have a lower than expected transport rate across the Caco-2 cell monolayers. Based upon confocal microscopy, it appears that ntPE, whether by itself or attached to NPs, was able to enter Caco-2 cell monolayers but stopped in the transcytosis process in a peri-nuclear compartment consistent with the Golgi apparatus or endoplasmic reticulum. By comparison, BSA by itself or after coupling to NPs failed to demonstrate a similar intracellular localisation.

Based upon all of these findings, it is hypothesised that defects in the intracellular trafficking pathways of the Caco-2 cells used in these studies may have led to the lower than expected transcytosis of ntPE. Importantly, GM1 was previously shown to affect ntPE transcytosis and its low expression in Caco-2 cells resulted in the low transcytosis of CT, which might explain the low transcytosis measured for ntPE (121, 267). Rather than perform an extensive series of studies in an attempt to understand/correct the trafficking defects observed in these *in vitro* studies, the focus of this research moved to assessing the transcytosis of these NPs *in vivo*.

Chapter 5 *In vivo* study of ntPE-coupled nanoparticles

Overview:

Aim: To test the transcytosis of nanoparticles mediated by ntPE in a rat model via intraluminal administration.

Methods: Transcytosis of fluorescent polystyrene nanoparticles (fPS NPs) and alginate chitosan nanoparticles (AC NPs) was tested in the jejunum region of the small intestine of rats using intraluminal injections. After the exposure of NPs on the epithelium for 15 min and 30 min, the tissues were isolated and processed by an immunofluorescence protocol. Nuclei in the epithelium were stained with DAPI, red fluorescent fPS NPs were observed using a confocal microscope. The location of AC NPs-ntPE was determined using immunofluorescence to detect ntPE on the surface of AC NPs. Green fluorescent protein (GFP) was used as a model biopharmaceutical (MW = 26 kDa; pI = 5.7) loaded into AC NPs-ntPE. GFP-loaded AC NPs were administered following the same protocol as previous NPs, and using the fluorescein labelled antibody to track GFP using confocal microscopy.

Results: Localisation of blank fPS NPs or those conjugated with BSA or ntPE was assessed in the *lamina propria* at 15 min and 30 min following the injection of 166 µg fPS NPs-ntPE into the intestinal lumen. There were no detected fluorescence signals for blank fPS NPs nor fPS NPs-BSA in the villi, but fPS NPs-ntPE were found in the *lamina propria*. AC NPs and GFP-loaded AC NPs were also found in the *lamina propria* of the small intestine in a manner dependent upon the coupling of ntPE. Overall, ntPE-mediated NPs showed potential of being a trans-epithelial carrier for biopharmaceuticals.

5.1 Introduction

In chapter 4, the transcytosis of fPS NPs and AC NPs mediated by ntPE was tested in Caco-2 cell monolayers. Those studies failed to demonstrate a robust transport of these NPs in that *in vitro* model. It was concluded that the Caco-2 monolayer used possibly has low expression of GM1, which is important for the transport of ntPE, therefore this cell monolayer, may have not provided the normal transcytosis trafficking typically observed *in vivo* (248). Thus, the feasibility of using ntPE to facilitate the trans-epithelial transport of NPs was tested *in vivo*.

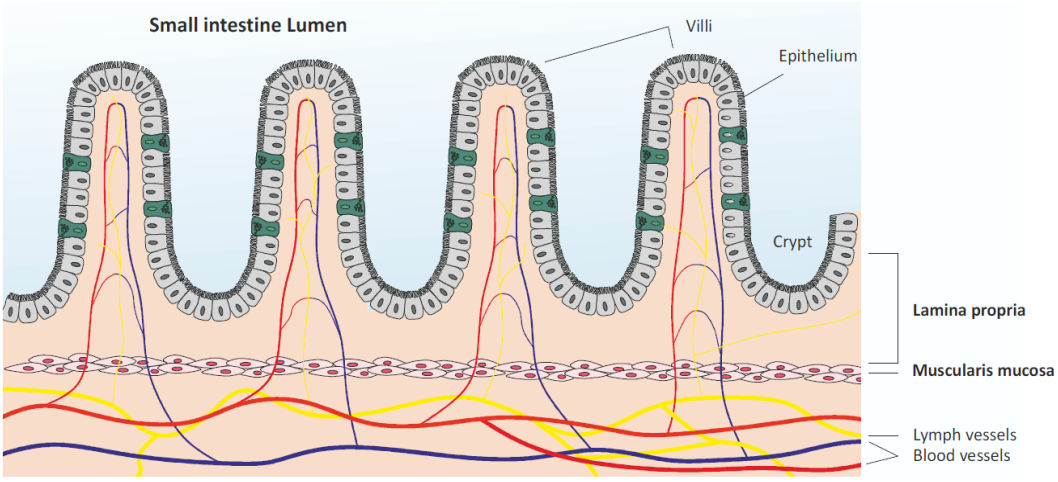

Figure 5-1: Illustration of the small intestinal mucosa. The epithelium rests upon an underlying layer of connective tissue, *lamina propria*, which it itself supported by layers of smooth muscles named as *muscularis mucosa*. The finger-like projections are named villi, and the wells between these epithelial-lined villi are called crypts. Image is from (2).

The anatomy of the intestinal epithelium was introduced in Chapter 1, these tissues will be discussed in additional detail here. Intestinal epithelium functions not only as a barrier to unwanted solutes, this tissue is also responsible for selectively absorbing nutrients from the lumen, as well as maintaining the homeostatic conditions of the small intestine (23). Underneath the epithelium is a loose connective tissue called *lamina propria* that functions to organise blood and lymphatic vessels (referring to central lacteal), as well as a wide variety of circulating immune cells and resident cells involved in local humoral and adaptive immunity (Figure 5-1). Dendritic cells (DCs) are one cell population in the *lamina propria* involved in antigen presentation, being able to extend processes between two adjacent enterocytes and sample bacteria from the lumen (268). Overall, the *lamina propria* is a place for regulating immune function, providing nourishment for the epithelium, and processing/passing nutrients absorbed across the epithelium.

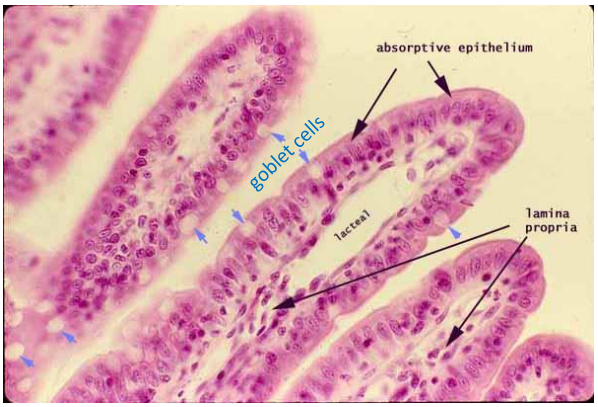

Figure 5-2: Image of villi in the small intestine. The villi are lined by simple columnar epithelial cells (enterocytes) and interspersed with goblet cells (blue arrows).

The intestinal epithelium consists of a monolayer of columnar epithelial cells covered by a mucus layer (Figure 5-2) (33). Enterocytes are the most common cells of the intestinal epithelium, with microvilli expressed at the apical (luminal) surface that are referred to as a brush border. Another commonly present cell type in the intestinal epithelium is the goblet cell. These cells produce mucin and release it onto the luminal surface of the intestinal epithelium. This mucus layer forms a barrier to help limit the invasion of pathogens or noxious substances (33). The mucoadhesive polymers chitosan and alginate were used in this study to form NPs, in order to increase interactions with the mucus at the surface of the epithelium (126).

Microfold (M) cells are located individually or in lymphoid follicle-associated epithelium. M cells play an important role in the immune response as they internalise antigens from the intestinal lumen via endocytosis, and deliver them to underlying lymphoid cells (35). M cells have less irregular microvilli and mucus layer compared to the enterocytes, and account for only ~1% of the surface area of the epithelium (77). For that reason, Hussain *et al.*(1997) pointed out that the importance of M cells for delivering biopharmaceuticals should not be over-emphasised (82). Nevertheless, M cells have attracted considerable interest as a transport route.

Non-toxic *Pseudomonas* exotoxin (ntPE) is able to transport across simple columnar epithelial cells, such as that present in the small intestine (229). ntPE was attached onto the surface of NPs in this work, and the feasibility of using ntPE to facilitate the transport of NPs across the epithelium was tested in a rat *in vivo* model.

Conventional *in vivo* studies assess the oral bioavailability of an agent by comparing the plasma level *vs.* time curves following oral administration to that of an intravenous (IV) administration (231). Oral gavage was not performed here, because the NPs' location and concentration within the intestine would be uncertain over time. Instead, intraluminal injection was performed to allow examination of specific intestinal locations to directly ascertain the potential for NP uptake. By using this method, the behaviours of NPs in the epithelium would be assessed specifically. Furthermore, intraluminal injection studies would allow the visualisation of the transport process, as well as localisation of transported NPs within the *lamina propria* of the small intestine. No IV administrations of the NPs was performed as the goal of these studies was to examine ways to facilitate NP delivery to the *lamina propria* and not the systemic circulation.

These *in vivo* studies also allowed assessment of mucus and intestinal motility on NP uptake, aspects that cannot be readily evaluated using polarised epithelial cell monolayer *in vitro*.

A non-degradable, commercial NP system (fPS NPs) was initially used to study the ntPE-mediated transport process. Although fPS NPs do not provide a viable carrier for the delivery of biopharmaceuticals, these NPs remain stable during the course of the experiment. By comparison, AC NPs are biodegradable and have the capacity to encapsulate biopharmaceuticals. The potential of using ntPE-mediated AC NPs for delivering biopharmaceuticals across the epithelium was tested, with green fluorescent protein (GFP), being loaded into AC NPs as a model for biopharmaceuticals.

5.2 Methods

5.2.1 *In vivo* transcytosis of fPS NPs

5.2.1.1 *In vivo* transcytosis assay protocol

Male Wistar rats (250-300 g; approximately 7-9 weeks old, bred in-house) were maintained on a 12 h light/day cycle. All experiments were conducted during the light phase. Animals were anesthetised under 5 % isoflurane and maintained in an anesthetised state using 4 % isoflurane (administered by mask) during surgery. Animals were placed on a warming pad throughout the procedure to maintain a stable body temperature. A 4 – 5 cm midline abdominal incision was used to expose the small intestine. After selection of a site within the mid-jejunum that contained minimal food, fPS NPs (166 µg or 332 µg for fPS NPs-ntPE, 332 µg for blank fPS NPs and fPS NPs-BSA) suspended in PBS (pH 7.3, Phosphate-buffered saline, Dulbecco "A" Tablets, BR0014G, Oxoid Ltd) were injected into the lumen using a 21 G needle (0.8 × 16 mm, BD Microlance™, 304434, Becton Dickinson). The adjacent mesentery was marked with indelible ink and the intestinal segment was returned to the abdominal cavity until the tissue to be harvested for analysis.

Concentrations of NPs and exposure times after injection are given in Table 5-1. fPS NPs-ntPE were used in condition 1 to condition 3, condition 1: 166 µg of with 15 min exposure time; condition 2: 166 µg with 30 min exposure time; and condition 3: 332 µg with 15 min exposure time. The condition for unmodified fPS NPs and fPS NPS-BSA was 332 µg with 15 min exposure time. After 15 or 30 min, the animal was euthanised using CO_2 and a 2 cm intestinal section encompassing the injection site was isolated. The dissected tissue was cut longitudinally and the luminal surface washed with ice-cold PBS prior to placing it (splayed flat) in a cassette with the lumen side facing up. The tissue was then fixed by applying 100 µL of 4 % PFA

(paraformaldehyde, P6148, Sigma-Aldrich) onto the luminal surface. After 20 min at 4 °C, fixed tissue was processed by tissue processor for 18 h (TP 1020, Leica Miscrosystems). Sections of small intestine (5 µm) were subsequently cut using a microtome (Biocut 2035, Leica Microsystems) and mounted onto polylysine slides (P4981, Thermo Scientific).

Table 5-1: Detailed information of different conditions

	Type of NPs	Concentration	Volume	Exposure time	Fluorescent tag
Condition 1	fPS NPs-ntPE	1666 µg/mL	100 µL	15 min	FluoSpheres® (E_x/E_m: 580/605)
Condition 2	fPS NPs-ntPE	1666 µg/mL	100 µL	30 min	FluoSpheres® (E_x/E_m: 580/605)
Condition 3	fPS NPs-ntPE	1666 µg/mL	200 µL	15 min	FluoSpheres® (E_x/E_m: 580/605)
Condition 4	AC NPs-ntPE	86 µg/mL	250 µL	15 min	Alexa Fluor® 546 (E_x/E_m: 556/573)
Condition 5	AC NPs-ntPE	86 µg/mL	250 µL	30 min	Alexa Fluor® 546 (E_x/E_m: 556/573)
Condition 6	GFP-AC NPs-ntPE	86 µg/mL	250 µL	30 min	Fluorescein (E_x/E_m: 490/525)

5.2.1.2 Immunohistochemistry

Slide-mounted cut sections were processed by successive 5 min immersions of Histo-Clear (solution 1, HS-200, National Diagnostics), Histo-Clear (solution 2), and 100 %, 90 %, 80 %, 70 % ethanol solutions (20821.330, VWR chemicals). Tissue sections were then washed three times with PBS for 5 min each time. Cell nuclei within the tissue sample were then stained by 30 min incubation with DAPI (4', 6-diamino-2-phenylindole, Dihydrochloride, D1306, Thermo Fisher Scientific) at RT. After rinsing with PBS and then water, sections were dehydrated in 70 % and 100 % ethanol for a few minutes each, followed by immersion in Histo-Clear solution 1 for 5 min and 100 % ethanol for a few minutes. Processed tissue sections were mounted using Fluoroshield Mounting Medium (ab104135, Abcam) prior to placement of a glass cover slip (12342118, 22×50 mm, Fisher Scientific). Confocal microscopy, performed using a Zeiss LSM 510 microscope, was used to identify and localise fPS NPs in processed tissue sections. The corrected total cryosection fluorescence (CTCF) was calculated by analysing 11 images of each condition (269). The equation used was:

CTCF=media of integrated density - (media of area of selected cell × mean fluorescence of background readings).

5.2.2 *In vivo* study of AC NPs

A volume of 250 µL of AC NPs (suspended in PBS, kept in 4 °C before injection) was administered using the same protocol as described above for fPS NPs (in section 5.2.1). Condition 4: 250 µL of AC NPs-ntPE for 15 min of exposure and condition 5: 250 µL of AC NPs-ntPE for 30 min of exposure. Following fixation, imbedding, sectioning and mounting onto polylysine slides, tissue samples were rehydrated by successive 5 min immersions into Histo-Clear (solution 1), Histo-Clear (solution 2), and 100 %, 90 %, 80 %, 70 % ethanol solutions and then washed three times with PBS for 5 min. AC NPs were tracked in a confocal microscope by using immunohistochemistry to stain ntPE. Antigen retrieval was performed by immersing slides in boiling 10 mM sodium citrate buffer at pH 6.0 for 10 min. After the antigen retrieval process, tissue sections were then permeabilised for 30 min at RT using 0.2 % Triton X-100 (X100-500ML, Sigma-Aldrich) in PBS and incubated at RT for 2 h in blocking buffer (containing 2 % BSA, A7906-100G, Sigma-Aldrich; 2 % donkey serum, D9663-10 mL, Sigma-Aldrich; and 0.1 % Triton-X 100 in PBS) prior to incubation in primary antibody (rabbit polyclonal anti-pseudomonas exotoxin A, P2318-1ML, diluted 1:1000) in PBS containing 0.1 % Triton X-100 and 1% BSA overnight at 4 °C. Excess primary antibody was removed by rinsing in PBS prior to incubation at RT for 2 h in a secondary antibody solution (Alexa Fluor® 546-conjugated donkey anti-rabbit polyclonal IgG, diluted 1:100, A10040, Life Technologies™) containing 0.1 % Triton X-100 in PBS. Afterwards, tissue sections were incubated with DAPI for 30 min at RT and rinsed using PBS and then water. After dehydration in 70 % and then 100 % ethanol for a few minutes each, tissue sections were exposed to Histo-Clear solution 1 for 5 min and 100 % ethanol for a few minutes prior to the addition of Fluoroshield Mounting Medium (ab104135, Abcam). A glass cover-slip was placed onto the tissue sample which was then analysed in a Zeiss LSM 510 microscope. The CTCF was calculated from 16 images of each injection condition.

Examination of CD11c$^+$ dendritic cells by immunohistochemistry staining

Dendritic cells in the *lamina propria* of rat jejunum were visualised using immunofluorescence staining. After antigen retrieval process, tissue sections were permeabilised for 30 min at RT using 0.2 % Triton X-100 in PBS and incubated at RT for 2 h in blocking buffer (containing 2 % BSA, 2 % donkey serum, and 0.1 % Triton-X 100 in PBS) prior to incubation in primary antibody (rabbit polyclonal anti-*Pseudomonas* exotoxin A and mouse monoclonal anti-CD11c antibody, diluted 1:1000) in PBS containing 0.1 % Triton X-100 and 1 % BSA overnight at 4 °C. Excess primary antibody was removed by rinsing in PBS prior to incubation at RT for 2 h in a secondary antibody solution (Alexa Fluor® 546-conjugated donkey anti-rabbit polyclonal IgG, and Alexa

Fluor® 488 conjugated donkey anti-mouse polyclonal IgG, (ab150109, Abcam) diluted 1:100) containing 0.1% Triton X-100 in PBS. Afterwards, tissue sections were incubated with DAPI for 30 min at RT and rinsed using PBS and then water. After dehydration in 70 % and then 100 % ethanol for a few minutes each, tissue sections were exposed to Histo-Clear solution 1 for 5 min and 100 % ethanol a few minutes prior to the addition of Fluoroshield Mounting Medium (ab104135, Abcam). A glass cover-slip was placed onto the tissue sample, which was then analysed in a Zeiss LSM 510 microscope.

5.2.3. *In vivo* study of GFP-loaded AC NPs

GFP-loaded NPs were prepared by adding GFP into AC NPs suspensions. The details can be found in Chapter 2.2.4. A 250 µL volume of GFP-loaded AC NPs-ntPE and GFP-loaded AC NPs-BSA (suspended in PBS, kept in 4 °C before injection) was injected into the lumen of rat small intestine for 30 min. Tissue preparations used for confocal microscopy closely followed the protocol described in section 5.2.1.2, the only difference was the immunofluorescence staining was performed to determine GFP, refer to Table 5-1. Blocking buffer containing 2 % BSA, 2 % goat serum (G9023-10 mL, Sigma-Aldrich), and 0.1 % Triton-X 100 in PBS was used, the primary antibody was rabbit polyclonal anti-GFP (ab6556, Abcam) and the secondary antibody was fluorescein goat anti-rabbit IgG (F1-1000, Vector).

5.3 Results

5.3.1 *In vivo* transcytosis of fPS NPs

Rat jejunum tissues exposed to NPs for different times (15 min and 30 min) and at different doses (166 µg and 332 µg) were collected and processed as described in section 5.2. Internalisation of fPS NPs occurred shortly after the intraluminal injection (Figure 5-3) shown in confocal microscopy. The finger-like structures (in Figure 5-3a, c, d, e and f) were identified as villi, and the nuclei of cells were stained by DAPI. Goblet cells can be found between two enterocytes (yellow arrows in Figure 5-3a and b). They are responsible for secreting glycoproteins named mucins, which generate a protective mucus blanket overlying the epithelial surface (270).

With the treatment of 166 µg fPS NPs-ntPE for 15 min (condition 1) on the luminal side of epithelium, some red fluorescence signals were found in the *lamina propria* (Figure 5-3, white arrows) and they were considered to be the accumulation of fPS NPs-ntPE.

Images in Figure 5-4 show the tissue segments following exposure to fPS NPs-ntPE for an increased exposure time of 30 min (condition 2). The same dose of 166 µg as the previous study was used. Red fluorescent dots were found in the *lamina propria* using confocal microscopy (Figure 5-4), this outcome was consistent with the 15-min study (Figure 5-3). The observed fluorescent signals refer to the accumulated NPs in the tissue, since confocal microscopy is unable to track individual NPs.

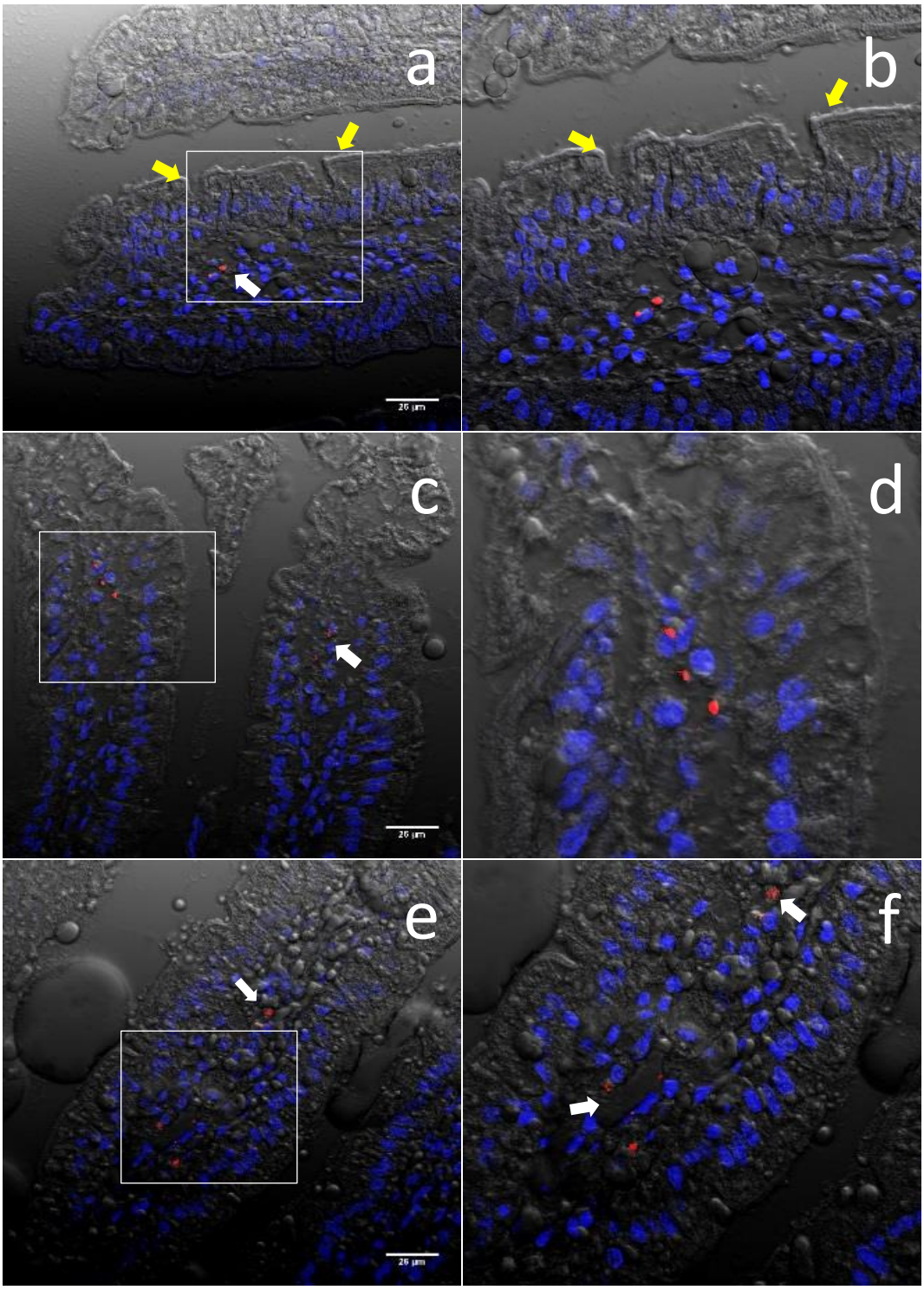

Figure 5-3: Representative confocal images of fPS NPs-ntPE in the villi (condition 1: 166 µg for 15 min). After exposing to NPs for 15 min, red fluorescence suggesting fPS NPs-ntPE were collected in the villi. Goblet cells in the epithelium were indicated by yellow arrows in (a) and (b), the internalised and collected NPs are pointed in (c), (e), and (f) by white arrows. Images on the right column are magnified from the white frame, can be found in the images on the left column (red: fPS NPs, blue: nuclei, scale bar=26 µm).

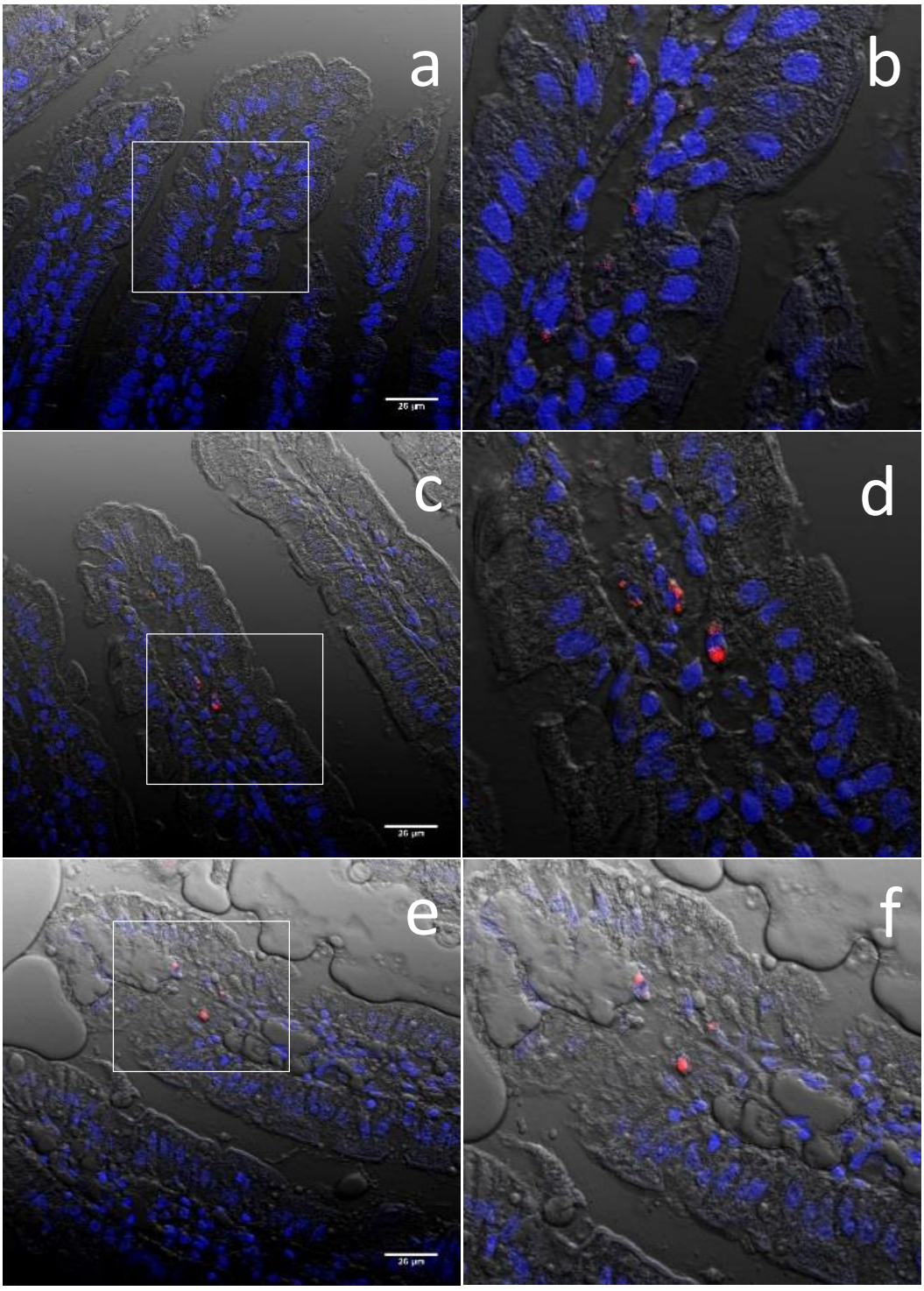

Figure 5-4: Representative confocal images of fPS NPs-ntPE (condition 2: 166 µg for 30 min). Red fluorescence signals (representing fPS NPs-ntPE) were detected in the *lamina propria* after exposing lumen to fPS NPs-ntPE for 30 min, suggesting the uptake and transport of fPS NPs-ntPE was still occurring at 30 min after the intraluminal injection. fPS NPs-ntPE appeared to be in close proximity with the DAPI-stained nuclei in the *lamina propria* in (d). Images on the right column are magnified from the white frame, found in the images on the left column (red: fPS NPs-ntPE, blue: nuclei, scale bar=26 µm).

A longer transcytosis study was not carried out, given exposure times longer than 30 min are perhaps not meaningful to study; rapid internalisation is preferred for delivering biopharmaceuticals via the oral route, considering the harsh environment in the lumen might affect the bioactivity of the delivered cargos (271).

fPS NPs-ntPE were found in the *lamina propria* regardless of the exposure time (15 min or 30 min). This outcome showed that fPS NPs had gone across the epithelium, but the transport route is unknown. Quantifying these NPs in the *lamina propria* is desirable, although no standard method exists (272). Generally speaking, two approaches have been undertaken to quantify measures in fluorescence microscopy images, concrete statistics and abstract statistics. Concrete statistics include counting measures such as volume occupied by a structure, and the number of structures in a region. While, the abstract statistics measure properties of an image such as morphology or texture (273). In this study, concrete statistics was chosen and carried out by summing up the red fluorescence intensity in the villi using software Image J (from 11 images). The summed values were considered to represent the amounts of fPS NPs found in the villi (274). The background fluorescence was subtracted from the fluorescence intensity in each image, and the intensity of fluorescence signals was calculated using a reported equation (corrected total crysection fluorescence, CTCF) (269).

The total calculated red fluorescence intensity in the tissue after exposure for 15 min, was in a similar range as the isolated tissues after 30 min-treatment (Figure 5-5). This might suggest that fPS NPs-ntPE were translocated via the blood or lymphatic vesicles, or were taken up by the immune cells in the *lamina propria*. If there was no translocation of fPS PS-ntPE occurring, more and more internalised fPS NPs would be accumulated in the *lamina propria* rather than in a sustained amount as observed. It is unlikely for the internalised NPs to stay in cells/tissues for 30 min, since this transport study was performed in a living rat. It is important to note that this interpretation is only based on the acquired confocal images, which were samples from part of the treated tissues. Regarding the dynamic transport process of NPs, a real-time tracking study would provide more information.

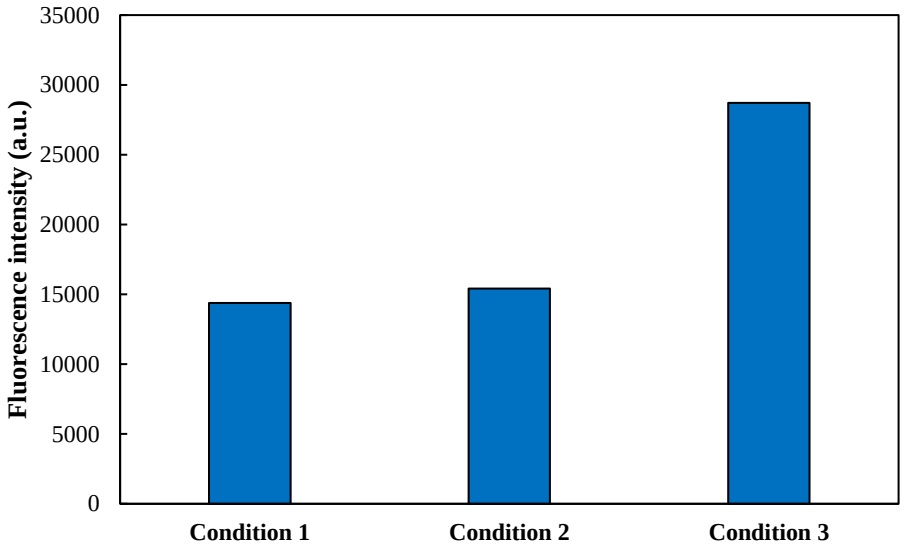

Figure 5-5: Comparison of the red fluorescence intensity from tissues being treated with fPS NPs-ntPE at different conditions. Condition 1: 166 µg for 15 min; condition 2: 166 µg for 30 min; and condition 3: 332 µg for 30 min. The amounts of red fluorescence intensity suggested the amounts of fPS NPs accumulated in the villi, condition 1 and condition 2 was in a similar range. The administration of double amounts of fPS NPs into the small intestine seemed to result in double amounts of measured red fluorescence intensities collected in the villi, which suggesting the transport of ntPE-mediated fPS NPs has a concentration effect.

To understand how the transport of fPS NPs might be influenced by concentration, the luminal side of the epithelium was exposed to 332 µg of fPS NPs-ntPE (condition 3), which was double the amount of NPs compared to the previous two conditions. Red fluorescent dots were the signals from the accumulated fPS NPs-ntPE in the villi, after 15 mins of intraluminal injection of NPs into the lumen side of small intestine (in Figure 5-6). The associations with these cells might suggest that fPS NPs were collected in the cells present in the *lamina propria*.

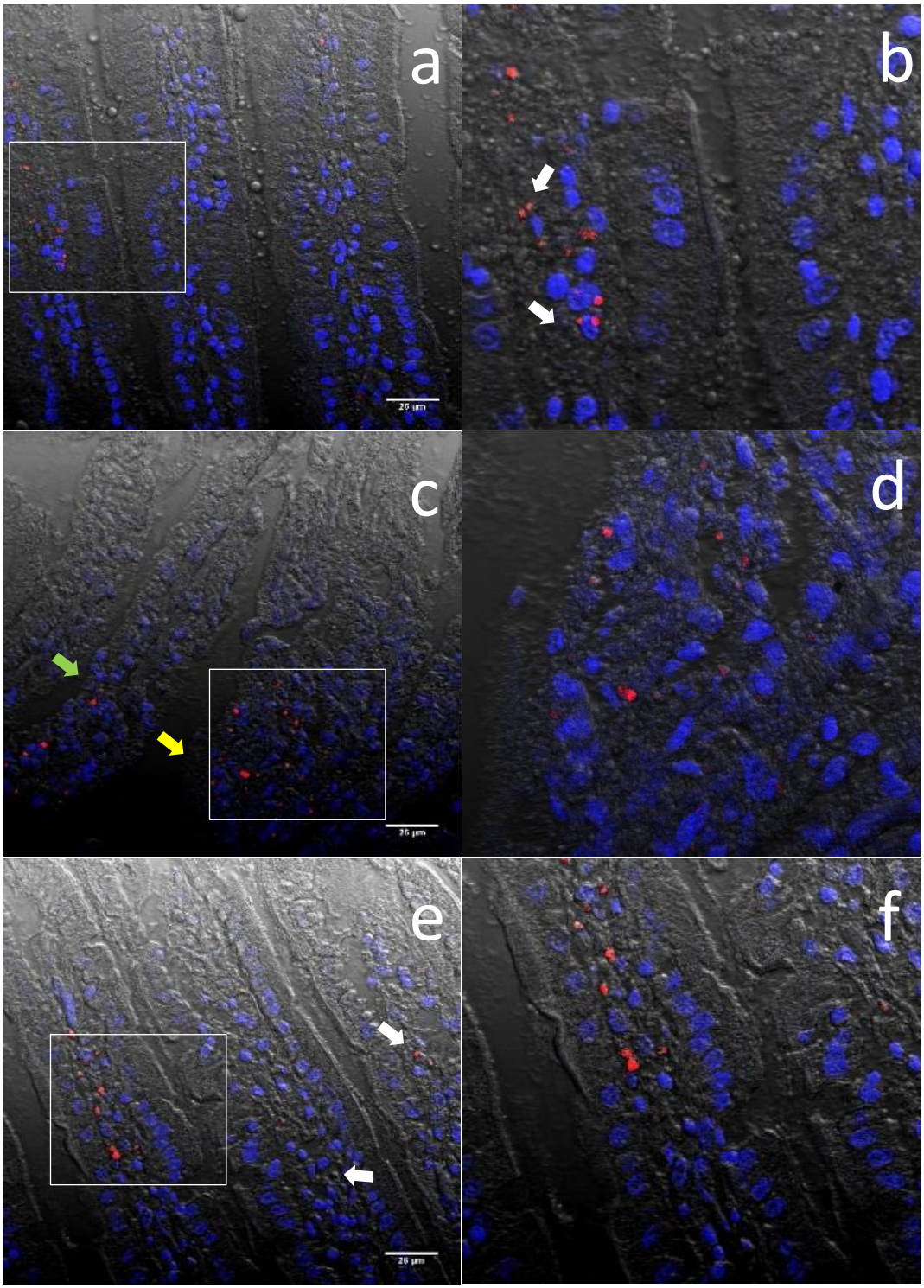

Figure 5-6: Representative confocal images of ntPE-coupled fPS NPs (condition 3: 332 µg for 15 min). As shown in (b), fPS NPs-ntPE were co-localised with DAPI-stained nuclei cells present in the *lamina propria*. The relatively wide structure found (yellow arrows) in figure (d) was considered to be the Peyer's patch, which has shown the ability to take up NPs. In the magnified image (d), these blue-stained cells were considered to be cells present in Peyer's patch, as they were less organised compared to the stained enterocytes in (b) and (f). Images on the right column are magnified from the white frame, which can be found in the images on the left column (red: fPS NPs-ntPE, blue: nuclei, scale bar=26 µm).

The thin finger-like structure (indicated by green arrows in Figure 5-6c) was identified as a villus, while on the right side of it, the round and wide structure appeared to be a Peyer's patch (yellow arrows in Figure 5-6c). The DAPI-stained cells in Figure 5-6d appeared to be in an irregular organisation compared to cells seen in Figure 5-6b and f. They might be M cells present in the Peyer's patches, which are responsible for transporting luminal antigens (and bacteria) to the underlying immune cells that either activate or inhibit the immune response (275). It is within expectation to see NPs accumulated in the Peyer's patch, as studies have demonstrated the Peyer's patch is able to absorb and assemble particles < 1 μm (276, 277). It is also possible that these irregular shaped cells were caused by the sample processing, particularly the sectioning part.

Compared to the intestinal tissues treated with 166 μg of fPS NPs-ntPE for 15 min (condition 1), double amounts of administrated fPS NPs-ntPE seemed to result in double amounts of measured fluorescence values (Figure 5-5). It is known that the variable microscope settings in different studies would bring difficulties in comparing images (278). Although these measured fluorescence values represent accumulated fPS NPs in selected slices of the isolated tissue (150-200 slices cut, only ~25 slices imaged), it is possible to compare between tissues prepared and visualised in the same protocol. The transport of fPS NPs mediated by ntPE appeared to have a concentration effect. Higher doses of fPS NPs are needed to be tested in future work, for a more comprehensive understanding of ntPE-mediated transport of NPs.

To investigate the role of ntPE in the transport of fPS NPs, unmodified fPS NPs and fPS NPs-BSA were also administered to the luminal side of epithelium for 15 min. No red fluorescence signals were detected in the villi using a confocal microscope (Figure 5-7a). Following the isolation of tissue from the animal, extensive rinsing was carried out to wash away any residues on the lumen side, perhaps the unspecific-attached NPs were washed away. It is also possible that confocal microscopy is unable to detect these NPs, as they were in small amounts and the fluorescence intensity might be below the detection limit of confocal microscopy. In addition, this observation cannot exclude the possibility that unmodified fPS NPs and fPS NPs-BSA were quickly taken up and translocated, therefore, they could not be detected in the villi any more. fPS NPs-BSA were found to accumulate on the edge of the epithelium (Figure 5-7b), although no trace of fPS NPs-BSA was detected in the other 10 confocal images for this condition. This outcome suggested the importance of ntPE for the internalisation of fPS NPs.

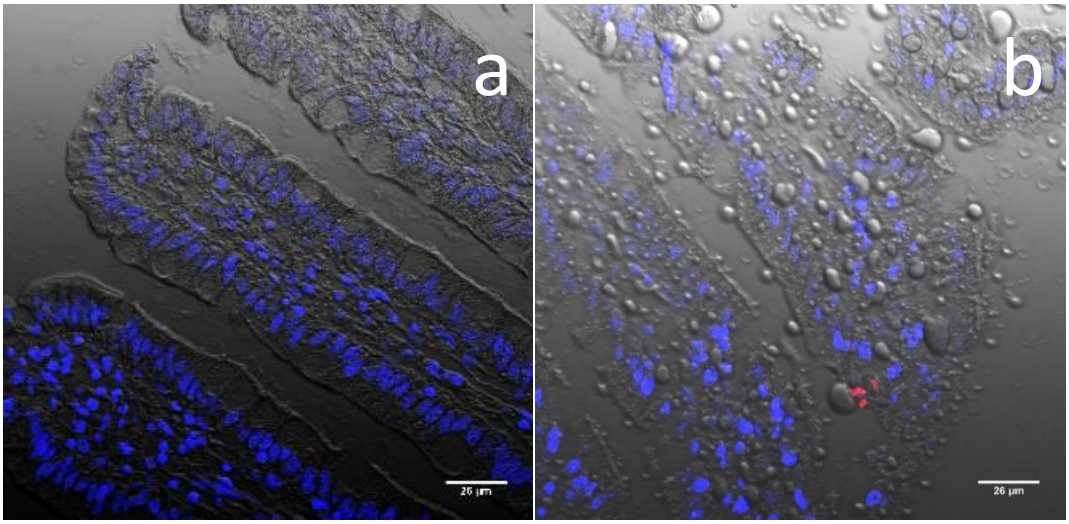

Figure 5-7: Representative confocal images of unmodified fPS NPs and fPS NPs-BSA in the villi. (a) No red fluorescence was detected in the villi of which lumen side had been exposed to 332 µg of unmodified fPS NPs for 15 min; and (b) BSA coupled-fPS NPs seemed to be accumulated on the surface of the epithelium (red: fPS NPs, blue: nuclei, scale bar=26 µm).

Following the administration of fPS NPs-ntPE into the lumen of rat small intestine, fPS NPs-ntPE appeared to accumulate underneath the epithelium observed using confocal microscopy. This outcome supports the hypothesis that ntPE is able to facilitate the transport of NPs across the epithelium. Therefore, its feasibility to mediate a nano-carrier loaded with biopharmaceutical to transport across the intestinal barrier will be tested.

5.3.2 *In vivo* transcytosis of AC NPs

AC NPs have shown the ability to encapsulate proteins in Chapter 2. Prior to using this nano-carrier to deliver biopharmaceuticals, the transport of AC NPs mediated by ntPE was tested *in vivo* using the same protocol as fPS NPs-ntPE. Unlike fPS NPs which have impregnated fluorophores, AC NPs were visualised using Alexa Fluor® 546-conjugated antibody to track ntPE on the surface of NPs. Several attempts were made to visualise the fluorescence labelled AC NPs, while no fluorescence signals were detected using confocal microscopy, this might be due to the damage brought by the fixation process.

Red fluorescence dots in the *lamina propria* represented the accumulation of AC NPs, which can also be found on the surface of the epithelium, shown in Figure 5-8. AC NPs appeared to accumulate under the basolateral side (yellow arrows, Figure 5-8d), and be collected in a DAPI-stained cells (white arrows, Figure 5-8).

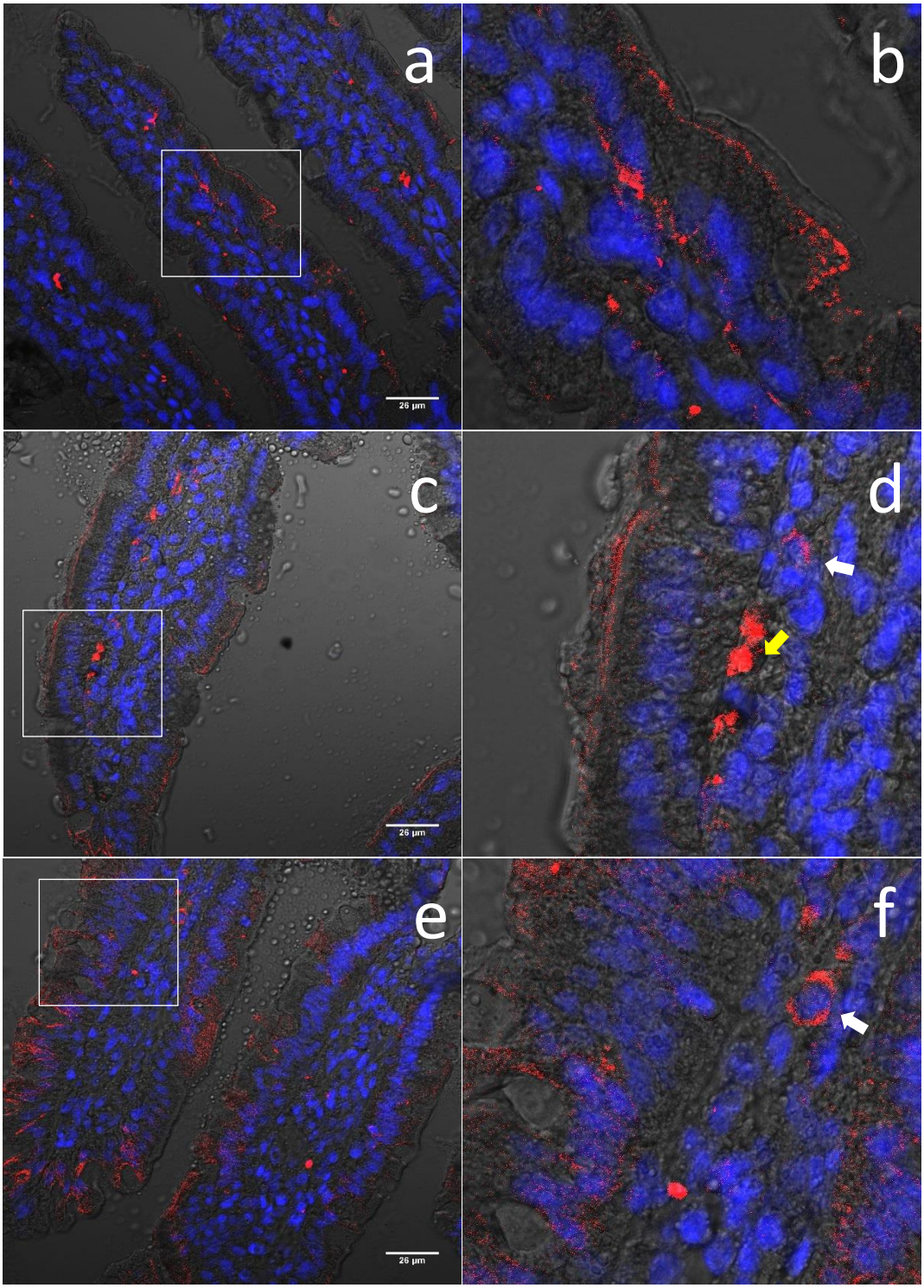

Figure 5-8: Representative confocal images of AC NPs-ntPE in the villi (condition 4: 250 µL for 15 min). Red fluorescent dots in the *lamina propria* suggested the accumulation of AC NPs-ntPE, red fluorescence can also be found on the surface of the epithelium and on the basolateral side of the epithelium (yellow arrows). Images on the right column are magnified from the white frame, found in the images on the left column (red: AC NPs-ntPE, blue: nuclei, scale bar=26 µm).

After the intraluminal injection of AC NPs-ntPE with 30 min exposure, red fluorescence signals were still found in the villi (Figure 5-9). Apart from locating in the *lamina propria*, some collected AC NPs were found in a close proximity to the DAPI-stained nuclei of the enterocytes in Figure 5-9b (yellow arrows), and Figure 5-9e (yellow arrows). Mathiowitz *et al*. (1997) demonstrated that NPs (made by polyanhydride copolymer of fumaric and sebacic acid) were taken up by the absorptive enterocytes observed using transmission electron microscopy; and NPs were visible in the dilated Golgi apparatus and secretory vesicles near the lateral edge of the cells. The mechanism of entry was not clear (277).

Red arrow (in Figure 5-9b) indicates the goblet cell in the epithelium. McDole *et al.* (2012) showed that goblet cells would allow small soluble protein antigens to the *lamina propria* via the goblet cell-associated pathway, and this pathway is size-dependent, as particles bigger than 20 nm did not enter this pathway (279). For this reason, it was unlikely for AC NPs (~200 nm diameter) in this study to undertake the goblet cell-associated pathway. Later on, Howe *et al.* (2014) supported the importance of particle size on the internalisation via goblet cell-associated cells, and suggested that NPs (polystyrene, 40 nm) can be taken up by enterocytes via a clathrin-mediated endocytosis. Besides, Howe *et al.* (2014) also observed that NPs in the *lamina propria* co-localised with $CD11c^+$ dendritic cells, following 30 min of exposure after intraluminal injection (280).

CD 11c are membrane proteins expressed in dendritic cells, macrophages and neutrophils (281, 282). AC NPs' accumulation appeared to co-localise with CD $11c^+$ cells using a fluorescence antibody bound to CD 11c (Figure 5-10). It is well known that dendritic cells play a key role in the regulation of the intestinal immune response (283). Farache *et al.* (2013) showed dendritic cells can sample antigen directly from the intestinal lumen, likely using tight junction proteins to penetrate the epithelium (284). This uptake route might also occurred in the transport of AC NPs-ntPE herein, considering CD 11c is highly expressed in dendritic cells. Green fluorescent signals (for CD 11 c^+) were found in the enterocyte and between two adjacent enterocytes (white arrows, in Figure 5-10b), this might suggest that these immune cells travel across the intraepithelial route to take up antigens from the lumen, particularly dendritic cells (285). An attempt to understand the role of macrophages in the uptake of NPs was not performed, due to the lack of appropriate fluorescent antibody for visualising.

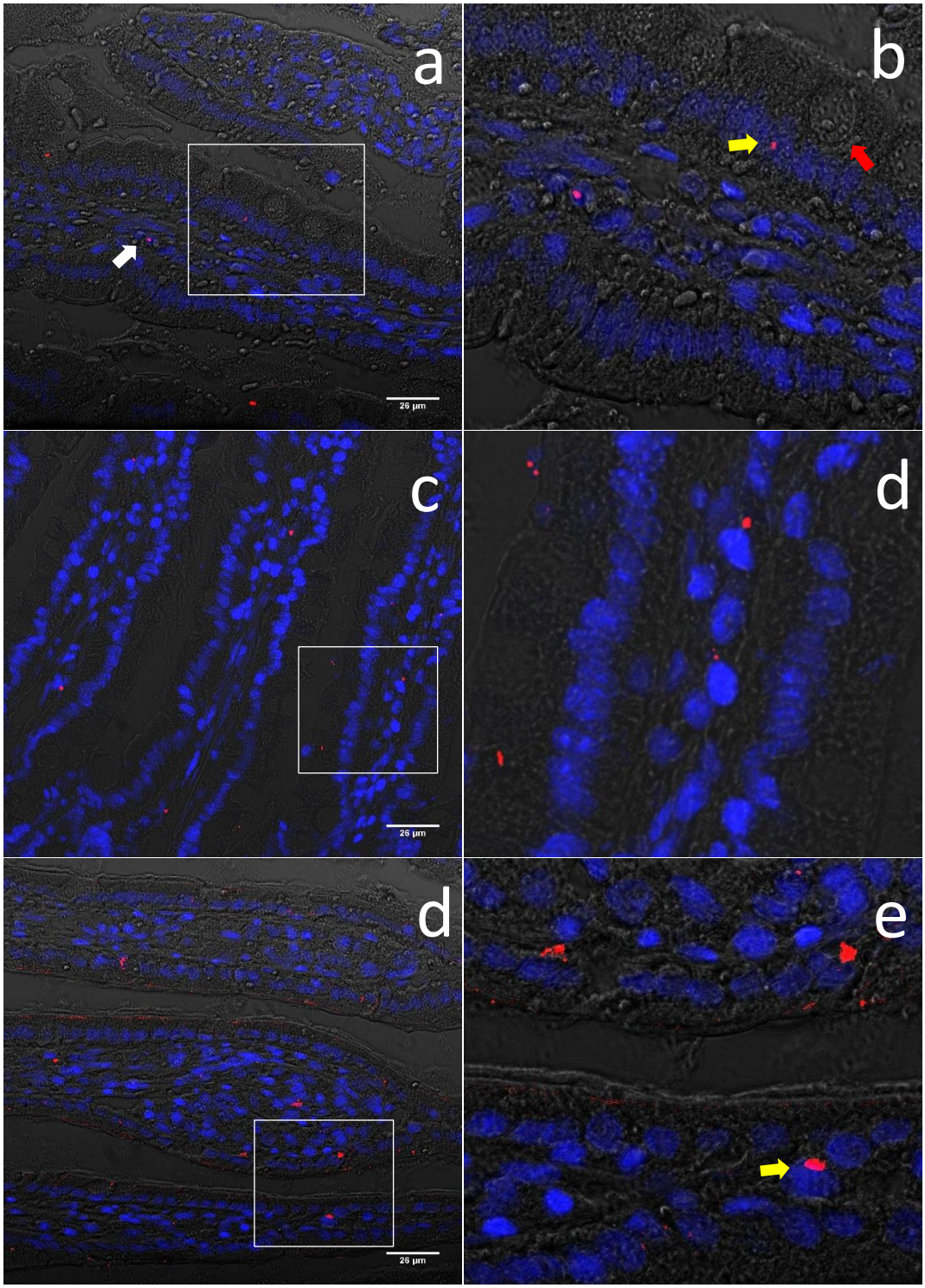

Figure 5-9: Representative confocal images of AC NPs-ntPE in the villi (condition 5: 250 µL for 30 min). AC NPs-ntPE (red fluorescence) were still detectable after 30 min of exposure time. AC NPs-ntPE accumulated on the basolateral sides of epithelium, and were also in close proximity to the enterocytes (yellow arrows). Images on the right column are magnified from the white frame, can be found in the images on the left column (red: AC NPs-ntPE, blue: nuclei, scale bar=26 µm).

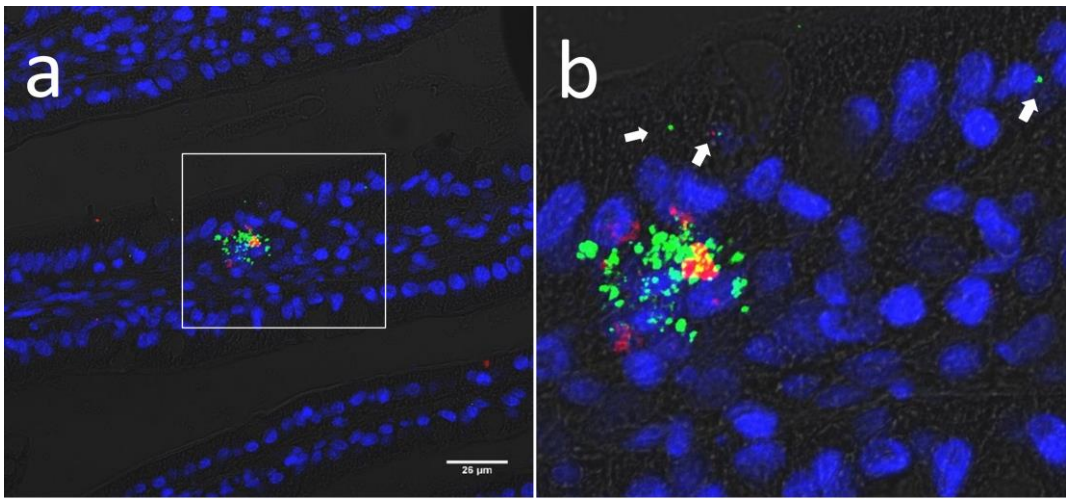

Figure 5-10: Representative confocal images of AC NPs-ntPE in the villi co-localising with CD 11c$^+$ cells. AC NPs-ntPE were stained by the red fluorescence, cells expressing CD 11c were presented by green fluorescence, and nuclei were in blue. The accumulated AC NPs-ntPE were found to be co-localised with CD 11c$^+$ cells. Green fluorescence labelled CD 11c$^+$ cells can also be found on the surface of the epithelium and between two enterocytes, suggesting these immune cells were in the process of taking up and transporting antigens (scale bar= 26 µm).

The red fluorescence intensity in the villi after 15 min- and 30 min- treatment with AC NPs-ntPE was measured and summed up from 16 images (Figure 5-11). The tissue exposed to AC NPs-ntPE for 30 min seemed to have lower fluorescence values compared to 15min tissue-exposure time. It is consistent with the observation from the confocal images, that fewer red fluorescence signals were found on the surface of the epithelium for 30-min treatment. Although confocal images may not represent the whole uptake and trans-epithelium process of AC NPs-ntPE, at least it showed that AC NPs-ntPE can be taken up and translocated within 15 min. In terms of delivering biopharmaceuticals, a short exposure time to the harsh environment is beneficial for preserving the structure of biopharmaceuticals (23).

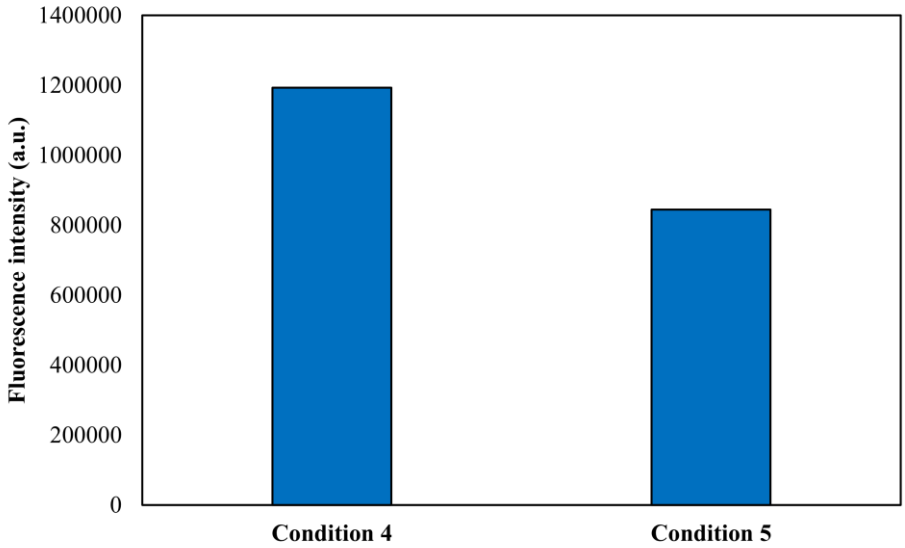

Figure 5-11: Comparison of the fluorescence intensity of AC NPs-ntPE in two isolated tissues. Condition 4 was for tissue of which lumen side was exposed to 250 µL AC NPs-ntPE for 15 min, and condition 5 was for 30 min. The uptake of AC NPs-ntPE occurred quickly after the intraluminal injection, and it seemed to slow down after 15 min.

5.3.3 *In vivo* transcytosis of GFP loaded AC NPs

ntPE seemed to facilitate AC NPs transport across the epithelium, thus to evaluate whether these ntPE-coupled nano-carriers are able to deliver biopharmaceuticals or not, GFP was loaded into AC NPs. The GFP-loaded AC NPs were prepared and administered into rat small intestine by intraluminal injection, and the transport was evaluated by tracking GFP using a fluorescein-labelled secondary antibody using confocal microscopy.

Although GFP is auto-fluorescent, the fixation process damaged the fluorescent signals, so that GFP was tracked by using a fluorescent antibody. The confocal images in Figure 5-12 captured the moment of transporting GFP-loaded AC NPs-ntPE across the epithelium. Green fluorescence signals representing the accumulated AC NPs, can be found on the surface of epithelium (yellow arrows, Figure 5-12f and c) and inside of the enterocytes (red arrows, Figure 5-12b and Figure 5-12c); and some were located in the *lamina propria* (white arrows).

It is understood that the detection of GFP in the confocal microscopy does not necessarily indicate these proteins were still encapsulated in AC NPs. Furthermore, the bioactivity of the delivered proteins needs to be evaluated in the future.

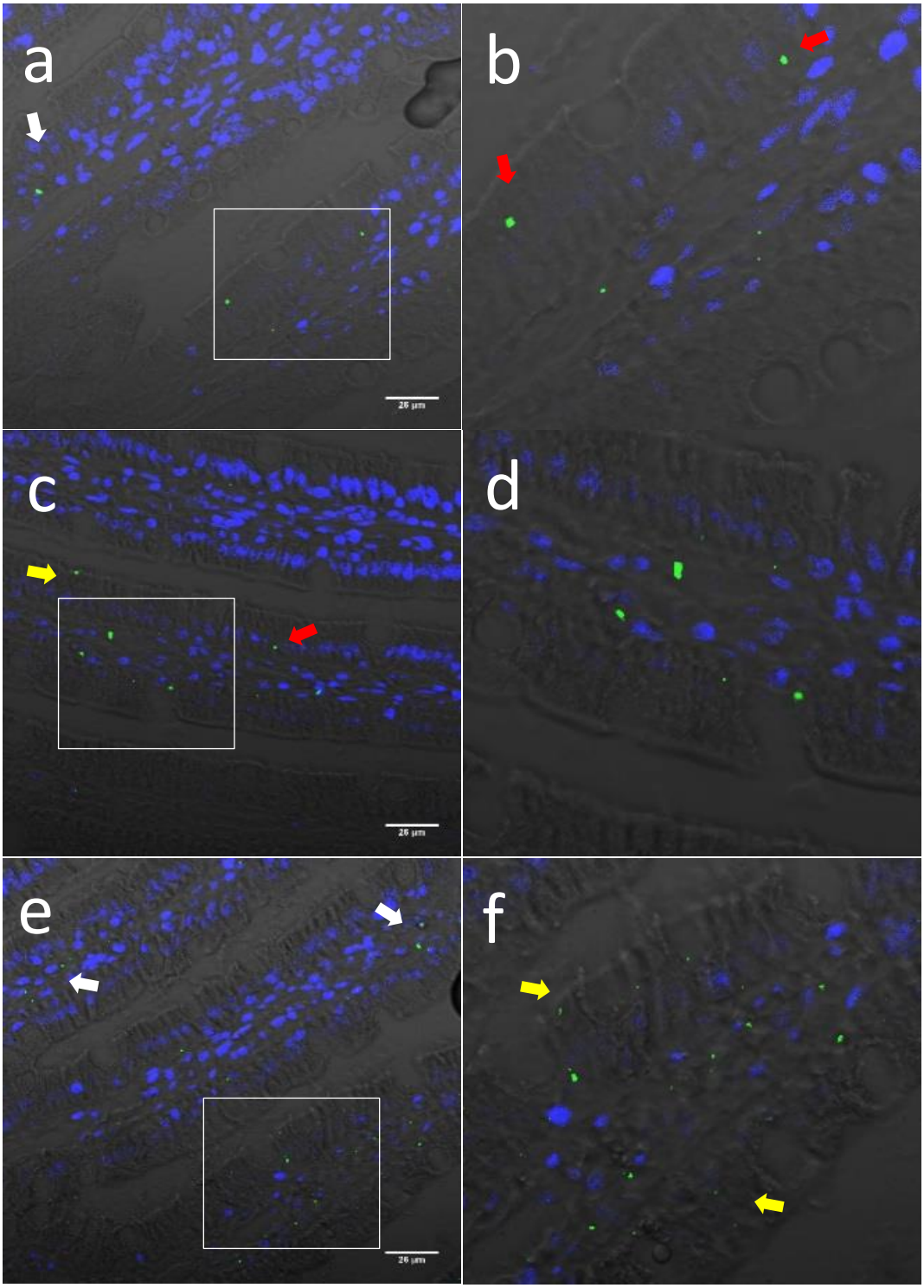

Figure 5-12: Representative confocal images of GFP-loaded AC NPs (condition 6: 250 µL for 30 min). Green fluorescent dots (representing the accumulated GFP-loaded AC NPs) can be found on the surface of the epithelium (yellow arrows); inside of the enterocytes (red arrows); and in the *lamina propria*. Images on the right column are magnified from the white frame, can be found in the images on the left column (green: GFP-loaded AC NPs-ntPE, blue: nuclei, scale bar=26 µm).

An equivalent negative control was prepared by loading GFP into AC NPs-BSA and was administered into the lumen using the same protocol as GFP-loaded AC NPs-ntPE. Green

fluorescent signals (perhaps from GFP-loaded AC NPs-BSA) were located outside of the villi (white arrows in Figure 5-13b) and some were associated with the epithelium (yellow arrows in Figure 5-13). No accumulation of AC NPs was detected in the villi, this might suggest that these NPs did not travel across the epithelium (as ntPE-coupled NPs did) or that they had been internalised and were no longer located in the villi. Certainly, more quantification strategies are needed to assess the ntPE-mediated transport and evaluate its feasibility as a carrier for trans-epithelial drug delivery in the future. It is also important to note that the detected fluorescence signals only represent the location of GFP, might not always indicate the location of AC NPs.

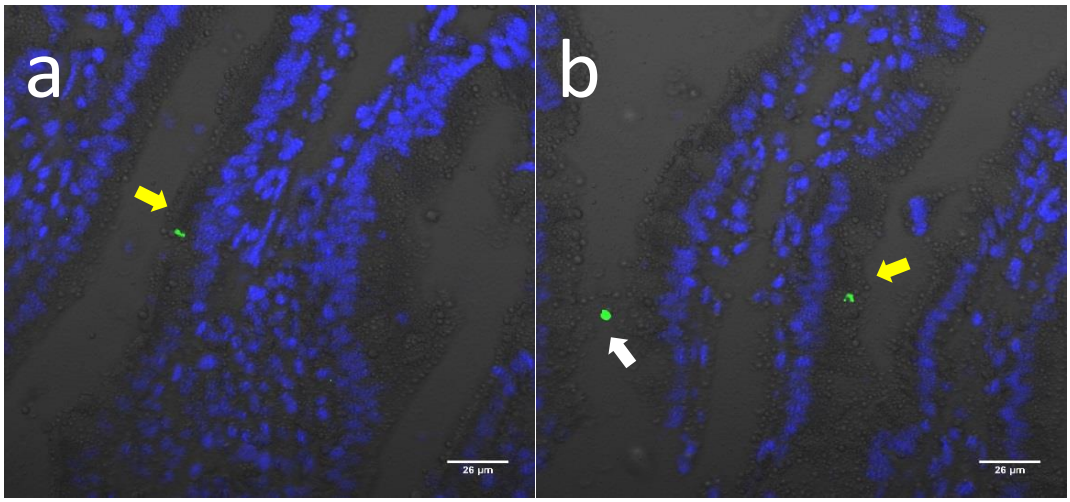

Figure 5-13: Representative confocal images of GFP-loaded AC NPs-BSA in the villi. Green fluorescence representing the accumulation of GFP-loaded AC NPs-BSA was found on the surface of the epithelium or in the luminal side, indicating that AC NPs-BSA did not carry GFP across the epithelium (Green: GFP-loaded AC NPs-BSA, blue: nuclei, scale bar=26 µm).

5.4 Conclusion

This study has supported the hypothesis that ntPE attached to the surface of NPs can facilitate the delivery of NPs to a selected cell population within the *lamina propria*. NPs conjugated with BSA, a molecule with similar physicochemical properties as ntPE, or unmodified NPs failed to demonstrate similar delivery to the *lamina propria*. These control samples have been tested closely following the protocol used for ntPE coupled NPs. While this study was carried out in rats, *Pseudomonas aeruginosa* is known to be a human pathogen and the actions of ntPE could therefore be considered in potential clinical applications. These studies were restricted to the jejunum, but it is quite possible for ntPE to similarly facilitate the delivery of NPs to other segments of the small intestine and possibly the large intestine as well.

The size of the NPs used in these studies were restricted to ~200 nm in diameter or less. LRP-1 has shown to be the surface receptor for ntPE and the internalisation of ntPE is reported to be via clathrin-mediated vesicle endocytosis (226). Clathrin-coated endosomes are very consistent in size due to the geometry of organised triskelion proteins, resulting in a size limitation up to 200 nm diameter (286). Larger NPs could enter cells via pathways involving phagocytosis or pinocytosis without the involvement of clathrin (287). Such uptake is more commonplace in M-cells where the microfold characteristic is more accommodating to larger particles (224).

NPs (~ 100 – 200 nm in diameter) were very difficult to observe individually by the confocal microscope available for these studies. Individual NPs crossing the epithelium of rat small intestine could not be observed since they are not visible until they were collected into locations, such as in phagocytic/antigen presentation cells present in the *lamina propria.* This was validated using an antibody to detect CD 11c, which is highly expressed in dendritic cells. Thus, the transport of NPs across rat epithelium was only inferred by the detection of clustered NPs after their delivery to the *lamina propria*. Future studies with a higher resolution confocal, and detection of antigens specific to vesicle compartments that define the various intracellular trafficking routes, would provide valuable information regarding the transcytosis route of these NPs.

The quantity of fPS NPs detected in the *lamina propria* was observed at 15 and 30 min, and it correlated with high levels of NPs applied to the luminal surface of the epithelium. NPs were observed to be collecting in discrete cells of the *lamina propria* by 15 min, and these clustered NPs were more prominent 30 min after their introduction into the intestinal lumen. These observations suggest that ntPE-mediated NPs transport rat epithelium can occur shortly after the injection. Such a transport timeline is consistent with the other transcytosis processes that utilise ATP to ensure directed, rather than random, movement of vesicles within the cell.

Overall, these *in vivo* studies showed the importance of ntPE for the transport of NPs across the intestinal epithelium, and these ntPE-coupled NPs are worthy of continued research. Stable fPS NPs-ntPE appear to provide a tool for future studies to better define the route of NPs across the intestinal epithelium and fate within the *lamina propria*. The demonstration of GFP delivery to the *lamina propria* using GFP-loaded AC NPs-ntPE, however, shows the potential pharmaceutical promise of this approach. While future studies with fPS NPs-ntPE might be more amenable for pharmacokinetic types of outcomes, therapeutic protein-loaded AC NPs-ntPE should provide opportunities to examine outcomes associated with the pharmacodynamics of this oral route of administration.

Chapter 6 General discussion and future work

The aim of this thesis was to develop a nano-carrier that could be used for the delivery of biopharmaceuticals across the intestinal epithelium, following oral administration in a dosage form that would protect the material during passage through the stomach. Specifically, the strategy presented herein was organised to identify and validate a polymeric biodegradable NP, which could be chemically conjugated at its surface with a non-toxic form of a bacterial exotoxin that had been previously suggested to traffic across polarised intestinal epithelia. To achieve and evaluate this strategy the following steps were performed: (a) biodegradable NPs using alginate and chitosan (AC NPs) were prepared and their characteristics to favour uptake and transcytosis were optimised; (b) these NPs were chemically conjugated to a non-toxic version of *Pseudomonas aeruginosa* toxin (ntPE); (c) transcytosis of the ntPE-coupled NPs was evaluated *in vitro* using Caco-2 cell monolayers; (d) the trans-epithelial transport of the ntPE-coupled NPs *in vivo* was tested by direct injection into the rat small intestine; and finally (e) the potential of these NPs to deliver biopharmaceuticals across the intestinal epithelium was evaluated, by examining the loading of a model protein (green fluorescent protein; GFP) into AC NPs. The following discussion is based upon key aspects and outcomes of these studies.

Characteristics of nanoparticles

Nano-carrier size is an important property that can directly affect their interactions with and trafficking within polarised intestinal epithelial cells. As expected, size measurement in DLS and TEM were different for the NPs prepared in these studies. Size measured by DLS was considered to be more relevant for these studies, since both alginate and chitosan are hydrophilic polymers and their application would be affected by their properties in a hydrated environment. Thus, the hydrodynamic size measured by DLS should best represent the physiological conditions for their ultimate use *in vivo*.

Based upon information available for the transport of NPs in intestinal epithelial cells, 100 – 200 nm is the optimal size range. It is anticipated that NPs conjugated at their surface with ntPE would utilise the transport route involving clathrin-coated vesicle entry, which restricts entering materials to a size of < 200 nm in diameter.

The characteristics of NPs were affected by changes in preparation parameters. For instance, the concentration and ratio of the polymers used had a direct impact on NP size, while the pH had great influence on NP size and surface charge as assessed by zeta potential measurement. Alteration of zeta potential in response to changes in pH was considered to be due to changes in

ionisation state of the polymers used and their solution conformation. In this regard, the present studies identified pH 4.5 as optimal to produce NPs in the desired size range of 100 – 200 nm. Higher or lower pH conditions led to solubility problems of chitosan or alginate that compromised the ability to generate NPs with the desired characteristics.

Surface charge has also been demonstrated as a parameter that affects NP transcytosis. While this would be affected to some extent by the surface coupling of ntPE, we assumed this physicochemical property to not be extensively affected. BSA-coupled NPs were prepared with similar characteristics as ntPE-coupled NPs. Due to difficulties with the Caco-2 cell monolayer model that was used to examine this question *in vitro*, a definitive outcome regarding the effects of surface charge on NP transcytosis was not obtainable. Studies performed with Caco-2 monolayers resulted in apical uptake of NPs but their transcytosis was halted within the cells at a location consistent with the Golgi network or endoplasm reticulum.

Density of transport ligands on the NP surface is another important factor. As different ligand density would lead to different characteristics of NPs as discussed earlier, ultimately this would have impacts on cell uptake and transport. It is challenging to report a precise ligand density, due to the lack of an accurate method of counting NPs, which is important information to determine the number of ligands on each NP. Future work on quantification of NPs would upgrade the understanding of the ligand-coupled NPs to a more sophisticated level.

In vitro and *in vivo* studies

The attachment of ntPE onto AC NPs was carried out to test the hypothesis that NPs could be ferried across intact, polarised intestinal epithelium using the transcytosis pathway utilised by this exotoxin. While this could not be readily assessed *in vitro* due to technical problems with the Caco-2 monolayers, *in vivo* studies were successful.

It remains unclear why the Caco-2 monolayers performed so poorly as an *in vitro* model for NP transcytosis in these studies. The Caco-2 monolayers used were verified to express LRP1, the receptor known to be used by PE (and ntPE) to enter cells. Its presence was consistent with the finding that ntPE-NPs entered into these monolayers, but they simply failed to complete the process of transcytosis and appeared to become trapped in an intracellular compartment. Some unpublished studies have suggested that PE (and ntPE) also engages the ganglioside GM1 as part of the transcytosis pathway utilised by this exotoxin. Since the nature of this potential interaction is still poorly understood, the issue of GM1 levels or GM1 localisation within polarised epithelial cells was not followed up.

In vivo studies demonstrated that BSA-coupled NPs were poorly absorbed compared to ntPE-coupled NPs at 15 and 30 min after intraluminal injection into rat jejunum. BSA has comparable physicochemical properties to ntPE and was used as a protein that could be coupled to the surface of NPs, as a control for presence of a surface-coupled protein. NtPE-coupled NPs were observed to accumulate in the *lamina propria* of rat small intestine, ntPE-NPs strikingly out-performed the BSA-NPs in terms of the number of particles undergoing transcytosis and the extent of cells in the *lamina propria* which had concentrated these NPs after transcytosis. Importantly, these studies supported the concept that ntPE-NPs moved across intestinal epithelial cells in a time course and via intracellular locations that are consistent with a receptor-mediated, energy-driven, vesicular pathway.

For ntPE-coupled NPs, it appeared that they were sequestered in the immune cells (i.e. macrophage and dendritic cells) present in the *lamina propria*. There are two main reasons for this assumption. Firstly, macrophages function to clear particles from a tissue, and dendritic cells are antigen-presenting cells and patrol the *lamina propria*. Secondly, PE (and ntPE) are known to target macrophage and dendritic cells, since the receptor (LRP1) for PE (and ntPE) is expressed by these cells. Future work on identifying the location of ntPE in the *lamina propria* is worth pursuing.

It is important to state that confocal microscopy is a qualitative, but not quantitative method to detect the NPs tested in these studies. Further, the extent of NPs that have undergone transcytosis is assessed by their presence in the epithelial cells and retention in the *lamina propria*. While the data presented suggests that ntPE-NPs were much more efficiently transported than BSA-NPs, it is possible that large amounts of BSA-NPs could have crossed the epithelium and were removed from the *lamina propria* by vascular and/or lymphatic vessels. For accurate tracking of individual NPs at a systemic level (*in vivo*), more precise equipment, such as an IVIS® Imaging System with high resolution, would be necessary.

A fluorescent dye was used to localise NPs during their transcytosis and fate within the *lamina propria*. When GFP loaded into AC NPs-ntPE was detected, it suggested that this model protein was being transported across the intestinal epithelium and sequestered into the *lamina propria*. Whether the GFP molecules detected were still encapsulated inside the NPs is unknown. GFP signal was localised within enterocytes as well as within cells of the *lamina propria*. This was consistent with the transcytosis and macrophage fate previously observed for markers used to define the NPs coupled with ntPE. Interestingly, in the case of BSA-coupled NPs both the NPs and the GFP localisation within the epithelium were not consistent with the pathway observed for ntPE-NPs.

Oral delivery of biopharmaceuticals

Nano-carriers have the potential to facilitate the delivery of biopharmaceuticals via the oral route. While extensive studies have been carried out in this field, there are still many challenges that need to be addressed.

Protein stability is critical for maintaining its specific functions. In this regard, nano-carriers can be used to protect loaded biopharmaceuticals. A conjugated surface ligand, in this case ntPE, is also a component that must remain stable. While the general size of AC NPs prepared here remained the same for 7 days, longer storage studies that include different conditions need to be considered in the future to ensure stability. Means of improving the stability of these nano-carriers would be valuable for the future work, as some precipitation was noticed in the suspension after 24 h storage.

The relatively large surface area of NPs offers the advantage of high drug loading, related to this the control of accurate dose appears to be fundamental. Even though the reproducibility of NP formation and biopharmaceutical loading/encapsulation can be solved, the reproducibility in the release of loaded drugs must be also studied for developing a final oral formulation.

Overall, this work has provided data to support the hypothesis that a novel strategy using bacterial toxin-coupled NPs to transport biopharmaceuticals across the intestinal epithelium is feasible. These NPs were shown to transport across the intestinal epithelium and accumulate in the *lamina propria* of the rat small intestine. There are still, however, many challenges (such as stability, release, toxicity and dose uniformity) for developing this strategy into a feasible oral formulation approach.

Chapter 7 References

1. Kansas Medical Clinic. Gastroenterology. 2017 [cited 2017 12 March]; Available from: http://www.kmcpa.com/gastroenterology/patient-education/gas-in-the-digestive-tract/.
2. Laurent F. Characterization of the trafficking pathway used by Pseudomonas aeruginosa Exotoxin A and application to oral drug delivery: University of Bath; 2015.
3. Bruchet M, Melman A. Fabrication of patterned calcium cross-linked alginate hydrogel films and coatings through reductive cation exchange. Carbohydr Polym. 2015;131:57-64.
4. Grenha A. Chitosan nanoparticles: a survey of preparation methods. J Drug Target. 2012;20(4):291-300.
5. Roopenian D, Akilesh S. FcRn: the neonatal Fc receptor comes of age. Nat Rev Immunol. 2007;7(9):715-25.
6. University of Tokyo. Introduction to LIFE SCIENCE. 2010 [cited 2017 10 March]; Available from: http://csls-text2.c.u-tokyo.ac.jp/inactive/08_02.html.
7. Gotoh T, Matsushima K, *et al*. Preparation of alginate–chitosan hybrid gel beads and adsorption of divalent metal ions. Chemosphere. 2004;55(1):135-40.
8. Giepmans B, van IJzendoorn S, *et al*. Epithelial cell–cell junctions and plasma membrane domains. Biochim Biophys Acta. 2009;1788(4):820-31.
9. Goldberg M, Gomez-Orellana I. Challenges for the oral delivery of macromolecules. Nat Rev Drug Discov. 2003;2(4):289-95.
10. Michalska M, Wolf P. Pseudomonas Exotoxin A: optimized by evolution for effective killing. Front Microbiol. 2015;6:1-7.
11. Walsh G. Biopharmaceutical benchmarks. Nature Biotechnol. 2000;18(8):831-3.
12. Sanchez-Garcia L, Martín L, *et al*. Recombinant pharmaceuticals from microbial cells: a 2015 update. Microb Cell Fact. 2016;15(33):1-7.
13. Walsh G. Biopharmaceutical benchmarks 2014. Nature Biotechnol. 2014;32(10):992-1000.
14. Antosova Z, Mackova M, *et al*. Therapeutic application of peptides and proteins: parenteral forever? Trends Biotechnol. 2009;27(11):628-35.
15. BCC research. Biologic Therapeutic Drugs: Technologies and Global Markets. 2015 [cited 2017 08 March]; Available from: http://www.bccresearch.com/market-research/biotechnology/biologic-therapeutic-drugs-technologies-markets-report-bio079c.html.
16. Grewal I. Emerging protein biotherapeutics. New York: CRC Press; 2009.
17. Leader B, Baca Q, *et al*. Protein therapeutics: a summary and pharmacological classification. Nat Rev Drug Discov. 2008;7(1):21-39.
18. Renukuntla J, Vadlapudi A. Approaches for enhancing oral bioavailability of peptides and proteins. Int J Pharm. 2013;447(1):75-93.
19. Hanas R, Ludvigsson J. Experience of pain from insulin injections and needle-phobia in young patients with IDDM. Practical Diabetes Int. 1997;14(4):95-9.
20. Shaji J, Patole V. Protein and peptide drug delivery: oral approaches. Indian J Pharm Sci. 2008;70(3):269-77.
21. Muheem A, Shakeel F, *et al*. A review on the strategies for oral delivery of proteins and peptides and their clinical perspectives. Saudi Pharm J. 2016;24(4):413-28.
22. Arbit E, Kidron M, *et al* Oral insulin: the rationale for this approach and current developments. J Diabetes Sci Technol. 2009;3(3):562-7.
23. Madara J. Functional morphology of epithelium of the small intestine. Compr Physiol. 2011:83-120.
24. Daugherty A, Mrsny R. Transcellular uptake mechanisms of the intestinal epithelial barrier Part one. Pharm Sci Technolo Today. 1999;2(4):144-51.
25. Clevers H. The intestinal crypt, a prototype stem cell compartment. Cell. 2013;154(2):274-84.

26. Ahlman H, Nilsson O. The gut as the largest endocrine organ in the body. Ann Oncol. 2001;12(suppl 2):63-8.
27. Louvard D, Kedinger M, *et al*. The differentiating intestinal epithelial cell: establishment and maintenance of functions through interactions between cellular structures. Annu Rev Cell Biol.1992;8(1):157-95.
28. Caplan M. Membrane polarity in epithelial cells: protein sorting and establishment of polarized domains. Am J Physiol. 1997;272(4):F425-F9.
29. Garrod D, Chidgey M. Desmosome structure, composition and function. Biochim Biophys Acta. 2008;1778(3):572-87.
30. Hartsock A, Nelson W. Adherens and tight junctions: structure, function and connections to the actin cytoskeleton. Biochim Biophys Acta. 2008;1778(3):660-9.
31. Van Itallie C, Anderson J. Claudins and epithelial paracellular transport. Annu Rev Physiol. 2006;68:403-29.
32. Chiba H, Osanai M, *et al*. Transmembrane proteins of tight junctions. Biochim Biophys Acta. 2008;1778(3):588-600.
33. Ensign L, Cone R, *et al*. Oral drug delivery with polymeric nanoparticles: the gastrointestinal mucus barriers. Adv Drug Deliv Rev. 2012;64(6):557-70.
34. Devriendt B, De Geest B, *et al*. Crossing the barrier: Targeting epithelial receptors for enhanced oral vaccine delivery. J Control Release. 2012;160(3):431-9.
35. Neutra M, Kraehenbuhl J. Transepithelial transport and mucosal defence I: the role of M cells. Trends Cell Biol. 1992;2(5):134-8.
36. Smart A, Gaisford S, *et al*. Oral peptide and protein delivery: intestinal obstacles and commercial prospects. Expert Opin Drug Deliv. 2014;11(8):1323-35.
37. Mahato R, Narang A, *et al*. Emerging trends in oral delivery of peptide and protein drugs. Crit Rev Ther Drug Carrier Syst. 2003;20(2-3):153-214.
38. Herrero E, Alonso M, *et al*. Polymer-based oral peptide nanomedicines. Ther Deliv. 2012;3(5):657-68.
39. Allen A. Structure and function of gastrointestinal mucus. New York: Raven Press; 1981.
40. Lai S, Wang Y. Mucus-penetrating nanoparticles for drug and gene delivery to mucosal tissues. Adv Drug Deliv Rev. 2009;61(2):158-71.
41. Kim Y, Ho S. Intestinal goblet cells and mucins in health and disease: recent insights and progress. Curr Gastroenterol Rep. 2010;12(5):319-30.
42. Frey A, Giannasca K, *et al*. Role of the glycocalyx in regulating access of microparticles to apical plasma membranes of intestinal epithelial cells: implications for microbial attachment and oral vaccine targeting. J Exp Med. 1996;184(3):1045-59.
43. Corfield A, Carroll D, *et al*. Mucins in the gastrointestinal tract in health and disease. Front Biosci. 2001;6(10):D1321-57.
44. Donovan M, Flynn G, *et al*. Absorption of polyethylene glycols 600 through 2000: the molecular weight dependence of gastrointestinal and nasal absorption. Pharm Res. 1990;7(8):863-8.
45. Tibbitts J, Canter D, *et al*, editors. Key factors influencing ADME properties of therapeutic proteins: A need for ADME characterization in drug discovery and development. MAbs; 2016: Taylor & Francis.
46. Pade V, Stavchansky S. Estimation of the relative contribution of the transcellular and paracellular pathway to the transport of passively absorbed drugs in the Caco-2 cell culture model. Pharm Res. 1997;14(9):1210-5.
47. Bernkop-Schnürch A. The use of inhibitory agents to overcome the enzymatic barrier to perorally administered therapeutic peptides and proteins. J Control Release. 1998;52(1):1-16.
48. Yamamoto A, Taniguchi T, *et al*. Effects of various protease inhibitors on the intestinal absorption and degradation of insulin in rats. Pharm Res. 1994;11(10):1496-500.
49. Hutton D, Pearson J, *et al*. Mucolysis of the colonic mucus barrier by faecal proteinases: inhibition by interacting polyacrylate. Clin Sci (Lond). 1990;78(3):265-71.
50. Lueßen H, Verhoef J, *et al*. Mucoadhesive polymers in peroral peptide drug delivery. II. Carbomer and polycarbophil are potent inhibitors of the intestinal proteolytic enzyme trypsin. Pharm Res. 1995;12(9):1293-8.
51. Carey M, Small D. Micelle formation by bile salts: physical-chemical and thermodynamic considerations. Arch Intern Med. 1972;130(4):506-27.

52. Aungst J. Absorption enhancers: applications and advances. AAPS J. 2012;14(1):10-8.
53. Thanou M, Verhoef J, *et al*. Oral drug absorption enhancement by chitosan and its derivatives. Adv Drug Deliv Rev. 2001;52(2):117-26.
54. Bai J, Chang L, *et al*. Effects of polyacrylic polymers on the degradation of insulin and peptide drugs by chymotrypsin and trypsin. J Pharm Pharmacol. 1996;48(1):17-21.
55. Mesiha M, Ponnapula S, *et al*. Oral absorption of insulin encapsulated in artificial chyles of bile salts, palmitic acid and α-tocopherol dispersions. Int J Pharm. 2002;249(1):1-5.
56. Stojančević M, Pavlović N, *et al*. Application of bile acids in drug formulation and delivery. Front Life Sci. 2013;7(3-4):112-22.
57. Hwang S, Byun Y. Advances in oral macromolecular drug delivery. Expert Opin Drug Deliv. 2014;11(12):1955-67.
58. Balakrishnan A, Polli J. Apical sodium dependent bile acid transporter (ASBT, SLC10A2): a potential prodrug target. Mol Pharm. 2006;3(3):223-30.
59. Hashizume M, Douen T, *et al*. Improvement of large intestinal absorption of insulin by chemical modification with palmitic acid in rats. J Pharm Pharmacol. 1992;44(7):555-9.
60. Clement S, Still J, *et al*. Oral insulin product hexyl-insulin monoconjugate 2 (HIM2) in type 1 diabetes mellitus: the glucose stabilization effects of HIM2. Diabetes Technol Ther. 2002;4(4):459-66.
61. Kipnes M, Dandona P, *et al*. Control of postprandial plasma glucose by an oral insulin product (HIM2) in patients with type 2 diabetes. Diabetes Care. 2003;26(2):421-6.
62. Kreuter J. Nanoparticles—a historical perspective. Int J Pharm. 2007;331(1):1-10.
63. Mohanraj V, Chen Y. Nanoparticles-a review. Trop J Pharm Res. 2006;5(1):561-73.
64. Pridgen E, Alexis F, *et al*. Polymeric nanoparticle drug delivery technologies for oral delivery applications. Expert Opin Drug Deliv. 2015;12(9):1459-73.
65. Date A, Hanes J, *et al*. Nanoparticles for oral delivery: Design, evaluation and state-of-the-art. J Control Release. 2016;240:504-26.
66. Kolybaba M, Tabil L, *et al*, editors. Biodegradable polymers: past, present, and future. An ASAE Meeting Presentation; 2003; North Dakota, USA.
67. Wikipedia. Biodegradable polymer. [cited 2017 10 March]; Available from: https://en.wikipedia.org/wiki/Biodegradable_polymer.
68. Vroman I, Tighzert L. Biodegradable polymers. Materials. 2009;2(2):307-44.
69. Lendlein A, Sisson A. Handbook of biodegradable polymers: isolation, synthesis, characterization and applications: John Wiley & Sons; 2011.
70. Soppimath K, Aminabhavi T, *et al*. Biodegradable polymeric nanoparticles as drug delivery devices. J Control Release. 2001;70(1):1-20.
71. Thakral S, Thakral N, *et al*. Eudragit®: a technology evaluation. Expert Opin Drug Deliv. 2013;10(1):131-49.
72. Anderson J, Van Itallie C, *et al*. Physiology and function of the tight junction. Cold Spring Harb Perspect Biol. 2009;1(2):1-16.
73. Chuang E, Lin K, *et al*. Calcium depletion-mediated protease inhibition and apical-junctional-complex disassembly via an EGTA-conjugated carrier for oral insulin delivery. J Control Release. 2013;169(3):296-305.
74. Lin Y, Mi F, *et al*. Preparation and characterization of nanoparticles shelled with chitosan for oral insulin delivery. Biomacromolecules. 2007;8(1):146-52.
75. Yeh T, Hsu L, *et al*. Mechanism and consequence of chitosan-mediated reversible epithelial tight junction opening. Biomaterials. 2011;32(26):6164-73.
76. Pappenheimer J. Physiological regulation of transepithelial impedance in the intestinal mucosa of rats and hamsters. J Membr Biol. 1987;100(1):137-48.
77. Yun Y, Cho Y, *et al*. Nanoparticles for oral delivery: targeted nanoparticles with peptidic ligands for oral protein delivery. Adv Drug Deliv Rev. 2013;65(6):822-32.
78. Eldridge J, Hammond C, *et al*. Controlled vaccine release in the gut-associated lymphoid tissues. I. Orally administered biodegradable microspheres target the Peyer's patches. J Control Release. 1990;11(1-3):205-14.
79. Plapied L, Duhem N, *et al*. Fate of polymeric nanocarriers for oral drug delivery. Curr Opin Colloid Interface Sci. 2011;16(3):228-37.

80. Yin L, Ding J, *et al*. Drug permeability and mucoadhesion properties of thiolated trimethyl chitosan nanoparticles in oral insulin delivery. Biomaterials. 2009;30(29):5691-700.
81. Woitiski C, Sarmento B, *et al*. Facilitated nanoscale delivery of insulin across intestinal membrane models. Int J Pharm. 2011;412(1):123-31.
82. Hussain N, Jani P, *et al*. Enhanced oral uptake of tomato lectin-conjugated nanoparticles in the rat. Pharm Res. 1997;14(5):613-8.
83. Fievez V, Plapied L, *et al*. Targeting nanoparticles to M cells with non-peptidic ligands for oral vaccination. Eur J Pharm Biopharm. 2009;73(1):16-24.
84. Russell-Jones G. The potential use of receptor-mediated endocytosis for oral drug delivery. Adv Drug Deliv Rev. 1996;20(1):83-97.
85. Chalasani K, Russell-Jones G, *et al*. Effective oral delivery of insulin in animal models using vitamin B12-coated dextran nanoparticles. J Control Release. 2007;122(2):141-50.
86. Fowler R, Vllasaliu D, *et al*. Uptake and transport of B 12-conjugated nanoparticles in airway epithelium. J Control Release. 2013;172(1):374-81.
87. Clardy S, Allis D, *et al*. Vitamin B12 in drug delivery: breaking through the barriers to a B12 bioconjugate pharmaceutical. Expert Opin Drug Deliv 2011;8(1):127-40.
88. Bies C, Lehr C, *et al*. Lectin-mediated drug targeting: history and applications. Adv Drug Deliv Rev. 2004;56(4):425-35.
89. Irache J, Durrer C, *et al*. Preparation and characterization of lectin-latex conjugates for specific bioadhesion. Biomaterials. 1994;15(11):899-904.
90. Irache JM, Durrer C, *et al*. Bioadhesion of lectin-latex conjugates to rat intestinal mucosa. Pharm Res. 1996;13(11):1716-9.
91. Russell-Jones G, Veitch H, *et al*. Lectin-mediated transport of nanoparticles across Caco-2 and OK cells. Int J Pharm. 1999;190(2):165-74.
92. Wolf J, Bye W. The membranous epithelial (M) cell and the mucosal immune system. AnnU Rev Med. 1984;35(1):95-112.
93. Yin Y, Chen D, *et al*. Preparation and evaluation of lectin-conjugated PLGA nanoparticles for oral delivery of thymopentin. J Control Release. 2006;116(3):337-45.
94. Yin Y, Chen D, *et al*. Lectin-conjugated PLGA nanoparticles loaded with thymopentin: ex vivo bioadhesion and in vivo biodistribution. J Control Release. 2007;123(1):27-38.
95. Naisbett B, Woodley J. The potential use of tomato lectin for oral drug delivery: 4. Immunological consequences. Int J Pharm. 1995;120(2):247-54.
96. Low S, Nunes S, *et al*. Oral and pulmonary delivery of FSH–Fc fusion proteins via neonatal Fc receptor-mediated transcytosis. Hum Reprod. 2005;20(7):1805-13.
97. Dickinson B, Badizadegan K, *et al*. Bidirectional FcRn-dependent IgG transport in a polarized human intestinal epithelial cell line. J Clin Invest. 1999;104(7):903-11.
98. Rojas R, Apodaca G. Immunoglobulin transport across polarized epithelial cells. Nat Rev Mol Cell Biol. 2002;3(12):944-56.
99. Vllasaliu D, Alexander C, *et al*. Fc-mediated transport of nanoparticles across airway epithelial cell layers. J Control Release. 2012;158(3):479-86.
100. Pridgen E, Alexis F, *et al*. Transepithelial transport of Fc-targeted nanoparticles by the neonatal fc receptor for oral delivery. Sci Transl Med. 2013;5(213):1-19.
101. Widera A, Norouziyan F, *et al*. Mechanisms of TfR-mediated transcytosis and sorting in epithelial cells and applications toward drug delivery. Adv Drug Deliv Rev. 2003;55(11):1439-66.
102. Narang A, Mahato R. Targeted delivery of small and macromolecular drugs. New York: CRC press; 2010.
103. Banerjee D, Flanagan P, *et al*. Transferrin receptors in the human gastrointestinal tract: relationship to body iron stores. Gastroenterology. 1986;91(4):861-9.
104. Xia C, Wang J, *et al*. Hypoglycemic effect of insulin-transferrin conjugate in streptozotocin-induced diabetic rats. J Pharm Exp Ther. 2000;295(2):594-600.
105. Lim C, Shen W. Comparison of monomeric and oligomeric transferrin as potential carrier in oral delivery of protein drugs. J Control Release. 2005;106(3):273-86.
106. Mrsny R. Lessons from nature:"Pathogen-Mimetic" systems for mucosal nano-medicines. Adv Drug Deliv Rev. 2009;61(2):172-92.

107. Guan C, Ji J, *et al*. Expression of cholera toxin B subunit–lumbrokinase in edible sunflower seeds–the use of transmucosal carrier to enhance its fusion protein's effect on protection of rats and mice against thrombosis. Biotechnol Prog. 2014;30(5):1029-39.
108. Salman H, Gamazo C, *et al*. Salmonella-like bioadhesive nanoparticles. J Control Release. 2005;106(1-2):1-13.
109. Hussain N, Florence A. Utilizing bacterial mechanisms of epithelial cell entry: invasin-induced oral uptake of latex nanoparticles. Pharm Res. 1998;15(1):153-6.
110. Weldon J, Pastan I. A guide to taming a toxin–recombinant immunotoxins constructed from Pseudomonas exotoxin A for the treatment of cancer. FEBS J. 2011;278(23):4683-700.
111. McKee M, FitzGerald D. Reduction of furin-nicked Pseudomonas exotoxin A: an unfolding story. Biochemistry. 1999;38(50):16507-13.
112. Ogata M, Chaudhary V. Processing of Pseudomonas exotoxin by a cellular protease results in the generation of a 37,000-Da toxin fragment that is translocated to the cytosol. J Biol Chem. 1990;265(33):20678-85.
113. Jackson M, Simpson J, *et al*. The KDEL retrieval system is exploited by Pseudomonas exotoxin A, but not by Shiga-like toxin-1, during retrograde transport from the Golgi complex to the endoplasmic reticulum. J Cell Sci. 1999;112(4):467-75.
114. Smith D, Spooner R, *et al*. Internalized Pseudomonas exotoxin A can exploit multiple pathways to reach the endoplasmic reticulum. Traffic. 2006;7(4):379-93.
115. Chaudhary V, Jinno Y, *et al*. Pseudomonas exotoxin contains a specific sequence at the carboxyl terminus that is required for cytotoxicity. Proc Natl Acad Sci U S A 1990;87(1):308-12.
116. Kreitman R, Tallman M, *et al*. Phase I trial of anti-CD22 recombinant immunotoxin moxetumomab pasudotox (CAT-8015 or HA22) in patients with hairy cell leukemia. J Clin Oncol. 2012;30(15):1822-8.
117. Kreitman R, Hassan R, *et al*. Phase I trial of continuous infusion anti-mesothelin recombinant immunotoxin SS1P. Clin Cancer Res. 2009;15(16):5274-9.
118. Daugherty A, McKee M, *et al*. Epithelial application of Pseudomonas aeruginosa exotoxin A results in a selective targeting to cells in the liver, spleen and lymph node. J Control Release. 2000;65(1):297-302.
119. Douglas C, Collier R. Exotoxin A of Pseudomonas aeruginosa: substitution of glutamic acid 553 with aspartic acid drastically reduces toxicity and enzymatic activity. J Bacteriol. 1987;169(11):4967-71.
120. Mohammed A, Abdul-Wahid A, *et al*. The Pseudomonas aeruginosa exotoxin A translocation domain facilitates the routing of CPP–protein cargos to the cytosol of eukaryotic cells. J Control Release. 2012;164(1):58-64.
121. Carter E. The Involvement of Phosphoinositide 3-kinase in Murine Lung Branching Morphogenesis and Insights into Protein Mediated Drug Delivery: University of Bath; 2014.
122. Mathiowitz E, ChickeringIII D, *et al*. Fundamentals of bioadhesion. New York: CRC Press; 1999.
123. Boddupalli B, Mohammed Z, *et al*. Mucoadhesive drug delivery system: An overview. J Adv Pharm Technol Res. 2010;1(4):381-7.
124. Rajaonarivony M, Vauthier C, *et al*. Development of a new drug carrier made from alginate. J Pharm Sci. 1993;82(9):912-7.
125. Peppas N, Huang Y. Nanoscale technology of mucoadhesive interactions. Adv Drug Deliv Rev. 2004;56(11):1675-87.
126. Wittaya-areekul S, Kruenate J, *et al*. Preparation and in vitro evaluation of mucoadhesive properties of alginate/chitosan microparticles containing prednisolone. Int J Pharm. 2006;312(1):113-8.
127. Chen F, Zhang Z, *et al*. In vitro and in vivo study of N-trimethyl chitosan nanoparticles for oral protein delivery. Int J Pharm. 2008;349(1):226-33.
128. Yue Z, Wei W. Surface charge affects cellular uptake and intracellular trafficking of chitosan-based nanoparticles. Biomacromolecules. 2011;12(7):2440-6.
129. Mukhopadhyay P, Mishra R, *et al*. Strategies for effective oral insulin delivery with modified chitosan nanoparticles: A review. Prog Polym Sci. 2012;37(11):1457-75.
130. Csaba N, Köping-Höggård M, *et al*. Ionically crosslinked chitosan/tripolyphosphate nanoparticles for oligonucleotide and plasmid DNA delivery. Int J Pharm. 2009;382(1):205-14.

131. Ohya Y, Shiratani M. Release behavior of 5-fluorouracil from chitosan-gel nanospheres immobilizing 5-fluorouracil coated with polysaccharides and their cell specific cytotoxicity. J Macromol Sci, Pure Appl Chem. 1994;31(5):629-42.
132. Tokumitsu H, Ichikawa H, *et al*. Chitosan-gadopentetic acid complex nanoparticles for gadolinium neutron-capture therapy of cancer: preparation by novel emulsion-droplet coalescence technique and characterization. Pharm Res. 1999;16(12):1830-5.
133. El-Shabouri M. Positively charged nanoparticles for improving the oral bioavailability of cyclosporin-A. Int J Pharm. 2002;249(1):101-8.
134. Hartig S, Greene R, *et al*. Multifunctional nanoparticulate polyelectrolyte complexes. Pharm Res. 2007;24(12):2353-69.
135. Sosnik A. Alginate particles as platform for drug delivery by the oral route: state-of-the-art. ISRN Pharm. 2014;2014(2014):1-14.
136. Machado AH, Lundberg D, *et al*. Preparation of calcium alginate nanoparticles using water-in-oil (W/O) nanoemulsions. Langmuir. 2012;28(9):4131-41.
137. Win K, Feng S. Effects of particle size and surface coating on cellular uptake of polymeric nanoparticles for oral delivery of anticancer drugs. Biomaterials. 2005;26(15):2713-22.
138. Desai M, Labhasetwar V, *et al*. The mechanism of uptake of biodegradable microparticles in Caco-2 cells is size dependent. Pharm Res. 1997;14(11):1568-73.
139. Blanco E, Shen H, *et al*. Principles of nanoparticle design for overcoming biological barriers to drug delivery. Nat Biotechnol. 2015;33(9):941-51.
140. Jiang X, Dausend J, *et al*. Specific effects of surface carboxyl groups on anionic polystyrene particles in their interactions with mesenchymal stem cells. Nanoscale. 2011;3(5):2028-35.
141. Bannunah M, Vllasaliu D, *et al*. Mechanisms of nanoparticle internalization and transport across an intestinal epithelial cell model: effect of size and surface charge. Mol Pharm. 2014;11(12):4363-73.
142. Paques JP, van der Linden E, *et al*. Preparation methods of alginate nanoparticles. Adv Colloid Interface Sci. 2014;209:163-71.
143. Sarmento B, Ribeiro A, *et al*. Alginate/chitosan nanoparticles are effective for oral insulin delivery. Pharm Res. 2007;24(12):2198-206.
144. Chithrani B, Ghazani A, *et al*. Determining the size and shape dependence of gold nanoparticle uptake into mammalian cells. Nano Lett. 2006;6(4):662-8.
145. Wang S, Lee C. Size-dependent endocytosis of gold nanoparticles studied by three-dimensional mapping of plasmonic scattering images. J Nanobiotechnology. 2010;8(1):33.
146. Harush-Frenkel O, Rozentur E, *et al*. Surface charge of nanoparticles determines their endocytic and transcytotic pathway in polarized MDCK cells. Biomacromolecules. 2008;9(2):435-43.
147. Mailander V, Landfester K. Interaction of nanoparticles with cells. Biomacromolecules. 2009;10(9):2379-400.
148. Reis C, Neufeld R, *et al* Nanoencapsulation I. Methods for preparation of drug-loaded polymeric nanoparticles. Nanomed Nanotech Biol Med 2006;2(1):8-21.
149. Lankalapalli S, Kolapalli V. Polyelectrolyte complexes: A review of their applicability in drug delivery technology. Indian J Pharm Sci. 2009;71(5):481-7.
150. Bodnar M, Hartmann J, *et al*. Preparation and characterization of chitosan-based nanoparticles. Biomacromolecules. 2005;6(5):2521-7.
151. Kovtun A, Heumann R, *et al*. Calcium phosphate nanoparticles for the transfection of cells. Biomed Mater Eng. 2009;19(2-3):241-7.
152. Morçöl T, Nagappan P, *et al*. Calcium phosphate-PEG-insulin-casein (CAPIC) particles as oral delivery systems for insulin. Int J Pharm. 2004;277(1):91-7.
153. Banik M, Basu T. Calcium phosphate nanoparticles: a study of their synthesis, characterization and mode of interaction with salmon testis DNA. Dalton Trans. 2014;43(8):3244-59.
154. Ramachandran R, Paul W, *et al*. Synthesis and characterization of PEGylated calcium phosphate nanoparticles for oral insulin delivery. J Biomed Mater Res B Appl Biomater. 2009;88(1):41-8.
155. De S, Robinson D. Polymer relationships during preparation of chitosan–alginate and poly-l-lysine–alginate nanospheres. J Control Release. 2003;89(1):101-12.

156. Bodmeier R, Oh K, *et al*. Preparation and evaluation of drug-containing chitosan beads. Drug Dev Ind Pharm. 1989;15(9):1475-94.
157. Rampino A, Borgogna M, *et al*. Chitosan nanoparticles: Preparation, size evolution and stability. Int J Pharm. 2013;455(1):219-28.
158. Dong Y, Ng W, *et al*. Scalable ionic gelation synthesis of chitosan nanoparticles for drug delivery in static mixers. Carbohydr Polym. 2013;94(2):940-5.
159. Koukaras E, Papadimitriou S, *et al*. Insight on the formation of chitosan nanoparticles through ionotropic gelation with tripolyphosphate. Mol Pharm. 2012;9(10):2856-62.
160. Albee F. Studies in bone growth: triple calcium phosphate as a stimulus to osteogenesis. Ann Surg. 1920;71(1):32.
161. Habraken W, Habibovic P, *et al*. Calcium phosphates in biomedical applications: materials for the future? Mater Today. 2016;19(2):69-87.
162. Paul W, Sharma C. Tricalcium phosphate delayed release formulation: A proof of concept study. J Pharma Sci. 2007;97(2):875-82.
163. Khan M, Wu V, *et al*. Gene delivery using calcium phosphate nanoparticles: Optimization of the transfection process and the effects of citrate and poly (l-lysine) as additives. J Colloid Interface Sci 2016;471:48-58.
164. Karimi M, Hesaraki S, *et al*. A facile and sustainable method based on deep eutectic solvents toward synthesis of amorphous calcium phosphate nanoparticles: The effect of using various solvents and precursors on physical characteristics. J Non-Cryst Solids. 2016;443:59-64.
165. Choi M, Briancon S, *et al*. Effect of freeze-drying process conditions on the stability of nanoparticles. Drying Technol. 2004;22(1-2):335-46.
166. Moore T, Rodriguez-Lorenzo L, *et al*. Nanoparticle colloidal stability in cell culture media and impact on cellular interactions. Chem Soc Rev. 2015;44(17):6287-305.
167. Ramachandran R, Paul W, *et al*. Synthesis and characterization of PEGylated calcium phosphate nanoparticles for oral insulin delivery. J Biomed Mater Res B Appl Biomater. 2009;88(1):41-8.
168. Dautova Y, Kozlova D, *et al*. Fetuin-A and albumin alter cytotoxic effects of calcium phosphate nanoparticles on human vascular smooth muscle cells. PloS one. 2014;9(5):1135-43.
169. Yavorskyy A, Hernandez-Santana A, *et al*. Detection of calcium phosphate crystals in the joint fluid of patients with osteoarthritis–analytical approaches and challenges. Analyst. 2008;133(3):302-18.
170. Lawrie G, Keen I, *et al*. Interactions between alginate and chitosan biopolymers characterized using FTIR and XPS. Biomacromolecules. 2007;8(8):2533-41.
171. Hermanson G. Bioconjugate Techniques. Tokyo: Academic press; 2013.
172. Ruda G, Alibu V, *et al*. Synthesis and Biological Evaluation of Phosphate Prodrugs of 4-Phospho-D-erythronohydroxamic Acid, an Inhibitor of 6-Phosphogluconate Dehydrogenase. ChemMedChem. 2007;2(8):1169-80.
173. McHugh D. Production, properties and uses of alginates. Production and Utilization of Products from Commercial Seaweeds FAO Fish Tech Pap. 1987;288:58-115.
174. Daemi H, Barikani M. Synthesis and characterization of calcium alginate nanoparticles, sodium homopolymannuronate salt and its calcium nanoparticles. Sci Iran. 2012;19(6):2023-8.
175. Mi F, Sung H, *et al*. Drug release from chitosan–alginate complex beads reinforced by a naturally occurring cross-linking agent. Carbohydr Polym. 2002;48(1):61-72.
176. Douglas K, Tabrizian M. Effect of experimental parameters on the formation of alginate–chitosan nanoparticles and evaluation of their potential application as DNA carrier. J Biomater Sci Polym Ed. 2005;16(1):43-56.
177. George M, Abraham T. Polyionic hydrocolloids for the intestinal delivery of protein drugs: alginate and chitosan—a review. J Control Release. 2006;114(1):1-14.
178. Tian X, Tian D, *et al*. Synthesis and evaluation of chitosan-Vitamin C complex. Indian J Pharm Sci. 2009;71(4):371.
179. Motwani S, Chopra S, *et al*. Chitosan–sodium alginate nanoparticles as submicroscopic reservoirs for ocular delivery: formulation, optimisation and in vitro characterisation. Eur J Pharm Biopharm. 2008;68(3):513-25.
180. Sarmento B, Ferreira D, *et al*. Probing insulin's secondary structure after entrapment into alginate/chitosan nanoparticles. Eur J Pharm Biopharm. 2007;65(1):10-7.

181. Flory P. Principles of polymer chemistry. New York: Cornell University Press; 1953.
182. Dutta P, Dutta J, *et al*. Chitin and chitosan: Chemistry, properties and applications. J Sci Ind Res. 2004;63:20-31.
183. Lavertu M, Methot S*ea*. High efficiency gene transfer using chitosan/DNA nanoparticles with specific combinations of molecular weight and degree of deacetylation. Biomaterials. 2006;27(27):4815-24.
184. Gan Q, Wang T. Chitosan nanoparticle as protein delivery carrier—systematic examination of fabrication conditions for efficient loading and release. Colloids Surf B Biointerfaces. 2007;59(1):24-34.
185. Chernyshev V, Rachamadugu R, *et al*. Size and shape characterization of hydrated and desiccated exosomes. Anal Bioanal Chem. 2015;407(12):3285-301.
186. Zheng T, Bott S, *et al*. Techniques for accurate sizing of gold nanoparticles using dynamic light scattering with particular application to chemical and biological sensing based on aggregate formation. ACS Appl Mater Interfaces. 2016;8(33):21585-94.
187. Fallingborg J. Intraluminal pH of the human gastrointestinal tract. Dan Med Bull. 1999;46(3):183-96.
188. Lee K, Mooney J. Alginate: properties and biomedical applications. Prog Polym Sci. 2012;37(1):106-26.
189. Fan W, Yan W, *et al*. Formation mechanism of monodisperse, low molecular weight chitosan nanoparticles by ionic gelation technique. Colloids Surf B Biointerfaces 2012;90:21-7.
190. Bergisadi JA, N. Effect of formulation variables on cis-platin loaded chitosan microsphere properties. J Microencapsul. 1999;16(6):697-703.
191. Xu Y, Du Y. Effect of molecular structure of chitosan on protein delivery properties of chitosan nanoparticles. Int J Pharm. 2003;250(1):215-26.
192. Vandenberg G, Drolet C, *et al*. Factors affecting protein release from alginate–chitosan coacervate microcapsules during production and gastric/intestinal simulation. J Control Release. 2001;77(3):297-307.
193. Vila A, Sánchez A, *et al*. Low molecular weight chitosan nanoparticles as new carriers for nasal vaccine delivery in mice. Eur J Pharm Biopharm. 2004;57(1):123-31.
194. Köping-Höggård M, Tubulekas I, *et al*. Chitosan as a nonviral gene delivery system. Structure-property relationships and characteristics compared with polyethylenimine in vitro and after lung administration in vivo. Gene Ther. 2001;8(14):1108-21.
195. Scientific T. Thermo scientific pierce-crosslinking technical handbook. 2011.
196. Bernkop-Schnürch A, Hornof M, *et al*. Thiolated chitosans. Eur J Pharm Biopharm. 2004;57(1):9-17.
197. He B, Lin P, *et al*. The transport mechanisms of polymer nanoparticles in Caco-2 epithelial cells. Biomaterials. 2013;34(25):6082-98.
198. Lukac M, Pier G, *et al*. Toxoid of Pseudomonas aeruginosa exotoxin A generated by deletion of an active-site residue. Infect Immun. 1988;56(12):3095-8.
199. Hein C, Liu X, *et al*. Click chemistry, a powerful tool for pharmaceutical sciences. Pharm Res. 2008;25(10):2216-30.
200. Allured V, Collier R, *et al.* Structure of exotoxin A of Pseudomonas aeruginosa at 3.0-Angstrom resolution. Proc Nal Acad Sci U S A. 1986;83(5):1320-4.
201. Huang B, Kim H, *et al*. Probing three-dimensional structure of bovine serum albumin by chemical cross-linking and mass spectrometry. J Am Soc Mass Spectrom. 2004;15(8):1237-47.
202. McNeil S. Characterization of nanoparticles intended for drug delivery. Mumbai: Humana Press; 2011.
203. Bartczak D, Kanaras A. Preparation of peptide-functionalized gold nanoparticles using one pot EDC/sulfo-NHS coupling. Langmuir. 2011;27(16):10119-23.
204. Röcker C, Pötzl M, *et al*. A quantitative fluorescence study of protein monolayer formation on colloidal nanoparticles. Nat Nanotechnol. 2009;4(9):577-80.
205. Zhang Y, Sun Y, *et al*. Fluorescein-5-thiosemicarbazide as a probe for directly imaging of mucin-type O-linked glycoprotein within living cells. Glycoconj J. 2012;29(5-6):445-52.
206. Mergulhao F, Summers D, *et al*. Recombinant protein secretion in Escherichia coli. Biotechnol Adv. 2005;23(3):177-202.

207. Gasteiger E, Hoogland C, *et al*. Protein identification and analysis tools on the ExPASy server. In: Walker J, editor. The Proteomics Protocols Handbook. Totowa, New Jersey: Humana Press; 2005. p. 571-607.
208. Kale A, Torchilin V. Environment-responsive polymers for coating of pharmaceutical nanocarriers. Polym Sci Ser A Chem Phys. 2009;51(6):730-7.
209. Rudolf B, Palusiak M, *et al*. Sulfhydryl-Selective, Covalent Labeling of Biomolecules with Transition Metallocarbonyl Complexes. Synthesis of (η5-C5H5) M (CO) 3 (η1-N-Maleimidato)(M= Mo, W), X-ray Structure, and Reactivity Studies. Bioconjug Chem. 2005;16(5):1218-24.
210. Townsend SA, Evrony G, *et al*. Tetanus toxin C fragment-conjugated nanoparticles for targeted drug delivery to neurons. Biomaterials. 2007;28(34):5176-84.
211. Moghimi S. Chemical camouflage of nanospheres with a poorly reactive surface: towards development of stealth and target-specific nanocarriers. Biochim Biophys Acta. 2002;1590(1):131-9.
212. Ge S, Kojio K, *et al*. Bovine serum albumin adsorption onto immobilized organotrichlorosilane surface: influence of the phase separation on protein adsorption patterns. J Biomater Sci Polym Ed. 1998;9(2):131-50.
213. Serizawa T, Uchida T, *et al*. Synthesis of polystyrene nanospheres having lactose-conjugated hydrophilic polymers on their surfaces and carbohydrate recognition by proteins. J Biomater Sci Polym Ed. 1999;10(3):391-401.
214. Jiang W, Kim B, *et al*. Nanoparticle-mediated cellular response is size-dependent. Nat Nanotechnol. 2008;3(3):145-50.
215. Shang J, Gao X. Nanoparticle counting: towards accurate determination of the molar concentration. Chem Soc Rev. 2014;43(21):7267-78.
216. Pandithage R. Brief Introduction to Contrasting for EM Sample Preparation. 2013 [12 Feb 2017]; Available from: http://www.leica-microsystems.com/science-lab/brief-introduction-to-contrasting-for-em-sample-preparation/.
217. Lakowicz J, Masters B. Principles of fluorescence spectroscopy. Journal of Biomedical Optics. 2008;13(2):9901.
218. Simsek-Ege F, Bond G, *et al*. Polyelectrolyte complex formation between alginate and chitosan as a function of pH. J Appl Polym Sci. 2003;88(2):346-51.
219. Ahmed T, Aljaeid B. Preparation, characterization, and potential application of chitosan, chitosan derivatives, and chitosan metal nanoparticles in pharmaceutical drug delivery. Drug Des Devel Ther. 2016;10:483-507.
220. Bhunchu S, Rojsitthisak P, *et al*. Effects of preparation parameters on the characteristics of chitosan–alginate nanoparticles containing curcumin diethyl disuccinate. J Drug Deliv Sci Technol. 2015;28:64-72.
221. Byler D, Susi H. Examination of the secondary structure of proteins by deconvolved FTIR spectra. Biopolymers. 1986;25(3):469-87.
222. Jahn K, Biazik J, *et al*. GM1 expression in caco-2 cells: Characterisation of a fundamental passage-dependent transformation of a cell line. J Pharm Sci. 2011;100(9):3751-62.
223. des Rieux A, Fievez V, *et al*. Nanoparticles as potential oral delivery systems of proteins and vaccines: a mechanistic approach. J Control Release. 2006;116(1):1-27.
224. Jang M, Kweon M, *et al*. Intestinal villous M cells: an antigen entry site in the mucosal epithelium. Proc Nal Acad Sci U S A. 2004;101(16):6110-5.
225. Mrsny R. Methods and compositions for needleless delivery of binding partners. Google Patents; 2006.
226. Kounnas M, Morris R, *et al*. The alpha 2-macroglobulin receptor/low density lipoprotein receptor-related protein binds and internalizes Pseudomonas exotoxin A. J Biol Chem. 1992;267(18):12420-3.
227. Voulhoux R, Taupiac M, *et al*. Influence of deletions within domain II of exotoxin A on its extracellular secretion from Pseudomonas aeruginosa. J Bacteriol. 2000;182(14):4051-8.
228. Hwang J, Fitzgerald D, *et al*. Functional domains of Pseudomonas exotoxin identified by deletion analysis of the gene expressed in E. coli. Cell. 1987;48(1):129-36.
229. Mrsny R, Daugherty A, *et al*. Bacterial toxins as tools for mucosal vaccination. Drug Discov Today. 2002;7(4):247-58.

230. Hidalgo I, Raub T, *et al*. Characterization of the human colon carcinoma cell line (Caco-2) as a model system for intestinal epithelial permeability. Gastroenterology. 1989;96(3):736-49.
231. Antunes F, Andrade F, *et al*. Models to predict intestinal absorption of therapeutic peptides and proteins. Curr Drug Metab. 2013;14(1):4-20.
232. Cabezas F, Lagos J, *et al*. Megalin/LRP2 expression is induced by peroxisome proliferator-activated receptor-alpha and-gamma: implications for PPARs' roles in renal function. PloS One. 2011;6(2):1-17.
233. Ge Y, Zhang Y, *et al*. Fluorescence modified chitosan-coated magnetic nanoparticles for high-efficient cellular imaging. Nanoscale Res Lett. 2009;4(4):287-95.
234. Husband F, Garrood M, *et al*. Adsorbed protein secondary and tertiary structures by circular dichroism and infrared spectroscopy with refractive index matched emulsions. J Agric Food Chem. 2001;49(2):859-66.
235. Whitmore L, Wallace B. Protein secondary structure analyses from circular dichroism spectroscopy: methods and reference databases. Biopolymers. 2008;89(5):392-400.
236. Fowler R, Vllasaliu D, *et al*. Nanoparticle transport in epithelial cells: pathway switching through bioconjugation. Small. 2013;9(19):3282-94.
237. Kim K, Malik A. Protein transport across the lung epithelial barrier. Am J Physiol Lung Cell Mol Physiol. 2003;284(2):247-59.
238. Howard K, Bienk K, *et al*. Modified payload molecules and their interactions and uses. Google Patents; 2014.
239. des Rieux A, Ragnarsson E, *et al*. Transport of nanoparticles across an in vitro model of the human intestinal follicle associated epithelium. Eur J Pharm Sci. 2005;25(4):455-65.
240. Carney R, Carney T, *et al*. Dynamic cellular uptake of mixed-monolayer protected nanoparticles. Biointerphases. 2012;7(1):17.
241. Srinivasan B, Kolli A, *et al*. TEER measurement techniques for in vitro barrier model systems. J Lab Autom. 2015;20(2):107-26.
242. Johannes L, Popoff V. Tracing the retrograde route in protein trafficking. Cell. 2008;135(7):1175-87.
243. Cartiera M, Johnson K, *et al*. The uptake and intracellular fate of PLGA nanoparticles in epithelial cells. Biomaterials. 2009;30(14):2790-8.
244. Rowland R, Taylor P, *et al*. Attachment, uptake and transport of nanoparticles coated with an internalin A fragment in Caco-2 cell monolayers. J Drug Deliv Sci Technol. 2005;15(4):313-7.
245. Fröhlich E. The role of surface charge in cellular uptake and cytotoxicity of medical nanoparticles. Int J Nanomedicine. 2012;7(1):5577-91.
246. Dos Santos T, Varela J, *et al*. Effects of transport inhibitors on the cellular uptake of carboxylated polystyrene nanoparticles in different cell lines. PloS one. 2011;6(9):1-10.
247. Dausend J, Musyanovych A, *et al*. Uptake mechanism of oppositely charged fluorescent nanoparticles in HeLa cells. Macromol Biosci. 2008;8(12):1135-43.
248. Lennernäs H, Palm K, *et al*. Correlation between paracellular and transcellular drug permeability in the human jejunum and Caco-2 monolayers. Int J Pharm. 1996;127:103-7.
249. Toquet C, Jarry A, *et al*. Altered Calreticulin expression in human colon cancer: maintenance of Calreticulin expression is associated with mucinous differentiation. Oncol Rep. 2007;17(5):1101-8.
250. Seyrek E, Dubin P, *et al*. Ionic strength dependence of protein-polyelectrolyte interactions. Biomacromolecules. 2003;4(2):273-82.
251. Thanou M, Verhoef J. Chitosan and its derivatives as intestinal absorption enhancers. Adv Drug Deliv Rev. 2001;50:S91-S101.
252. Li P, Dai Y, *et al*. Chitosan-alginate nanoparticles as a novel drug delivery system for nifedipine. Int J Biomed Sci. 2008;4(3):221-8.
253. Katuwavila N, Perera A, *et al*. Chitosan-Alginate Nanoparticle System Efficiently Delivers Doxorubicin to MCF-7 Cells. J Nanomater. 2016;2016:1-12.
254. Das R, Kasoju N, *et al*. Encapsulation of curcumin in alginate-chitosan-pluronic composite nanoparticles for delivery to cancer cells. Nanomedicine. 2010;6(1):153-60.
255. Ma Z, Lim L. Uptake of chitosan and associated insulin in Caco-2 cell monolayers: a comparison between chitosan molecules and chitosan nanoparticles. Pharm Res. 2003;20(11):1812-9.

256. Collins C, Collier R. Circular dichroism of diphtheria toxin, Pseudomonas aeruginosa exotoxin A, and various derivatives. Biochim Biophys Acta. 1985;828(2):138-43.
257. Sreerama N, Woody R. Estimation of protein secondary structure from circular dichroism spectra: comparison of CONTIN, SELCON, and CDSSTR methods with an expanded reference set. Anal Biochem. 2000;287(2):252-60.
258. Gordon D, Leinart A, *et al*. Portal copper transport in rats by albumin. Am J Physiol. 1987;252(3):327-33.
259. van der Vusse G. Albumin as fatty acid transporter. Drug Metab Pharmacokinet. 2009;24(4):300-7.
260. Schnitzer J, Oh P. Albondin-mediated capillary permeability to albumin. Differential role of receptors in endothelial transcytosis and endocytosis of native and modified albumins. J Biol Chem. 1994;269(8):6072-82.
261. Tiruppathi C, Song W, *et al*. Gp60 activation mediates albumin transcytosis in endothelial cells by tyrosine kinase-dependent pathway. J Biol Chem. 1997;272(41):25968-75.
262. Birn H, Fyfe J, *et al*. Cubilin is an albumin binding protein important for renal tubular albumin reabsorption. J Clin Invest. 2000;105(10):1353-61.
263. Cui S, Verroust P, *et al*. Megalin/gp330 mediates uptake of albumin in renal proximal tubule. Am J Physiol. 1996;271(4):900-7.
264. Merlot A, Kalinowski D, *et al*. Unraveling the mysteries of serum albumin—more than just a serum protein. Front Physiol. 2014;5:1-7.
265. White J, Johannes L, *et al*. Rab6 coordinates a novel Golgi to ER retrograde transport pathway in live cells. J Cell Biol. 1999;147(4):743-60.
266. Lencer W, Saslowsky D. Raft trafficking of AB 5 subunit bacterial toxins. Biochim Biophys Acta. 2005;1746(3):314-21.
267. Pang H, Le P, *et al*. Ganglioside GM1 levels are a determinant of the extent of caveolae/raft-dependent endocytosis of cholera toxin to the Golgi apparatus. J Cell Sci. 2004;117(8):1421-30.
268. Rescigno M, Urbano M, *et al*. Dendritic cells express tight junction proteins and penetrate gut epithelial monolayers to sample bacteria. Nat Immunol. 2001;2(4):361-7.
269. Potapova T, Sivakumar S, *et al*. Mitotic progression becomes irreversible in prometaphase and collapses when Wee1 and Cdc25 are inhibited. Mol Biol Cell. 2011;22(8):1191-206.
270. Specian R, Oliver M. Functional biology of intestinal goblet cells. Am J Physiol. 1991;260(2):183-93.
271. Grivel M, Ruckebusch Y. The propagation of segmental contractions along the small intestine. J Physiol. 1972;227(2):611-25.
272. Waters J. Accuracy and precision in quantitative fluorescence microscopy. J Cell Biol. 2009;185(7):1135-48.
273. Hamilton N. Quantification and its applications in fluorescent microscopy imaging. Traffic. 2009;10(8):951-61.
274. Jensen E. Quantitative analysis of histological staining and fluorescence using ImageJ. Anat Rec. 2013;296(3):378-81.
275. Jung C, Hugot J, *et al*. Peyer's patches: the immune sensors of the intestine. Int J Inflam. 2010;2010:1-12.
276. Jani P, Halbert G, *et al*. The uptake and translocation of latex nanospheres and microspheres after oral administration to rats. J Pharm Pharmacol. 1989;41(12):809-12.
277. Mathiowitz E, Jacob J, *et al*. Biologically erodable microspheres as potential oral drug delivery systems. Nature. 1997;386(6623):410-4.
278. Jensen E. Quantitative analysis of histological staining and fluorescence using ImageJ. Anat Rec. 2013;296(3):378-81.
279. McDole J, Wheeler L, *et al*. Goblet cells deliver luminal antigen to CD103+ dendritic cells in the small intestine. Nature. 2012;483(7389):345-9.
280. Howe S, Lickteig D, *et al*. The uptake of soluble and particulate antigens by epithelial cells in the mouse small intestine. PloS one. 2014;9(1):1-11.
281. Murray P, Wynn T. Protective and pathogenic functions of macrophage subsets. Nat Rev Immunol. 2011;11(11):723-37.

282. Lewis S, Treacher D, *et al*. Expression of CD11c and EMR2 on neutrophils: potential diagnostic biomarkers for sepsis and systemic inflammation. Clin Exp Immunol. 2015;182(2):184-94.
283. Iwasaki A. Mucosal dendritic cells. Annu Rev Immunol. 2007;25:381-418.
284. Farache J, Koren I, *et al*. Luminal bacteria recruit CD103+ dendritic cells into the intestinal epithelium to sample bacterial antigens for presentation. Immunity. 2013;38(3):581-95.
285. Persson E, Scott C, *et al*. Dendritic cell subsets in the intestinal lamina propria: ontogeny and function. Eur J Immunol. 2013;43(12):3098-107.
286. Cureton D, Massol R, *et al*. Vesicular stomatitis virus enters cells through vesicles incompletely coated with clathrin that depend upon actin for internalization. PLoS Pathog. 2009;5(4):1-15.
287. Doherty G, McMahon H. Mechanisms of endocytosis. Annu Rev Biochem. 2009;78:857-902.

Appendix 1 Protocol for Sodium dodecyl sulphate polyacrylamide gel electrophoresis

Recipes:

Reducing sample buffer 2X (1 mL): 500 µL of 4X NuPAGE® LDS buffer, 200 µL of NuPAGER reducing agent 200, and 300 µL of MQ H_2O.

Running buffer (Tris-Glycine) 10X (1 L): 30.3 g of Tris, 144 g of glycine, and 10 g of sodium dodecyl sulphate.

Staining solution (1 L): 500 mg of Coomassie Brilliant Blue R-250, 400 mL of ethanol, 100 mL of glacial acetic acid, and 500 mL of MQ H_2O.

Destain Solution (1 L): 100 mL of methanol, 70 mL of glacial acetic acid, and 830 mL of MQ H_2O.

Recipes for 10 polyacrylamide gels. 12% Bio-Tris acrylamide, 1 mm thick gels:

Resolving gel: 16.8 mL of 40 % Bis-Tris acrylamide, 14.0 mL of 1.5 M Tris-HCl pH 8.8, 560 µL of 10% SDS, 560 µL of 10% ammonium persulfate, 56 µL of tetramethylethylenediamine, and 24.0 mL of MQ H_2O.

Stacking gel: 3.0 mL of 40% Bis-Tris acrylamide, 5.0 mL of 0.5 M Tris-HCl pH 6.8, 200 µL of 10% SDS, 200 µL of 10% ammonium persulfate, 20 µL of tetramethylethylenediamine and 11.6 mL of MQ H_2O.

The mixtures for resolving gel were poured into gel cassettes to about 75 % total volume. Butanol was used to fill up the gel cassettes, in order to ensure that the gel set flat and without bubbles. Gels were allow to polymerise for 45 min at room temperature. Later on, the butanol was discarded and the stacking gel solution was applied. Gel combs containing 12 wells were inserted into the stacking gel at the top of the cassette prior to polymerisation and gels were left to set for another 30 min.

Procedures:

10 µL of samples (collected protein fractions) were mixed with 50 µL of reducing sample buffer and 20 µL of the mixture were loaded onto polymerised gel which was placed on an XCell™ Sure lock® Mini-cell tank with running buffer.

The first well was filled with 15 µL of a standard protein ladder (10-170 KDa). Gels were allowed to run for 35-40 min at 220 V. Following electrophoresis, gels were incubated overnight in

Coomassie stain solution on a rocking platform. Finally, protein bands were observed after the gels were destained many times.

Appendix 2 Ellman's reagent reaction

Materials preparation:

Reaction buffer: 0.1 M sodium phosphate, 1 mM EDTA, and 50 mL of MQ H_2O, at pH 8.0.

Ellman's Reagent solution: 4 mg Ellman's reagent were dissolved in 1 mL of reaction buffer.

0.15 mM cysteine solution (dissolved in PBS) was prepared as positive control.

Measurement:

50µL of Ellman's Reagent solution and 2.5 mL of reaction buffer were added into a 5 mL Eppendorf tubes. 250 µL of unknown sample was added into tube 1, 250 µL of reaction buffer was added to a tube 2 as a blank, and 250 µL of 0.15mM cysteine solution was added into tube 3 as a positive control. All these solutions were mixed and incubated at RT for 15 min. Absorbance of each sample was measured at the wavelength of 412nm using a spectrophotometer. The concentration of the free thiol groups in the unknown sample was calculated using the adapted equation follows: $c = \frac{11.2A}{bE}$, where A=absorbance, b=path length in centimetres, E= molar extinction coefficient, which is 14,150 $M^{-1}cm^{-1}$.